REACTION OF BULKY MAIN GROUP METAL(II) AMIDES WITH POLYFUNCTIONAL PHENOL SUBSTRATES

By

Anthony E. Wetherby Jr.

Bachelor of Science in Chemistry
Clarkson University
Potsdam, New York
2004

Submitted to the Faculty of the
Graduate College of the
Oklahoma State University
in partial fulfillment of
the requirements for
the Degree of
DOCTOR OF PHILOSOPHY OR OTHER
July, 2009

REACTION OF BULKY MAIN GROUP

METAL(II) AMIDES WITH

POLYFUNCTIONAL PHENOL SUBSTRATES

Dissertation Approved:

Dr. Charles S. Weinert

Dissertation Adviser

Dr. Allen Apblett

Dr. Nicholas Materer

Dr. LeGrande Slaughter

Dr. Earl Mitchell Jr.

Dr. A. Gordon Emslie

Dean of the Graduate College

Dedication

To my wife Mary and daughter Kiera: Thank you for your unconditional love and support. Without you none of what I have accomplished would be possible.

Acknowledgements

I first wish to thank my wife, daughter, and family without whom none of this work would be possible. You support and inspire me always and for that I am eternally grateful. Thank you to my advisor Dr. Charles S. Weinert for your teachings and advising. I have learned more from you than I could ever thank you for. You have improved my skills and shown me what it takes to be truly successful in this field. Thank you also for the experiences at the Gordo, which I enjoyed immensely. To my graduate committee, thank you for the classes you have taught and the guidance and lessons you have given me. Thank you to Dr. Iob and Gianna for their assistance with instrumentation and guidance throughout my graduated experience. To the Clemons family, thank you for being our family away from home and giving my family strength in trying times. To my friends thank you for all of your help and the experiences here that have made the work worth it. I will miss you all. To the hallmark girls, past and present, thank you for extra work, the entertainment and Henrys. To the Weinert group members, who are also my good friends, thank you for ice cream babies, explosions, broken glassware and headaches. Thank you also for our discussions, team work and enjoyable working environment. The success of our group and its individual members is a direct

result of our cohesive nature, desire to teach each other things and a willingness to go the extra mile and help each other without thought of personal gains. To all I have met here, thank you and good luck in your future endeavors. And lastly, thank you to Jameson. You are the only one that is always happy to see me.

TABLE OF CONTENTS

Chapter **Page**

Chapter **Page**

LIST OF TABLES

Table **Page**

Chapter 1

Chapter 2

Chapter 3

Table **Page**

Chapter 4

Chapter 5

LIST OF SCHEMES

Schemes **Page**

Chapter 1

Schemes **Page**

Chapter 2

Schemes **Page**

Chapter 3

Chapter 4

Schemes **Page**

Chapter 5

LIST OF FIGURES

Figure **Page**

Chapter 1

Chapter 2

Figure **Page**

Chapter 3

Chapter 4

Figure **Page**

Chapter 5

Figure **Page**

CHAPTER I

INTRODUCTION

The initial interest in organogermanium compounds was a result of their perceived technological importance. Nearly 62 years later technological applications still drive this chemistry, with research having intensified, citing the thermochromic nature of these compounds as well as their uses in the field of semi-conductors and their prospective biological and optical applications[1]. As a result of this interest, the chemistry germylene compounds, pioneered in 1948 by M. Lesbre and J. Satgé at University of Toulouse, France, has grown considerably over this time in order to meet technological demands. Steady advances in the synthesis and characterization of these compounds have been achieved due greatly to the advances made in spectroscopic methods. Impressive efforts made in both carbene and stannylene chemistry has also furthered the progress of germylene chemistry. This is due to the fact that germylenes can be regarded as heavy carbene anologues[1] and compliment the analogous stannylene type reactions, since they often demonstrate similar reactivity. One example of stannylene and germylene compounds reacting similarly is the reaction of $Sn(NR_2)_2$ or $Ge(NR_2)_2$ (R = $N(SiMe_3)$) with $M(CO)_6$ (M = Cr, Mo, or W).[2] It has been observed that both the $Sn(NR_2)_2$ **(Scheme 1.1)**[2] and the $Ge(NR_2)_2$ (**Scheme 1.2**)[2] reactions result in ligand substitution reactions which afford a final transition metal containing product that

has one of the CO ligands replaced with a $M(NR_2)_2$ (M = Sn or Ge).

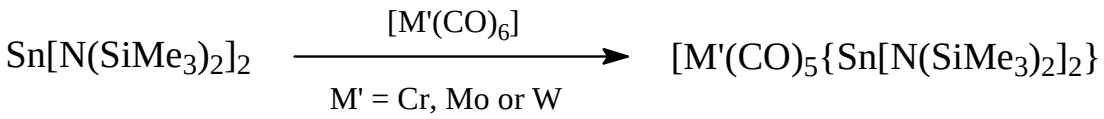

Scheme 1.1: Reaction of $M(CO)_6$ (M = Cr, Mo, or W) with $Sn(NR_2)_2$.[2]

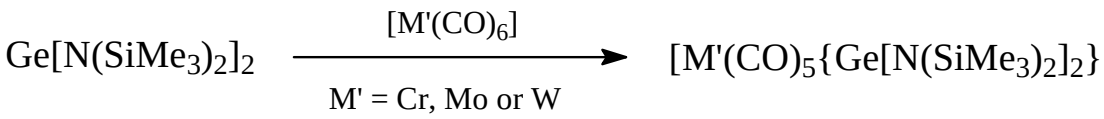

Scheme 1.2: Reaction of $M(CO)_6$ (M = Cr, Mo, or W) with $Ge[N(SiMe_3)_2]_2$.[2]

Germylene compounds have been observed as a number of forms including polymers, dimers, and monomeric species. The type of compound formed is greatly influenced by the ligands attached to the germanium atom, with species containg bulky, electron withdrawing ligands having been shown to stabilize the formation of monomeric germylenes. In these cases the electronic configuration of the germanium(II) compound, which consists of a lone pair of electrons and a vacant p-orbital, results in diverse chemistry. The lone pair of electrons, housed in a sp^2 hybridized orbital, allows the germylene to act as a lewis base via donation of its electron density to other species. Germylenes also exhibit lewis acidity resulting from the acceptance of electron density into their vacant p-orbitals.[3]

To date several methods for the synthesis of germylene compounds are known. One of the more common methods for the synthesis of free germylene compounds consists of the reaction between tetraphenylgermole and dehydrobenzene **(Scheme 1.3)**.[1] This reaction results in the formation of a 7,7-disubstituted -7-germabenzonorbornadiene intermediate. Subsequent heating or UV irradiation affords the germylene product which can then be isolated via a hydrocarbon matrix at 77 K to prevent the formation of a polymeric species.[1]

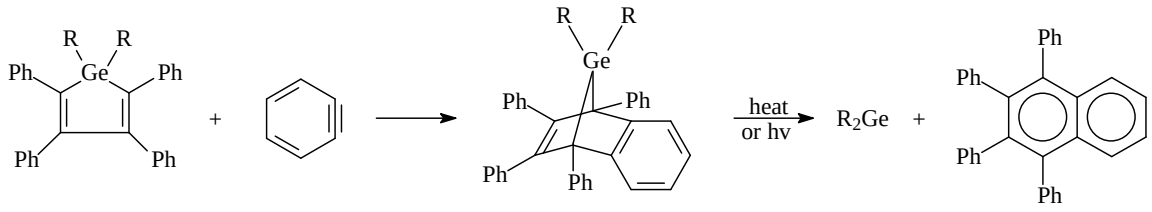

R = Me, Et, Bu, Ph or 4-MePh

Scheme 1.3: Reaction of 7,7-disubstituted-7-germabenzonorbornadiene to yield R_2Ge.[1]

Other reactions affording germylenes include UV irradiation of diaryl bissilylgermanium compounds **(Scheme 1.4)**[1], the photochemical deazotination of dimethyldiazidogermane ($Me_2Ge(N_3)_2$) **(Scheme 1.5)**[1], and the photolytical cleavage of strained cyclogermanes containing Ge-Ge bonds **(Scheme 1.6)**.[1]

Ar = e.g. Ph, 4-MePh, 2,6-Me_2Ph, 2,6-Et_2-Ph, Mesityl and 2,4,6-$^{i}Pr_3$-Ph

Scheme 1.4: UV irradiation of diaryl bissilylgermanium compounds.[1]

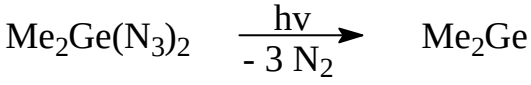

Scheme 1.5: Photochemical deazotination of dimethyldiazidogermane ($Me_2Ge(N_3)_2$).[1]

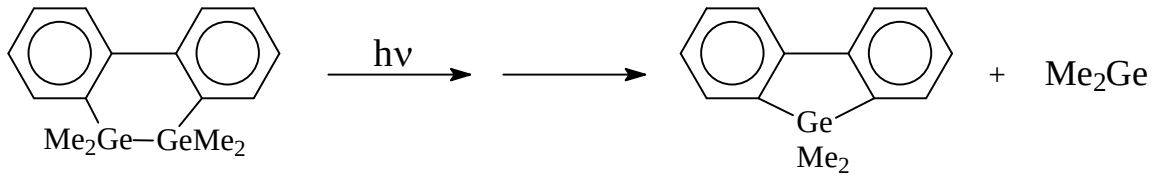

Scheme 1.6: Photolytical splitting of strained cyclogermanes.[1]

Despite the multitude of synthetic routes for the preparation of germylenes, the isolation and characterization of these compounds has been difficult. This is a result of the fact that most monomeric germylenes, produced by these and related methods, are short-lived highly reactive species that undergo rapid polymerization. In order to study these compounds, it has been necessary to isolate them either in a hydrocarbon matrix at 77 K or via chemical trapping methods, which commonly employ 1,3-dienes or Benzil.[1]

Although most germylenes are unstable, stable compounds that are resistant toward polymerization have been prepared by the attachment bulky ligands to the germanium(II) center. These ligands include aryl, alkyl, amido, aryloxo and arylthiolato groups and have been shown to kinetically and thermodynamically stabilize germylenes such that they are present in a monomer-dimer equilibrium or in a completely monomeric state.[4] Of these ligand types, the two most commonly used bulky ligands to date are the disyl ($CH(SiMe_3)_2$) and trimethylsilylamido ($[N(SiMe_3)_2]$) groups, which afford the bis[bis(trimethylsilyl)methyl] germanium(II) ($Ge[CH(SiMe_3)_2]_2$) and bis[bis(trimethylsilyl)amido]germanium(II) ($Ge[N(SiMe_3)_2]_2$) germylenes (respectively). The monomeric nature of these germylenes stems from the selection of their significantly bulky ligands which aid in the stability of the species in two main ways. First, the absence of any β-hydrogens and the presence of a β-silicon impedes metal-ligand decomposition through a β-elimination pathway. The second way in which these bulky ligands stabilize the monomeric state is by inhibiting access to the metal center through steric effects which limits further reactivity. An additional feature that these two compounds share is the presence of a significant number of methyl groups. Along with providing steric bulk, the methyl groups provide the added benefit of enhancing the solubility of these compounds in hydrocarbon solvents. This in turn makes the manipulation of these germylenes facile.

Although similar in bulk, these two common germylenes are synthesized by different methods, exhibit different solid state structures, and have been shown to afford a wide range of reactivity. The first of the two best known stable germylenes,

bis[bis(trimethylsilyl)methyl] germanium(II) ($Ge[CH(SiMe_3)_2]_2$) can be prepared via the reaction of bis(trimethylsilyl)methyl-lithium and germanium(II) amide **(Scheme 1.7).**[5]

$$2Li[CH(SiMe_3)_2] + Ge[N(SiMe_3)_2]_2 \xrightarrow[0 \text{ to } -20\ ^oC]{OEt_2} Ge[CH(SiMe_3)_2]_2 + 2Li[N(SiMe_3)_2]$$

Scheme 1.7: Synthesis of bis[bis(trimethylsilyl)methyl] germanium(II) via reaction of bis(trimethylsilyl)methyl-lithium and germanium(II) amide.[5]

The resulting germylene has been observed to be dimeric in the crystalline state **(Figure 1.1)**[6], but in solution reacts as if it were monomeric. This monomeric reaction behavior can be attributed to the weak nature of germanium-germanium bond. The germanium-germanium bond measures 2.347(2)Å, which is indicative of a Ge=Ge double bond, while the average germanium-carbon bond distance measures 2.011(3)Å and the Ge-Ge-C bond angles are 113.7(3)° and 122.3(2)°.[6]

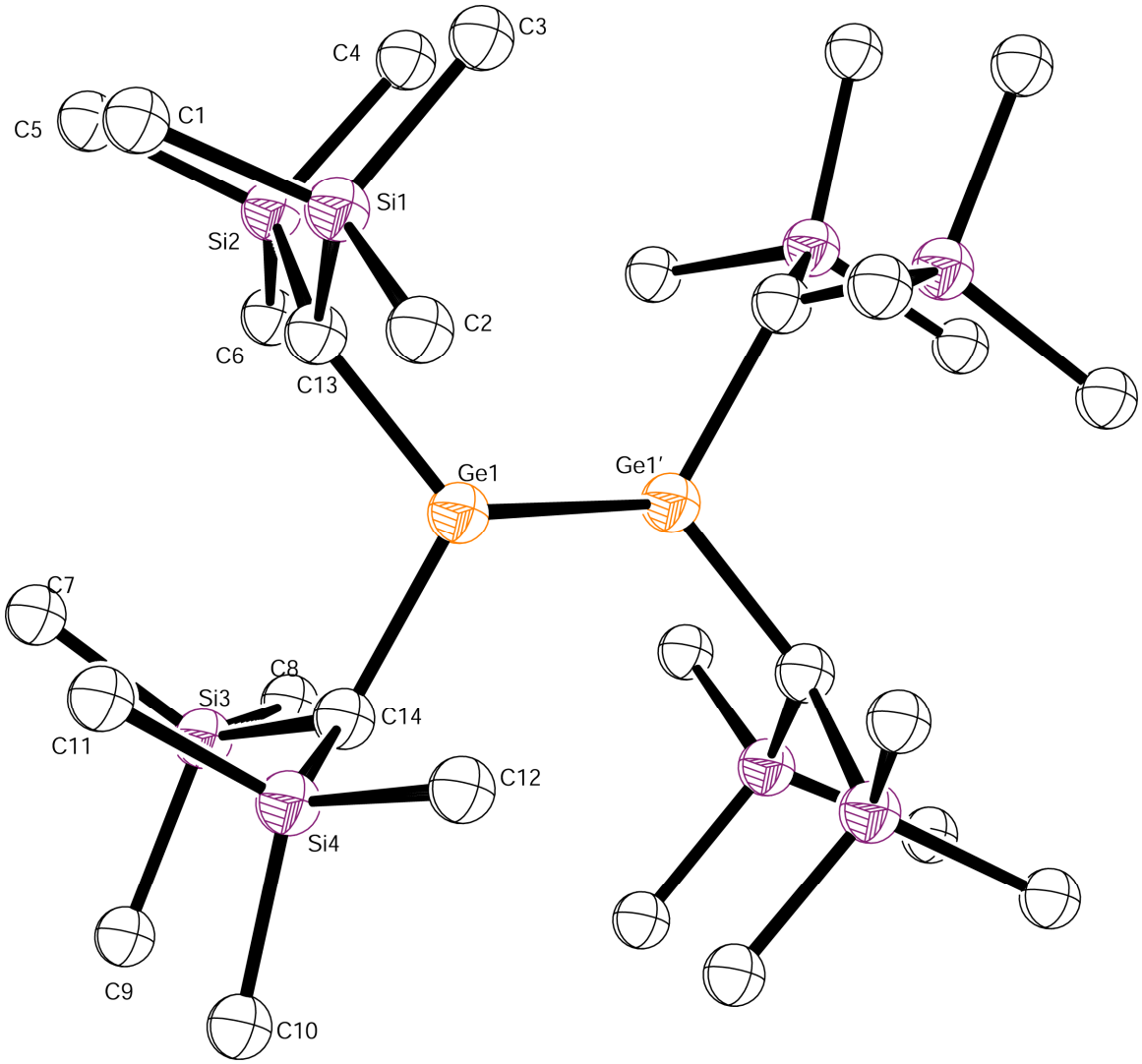

Figure 1.1: X-ray crystal structure of $\{Ge[CH(SiMe_3)_2]\}_2$.[6]

Table 1.1: Selected bond angles and distances for $\{Ge[CH(SiMe_3)_2]\}_2$.[6]

Bond Lengths	(Å)	Bond Angles	(°)
Ge(1) – Ge(1´)	2.347(2)	Ge(1´) – Ge(1) – C(14)	122.3(2)
Ge(1) – C(14)	1.979(9)	Ge(1) – C(13) – Si(1)	119.1(4)
Ge(1) – C(13)	2.042(8)	Ge(1) – C(13) – Si(2)	110.0(4)
		Ge(1) – C(14) – Si(3)	113.9(4)
		Ge(1) – C(14) – Si(4)	121.8(4)

Reactions involving $Ge[CH(SiMe_3)_2]_2$ generally involve CH activation in a variety of compounds including alkanes,[7] ethers,[7] cyanides,[8] amines[9] and ketones.[10] Most of these reactions require $MgCl_2$ or PhI to afford CH insertion, and have been shown to yield vastly different products in their absence. Several examples of these reactions are shown below **(Schemes 1.8-1.12)**.[7-10]

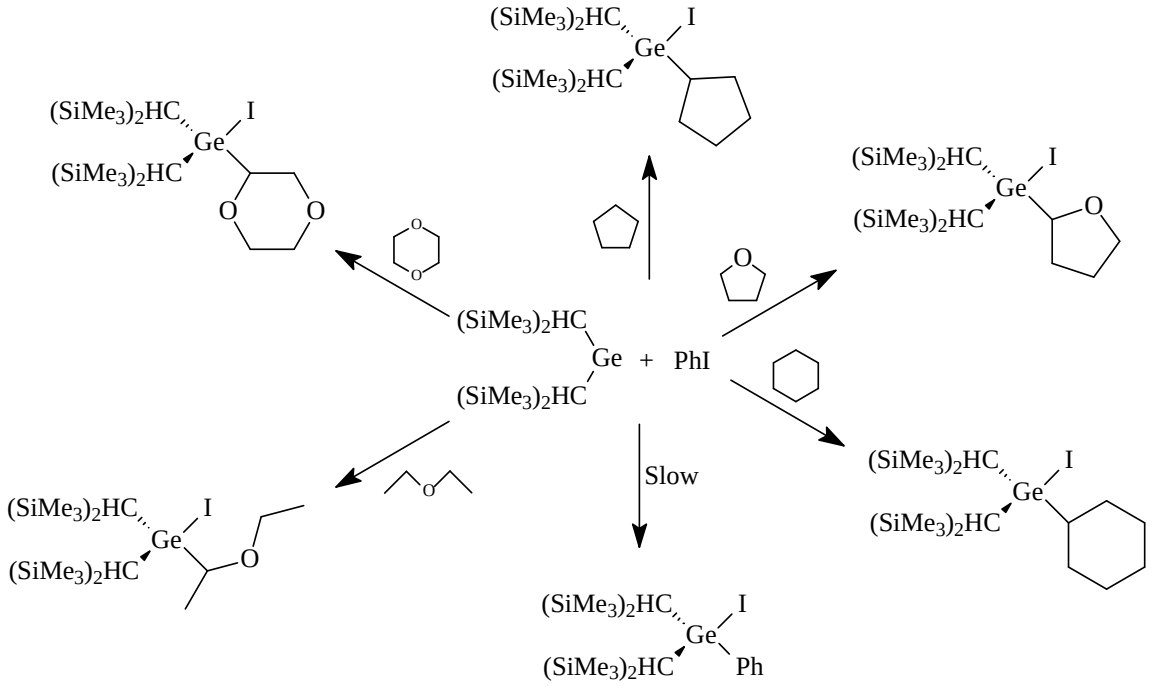

Scheme 1.8: CH activation of alkanes and ethers with $Ge[CH(SiMe_3)_2]_2$ and PhI.[7]

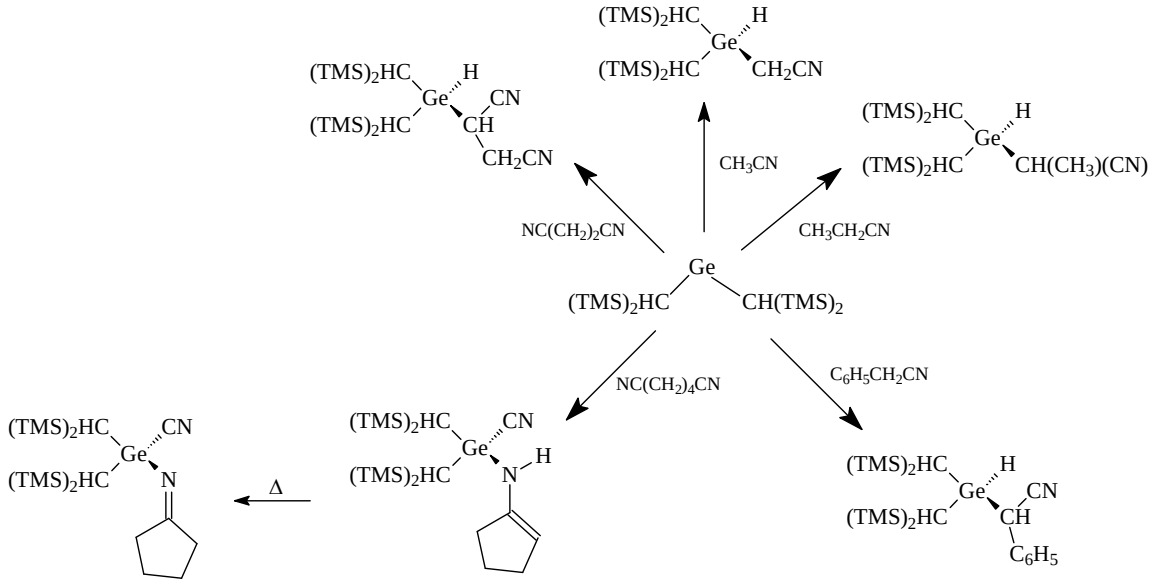

Scheme 1.9: CH activation of cyanide containing compounds with $Ge[CH(SiMe_3)_2]_2$and $MgCl_2$.[8]

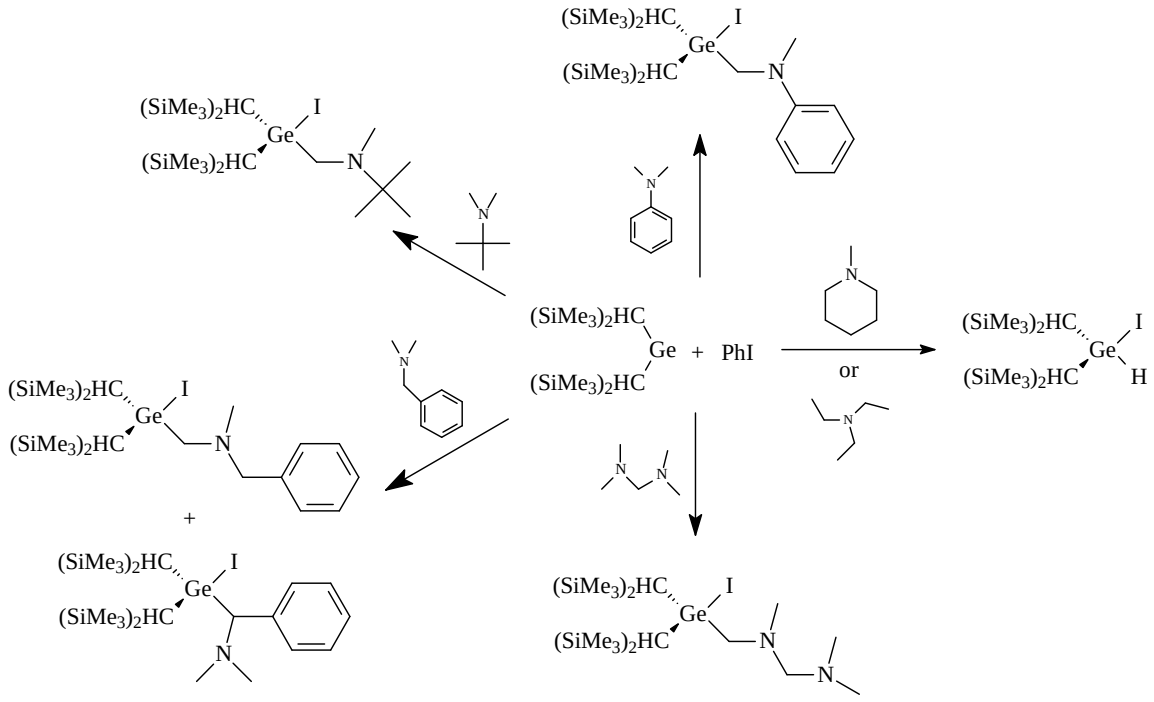

Scheme 1.10: CH activation of amine containing compounds with $Ge[CH(SiMe_3)_2]_2$ and PhI.[9]

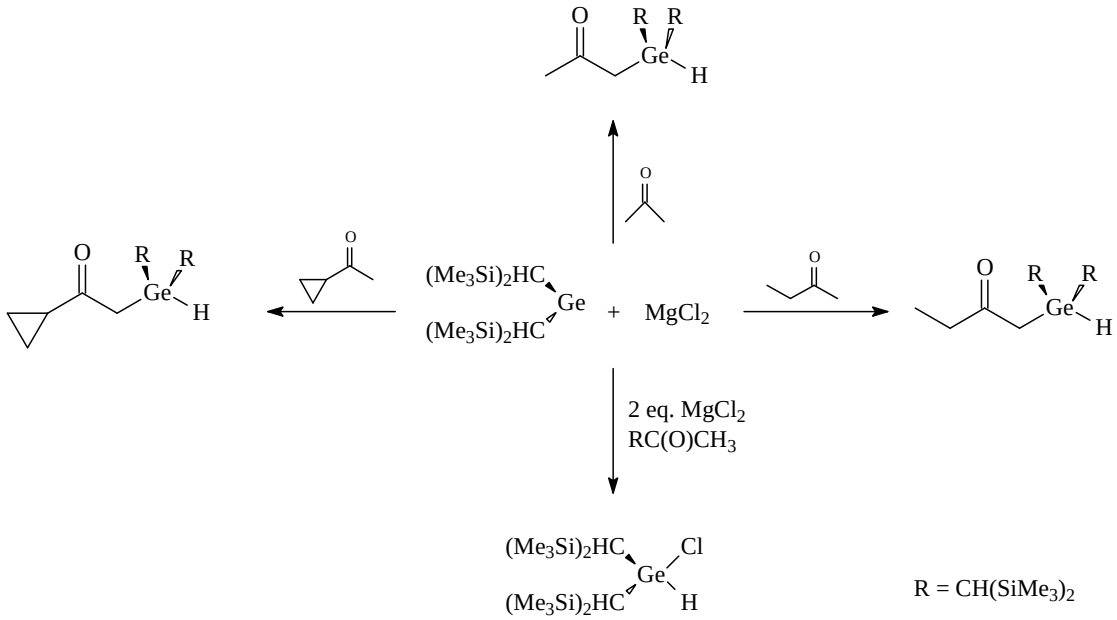

Scheme 1.11: Insertion of Ge[CH(SiMe$_3$)$_2$]2 into CH bonds of keytones in the presence of MgCl$_2$.[10]

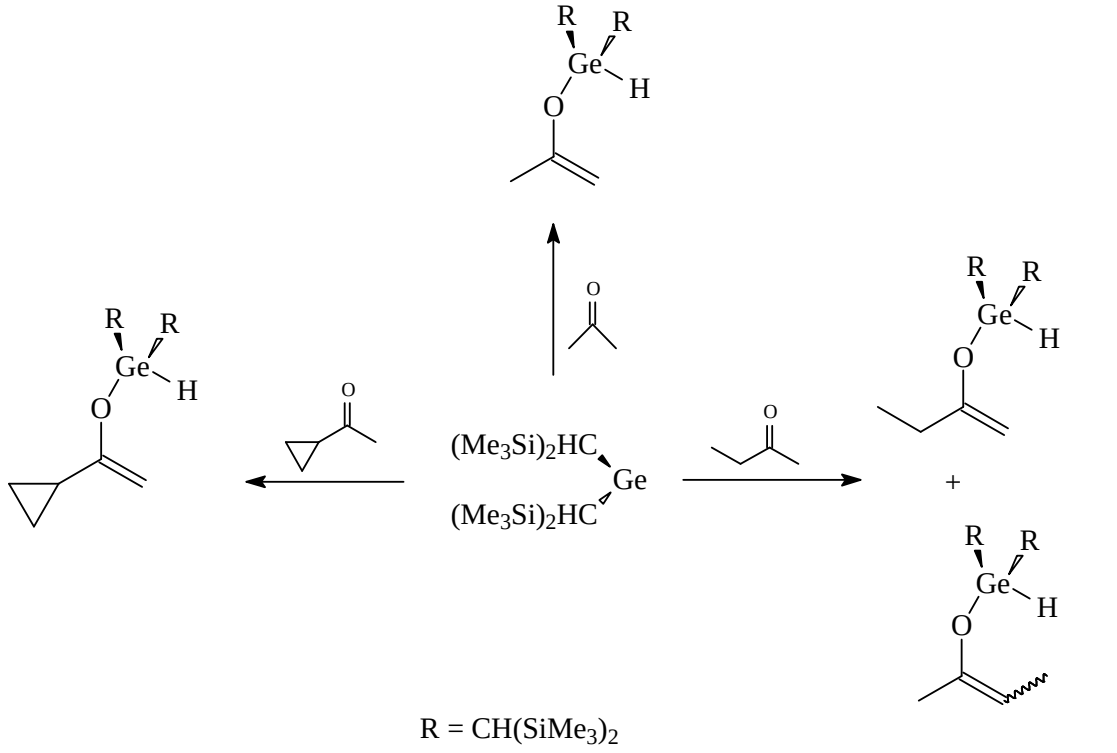

Scheme 1.12: Insertion of Ge[CH(SiMe$_3$)$_2$]$_2$ into OH bonds in the absence of MgCl$_2$.[10]

The second of the two most well-known bulky germylenes, germanium(II) amide, takes advantage of the use of the bulky, electron withdrawing trimethylsilylamido groups pioneered by Bürger and Wannagat[11] to stabilize the monomeric state. As found for the disyl ligand, the trimethylsilyl amido group stabilizes the monomeric state as a result of the absence of any β-hydrogens and the presence of a β-silicon. An additional feature that works to stabilize the monomeric state for this compound is the electron withdrawing nature of the trimethylsilylamido ligands which results in an electron deficient metal center, rendering the lone pair of electrons less reactive.

A thermochromic yellow/orange liquid at room temperature, $Ge[N(SiMe_3)_2]_2$ becomes colorless upon cooling to -196 °C[12], and is typically prepared via the reaction of germaniumdichloride·1,4-dioxane with two equivalents of lithium hexamethyldisilazane. This reaction results in the formation of the desired germylene, two equivalents of lithium chloride and 1,4-dioxane as the by-products (**Scheme 1.13**).[4]

$$GeCl_2(1,4\text{-dioxane}) + 2\ LiNR_2 \longrightarrow Ge(NR_2)_2 + 2\ LiCl + 1,4\text{-dioxane}$$

Scheme 1.13: Previous preparation of $Ge[N(SiMe_3)_2]_2$ ($NR_2 = N(SiMe_3)_2$).[4]

The X-ray crystal structure of germanium(II) amide **(Figure 1.2)**[4] exhibits a bent singlet state geometry rather than a linear triplet state **(Figure 1.3)**[11] with the germanium – nitrogen bond distances measuring 1.873(5) and 1.878(5) Å, while the N – Ge – N angle measures 107.1(2) ° **(Table 1.2)**.[4]

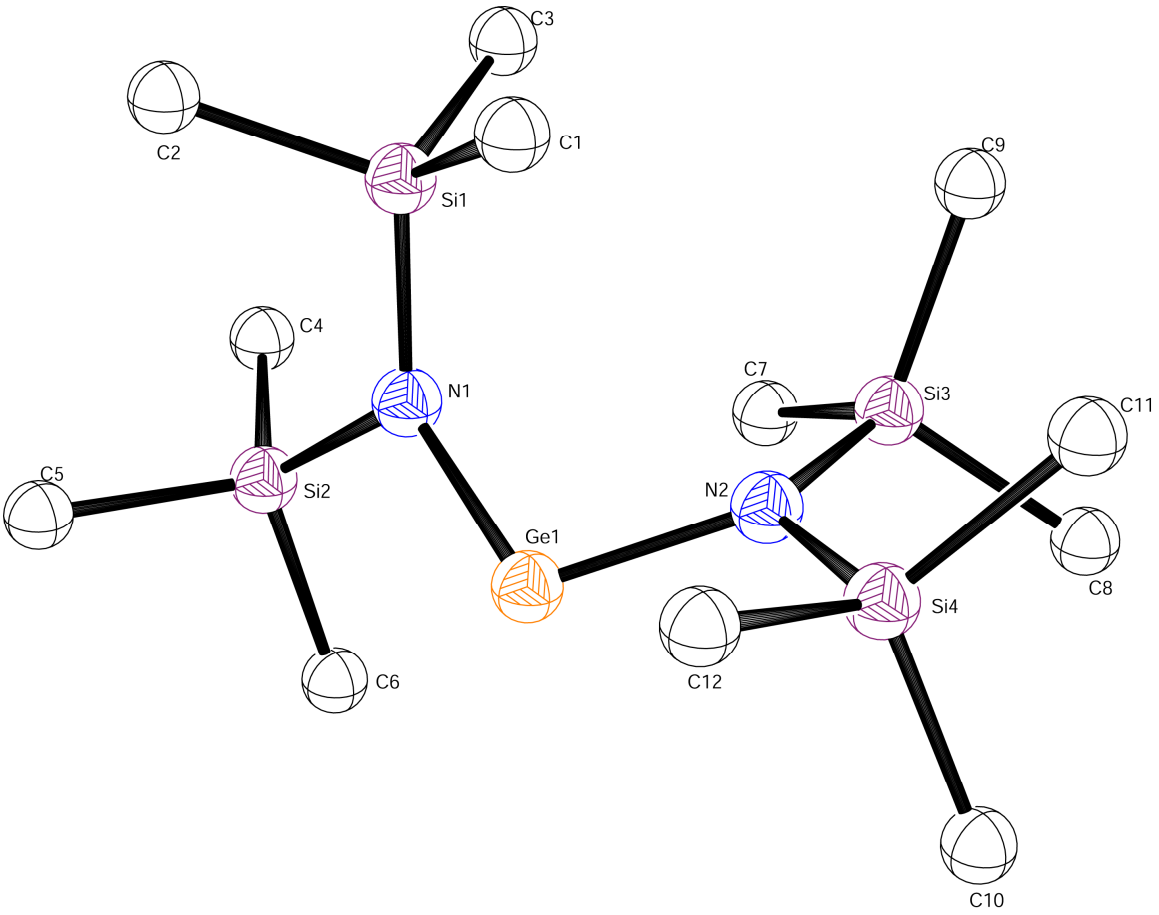

Figure 1.2: X-ray crystal structure of $Ge[N(SiMe_3)_2]_2$.[4]

(*a*) (*b*)

Figure 1.3: Expected structures for monomeric $M(NR^1R^2)_2$. (*a*) singlet and (*b*) triplet ground state.[11]

Table 1.2: Selected bond angles and distances for $Ge[N(SiMe_3)_2]_2$.[4]

Bond Lengths	(Å)	Bond Angles	(°)
Ge – N(1)	1.878(5)	N(1) – Ge – N(2)	107.1(2)
Ge – N(2)	1.873(5)	Si(1) – N(1) – Si(2)	120.7(3)
N(1) – Si(1)	1.751(5)	Si(3) – N(2) – Si(4)	120.5(3)
N(1) – Si(2)	1.749(5)	Ge – N(1) – Si(1)	124.4(3)
N(2) – Si(3)	1.757(5)	Ge – N(1) – Si(2)	113.0(3)
N(2) – Si(4)	1.749(6)	Ge – N(2) – Si(3)	125.3(3)
		Ge – N(2) – Si(4)	112.2(3)

Although feasible, the formation of $Ge[N(SiMe_3)_2]_2$ via the reaction of germaniumdichloride·1,4-dioxane with two equivalents of lithium hexamethyldisilazane results in only moderate yields. This is due to the presence of side reactions resulting from the highly acidic trichlorogermanium hydride intermediate produced during the synthesis of the germaniumdichloride·1,4-dioxane precursor compound **(Scheme 1.14)**.

Scheme 1.14: Synthesis of the germaniumdichloride·1,4-dioxane precursor compound via the formation of the highly acidic trichlorogermanium hydride intermediate.[6,13]

In an effort to improve upon the yield this synthetic route, Roskamp and coworkers reported a synthesis of $Ge[N(SiMe_3)_2]_2$ through a stabilized triphenylphosphoniumtrichlorogermanate intermediate in 1992.[13] This method involves a multistep synthesis beginning with the reaction of triphenylphosphine with germanium tetrachloride and tributyltinhydride in diethyl ether at room temperature to yield the triphenylphosphoniumtrichlorogermanate as well as tributyltinchloride (**Scheme 1.15**).[13] The triphenylphosphoniumtrichlorogermanate is then reacted with triethylamine to yield triethylammoniumtrichlorogermanate and triphenylphosphine (**Scheme 1.16**).[13] Lastly, triethylammoniumtrichlorogermanate is reacted with three equivalents of lithium hexamethyldisilazane to afford $Ge[N(SiMe_3)_2]_2$ in 70 – 77 % yield as well as triethylamine, lithium chloride and hexamethyldisilazane as by-products (**Scheme 1.17**).[13] In addition to the formation of a stabilized intermediate that reduces side reactions, most of the final by-products of this reaction are volatile which leads to a facile work-up.[13]

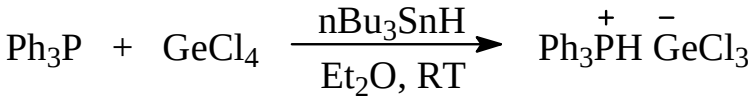

Scheme 1.15. Reaction of triphenylphosphine with germaniumtetrachloride and tributyltinhydride.[13]

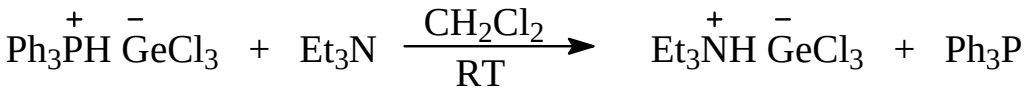

Scheme 1.16. Reaction of triphenylphosphoniumtrichlorogermanate with triethyl amine.[13]

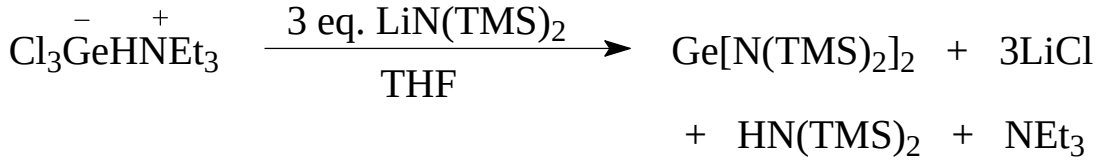

Scheme 1.17: Reaction of triethylammoniumtrichlorogermanate with three equivalents of lithium hexamethyldisilazane.[13]

The reactivity of $Ge[N(SiMe_3)_2]_2$ has been shown to be versatile, allowing for some CH insertion reactions similar to those observed for the $Ge[CH(SiMe_3)_2]_2$ as well as many different types of reactions involving both transition and main group metal compounds. This germanium(II) amide has also been used for the preparation of a variety of germanium aryloxides via a protonolysis reaction.

With regard to the reactivity of metal (II) amides (M = Ge or Sn) with transition metals, a variety of processes have been reported. These include the reaction of germylenes and stanylenes (MX_2) (M = Ge or Sn) with transition metal compounds of the general formula, L_nM'-X′. The versatility of these reagents has been studied and is exemplified by the fact that the reactions can be categorized into one of seven types. These seven types of reactions include MX_2 (*i*) acting as a terminal ligand, (*ii*) acting as a bridging ligand, (*iii*) inserting into a M′ – X′ bond which creates a new ligand with the formula MX_2X', (*iv*) reacting as a *N*-centered nucleophile with respect to a transition metal hydride containing compound to generate a new MX_2 species where X = M′L_n, (*v*) acting as a X^- transfer reagent, (*vi*) oxidatively adding to M′ center in a low oxidation state via a C – H bond insertion in $M(NR_2)_2$ with concomitant cyclometallation or (*vii*) acting as a reducing agent.[2] One example of a reaction of $Ge[N(SiMe_3)_2]_2$ with a transition metal was given in **Scheme 1.2**[2], and a few more examples of these types of reactions are provided below in **Scheme 1.18.**[2,14]

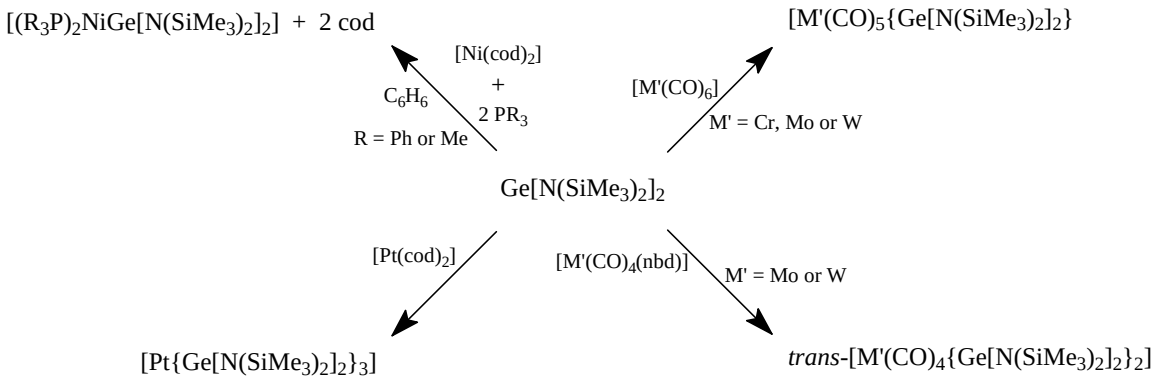

Scheme 1.18: A few reactions of $Ge[N(SiMe_3)_2]_2$ with transition metal compounds.[2,14]

The reactivity of $Ge[N(SiMe_3)_2]_2$ with organic molecules and other main group metals has also been observed to afford a wide range of products, including the formation of Ge-Si,[15] Ge-O,[16] Ge-N,[17] Ge-S,[18] Ge-Se,[18] and Ge-Te[18] bonds as well as many others. A variety of reactions are shown below in **Schemes 1.19-1.22**.[15-18]

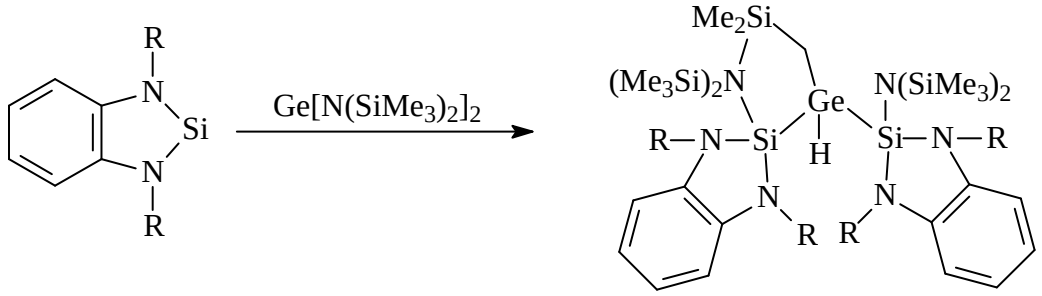

R = $CH_2{}^tBu$

Scheme1.19: Example of the formation of a Ge-Si bond.[15]

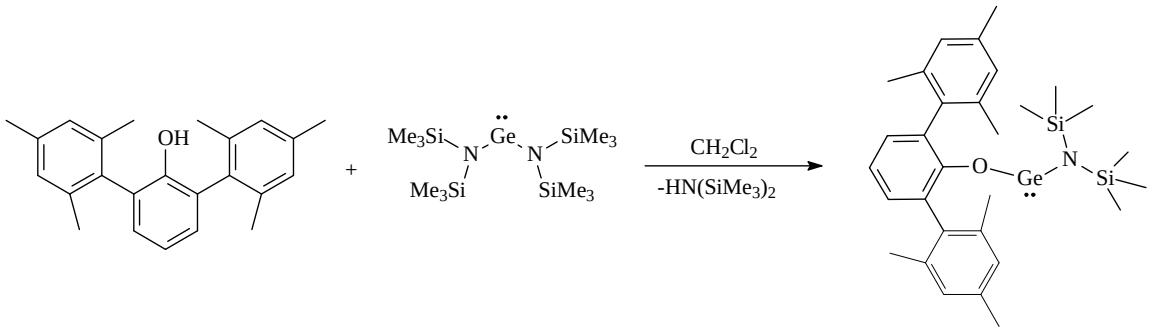

Scheme 1.20: Example of the formation of a Ge-O bond.[16]

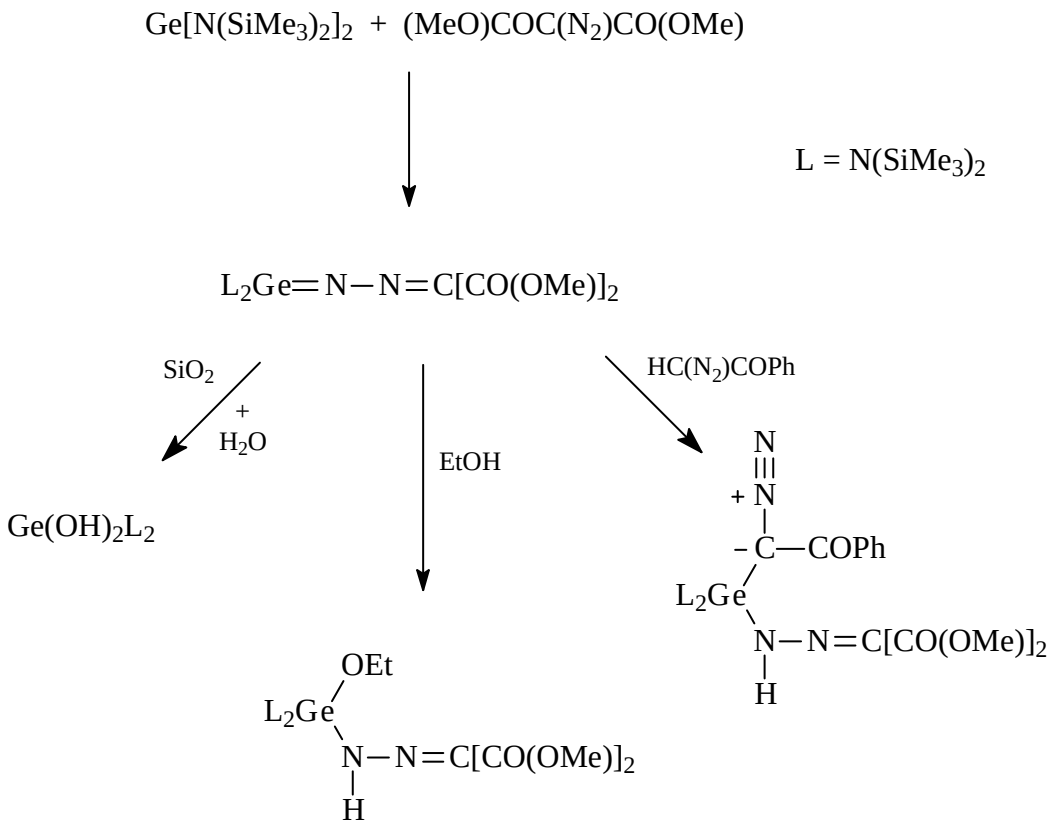

Scheme 1.21: Example of the formation of Ge-N bond and subsequent reactions.[17]

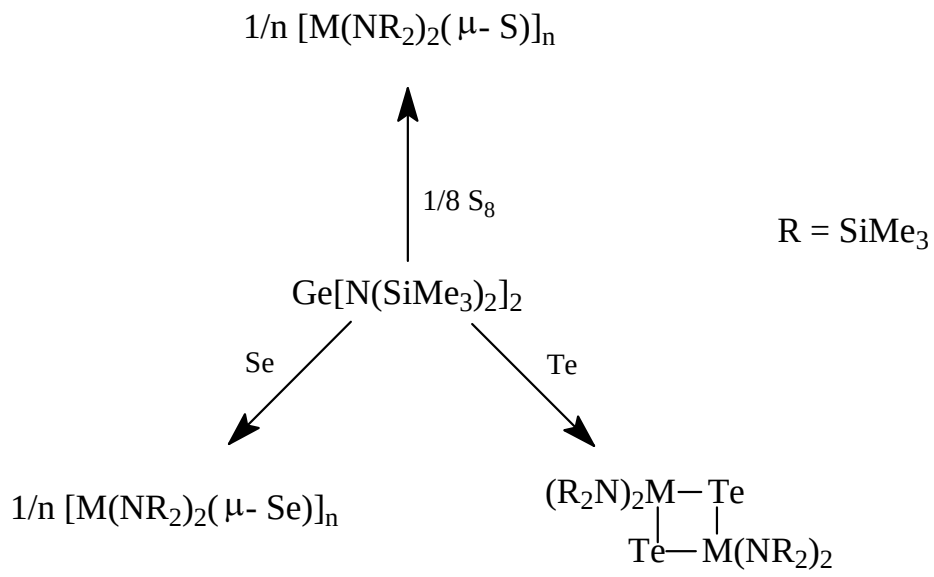

Scheme 1.22: Examples of the formation of Ge-S, Ge-Se and Ge-Te bonds.[18]

Along with the reactions between $Ge[N(SiMe_3)_2]_2$ with transition and main group metals, this species has been widely applied for the generation of germanium(II) aryloxides. The germanium(II) aryloxides form either monomers or dimers depending on the steric bulk of the ancillary ligands. Dimeric species have been observed when the aryl groups are either ($OC_6H_2Me_3$-2,4,6)[19] or ($OC_6H_3{}^iPr_2$-2,6).[19] The formation of monomeric species has been observed when the aryl groups are ($OC_6H_3Mes_2$),[16] (OC_6H_2Me-4-Bu^t_2-2,6),[20] ($OC_6H_3Ph_2$-2,6)[19] and (OC_6HPh_4-2,3,5,6).[19] Reaction schemes for synthesis of these compounds are given below in **Schemes 1.23-1.26**.[16,19,20]

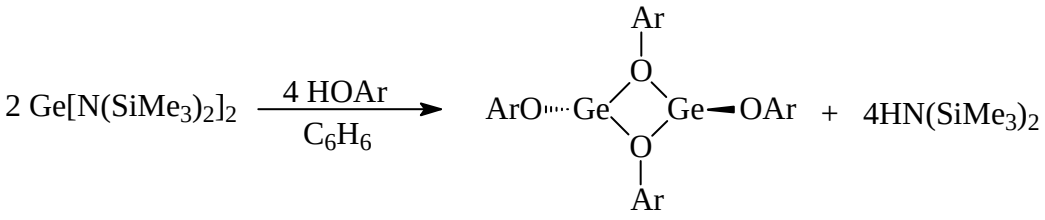

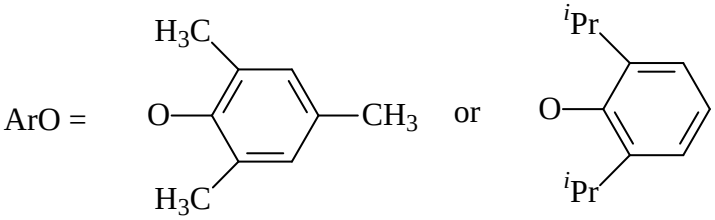

Scheme 1.23: Synthesis of $[Ge(OAr)_2]n$ (n = 2 and ArO = $OC_6H_2Me_3$-2,4,6 or OC6H3^{i}Pr2-2,6).[19]

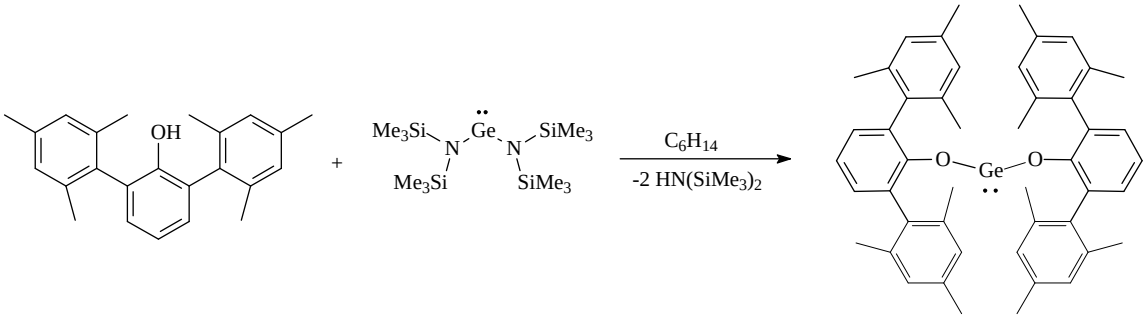

Scheme 1.24: Synthesis of $[Ge(OAr)_2]$ (ArO = $OC_6H_3Mes_2$).[16]

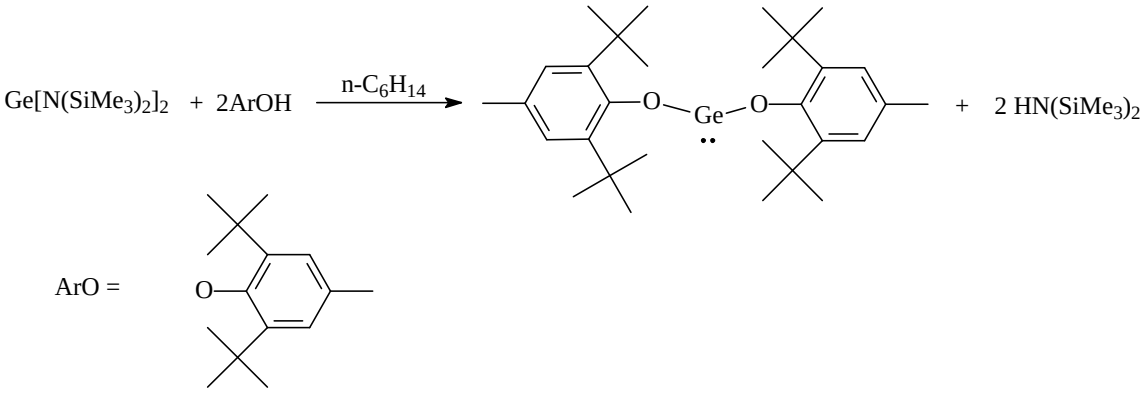

Scheme 1.25: Synthesis of $[Ge(OAr)_2]$ (ArO = OC_6H_2Me-4-Bu^t_2-2,6).[20]

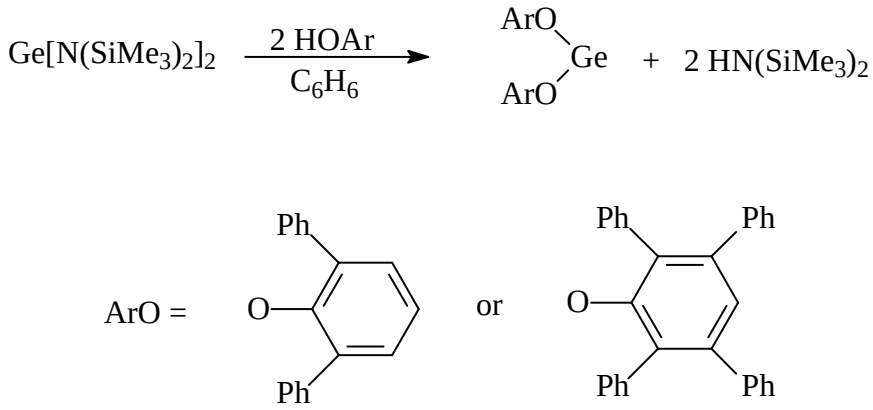

Scheme 1.26: Synthesis of $[Ge(OAr)_2]n$ (n = 1 and ArO = $OC_6H_3Ph_2$-2,6 or OC_6HPh_4-2,3,5,6).[19]

The germanium(II) amide $Ge[N(SiMe_3)_2]_2$ has also been observed to react with 3,3´-disubstituted binaphthols and the major calixarenes. In the former process, one of the two –OH groups of the binaphthol is converted to a silyl ether ($-OSiMe_3$) or a chelated binaphthoxide is generated. The product formation depends on the steric bulk of the 3,3´-substituents. Reactions of $Ge[N(SiMe_3)_2]_2$ with calixarenes generates complexes which contain germanium(II) sites bond to the phenolic oxygen atoms of the calixarene framework. These processes are the foci of the following chapters.

CHAPTER II

METAL-DEPENDENT REACTIONS OF BULKY METAL(II) AMIDES $M[N(SiMe_3)_2]_2$ WITH 3,3´-DISUBSTITUTED BINAPHTHOLS $(HO)_2C_{20}H_{10}(SiR_3)_2$-3,3´: SELECTIVE CONVERSION OF ONE EQUIVALENT –OH GROUP TO A SILYL ETHER $-OSiMe_3$

Introduction

The protection of a hydroxyl group is an important process in multistep organic synthesis, which allows for the manipulation of a compound and subsequent regeneration of the reactive –OH moiety. Of the various hydroxyl group protection schemes, the formation of silyl ethers is frequently used due to their ease of preparation, stability under a variety of conditions and the fact that the group can be cleaved to regenerate the –OH group in a facile manner by the fluoride ion as a result of the strength and stability of the Si-F bond.[21] Several preparative processes for silyl ethers exist, with the most common being the addition of trialkylsilyl groups. These groups include trimethylsilyl (TMS), triethylsilyl (TES), *tert*-butyldimethylsilyl (TBDMS), tri-*iso*-propylsilyl (TIPS), and *tert*-butyldiphenylsilyl (TBDPS).[22-33] Generally the protecting group is chosen on the basis of stability of the Si-O bond toward acids or bases. The stability of this bond has been found to be dependent on the identities of the alkyl groups bound to the silicon atom with

the Si-O bond of the -$OSiMe_3$ (OTMS) group being the weakest under both types of conditions.[23] One method of producing a trimethylsilyl ether involves the use ofhexamethyldisilazane $HN(SiMe_3)_2$ in the presence of various catalytic reagents. Molecular iodine[34], Me_3SiCl[35,36], amides or imides[37], copper(II) porphryins,[38] trimethylsilyl triflate,[39] tetrabutylammonium fluoride,[40] $ZnCl_2$,[41] metal chloride complexes,[42] tungstophosphoric acid,[43] silica chloride,[44] zirconium sulfophenyl phosphonate,[45] montmorillonite clay,[46] and zeolites[47] are some of the catalysts that can be used. Several examples of these interconversions are shown below in scheme 2.1.

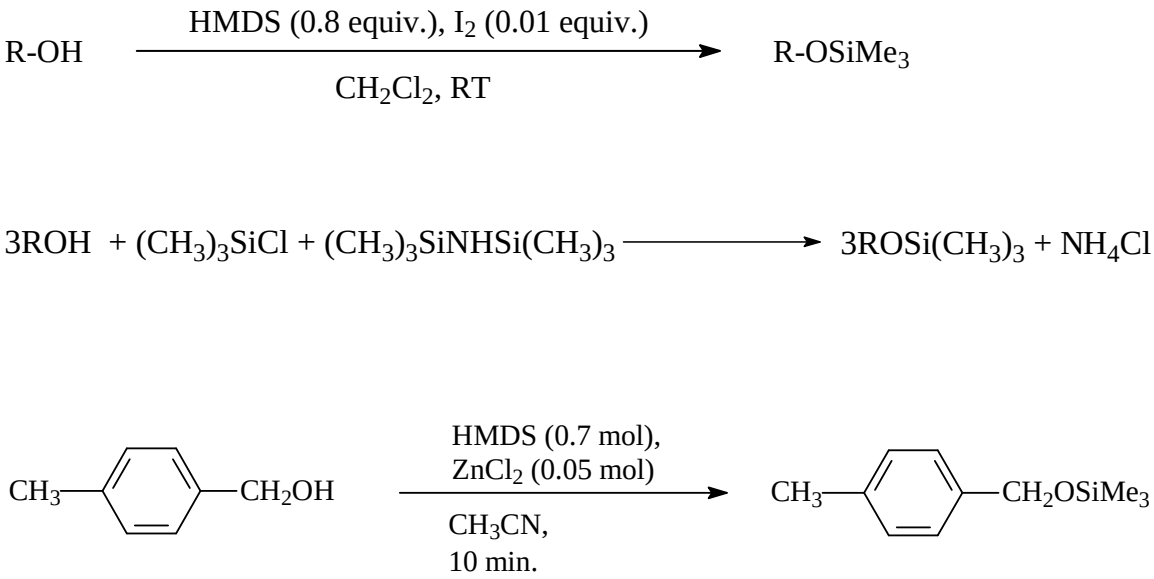

Scheme 2.1: Selected interconversions of alcohols to silyl ethers.

The selective silylation of one hydroxyl group in a molecule that contains two or more hydroxyl moieties is highly useful for synthetic applications. Many systems have been shown to afford silyl ether products,[40,42,43,46,48-52] such as 5,5-dimethyl-1,3-bis(trimethylsilyl)hydantoin or 5,5-dimethyl-1,3-bis(*tert*-butyldimethylsilyl)hydantoin,[40]

Ph_2PSiR_3 in the presence of diethyl azodicarboxylate and *p*-toluenesulfonate,[50] silyl methallylsulfinates,[51] and Et_3SiH in the presence of AuCl(xantphos),[52] which results in the preferential silylation of a primary alcohol in the presence of secondary and tertiary hydroxyls (some selective silylation reactions are shown below). Despite the synthetic relevance, however, regioselective silylation of one –OH group in the presence of other identical hydroxyl groups has yet to be reported.

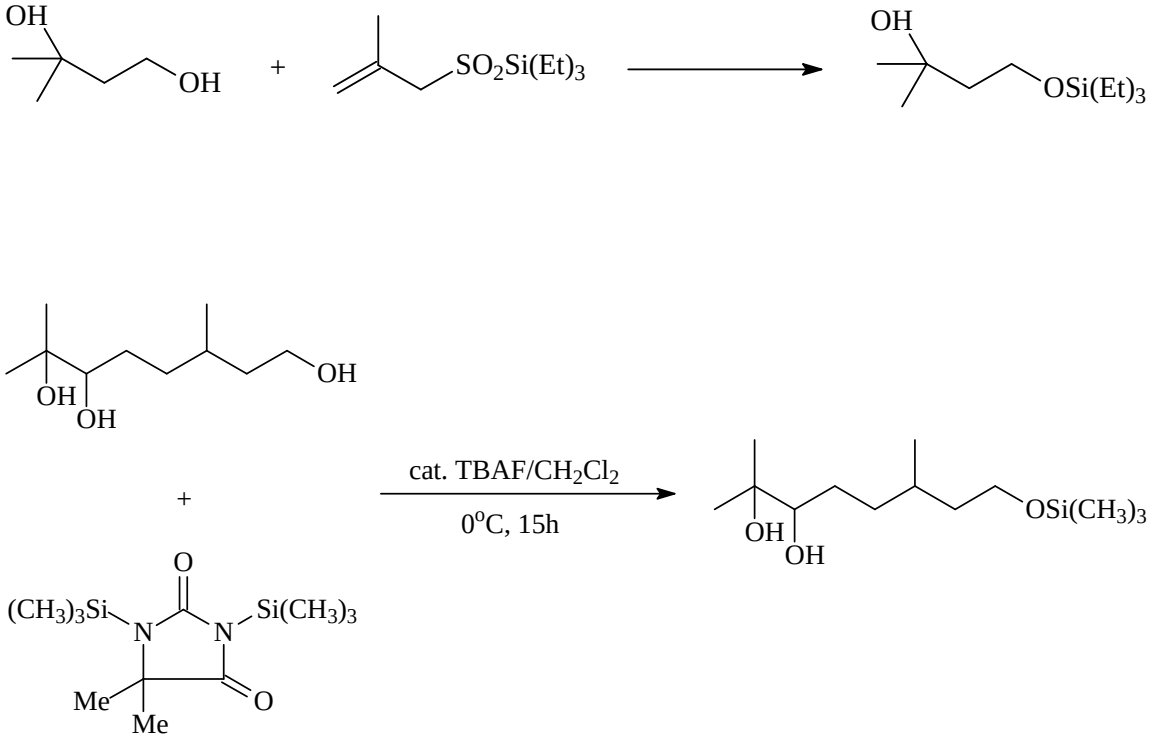

Scheme 2.2: Selective interconversions of alcohols to silyl ethers.

Bulky metal(II) amides $M[N(SiMe_3)_2]_2$ (M = Ge, Cd, Hg) have been shown to react with binapthols[53] and calixarenes[54] via a protonolysis reaction to yield several interesting products. The outcome of the reactions of metal(II) amides (M = Be, Mg, Ca,

Zn, Cd, Hg, Ge, Sn) with 3,3′-disubstituted binapthols was found to depend on the identity of the metal. The products obtained resulted from several different processes, including the cyclization of the Binaphthol substrate to furnish 1,7-disubstituted *peri*-xanthenoxanthanes, formation of polynuclear compounds having bridging binaphthoxide ligands,[55] complex formation,[55, 50] and the selective silylation of one of the two hydroxyl groups of the binaphthol.[55] The mercury(II) or cadmium(II) amides resulted in a cyclization reaction that generated previously unknown 1,7-disubstituted *peri*-xanthenoxanthanes,[53] while the germanium(II), beryllium(II), and zinc(II) amides produced mono-silylated binaphthol species. The results obtained clearly indicated that the identity of the metal not only affected the nature of the products obtained, but also the rate of the reaction.

Results and Discussion

The reaction between binapthol *(R)*-**1** and one equivalent of $M[N(SiMe_3)_2]_2$ (M = Be, Zn, Ge), was performed in a Schlenk tube in benzene and was heated at 85ºC for one hour **(Scheme 2.3)**. Upon completion of the reaction, and aqueous workup the monosilylated ether product *(R)*-**2** was isolated in greater than 85% yield in all three cases. The product was characterized by ^{1}H-NMR spectroscopy and high resolution mass spectrometry.

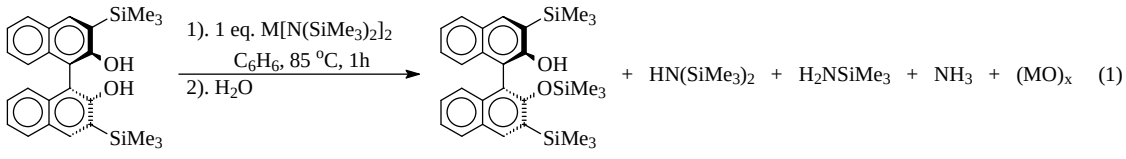

(*R*)-**1** (*R*)-**2**

M = Be, 91 %; M = Zn, 88 %; M = Ge, 89 %

Scheme 2.3: Reaction of *(R)*-**1** with 1 equivalent of $M[N(SiMe_3)_2]_2$ (M = Be, Zn, Ge)

Use of one equivalent of the metal(II) amide provided a product in which only one of the two equivalent hydroxyl groups was converted to a silyl ether, while the other group remained unchanged, thus leaving it available for use in subsequent reactions. The relative rates of these reactions were observed to be metal dependent, with the most rapid conversion of *(R)*-**1** to *(R)*-**2** taking place within 10 minutes when $Be[N(SiMe_3)_2]_2$ was employed as the silylation reagent. The use of $Zn[N(SiMe_3)_2]_2$ resulted in the conversion of *(R)*-**1** to *(R)*-**2** within 20 minutes. When the $Ge[N(SiMe_3)_2]_2$ reagent was used the rate of reaction was greatly diminished, requiring a reaction time of 40 minutes. Other silylation reactions were performed with various metal(II) amides to ascertain the dependence of the reaction rate on the identity of the metal. Because *(R)*-**1** and *(R)*-**2** exhibit distinct resonances for their respective hydroxyl protons, it was possible to use ^{1}H-NMR spectroscopy to probe the reaction of *(R)*-**1** with $M[N(SiMe_3)_2]_2 \cdot nTHF$ (M = Be, Zn, Ge, Sn, n = 0; M = Mg, Ca, n = 2), which allowed for the identification of several proposed intermediates in reaction pathway shown in **Scheme 2.4**.

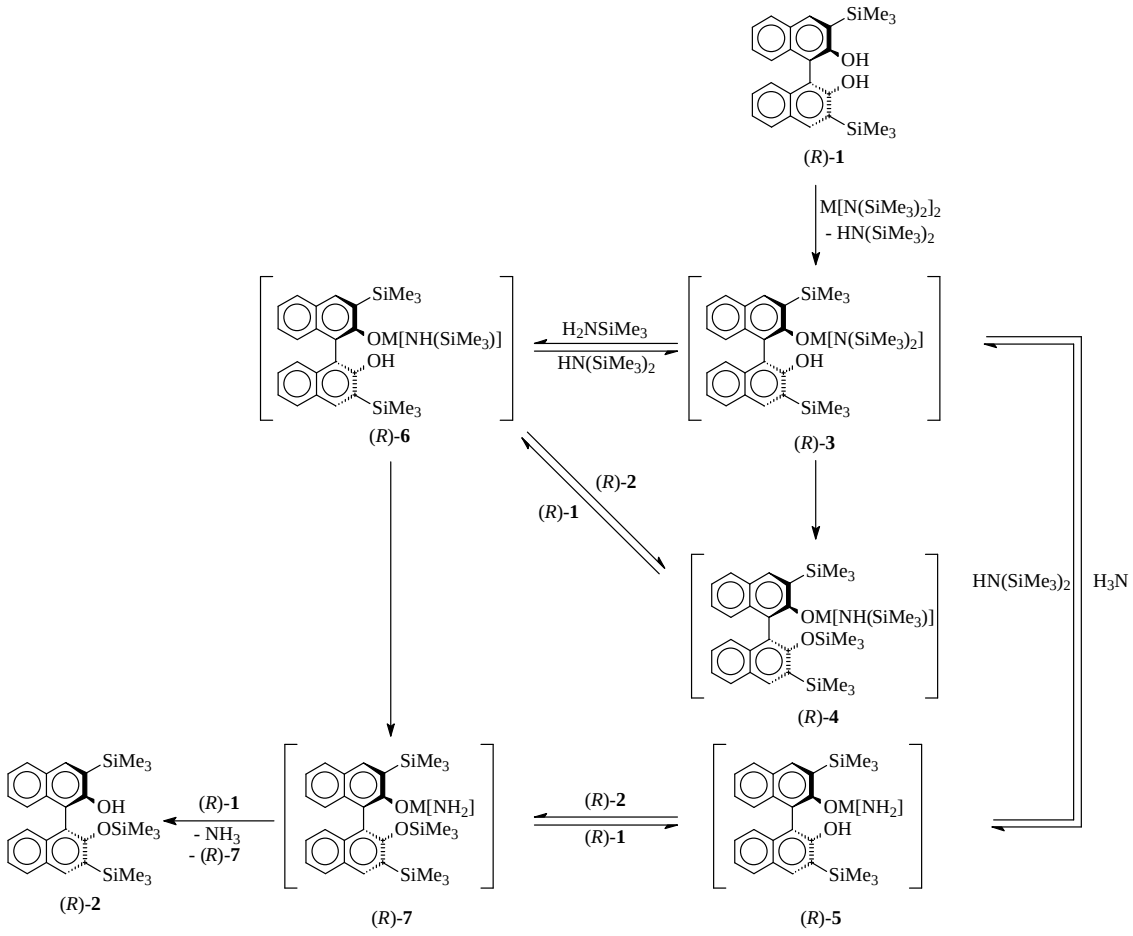

Scheme 2.4: Reaction of *(R)*-**1** with $M[N(SiMe_3)_2]_2$ (M = Be, Zn, Ge) proposed pathway.

The monosilylated intermediates were stable enough that they were detectable by ^{1}H-NMR spectroscopy even though they are present in a complex equilibrium with the reaction intermediates. All silylation reactions initially involve the loss of one –$N(SiMe_3)_2$ as the free hexamethyldisilazane ($HN(SiMe_3)_2$) . The metal of the remaining –$M[N(SiMe_3)_2]$ fragment is bound to one of the oxygen atoms of the binaphthol, leaving the –$SiMe_3$ groups in close enough proximity to permit the transfer of the trimethylsilyl group to the remaining hydroxyl.

^{1}H-NMR spectroscopy proved to be a useful tool for monitoring and evaluating the rates of silylation. A resonance was observed at a chemical shift of 5.02 ppm for the single hydroxyl of the monosilylated product *(R)*-**2**, where as a peak for the two equivalent hydroxyl groups of binapthol reactant *(R)*-**1** was observed at 4.87 ppm. In most cases a third resonance was seen at 5.30 ppm, which was attributed to the reaction intermediate *(R)*-**3**, the stability of which was observed to depend on the identity of the metal. **Table 2.1** illustrates the observed reaction times as well as the integrated intensities for each of the three hydroxyl resonances for a series of silylation reactions, while **Table 2.2** provides qualitative information about the range of reaction times and reactivity when varying the metal (II) amide employed. All data for **Tables 2.1- 2.2** were collected at 70ºC.

Table 2.1. ^{1}H NMR spectroscopic data for the reactions of $M[N(SiMe_3)_2]_2$ with *(R)*-**1**.

Entry	Equiv. $M[N(SiMe_3)_2]_2$	Time (min)	Intensity of Resonance for *(R)*-**2**	Intensity of Resonance for *(R)*-**1**	Intensity of Resonance for *(R)*-**3**
1	0.5 Be	5	93.5 %	6.5 %	0 %
		10	100 %	0 %	0 %
2	1.0 Be	5	69.5 %	30.5 %	0 %
		10	100 %	0 %	0 %
3	0.5 Mg [a]	5	7.5 %	92.5 %	< 1 %
		55	30 %	61.5 %	8.5 %
		155	33.5 %	58 %	8.5 %
4	1.0 Mg [a]	5	7.5 %	88 %	4.5 %
		55	19 %	72 %	9 %
		105	41.5 %	41.5 %	17 %
		190	72 %	7.5 %	20.5 %
5	0.5 Ca [a]	5	0 %	81 %	19 %
		155	0 %	83 %	17 %
6	0.5 Zn	5	10 %	84.5 %	5.5 %
		10	12 %	82 %	6 %
		15	23 %	75 %	2 %
		20	27 %	72 %	1 %
		40	35 %	65 %	0 %
7	1.0 Zn	5	75 %	0 %	25 %
		10	91 %	0 %	9 %
		15	97.5 %	0 %	2.5 %
		20	100 %	0 %	0 %
8	0.5 Ge	5	7.5 %	86.5 %	6 %
		10	7.5 %	86.5 %	6 %
		40	11 %	89 %	< 1 %
9	1.0 Ge	5	3.5 %	95 %	1.5 % [b]
		10	20.5 %	78 %	1.5 % [b]
		15	69.5 %	30.5 %	0 %
		20	100 %	0 %	0 %
10	0.5 Sn [a]	5	5 %	95 %	0 %
		10	6.5 %	93 %	0.5 %
		15	8 %	91 %	1 %
		45	11.5 %	87 %	1.5 %
		100	14.5 %	85.5 %	0 %

[a] Silylation and formation of a polynuclear species both occur.

Table 2.2: Results of silylation reactions using various metal (II) amides.

Metal	Reaction Completion Time (Min)
$Be[N(SiMe_3)_2]_2$	<5
$Zn[N(SiMe_3)_2)_2$	4-7
$Ge[N(SiMe_3)_2]_2$	20-25
$Mg[N(SiMe_3)_2]_2 \cdot 2THF$[a]	4^+ (hours)
$Sn[N(SiMe_3)_2]_2$[a]	12(hours)
$Ca[N(SiMe_3)_2]_2 \cdot 2THF$[b]	Unexpected Results
$Pb[N(SiMe_3)_2]_2$[b]	Unexpected Results
$Hg[N(SiMe_3)_2]_2$[c]	Unexpected Results
$Cd[N(SiMe_3)_2]_2$[c]	Unexpected Results

[a] Silylation and formation of a polynuclear species both occur

[b] Formation of polynuclear species exclusively

[c] Formation of cyclized species

These data clearly indicate a metal dependence on the rate of reaction. In both entries 1 and 2, the reaction of 0.5 and 1 equivalents of $Be[N(SiMe_3)_2]_2$ (respectively) with binaphthol *(R)*-**1**, produced no observable intermediate and the reaction reached completion within 10 minutes. The ^{1}H-NMR spectra of these reaction mixtures indicates that *(R)*-**1** is completely consumed in the reaction. Three additional resonances attributed to the formation of the monsilylated product *(R)*-**2** were also observed. Two of these resonances at δ 0.51 and 0.48 ppm arise from two distinct $–SiMe_3$ groups in the 3- and 3′-positions that are no longer magnetically equivalent after silylation. The third resonance is a result of the presence of the $-OSiMe_3$ group and was observed at δ -0.30 ppm.

To further investigate the reaction pathway, $Be[N(SiMe_3)_2]_2$ was treated with 1, 2, 3 and 4 molar equivalents of *(R)*-**1**, by adding successive equivalents of *(R)*-**1** to the NMR tube throughout the experiment. Using ^{9}Be NMR it was determined that all four $–SiMe_3$ groups present on the bisamide are available for use in product formation. These reactions also provided evidence for the formation of the reaction intermediates *(R)*-**4** and *(R)*-**7** **(Figure 2.1)**. As the ratio of $Be[N(SiMe_3)_2]_2$ to *(R)*-**1** was decreased, as sequential equivalents of *(R)*-**1** were added to the NMR tube, a change in the relative intensities of the resonances for the intermediate species was observed. It was expected that the intensity of the peak that corresponds to *(R)*-**4** would be diminished as compared to the resonance corresponding to *(R)*-**7** when the ratio of *(R)*-**1** to $Be[N(SiMe_3)_2]_2$ was increased because fewer $–SiMe_3$ groups are available for transfer to the adjacent –OH moiety in the binaphthol. The limited availability of the $–SiMe_3$ groups eventually results in the exclusive generation of the $–OM[NH_2]$ moiety of *(R)*-**7** rather than the production of the $–OM[NH(SiMe_3)]$ moiety of *(R)*-**4** as the ratio of $Be[N(SiMe_3)_2]_2$ to

(R)-**1** approaches 1:4. On the basis of these assumptions, the ^{9}Be chemical shifts for intermediates *(R)*-**4** and *(R)*-**7** were assigned by observing the relative intensity change of the two peaks as the stoichiometric ratio was varied.

The reaction of $Be[N(SiMe_3)_2]_2$ with 1 equivalent of *(R)*-**1** in C_6D_6 at 70 ^{o}C resulted in the appearance of two main features at δ 10.0 and 1.8 ppm in the ^{9}Be NMR spectrum. Both of these resonances were shifted from the peak of the starting bisamide which is observed at δ 9.4 ppm.[56,57] It was observed that the intensity of the peak at δ 10.0 ppm was approximately 1.5 times greater in intensity than the resonance at δ 1.8 ppm, leading to the assignment of these resonances to the intermediates *(R)*-**4** and *(R)*-**7** **(**respectively). In both the ^{1}H-NMR and ^{9}Be NMR spectra, no additional changes in the appearance of the spectra were observed after 1 hour. The rate of reaction indicates that all of the $Be[N(SiMe_3)_2]_2$ is consumed quickly and is supported by the fact that neither a resonance for intermediate *(R)*-**3** or the starting amide is observed in the ^{9}Be NMR spectrum. The corresponding ^{1}H-NMR spectrum for the reaction between 1 equivalent of $Be[N(SiMe_3)_2]_2$ and one equivalent of *(R)*-**1** provided further support for the proposed pathway, since seven peaks located in the chemical shift range of δ 0.4 to -0.3 ppm were observed. These peaks were attributed to the seven TMS groups present on the two intermediates *(R)*-**4** and *(R)*-**7**. Adding a second equivalent of *(R)*-**1** to the NMR tube resulted in spectra with the same resonances in the ^{9}Be NMR as shown below. However, the resonance attributed to *(R)*-**4** found at δ 10.0 ppm was now approximately half the intensity of that for the resonance of *(R)*-**7** found at δ 1.8 ppm. This indicated that the intermediate *(R)*-**7** was now present in greater abundance, as expected from the reaction stoichiometry.

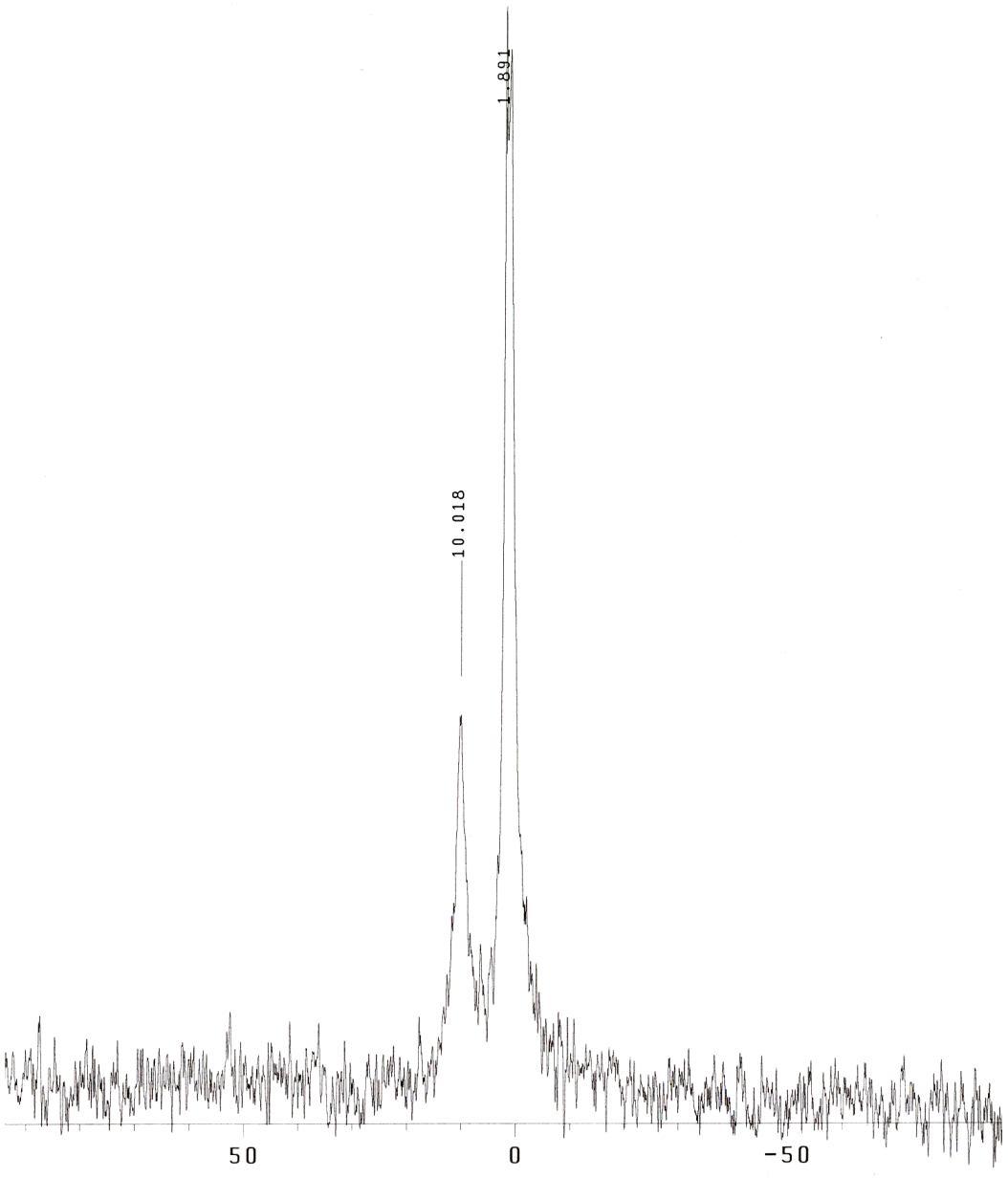

Figure 2.1: ^{9}Be NMR with 2 equivalents of *(R)*-1 to show intermediate peaks

The reaction of $Be[N(SiMe_3)_2]_2$ with four equivalents of *(R)*-**1** yielded a product with a spectrum that contained a single resonance at δ 1.8 ppm which corresponds to the intermediate *(R)*-**7**. This indicates that intermediate *(R)*-**7** remains in solution along with the product *(R)*-**2**; *(R)*-**7** subsequently results in product formation through the loss of NH_3, which is generated via the transfer of a proton from *(R)*-**1** to *(R)*-**7**. When the reaction is conducted on preparative scale all of intermediate *(R)*-**7** is converted product during aqueous workup. The quantity of the products formed and the intensities of the resonances in the NMR spectra indicate that all four $–SiMe_3$ groups are available for transfer to one of the hydroxyl groups of *(R)*-**1**, which occurs via cleavage of the nitrogen-silicon bond during the protonolysis reaction, resulting in the formation of the silylated product *(R)*-**2** as well as hexamethyldisilizane and ammonia. Precedence for reactivity of this nature has been observed in the reaction of $Be[N(SiMe_3)_2]_2$ with HSPh, which also produces NH_3.[58] The ^{1}H-NMR spectra **(Figure 2.2)** corresponding to the reaction of $Be[N(SiMe_3)_2]_2$ with 4 equivalents of *(R)*-**1** exhibits three non equivalent $–SiMe_3$ peaks for *(R)*-**7** at 0.43, 0.04 and -0.35 ppm as well as two resonances at 0.095 and 0.07 ppm. The resonance at 0.095 ppm is of weaker intensity than the peak at 0.07 and is attributed to free $HN(SiMe_3)_2$, where as the resonance at 0.07 ppm is assigned to H_2NSiMe_3.[59] The assignment of the feature at δ 0.07 ppm to H_2NSiMe_3 is tentative, however, since this species has been observed to undergo disproportionation to $HN(SiMe_3)_2$ and NH_3 at temperatures greater than room temperature.[59]

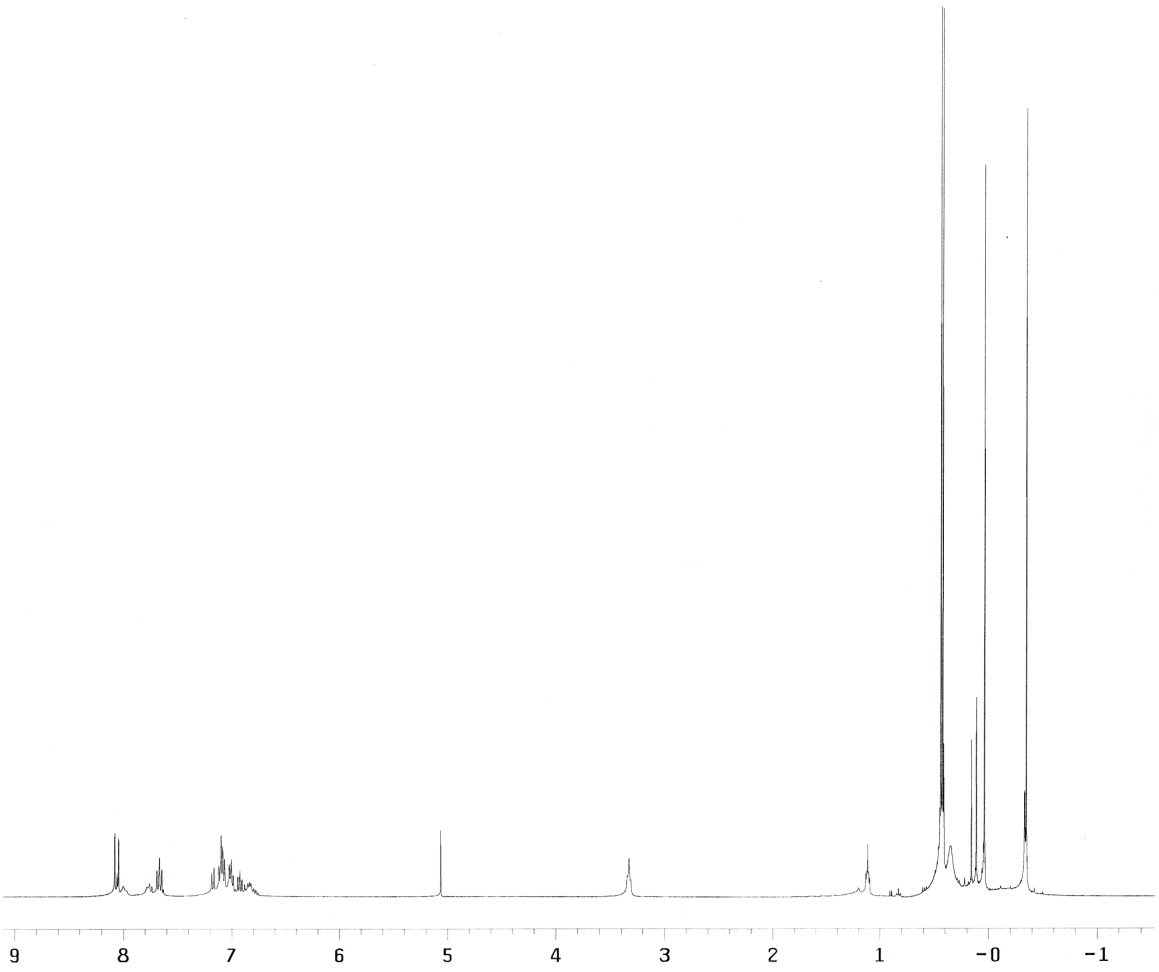

Figure 2.2: ^{1}H-NMR of the reaction product between TMS binol and 4 equivalents of *(R)*-1.

The reaction of the magnesium and calcium amides $M[N(SiMe_3)_2]_2 \cdot 2THF$ (M = Mg, Ca) with *(R)*-**1** occurred at a significantly slower rate than that observed for the beryllium amide as illustrated by entries 3-5 in Table 2.1. Reaction of *(R)*-**1** with 0.5 equivalents of $Mg[N(SiMe_3)_2]_2 \cdot 2THF$ resulted in only minimal product formation (35%) after 55 minutes as shown by ^{1}H-NMR. No change was observed in the spectrum after 24 hours, with the resonance at δ 5.30 ppm for the intermediate *(R)*-**3** being still visible in the ^{1}H-NMR spectrum. Similarly, the reaction using 1.0 equivalent of $Mg[N(SiMe_3)_2]_2 \cdot 2THF$ converts more of *(R)*-**1** to *(R)*-**2**, but also produces a significantly greater amount of *(R)*-**3**. Reacting 0.5 equivalents of $Ca[N(SiMe_3)_2]_2 \cdot 2THF$ with *(R)*-**1** resulted in no formation of *(R)*-**2**; however significant amounts of *(R)*-**3** were generated as shown by ^{1}H-NMR spectroscopy and were found to be stable in solution for long periods of time. In each of these three reactions a gelatinous material was present in the NMR tube. It is likely that the compound observed is a polynuclear metal complex that contains bridging binaphthoxide ligands. Attempts to react *(R)*-**1** with 1.0 equivalents of $Ca[N(SiMe_3)_2]_2 \cdot 2THF$ produced the gelatinous material relatively quickly such that a satisfactory NMR could not be obtained.

The formation of metal complexes having bridging binaphthoxide ligands has been reported for other large metals with ionic radii and electronegativities similar to that of Ca^{2+} (1.06Å and 1.00 (Pauling) respectively).[60,61-68] One example of such a complex results from the reaction of $La[N(SiMe_3)_2]_3$ with 3,3′-bis(diphenylphosphinoylmethyl)-1,1′-bi-2,2′-naphthol, which furnishes a dinuclear lanthanum complex incorporating three bridging binaphthoxide ligands.[68] (**Scheme 2.5** shown below)

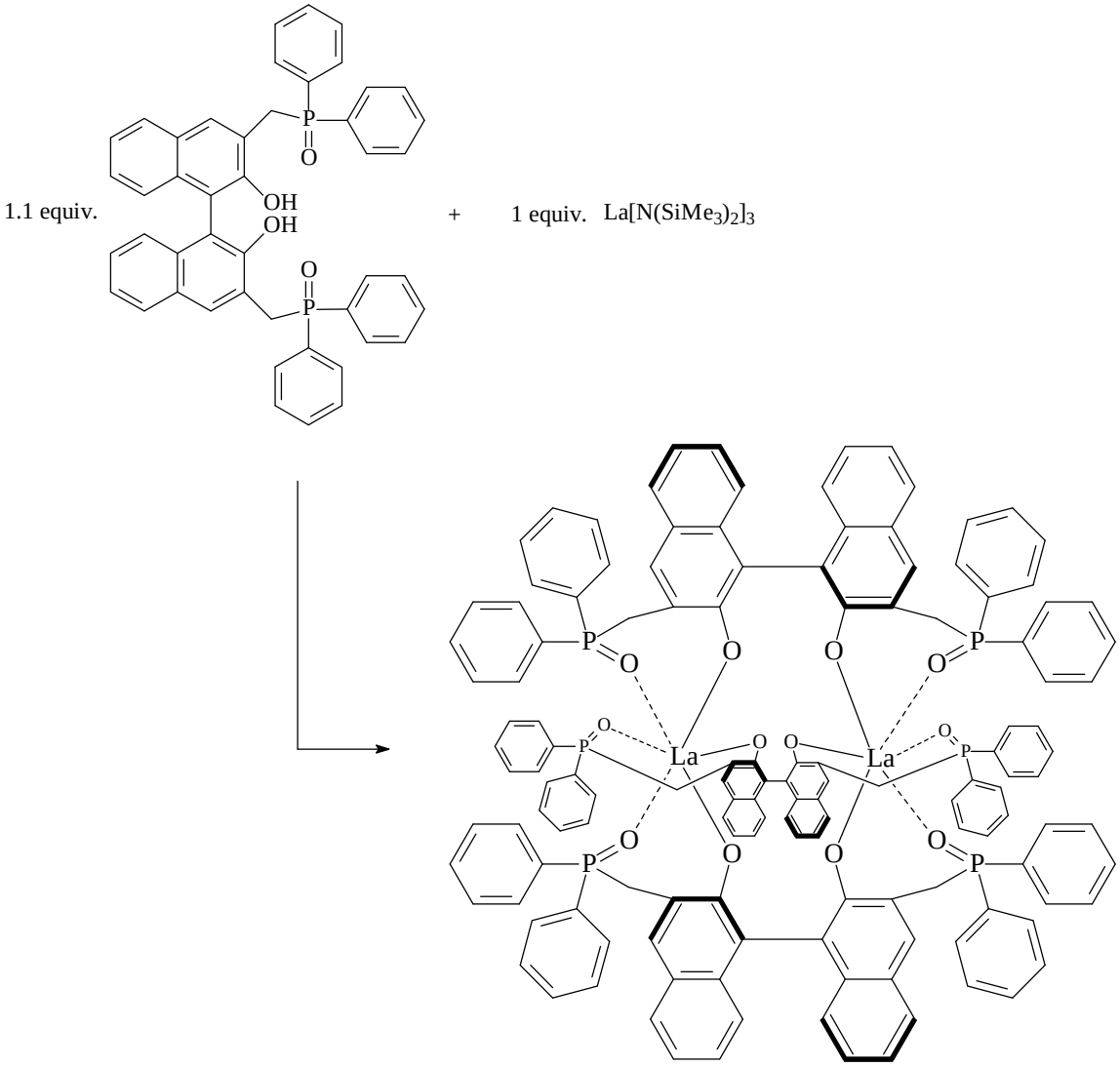

Scheme 2.5: Reaction of $Ln[N(SiMe_3)_2]_3$ with 1.1 equivalents of 3,3´-bis(diphenylphosphinoylmethyl)-1,1´-bi-2,2´-naphthol.

The generation of a related polynuclear complex may also be occurring in the reactions with the magnesium amide. However, this has not been confirmed since x-ray quality crystals of the product have not yet been obtained.

Based on the results observed in the magnesium and calcium experiments, it was determined that the stability of the intermediate *(R)*-**3** is an important factor in the outcome of the reaction, either resulting in the generation of a polynuclear complex with bridging binaphthoxide ligands (reaction **Scheme 2.6** shown below), or formation of the mono silylated product *(R)*-**2**. If the intermediate *(R)*-**3** was consumed rapidly, the reaction results in conversion of *(R)*-**3** to the other intermediates *(R)*-**4** and *(R)*-**7,** ultimately leading to the formation of the major product *(R)*-**2**. If the intermediate *(R)*-**3** remains in solution for extended periods of time, however, polynuclear complexes with bridging binapthoxide ligands result from the outcome of the reaction.

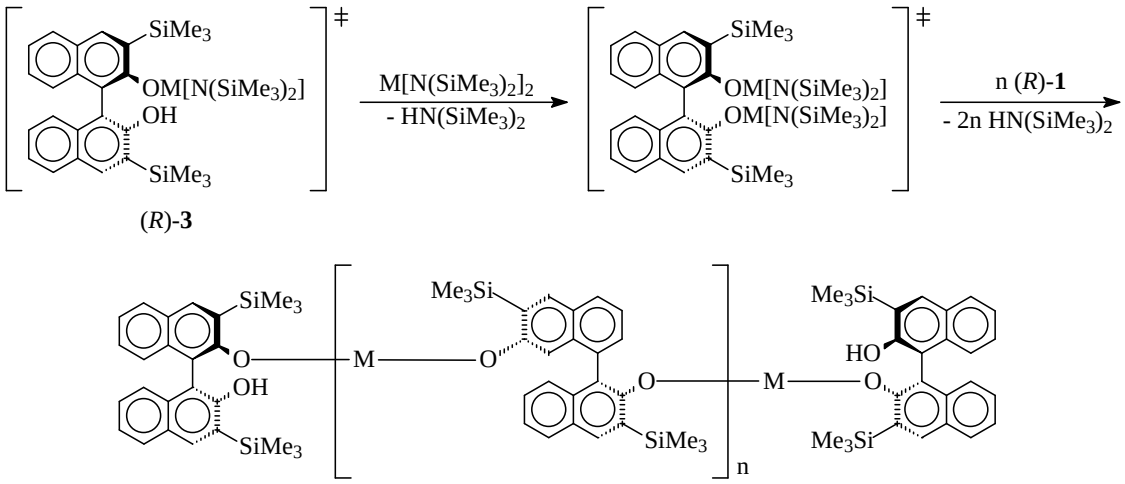

Scheme 2.6: Reaction of *(R)*-**1** with $M[N(SiMe_3)_2]_2$ (M = Ca, Mg).

There are three main factors that contribute to the stability of *(R)*-**3,** and hence the formation of the polynuclear complex in the cases of both magnesium and calcium bisamide. The first is the strength of the nitrogen-silicon bond. As the strength of this interaction increases, so does the stability of intermediate *(R)*-**3**, since the $–SiMe_3$ groups

are tightly bound to the nitrogen and thus the propensity for their transfer to the neighboring hydroxyl oxygen atom is inhibited. The ultimate effect of a strong Si-N bond is the impedance of the formation of the other intermediates *(R)*-**4** and *(R)*-**7** that are formed leading to the generation of *(R)*-**2**. Two additional interrelated factors include the strength of the metal-nitrogen bond and the strength of the metal-oxygen bond. If the metal-nitrogen bond strength is weaker than that of the metal-oxygen bond, the reaction will proceed towards the formation of the polynuclear complex via interaction of the intermediate *(R)*-**3** with an additional molecule of starting material *(R)*-**1** (**Scheme 2**) resulting in the loss of hexamethydisilazane $HN(SiMe_3)_2$. This can be used to rationalize why reactions involving $Ca[N(SiMe_3)_2]_2 \cdot 2THF$ formed the polynuclear complexes more readily than those involving the $Mg[N(SiMe_3)_2]_2 \cdot 2THF$ species. The metal-nitrogen bond strength is expected to decrease down a group, resulting in an increase in the nitrogen-silicon bond strength, which is consistent with the experimental data. Finally there is also a correlation with the absolute hardness of the metal centers[69] which suggests a stronger M-O bond would be formed with beryllium versus that with magnesium, calcium, and the other metals employed as a result of enhanced orbital overlap. A strong metal-oxygen bond coupled with a strong metal-nitrogen bond as in the beryllium case results in a weaker nitrogen-silicon bond, which allows for the migration of the trimethysilyl group to the adjacent oxygen atom of the remaining hydroxyl moiety. This results in a reduction of the stability of the intermediate *(R)*-**3**, and resulting in the formation of product *(R)*-**2** as opposed to the formation of the polynuclear complex.

Reactions of the group 12 metal(II) amides $M[N(SiMe_3)_2]_2$ (M=Zn, Cd, Hg) also were found to be metal dependent. Of these three species, only the zinc derivative

generated the silylated product *(R)*-**2** from *(R)*-**1**. The cadmium(II) and mercury(II) species instead result in an intramolecular electrophilic aromatic substitution reaction to furnish either a pentacyclic species or 1,7-bis(trimethylsilyl)*peri*-xanthenoxanthane depending on the reaction stoichiometry employed.[53] The reaction of $Zn[N(SiMe_3)_2]_2$ with *(R)*-**1** proceeds cleanly to provide the monosilylated binaphthol *(R)*-**2**. The success of this reaction is particularly advantageous because $Zn[N(SiMe_3)_2]_2$ is commercially available and is not highly air or moisture sensitive, which allows for its use in synthesis under a slow purge of nitrogen as rather than requiring the use of rigorous air-sensitive techniques. Thus, the ease of this reaction makes it a useful tool for organic synthesis.

The reactions of $Zn[N(SiMe_3)_2]_2$ with *(R)*-**1** were monitored by ^{1}H-NMR spectroscopy, and the experimental data is shown in entries 6 and 7 of **Table 2.1**. The reaction of 0.5 equivalents of $Zn[N(SiMe_3)_2]_2$ with *(R)*-**1** only yielded 35% of product *(R)*-**2** after 40 minutes. The hydroxyl resonance attributed to intermediate *(R)*-**3** was observed initially, but was found to be absent after a reaction time of 40 minutes. The peak at δ 0.20 ppm corresponding to the protons of $Zn[N(SiMe_3)_2]_2$ was also absent after 40 minutes; however, the two resonances at δ 0.090 and 0.48 ppm corresponding to free hexamethyldisilazane and unreacted *(R)*-**1** were still present after the reaction had reached completion (a series of ^{1}H-NMR spectra are shown in **Figure 2.3**). These data indicate that although all of the $Zn[N(SiMe_3)_2]_2$ had been completely consumed, intermediates species remain in addition to the formed monosilylated product *(R)*-**2** and free hexamethyldisilazane.

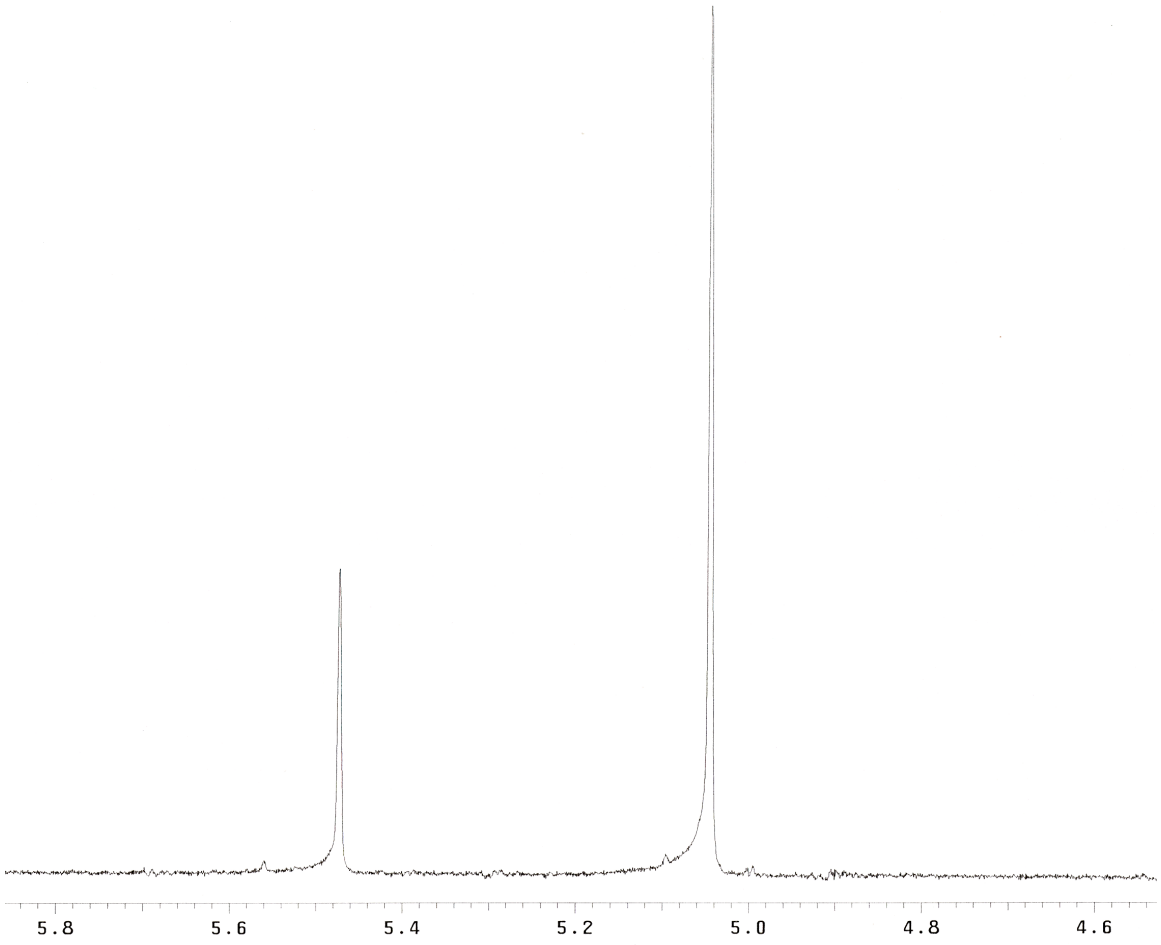

a)

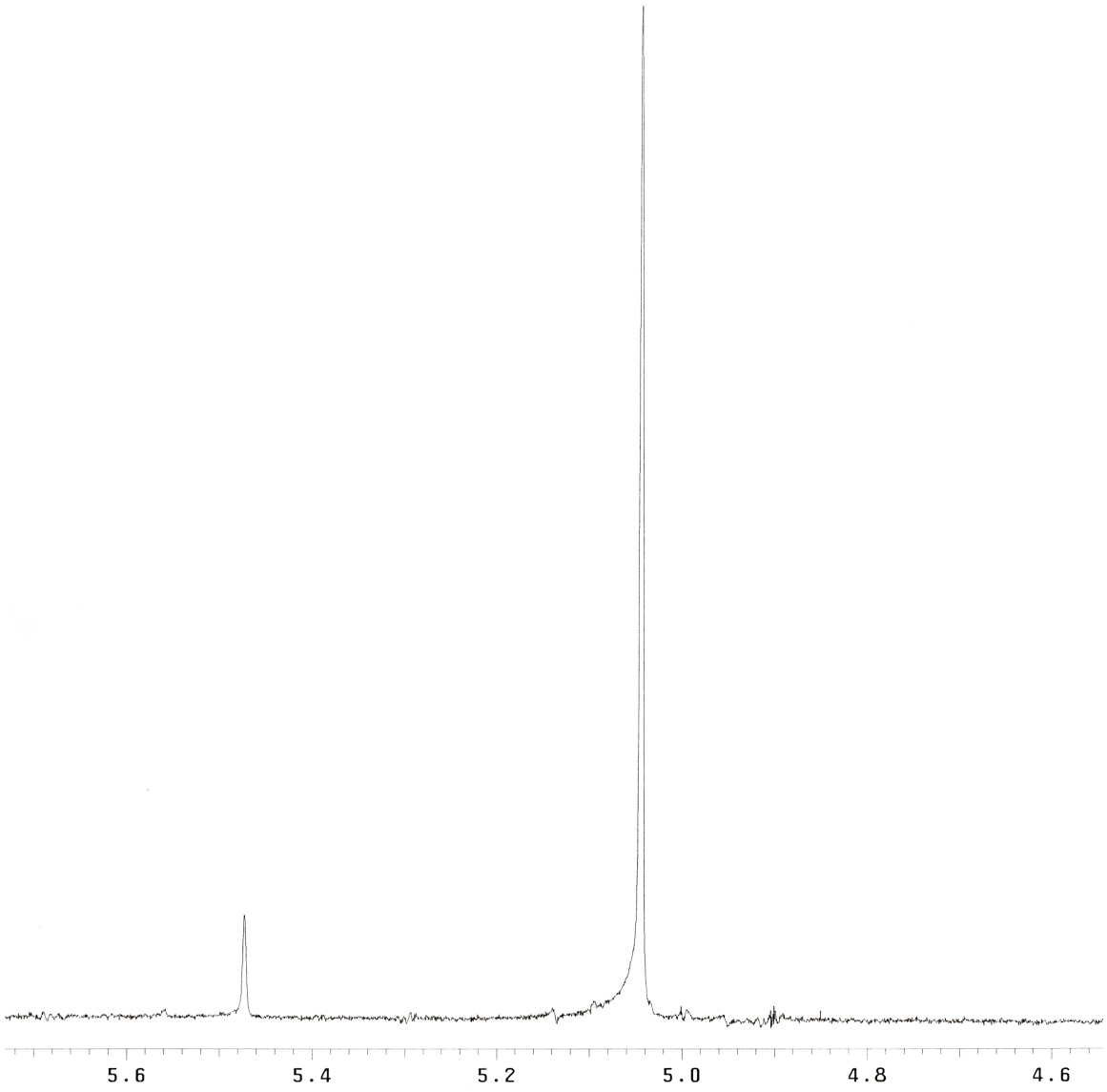

b)

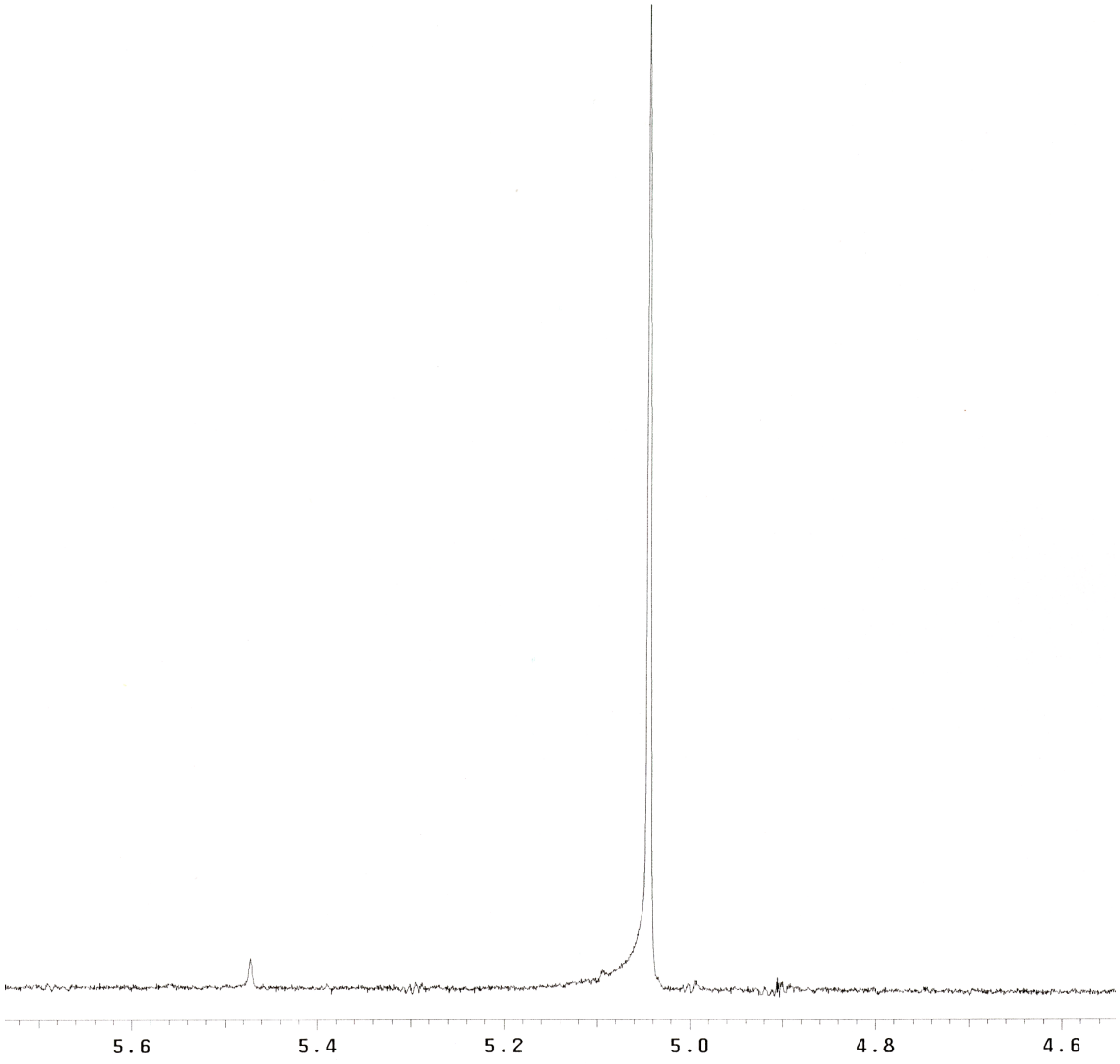

c)

Figure 2.3: A series of ^{1}H-NMR (hydroxyl proton region) with first half of $Zn[N(SiMe_3)_2]_2$ to show reaction rate. Spectrum *a)* was recorded within the first 5 minutes of reaction time. Subsequent spectra were recorded at 10 minute intervals.

The addition of a second 0.5 equivalent of $Zn[N(SiMe_3)_2]_2$ to the NMR tube resulted in the complete consumption of *(R)*-**1** and the formation of both *(R)*-**2** and *(R)*-**3** in a ratio of 96:4 after 5 minutes. After an additional 2 minutes of reaction time the resonance for the intermediate *(R)*-**3** had completely disappeared, and only the resonance for *(R)*-**2** and $HN(SiMe_3)_2$ remained. In a separate experiment, *(R)*-**1** was treated with 1 equivalent of $Zn[N(SiMe_3)_2]_2$ directly. The ^{1}H-NMR spectrum for this reaction exhibited peaks for *(R)*-**2** and *(R)*-**3** after 5 minutes, but the resonances for *(R)*-**1** were absent at this time **(Figure 2.4)**. After a reaction time of 20 minutes, only the resonance for *(R)*-**2** was present. These data suggest that treating $Zn[N(SiMe_3)_2]_2$ with *(R)*-**1** in a 1:1 ratio results in complete conversion to the silylated product *(R)*-**2**. Therefore, it can be concluded that the reactivity of $Zn[N(SiMe_3)_2]_2$ is similar to that of $Be[N(SiMe_3)_2]_2$, although the absence of a resonance for *(R)*-**3** in the reaction with the beryllium amide indicates that the reaction involving the Zn amide proceeds at a slightly slower rate.

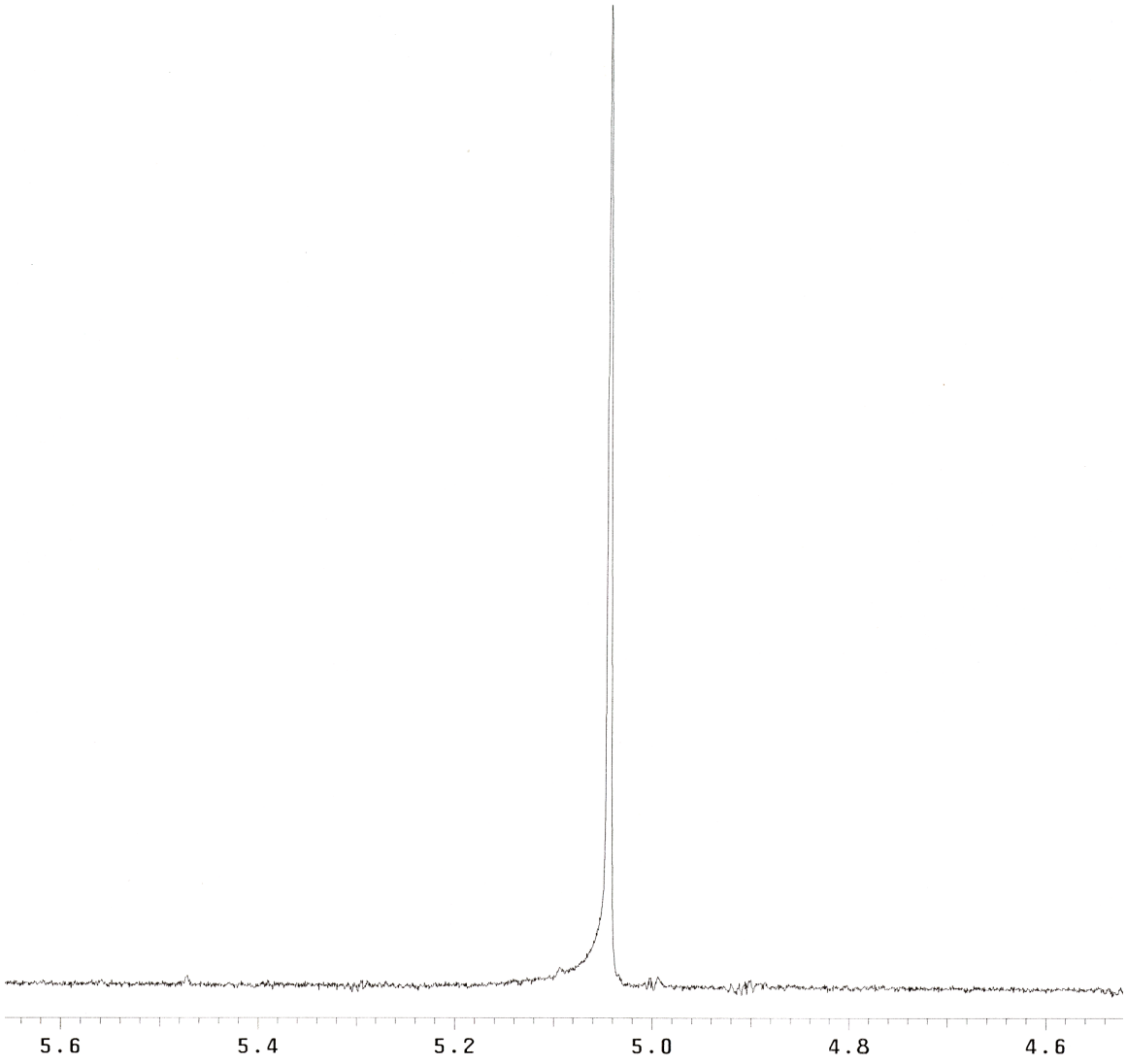

d)

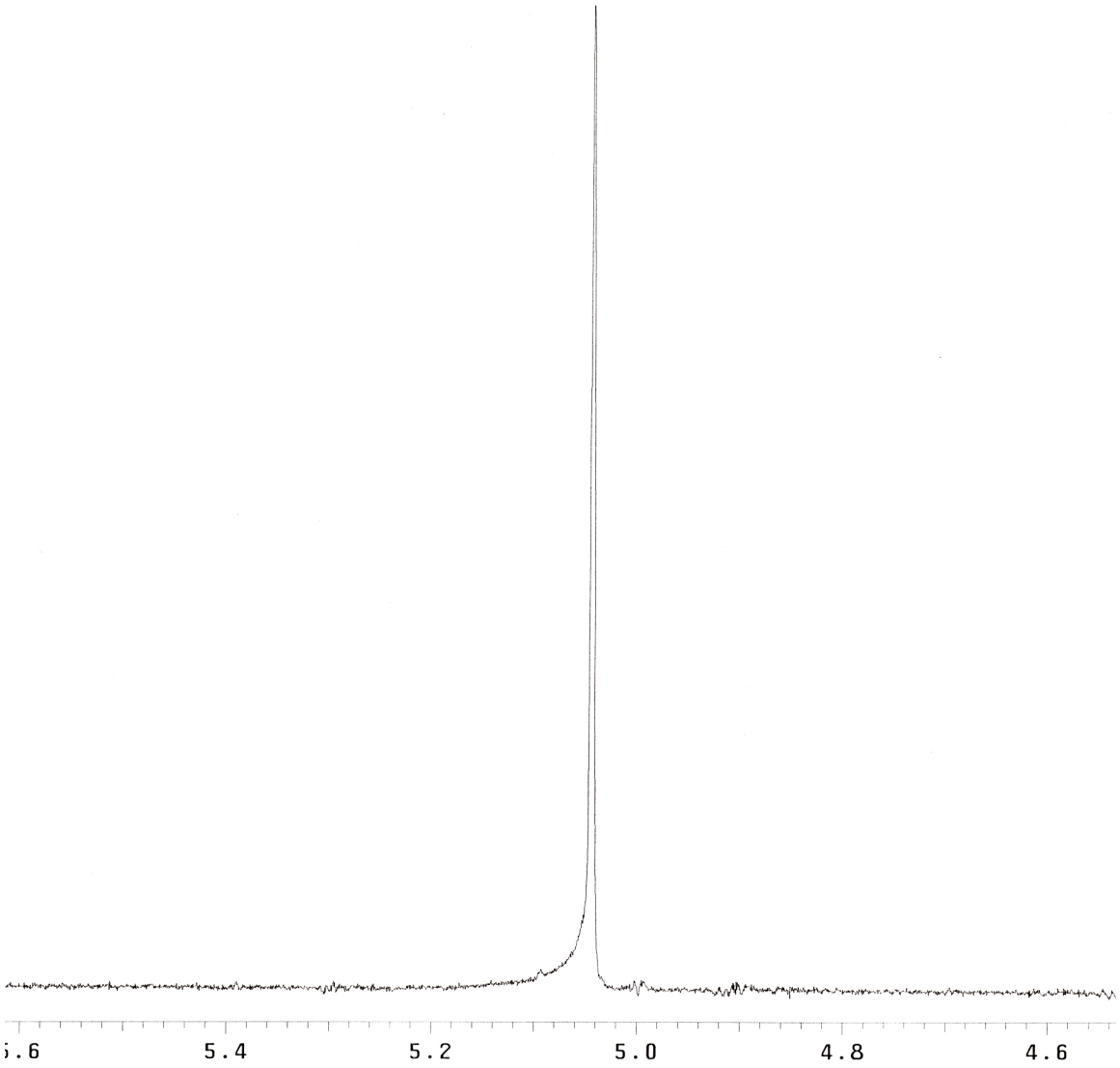

e)

Figure 2.4: Completion of ^{1}H-NMR series (hydroxyl proton region) after second half of $Zn[N(SiMe_3)_2]_2$ was added. Spectra *d* and *e* were recorded at 5 minute intervals.

The group 14 metal amides $Ge[N(SiMe_3)_2]_2$ and $Sn[N(SiMe_3)_2]_2$ have also been employed for the conversion of *(R)*-**1** to *(R)*-**2**. When 0.5 equivalents of $Sn[N(SiMe_3)_2]_2$ were reacted with *(R)*-**1,** only a 14.5% conversion to *(R)*-**2** was observed (**Table 2.1**, entry 10). Reacting 1.0 equivalent of $Sn[N(SiMe_3)_2]_2$ with *(R)*-**1** led to the formation of a viscous material consistent with the aforementioned polynuclear binaphthoxide complexes observed in the reactions of the magnesium and calcium amides. However, the germanium species was found to react in a similar manner to that of the beryllium and zinc amides. The treatment of *(R)*-**1** with 0.5 molar equivalents of $Ge[N(SiMe_3)_2]_2$ generated 11% of *(R)*-**2** after 40 minutes. The generation and subsequent consumption of *(R)*-**3** was also observed as the reaction proceeded. Adding a second equivalent of the Ge amide to the NMR tube resulted in the conversion of the remaining *(R)*-**1** to the product *(R)*-**2**, and the signal at δ 5.47 ppm for the intermediate *(R)*-**3** was no longer present.

Reaction of *(R)*-**1** with 1.0 equivalent of $Ge[N(SiMe_3)_2]_2$ resulted in the complete conversion of *(R)*-**1** to the product *(R)*-**2** within 20 minutes. During the reaction, the resonance for intermediate *(R)*-**3** was visible at δ 5.47 ppm for the first 12 minutes, after which time it was absent **(^{1}H-NMR comparison, Figure 2.5)**. A second downfield resonance was also visible during this time at δ 5.22 ppm, which was assigned to the second hydroxyl-containing intermediate species *(R)*-**6**. This species appears to be only transiently stable, and rapidly undergoes a silyl group transfer to form *(R)*-**7**. It was also found that the intensities of intermediates *(R)*-**3** and *(R)*-**6** decreased at the same rate and subsequently disappeared from the ^{1}H-NMR spectrum at the same time.

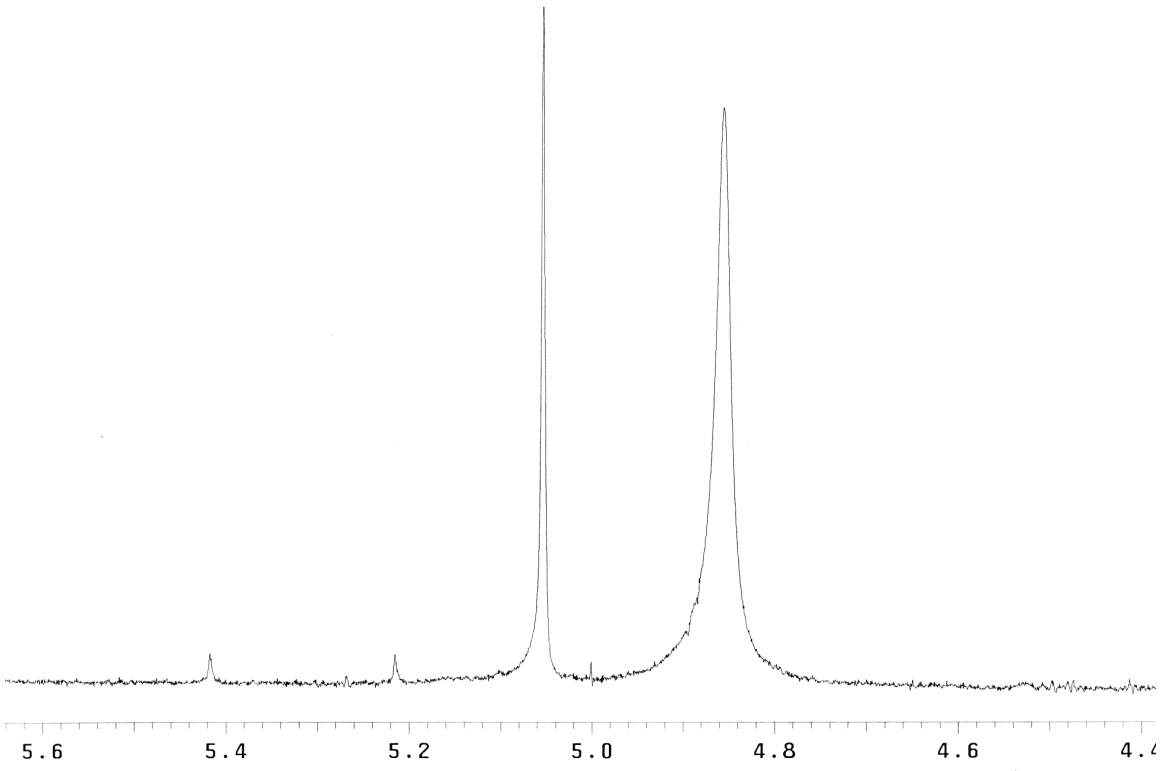

a)

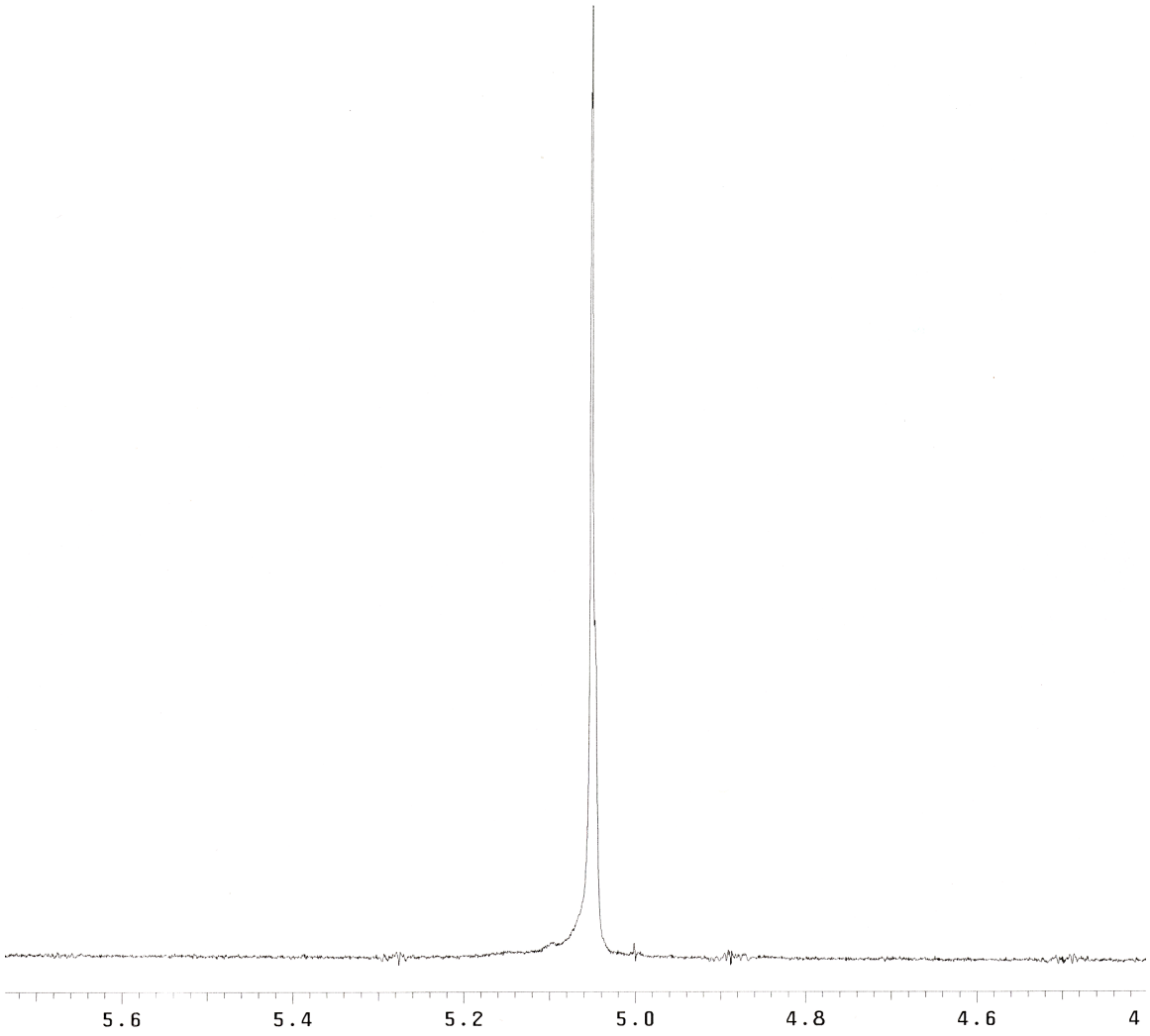

b)

Figure 2.5: ^{1}H-NMR comparison between a spectrum showing intermediate peaks during the reaction *(a)* and one showing no visible intermediates *(b)* upon reaction completion.

The reaction of metal(II) amides (M= Be, Zn, Ge) also occurs with the more sterically encumbered binaphthol *(S)*-3-3´-bis(dimethylphenylsilyl)-1,1´-bi-2,2´-naphthol *(S)*-**8**. The germanium species reacts with this substrate generating both *(S)*-**9** and a chelated germylene product *(S)*-**10** in 27% and 48% yields (respectively) when $Ge[N(SiMe_3)_2]_2$ is reacted with *(S)*-**8** in a 2:1 ratio. A similar outcome was not observed for the beryllium and zinc amides where only *(S)*-**9** was formed in the reaction. The formation of *(S)*-**10** results from the protonolysis reaction between $Ge[N(SiMe_3)_2]_2$ and *(S)*-**8** as shown in **Scheme 2.7**. Similar reactivity of the germanium(II) amide, but not for the other metal bisamides, has been reported for the reaction of $Ge[N(SiMe_3)_2]_2$ with *(R)*-**1** in a 2:1 molar ratio which resulted in the formation of the product *(R)*-**2**, as well as the bis (binaphthoxide) germylene complex (*(R,R)*-**11**) [70] as shown below in **Equation 2.8**.

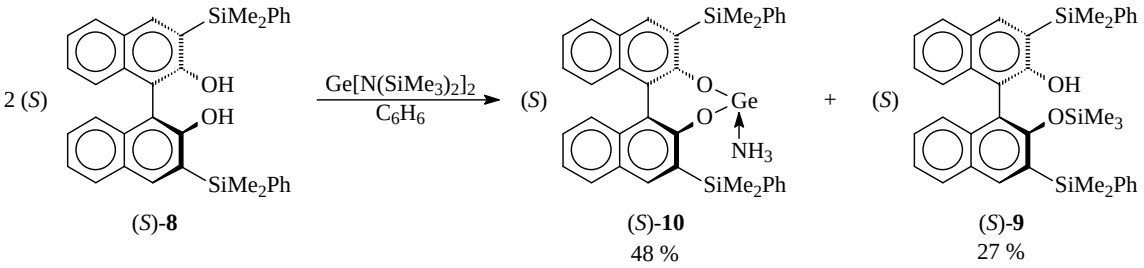

Scheme 2.7: Reaction of *(S)*-**8** with $Ge[N(SiMe_3)_2]_2$.

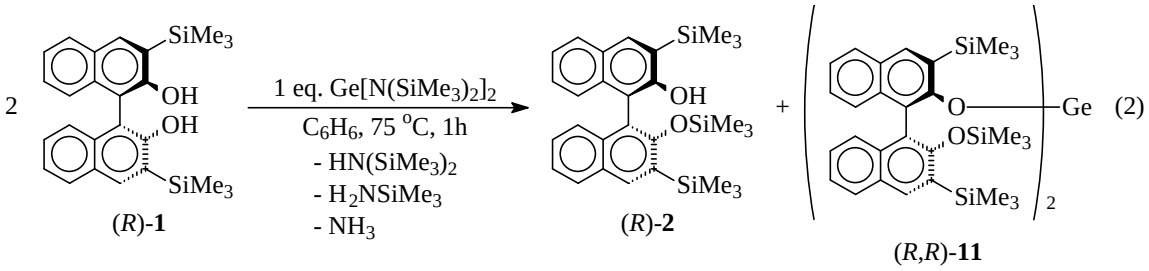

Scheme 2.8: Reaction of *(R)*-**1** with $Ge[N(SiMe_3)_2]_2$.

Reactions employing Be and Zn did not exhibit this reactivity presumably due to the more rapid rate at which these two species consume *(S)*-**8** to furnish the silylated product *(S)*-**9.**

The compound *(S)*-**10** was characterized by NMR spectroscopy and X-ray crystallography.[70] An ORTEP diagram of *(S)*-**10** is shown in **Figure 2.6** and bond distances and angles are collected in **Table 2.3**. The germanium-oxygen bond distances are slightly elongated when compared to those of the related species *(R,R)*-**11** at an average of length of 1.874(3)Å versus 1.814(2) Å. This is likely due to the larger 3,3´-substituents attached to the binaphthol rings in *(S)*-**10**, as well as the chelate effect of the seven-membered GeO_2C_4 ring. The O-Ge-O bond angle in product *(S)*-**10** was found to be 97.9(1)º, which is slightly larger than that of the *(R,R)*-**11** species which measures 89.4(7)º. This is a significant deviation from the expected ideal bond angle of 90º and may also be attributed to the chelating nature of the binaphthol. The two binaphthol rings are rotated by 64.6º relative to one another versus the parent binaphthol, where the relative orientation of the rings approaches 90º.[71] This is also an effect of the incorporation of the binaphthol ligand into the 7-membered ring. The Ge-N bond distance is relatively long at 2.107(4)Å, which is indicative of a dative interaction between the lone pair of electrons from the nitrogen atom and a vacant p-orbital of the

germanium(II) center. The presence of NH_3 in this crystal structure indicates that ammonia is being generated in this reaction as a product of the silylation reaction of *(S)*-**8** to furnish *(S)*-**9.**

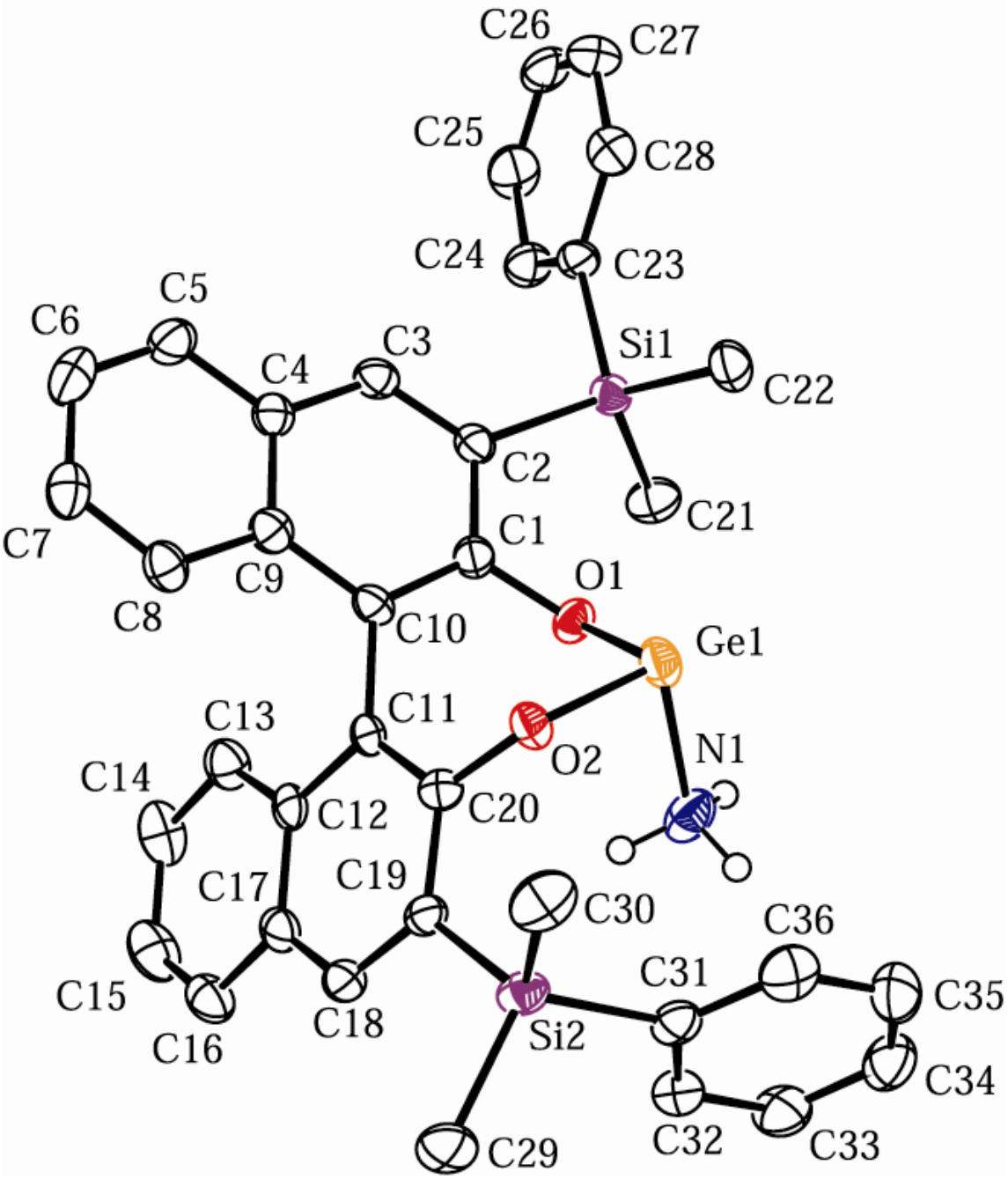

Figure 2.6: ORTEP diagram of *(S)*-**10**. Thermal ellipsoids are drawn at 50% probability.

Table 2.3. Selected bond distances (Å) and angles (deg) for (*S*)-**10**.

Ge(1) – O(1)	1.886(3)	O(1) – Ge(1) – O(2)	97.9(1)
Ge(1) – O(2)	1.863(3)	O(1) – Ge(1) – N(1)	81.6(1)
Ge(1) – N(1)	2.107(4)	O(2) – Ge(1) – N(1)	96.2(1)
O(1) – C(1)	1.363(5)	C(10) – C(1) – O(1)	120.7(4)
O(2) – C(20)	1.364(4)	C(11) – C(20) – O(2)	120.6(3)
C(10) – C(11)	1.501(5)	C(1) – O(1) – Ge(1)	118.9(2)
C(1) – C(10)	1.380(5)	C(20) – O(2) – Ge(1)	122.4(2)
C(11) – C(20)	1.390(5)	C(1) – C(10) – C(11) – C(20)	64.6(1)

Reaction of more sterically encumbered binaphthols with metal(II) amides were not successful. No reaction was observed upon treatment of either *(S)*-3,3´-bis(diphenylmethylsilyl)-1,1´-bi-2,2´-naphthol or *(S)*-3,3´-bis(triphenylsilyl)-1,1´-bi-2,2´-naphthol with the metal(II) amides $M[N(SiMe_3)_2]_2 \cdot nTHF$ (M = Be, Zn, Ge, Sn, n = 0; M = Mg, Ca, n = 2). Furthermore, the related strontium(II) amides did not serve for the conversion of *(R)*-**1** to *(R)*-**2**. The failure of these reactions is likely an effect of the steric bulk of the phenyl groups in the 3- and 3´- positions, which would hinder the accessibility of the hydroxyl groups and make it difficult to generate the intermediate *(R)*-**3**, which is key for the process to occur.

Conclusions

The bulky metal(II) amides $M[N(SiMe_3)_2]_2$ (M= Be, Zn, Ge) have been observed to cleanly transfer a $–SiMe_3$ group to an oxygen atom of one of the hydroxyl groups of either *(R)*-3,3′-bis(trimethylsilyl)-1,1′-bi-2,2′-naphthol (*(R)*-**1**) or *(S)*-3,3′-bis(dimethylphenylsilyl)-1,1′-bi-2,2′-napthol (*(S)*-**8**) to furnish a silyl ether group. The pathway of the reaction involves a cleavage of the Si-N bonds in the bis(trimethylsilyl)amido ligands of the $M[N(SiMe_3)_2]_2$ reagents, ultimately leading to the formation of ammonia and the silyl ether species. All four $–SiMe_3$ groups are potentially available for transfer in this reaction as shown by stiochiometric ^{9}Be NMR studies. The comparative rates and competing processes indicate that the relative strength of the Si-N bond of the metal(II) amide dictates the rate of the reaction.

Qualitative NMR experiments demonstrated that the reaction of *(R)*-**1** with one equivalent $M[N(SiMe_3)_2]_2 \cdot n$ THF (M = Be, Zn, Ge, Sn, n = 0; M = Mg, Ca, n = 2) is dependent on the identity of the metal. The metal(II) amides $M[N(SiMe_3)_2]_2$ (M = Be, Zn or Ge) were shown to cleanly and exclusively furnish the mono silyl ether product *(R)*-**2** in excellent yields, with the rate of reaction being observed to decrease in the order M=Be > M=Zn > M=Ge. The magnesium and tin amides produced some *(R)*-**2**, but were shown to preferentially react with *(R)*-**1** to form a polynuclear species having bridging naphthoxide ligands, and the reaction of $Ca[N(SiMe_3)_2]_2 \cdot 2$THF with *(R)*-**1** was observed to undergo the formation of the polynuclear species exclusively. When one methyl group of *(R)*-**1** is exchanged for a phenyl group in the 3,3′-silylsubstituents ((S)-**8**), the beryllium or zinc amides exclusively convert one –OH group of the substrate to a $–OSiMe_3$ moiety to furnish *(S)*-**9**, where as the germanium(II) amide produces *(S)*- **9** as a

minor product (yield = 27%) and the germanium(II) binaphthoxide complex *(S)*-**10** as the major product (yield = 48%).

The outcome of the reactions of beryllium, zinc and germanium amides with *(R)*-**1** all are similar despite the fact that they have significant differences in hardness and oxophilicity. Furthermore, the silylation reaction appears to be dependent on the proximity of the two hydroxyl moieties, since they must be close enough for the $–SiMe_3$ group transfer to occur during the intermediate phases of the reaction. Increasing the steric bulk of the substituents at the 3,3´ positions increases the distance between the two hydroxyl groups as the relative angle of rotation of the two naphtyl rings increases. When the hydroxyl groups are too far apart the reaction no longer proceeds, as demonstrated by the absence of the reaction of the metal(II) amides with the sterically encumbered 3,3´-(diphenylmethylsilyl) or 3,3´-(triphenylsilyl) binaphthols.

Experimental

General Considerations: *Caution! $Be[N(SiMe_3)_2]_2$ is toxic, a known carcinogen, and should be handled in a well-ventilated fume hood using proper personal protective equipment.* All manipulations were carried out using standard glovebox, Schlenk line, and syringe techniques.[72] ^{1}H, ^{13}C and ^{9}Be NMR spectra were recorded using a Varian Inova spectrometer operating at 400, 100.6, or 56.2 MHz (respectively). ^{1}H and ^{13}C NMR spectra were referenced to resonances for C_6D_6 while ^{9}Be NMR spectra were referenced to external 1.0 M $Be(NO_3)_2$ in D_2O. High resolution MS data were obtained at Purdue University and elemental analysis was provided by Desert Analytics.

Preparation of *(R)*-1

The reactant *(R)*-**1** was prepared following the standard preparation as described by Buisman *et al.* with a few modifications.[73] Protection of the two hydroxyl groups was achieved by adding 18.130g (23.95ml) of ethyl vinyl ether slowly via syringe to a solution of 18.0g of *(R)*-1,1´-Bi-2-naphthol in dichloromethane (50 to 100ml) in a 500ml schlenk flask under a nitrogen atmosphere. Once thoroughly mixed, a catalytic amount (1.578g, 10 mole %) of pyridinium toluene-4-sulfonate was added and the reaction was left to stir at room temperature for 3 days under an inert atmosphere (scheme 2.9). Upon the completion of the reaction the remaining catalyst was quenched with 100ml of deionized water resulting in a burnt orange colored product. Product isolation was achieved via extraction with diethyl ether (50-100ml, 3x) and a brine solution (50-100ml, 3x). The organic phase was separated and dried over anhydrous magnesium sulfate. Gravity filtration was used to remove the magnesium sulfate and the remaining organic solvent was removed *in vacuo* yielding the protected binaphthol product as a yellow oil.

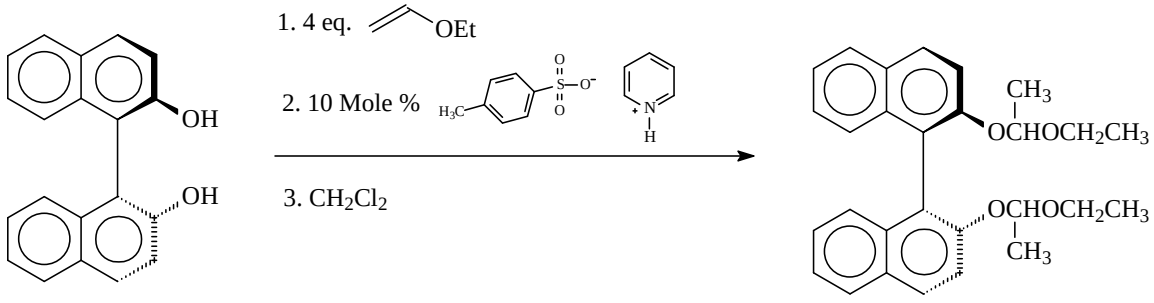

Scheme 2.9: Protection of 1,1´-Bi-2,2´-Naphthol.

Lithiation of the 3 and 3´ positions of the protected binapthol was achieved by reacting 69.3g (100ml, 4 molar equivalents) of n-butyl lithium (2.5M in hexanes) in diethyl ether with the protected binaphthol in manner similar to that of the protection reaction (**Scheme 2.10**). The mixture was stirred over night at room temperature under a nitrogen atmosphere. Product separation was achieved via Canulation of the brown colored solid product to a fritted filter using air sensitive procedures. The product was then washed three times with dry diethyl ether and dried under reduced pressure to remove any remaining ether.

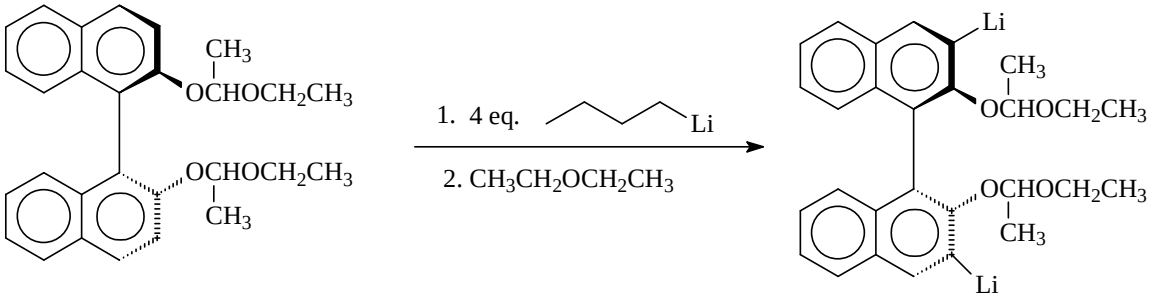

Scheme 2.10: Lithiation of protected binaphthol species.

Silylation of the 3 and 3´ positions was affected by reacting 3.10g of Me_3SiCl with 3.657g of the protected lithiated salt in tetrahydrofuran overnight (**Scheme 2.11**). The same aqueous work up that was used for the protection procedure was then applied to yield the protected trimethylsilyl binol.

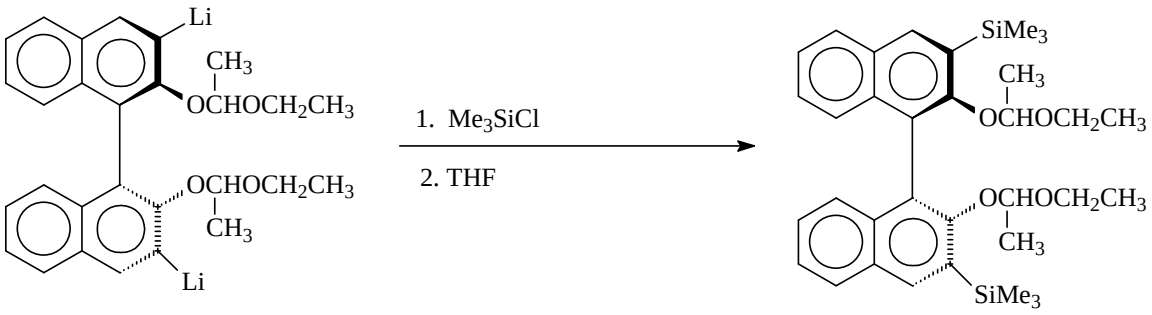

Equation 2.11: Silylation of lithiated species.

Deprotection of the protected trimethysilyl binaphthol was accomplished by reflux in anhydrous ethyl alcohol with 0.208g (10 % molar equivalents) the catalysts pyridinium toluene-4-sulfonate (**Scheme 2.12**). The reaction was allowed to cool and unreacted catalyst was quenched with deionized water. The organic layer was extracted with 100ml of diethyl ether (3x), followed by washes with a brine solution (100ml, 3x). The product was dried over anhydrous $MgSO_4$, filtered via gravity filtration. Lastly the product was subjected to column chromatography using a 1000ml flash column packed with .060-.200mm pore diameter silica gel from Agros chemicals. The eluent used consisted of an 80:20 hexane to ethyl acetate mixture. All fractions were rotovaped and evacuated on a Schlenk line to yield the desired product *(R)*-**1** as a white solid. The purity of each fraction was then assessed using ^{1}H-NMR.

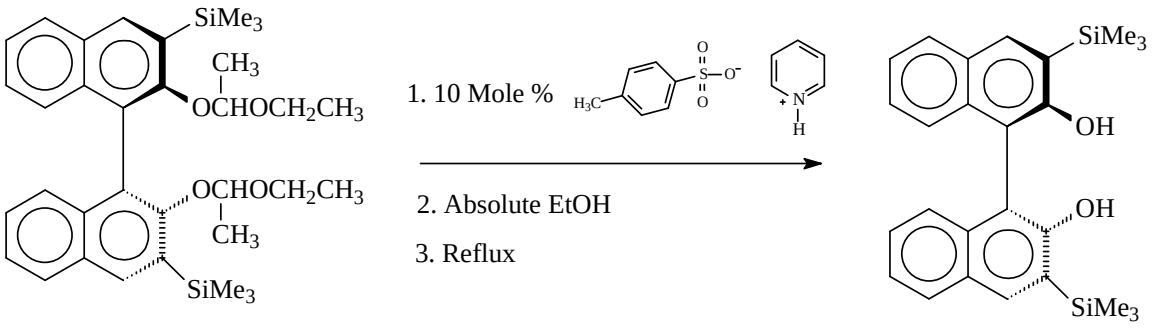

Scheme 2.12: Deprotection to afford the 3,3´-disubstituted binaphthol.

Preparation of *(R)*-8 and *(S)*-8

The preparation of reactants *(R)*-**8** and *(S)*-**8** followed the same protocol as was used for the synthesis of *(R)*-**1**, using $PhMe_2SiCl$ to afford silylation of the 3, 3´ positions rather than Me_3SiCl.

Preparation of $Ge[N(SiMe_3)_2]_2$

$Ge[N(SiMe_3)_2]_2$ was prepared following protocols similar to those found in the literature.[13,74] To a solution of germanium(IV) chloride (38.023g) in diethyl ether (200-250ml) in a 500ml schlenk flask was slowly added triphenyl phosphine (46.507g) and tributyl tin hydride (51.606g, 47.00ml). The reagents were allowed to stir for 15 minutes, after which time the diethyl ether was canulated off and dry dichloromethane (100ml) was added to the reaction vessel. The mixture was stirred until the entire solid dissolved. Fresh diethyl ether (50ml) was then added and the reaction was placed in a freezer to sit overnight. Removal of the solvents via canulation, followed by three washes with diethyl ether (50ml) and evacuation of the remaining volatiles under reduced pressure yielded $Ph_3PHGeCl_3$ as a pure white powder.

To a solution of $Ph_3PHGeCl_3$ (69.048g obtained from reaction 1) in dichloromethane (200ml) was slowly added triethyl amine (15.797g, 87.04ml, 4 molar equivalents) in a reaction vessel being cooled by a standard ice bath. Once all of the triethyl amine was added, the ice bath was removed and the reaction was allowed to come to, and stir at room temperature for 90 minutes. The solvent was then removed by way of Schlenk line evacuation procedures and the reaction was washed with hexane (50ml, 5x).

Lastly a solution of lithium bis(trimethylsilyl)amide (26.123g, 73.978ml, 2.8 molar equivalents) in tetrahydrofuran was canulated into the product from the previous reaction with the solution being kept at 0^oC via an ice bath. The solution was left to stir at room temperature overnight. Once complete the solvent was evacuated from the reaction and the remaining liquid was filtered through a fritted filter containing Celite. The remaining liquid was subjected to short path distillation at a temperature of 65^oC, under a reduced pressure, affording $Ge[N(SiMe_3)_2]_2$ as the final product in the form of a reddish-orange liquid. Allowing the product to cool to room temperature produced some crystalline material, with the product fully becoming a yellowish-orange crystalline solid after sitting in a freezer for a short time. ^{1}H-NMR was used to verify the composition and purity of the product.

Preparation of Other Metal(II) Amides

The other metal(II) amides $Be[N(SiMe_3)_2]_2$,[75] $Mg[N(SiMe_3)_2]_2 \cdot 2$ THF,[76,77] $Ca[N(SiMe_3)_2]_2 \cdot 2$ THF,[78] $Zn[N(SiMe_3)_2]_2$,[79] and $Sn[N(SiMe_3)_2]_2$[74] were prepared according to literature procedures or slight variations thereof.

Preparation of *(R)*-2 using $Be[N(SiMe_3)_2]_2$

To a solution of *(R)*-**1** (0.749 g, 1.74 mmol) in benzene (10 ml) was added a solution of $Be[N(SiMe_3)_2]_2$ (0.582 g, 1.76 mmol) in 20-30ml benzene. The reaction mixture was sealed in a Schlenk tube and heated at 85 ºC for 1 h. The tube was opened in air, the organic phase was washed with deionized water (2 x 10 ml). The organic phase was separated, dried over anhydrous $MgSO_4$, and the benzene was removed *in vacuo* to yield 0.795g (a 91% yield) of *(R)*-**2.** ^{1}H-NMR (C_6D_6, 25^{o}C) δ 8.15 (s, 1 H, 4-H), 8.12 (s, 1 H, 4′-H), 7.74 (d, 1 H, *J* = 9.0 Hz, 9-H), 7.70 (d, 1 H, *J* = 9.0 Hz, 9′-H), 7.28 – 6.94 (m, 6H, aromatics), 5.02 (s, 1 H, -O*H*), 0.51 (s, 9H, -$SiMe_3$-3), 0.48 (s, 9H, -$SiMe_3$-3′), -0.30 (s, 9H, -$OSiMe_3$) ppm. ^{13}C-NMR (C_6D_6, 25^{o}C) δ 158.0, 157.0, 139.1, 137.8, 136.0, 135.8, 130.8, 130.2, 130.0, 129.2, 129.0, 128.9, 127.7, 125.9, 125.8, 125.0, 123.9, 117.6, 115.4, 1.3, 0.5, -0.3 ppm. HRMS: Calcd. for $C_{29}H_{38}O_2Si_2$: *m/z* 502.2180. Found: 502.2180.

Preparation of *(R)*-2 using $Zn[N(SiMe_3)_2]_2$

In a manner identical to the reaction of *(R)*-**1** with $Be[N(SiMe_3)_2]_2$, a solution of *(R)*-**1** (1.571 g, 3.648 mmol) and $Zn[N(SiMe_3)_2]_2$ (1.425 g, 3.690 mmol) in 60 mL of benzene was heated at 85 °C for 1 h to furnish 1.612 g of *(R)*-**2** (88 %) after aqueous workup.

Preparation of *(R)*-2 using $Ge[N(SiMe_3)_2]_2$

In a manner identical to the reaction of *(R)*-**1** with $Be[N(SiMe_3)_2]_2$, a solution of *(R)*-**1** (0.775 g, 1.80 mmol) and $Ge[N(SiMe_3)_2]_2$ (0.712 g, 1.81 mmol) in 35 ml of

benzene was heated at 85 °C for 1 h to furnish 0.802 g of *(R)*-**2** (89 %) after aqueous workup.

NMR Scale Reactions of 1 equiv. $M[N(SiMe_3)_2]_2$ with *(R)*-1 (M = Be, Mg, Ca, Zn, Ge, Sn)

A representative procedure is as follows: To a solution of *(R)*-**1** (0.050 g, 0.12 mmol) in benzene-d_6 (0.50 mL) was added 0.5 equiv. $Zn[N(SiMe_3)_2]_2$ (0.022 g (0.057 mmol) in benzene-d_6 (0.25 mL) in an NMR tube, which was inserted into a preheated (70 ºC) NMR spectrometer. The spectrum was recorded at successive 5 min intervals after mixing the sample. After a total reaction time of 40 min, an additional 0.5 equiv. of $Zn[N(SiMe_3)_2]_2$ (0.022 g (0.057 mmol) in benzene-d_6 (0.25 mL) was added via syringe, and the spectrum was recorded at 5 min intervals. The reaction was shown to be complete after 20 min. An identical procedure was followed for the other $M[N(SiMe_3)_2]_2$ reagents using *(R)*-**1** (0.050 g, 0.12 mmol) and the following amounts for 0.5 equiv. of metal(II) amide: M = Be (0.019 g, 0.058 mmol); M = Mg (0.0238, 0.057 mmol); M = Ca (0.025, 0.057 mmol); M = Ge (0.023 g, 0.057 mmol); M = Sn (0.026 g, 0.057 mmol). For reactions using 1.0 equiv. metal(II) amide: M = Be (0.038 g, 0.12 mmol); M = Mg (0.050, 0.12 mmol); M = Ca (0.052, 0.12 mmol); M = Ge (0.046 g, 0.12 mmol); M = Sn (0.051 g, 0.12 mmol).

Reaction of $Be[N(SiMe_3)_2]_2$ with *(R)*-1: ^{9}Be NMR Study.

A solution of $Be[N(SiMe_3)_2]_2$ (0.078 g, 0.24 mmol) was prepared in benzene-d_6 (0.50 mL) in a NMR tube and its ^{9}Be NMR spectrum was recorded. A solution of *(R)*-**1**

(0.103 g, 0.239 mmol) in benzene-d_6 (0.20 mL) was added via syringe. The sample was mixed and inserted into the NMR spectrometer, which was preheated to at 70°C, and the ^{9}Be NMR spectrum was recorded 5 min after mixing. Additional spectra were recorded at regular (10 min) intervals over 1 h. Similarly, a second equiv. of *(R)*-**1** (0.103 g, 0.239 mmol) in benzene-d_6 (0.20 mL) was added to the tube, and the progress of the reaction was observed over a 1 h period. Addition of a further 2 equiv. of *(R)*-**1** (0.208 g, 0.483 mmol) in benzene-d_6 (0.20 mL) and monitoring the reaction by ^{9}Be NMR spectroscopy indicated the reaction had gone to completion.

Preparation of (*R,R*)-11/*(R)*-2[70]

To a solution of $Ge[N(SiMe_3)_2]_2$ (0.658 g, 1.67 mmol) in benzene (10 mL) was added a solution of *(R)*-**1** (1.46 g, 3.39 mmol) in benzene (5 ml)**.** The reaction mixture was sealed in a Schlenk tube and heated at 85°C for 18 h, after which time pale-yellow crystals had precipitated. The reaction mixture was allowed to cool and was filtered on a fritted glass funnel. The solvent was removed from the filtrate, and the resulting material was subsequently recrystallized twice to furnish more crystalline product, yielding a total of 0.573 g of (R,R)-**11** (32%). Evaporation of the combined mother liquors furnished 0.302 g of *(R)*-**2** (36%). ^{1}H-NMR for (R,R)-**11** (C_6D_6, 25 °C) δ 8.16 (s, 2 H, 4,4′ hydrogens), 7.69 (d, 2H, ^3J(H, H) = 8.1 Hz, 6,6′ hydrogens), 7.46 (d, 2 H, ^3J(H, H) = 8.1 Hz, 8,8′ hydrogens), 7.28-6.83 (aromatics, 14 H), 0.68 (s, 9 H, -OSiCH_3), 0.24 (s, 18 H, -SiCH_3), -0.28 (s, 18 H, - SiCH_3) ppm. ^{13}C NMR (C_6D_6): δ 157.3 (*C*-O-Ge), 138.2(*C*-O-$SiMe_3$), 134.9, 129.8, 128.9-126.8 (aromatics), 124.3 (*C*-$SiMe_3$), 123.9 (*C*-$SiMe_3$), 5.4

(OSi*C*H_3), 2.8 (Si*C*H_3), -0.6 (Si*C*H_3) ppm. Anal. Calcd. for $C_{58}H_{74}O_4Si_6Ge$: C, 64.72; H, 6.93. Found: C, 63.44; H, 6.83.

Preparation of *(S)*-9/*(S)*-10

To a solution of $Ge[N(SiMe_3)_2]_2$ (0.197 g, 0.50 mmol) in benzene (5ml) was added a solution of *(S)*-**9** (0.563 g, 1.02 mmol) in benzene (5 ml). The reaction mixture was sealed in a Schlenk tube and heated at 85 ºC for 18 h, after which time colorless crystals of *(S)*-**11** had precipitated. The reaction mixture was allowed to cool and was filtered on a glass fritted funnel to yield 0.145 g of *(S)*-**10** (48%). Evaporation of the mother liquor furnished 0.0885 g (27%) of *(S)*-**9**. ^{1}H-NMR for *(S)*-**10** (C_6D_6, 25 °C) δ 8.18 (s, 2 H, 4,4′ hydrogens), 7.79 (d, ^3J(H,H) = 8.1 Hz, 2 H, 6,6′ hydrogens), 7.58 (m, 4 H, aromatics), 7.35 (d, ^3J(H, H) = 8.4 Hz, 8,8′ hydrogens), 7.14 - 7.08 (m, 10 H, aromatics), 6.94 - 6.92 (m, 2 H, aromatics), 0.75 (s, 6 H, -Si(CH_3)$_2$Ph), 0.68 (s, 6 H, -Si(CH_3)$_2$Ph) ppm. ^{1}H-NMR for *(S)*-**9** (C_6D_6, 25 °C) δ 8.04 (s, 1 H, 4-H), 7.96 (s, 1 H, 4′-H), 7.90 (d, 1 H, *J* = 6.9 Hz, 9-H), 7.70 – 6.90 (m, 17 H, aromatics), 5.07 (s, 1 H, -O*H*), 0.76 (s, 6H, -Si(CH_3)$_2$Ph), 0.72 (s, 6H, -Si(CH_3)$_2$Ph), -0.50 (s, 9H, -OSiMe_3) ppm.

X-Ray Crystal Structure of *(S)*-10

A colorless block 0.10 x 0.10 x 0.10 mm^3 in size was mounted on a Cryoloop with Paratone oil. Data were then collected in a nitrogen gas stream at 208(2) K using phi and omega scans. Crystal-to-detector distance was 60 mm and the exposure time was 10 seconds per frame using a scan width of 0.3°. Data collection was 97.6% complete to 25.00° in θ. A total of 8663 reflections were collected covering the indices, -10<=*h*<=3,

-12<=*k*<=5, -45<=*l*<=47. 6711 reflections were found to be symmetry independent, with an R_{int} of 0.0278. Indexing and unit cell refinement indicated a primitive, orthorhombic lattice. The space group was found to be P2(1)2(1)2(1) (No. 19). The data were integrated using the Bruker SAINT software program and scaled using the SADABS software program. Solution by direct methods (SIR-2004) produced a complete heavy-atom phasing model consistent with the proposed structure. All non-hydrogen atoms were refined anisotropically by full-matrix least-squares (SHELXL-97). All hydrogen atoms were placed using a riding model. Their positions were constrained relative to their parent atom using the appropriate HFIX command in SHELXL-97. Selected crystallographic data for compound *(S)*-**10** is given below in **Table 2.4**.

Table 2.4. Crystallographic data for compound (*S*)-**10**

formula	$C_{36}H_{35}GeNO_2Si_2$
space group	$P2_12_12_1$
a (Å)	8.373(5)
b (Å)	10.529(6)
c (Å)	36.10(2)
α (°)	90
β (°)	90
γ (°)	90
V (Å^3)	3183(3)
Z	4
ρ_{calc} (g cm^{-1})	1.341
temperature (K)	208(2)
radiation	MoKα
wavelength (Å)	0.71073
R	0.0490
R_w	0.1069

CHAPTER III

REACTION OF BIS(BIS(TRIMETHYLSILYL)AMIDO)MERCURY(II) WITH 3,3´-DISUBSTITUTED BINAPHTHOLS: CYCLIZATION VIA AN INTRAMOLECULAR ELECTROPHILIC AROMATIC SUBSTITUTION REACTION

Introduction

Polycyclic aromatic and heteroaromatic compounds have been of significant interest due to their electronic properties and the fact that they might be used as organic conductors.[80-86] Recently, the long-known heteroaromatic species *peri*-xanthenoxanthene (6,12-dioxaanthanthrene, PXX) has been employed in a number of both organic[87,88] and inorganic[87] charge transfer complexes as well as conductive salts, including cobalt[87,89-93] salts and iron[94-96] phthalocyaninato complexes. The PXX compound and its complexes have been successfully used as organic and inorganic/organic conductors[97-99], with the PXX also having also found applications as pigment ingredients. Originally the hexacyclic species (6, 12-dioxaanthanthrene) was prepared by the reaction of 1,1´-bi-2,2´-naphthol with copper(II) acetate,[100] while the synthesis of substituted derivatives of PXX were previously unknown.

We have developed a methodology for the preparation of PXX and its derivatives using the sterically encumbered mercury(II) amide $Hg[N(SiMe_3)_2]_2$ (1).[79] The reaction of $Hg[N(SiMe_3)_2]_2$ with 1,1´-bi-2,2´-naphthol was shown to cleanly furnish PXX, while

similar reactions using 3,3′-disubstituted-1,1′-bi-2-naphtols were observed to afford 1,7-disubstitued derivatives of PXX in high yields, where the later materials are potentially useful in combinations with organic molecules and inorganic complexes to furnish potentially conductive materials. Four 1,7-silyldisubstituted derivatives of PXX were prepared, and the reaction leading to these species were investigated via ^{1}H and ^{199}Hg NMR spectroscopy.

Results and Discussions

The reaction of the mercury(II) amide $Hg[N(SiMe_3)_2]_2$ (**1**) with 3,3′-disubstituted-1,1′-bi-2,2′-naphthols (**2a-d**) or the unsubstituted parent molecule 1,1′-bi-2,2′-naphthol (**2e**) were observed to undergo an intramolecular electrophilic aromatic substitution reaction involving mercuration of the hydroxyl groups followed by attack at the 9-position of the adjacent naphthyl ring and subsequent extrusion of elemental mercury. This resulted in the formation of either pentacyclic or hexacyclic fused species depending on the reaction stoichiometry employed (Reaction **Schemes 3.1** and **3.2** are shown below).

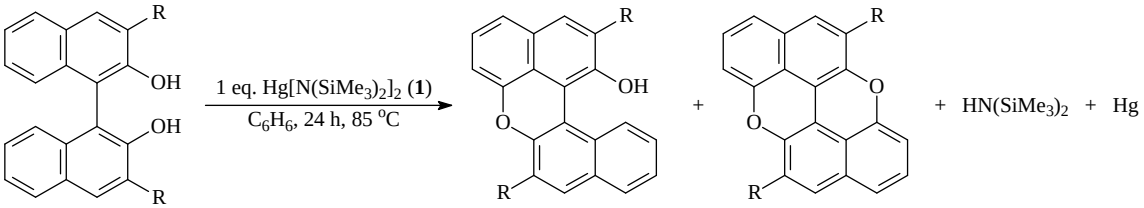

2a R = $SiMe_3$
2b R = $SiMe_2Ph$
2c R = $SiMePh_2$
2d R = $SiPh_3$
2e R = H

3a R = $SiMe_3$
3b R = $SiMe_2Ph$
3c R = $SiMePh_2$
3d R = $SiPh_3$
3e R = H

4a R = $SiMe_3$
4b R = $SiMe_2Ph$
4c R = $SiMePh_2$
4d R = $SiPh_3$
4e R = H (PPX)

Scheme 3.1: Reaction of 3,3′-disubstituted binaphthols (**2a-e)** with 1 equivalent of $Hg[N(SiMe_3)_2]_2$

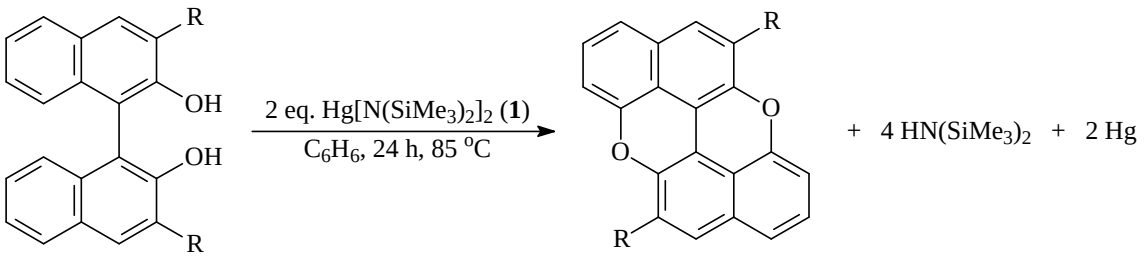

2a R = $SiMe_3$
2b R = $SiMe_2Ph$
2c R = $SiMePh_2$
2d R = $SiPh_3$
2e R = H

4a R = $SiMe_3$
4b R = $SiMe_2Ph$
4c R = $SiMePh_2$
4d R = $SiPh_3$
4e R = H (PXX)

Scheme 3.2: Reaction of 3,3′-disubstituted binaphthols (**2a-e)** with 2 equivalents of $Hg[N(SiMe_3)_2]_2$.

The reaction of one equivalent of $Hg[N(SiMe_3)_2]_2$ and **2a** was performed on a preparative scale in benzene at a temperature of 85°C over 12 hours. Throughout the course of the reaction, various color changes were observed. Initially, upon the addition of **2a** to the mecury(II) amide, the reaction mixture immediately turned dark yellow in color, and after five minutes of heating a dark purple/red solution was observed. Upon completion of the reaction, the solution was yellow/green in color and beads of mercury metal were clearly visible in the bottom of the reaction vessel. Filtration of the mixture in air and removal of solvent *in vacuo* yielded an orange/yellow solid. The crude product was then analyzed using ^{1}H-NMR spectroscopy, and four resonances were exhibited in the alkylsilyl region at δ 0.54, 0.51, 0.46, and 0.43 ppm indicating the presence of the starting material **2a** (δ 0.46 ppm) and two other species.

The crude product was recrystalized from a hot benzene solution to furnish the pentacyclic compound (Dibenzo[a,kl]xanthen-13-ol) **3a** in 37% yield. This was

confirmed via X-ray crystallographic analysis, ^{1}H and ^{13}C NMR spectroscopy, and by elemental analysis. An ORTEP diagram of the pentacyclic compound **3a** is shown in **Figure 3.1**, and selected bond angles and distances are collected in **Table 3.1**. The two intracyclic C-O bond distances of **3a** between O(1) and C(10) and O(1) and C(13) (1.383(2) Å and 1.380(2) Å, respectively) are nearly identical to the exocyclic O(2)-C(20) bond distance of 1.378(2) Å. Furthermore, the five-ring system is not planar, but rather puckered as indicated by the torsion angles of 6.64 ° and 4.44 ° in the central C_5O ring about O(1)-C(10)-C(9)-C(11) and O(1)-C(13)-C(12)-C(11), respectively.

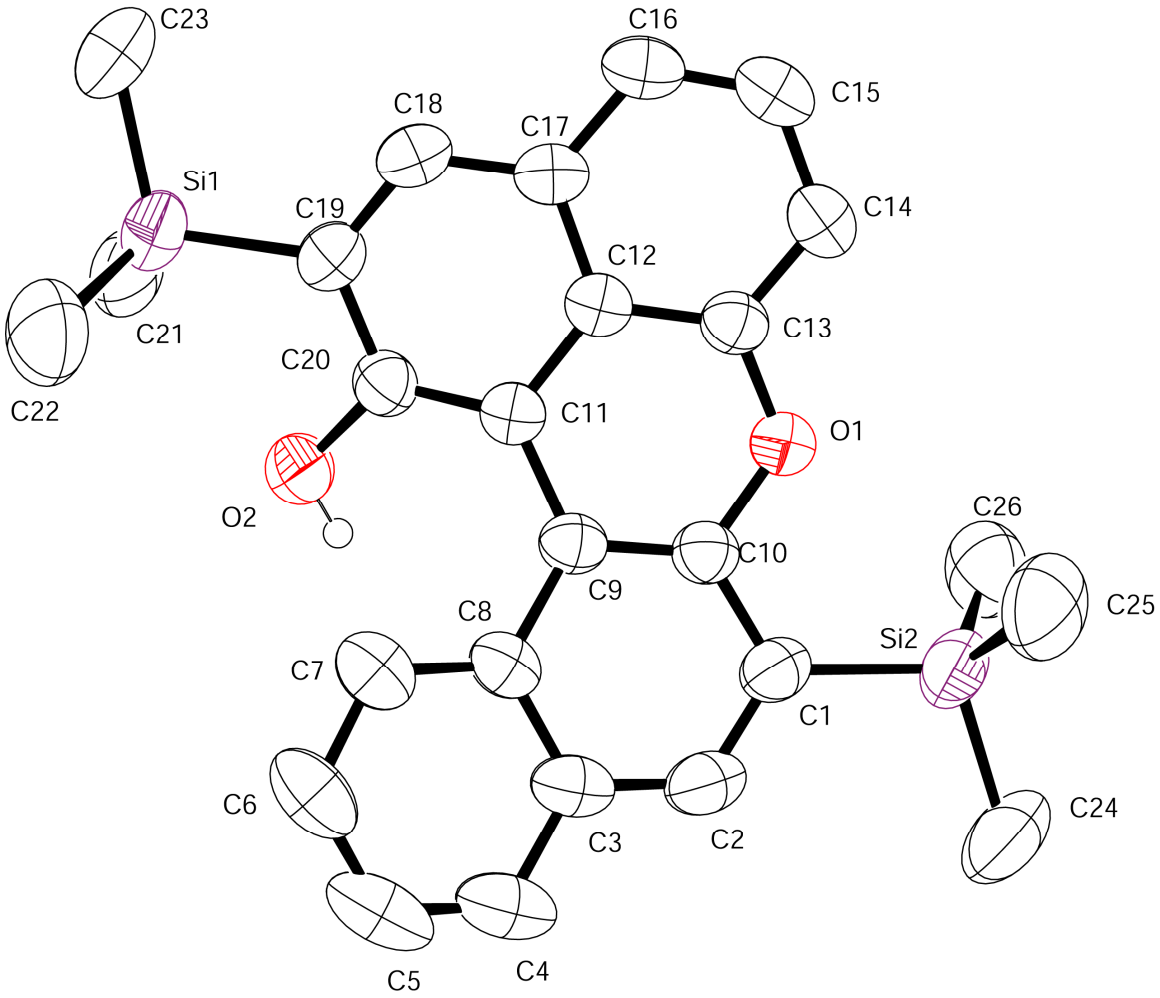

Fig. 3.1: ORTEP diagram of compound **3a**. Thermal ellipsoids are drawn at 50% probability.

Table 3.1. Selected bond distances (Å) and angles (°) for compound **3a**.

O(1) – C(10)	1.383(2)	C(9) – C(11)	1.473(2)
O(1) – C(13)	1.380(2)	Si(1) – C(19)	1.883(2)
O(2) – C(20)	1.378(2)	Si(2) – C(1)	1.882(2)
C(1) – C(2)	1.373(3)	C(11) – C(12)	1.428(2)
C(1) – C(10)	1.416(3)	C(11) – C(20)	1.386(2)
C(2) – C(3)	1.411(3)	C(12) – C(13)	1.404(2)
C(3) – C(4)	1.412(3)	C(12) – C(17)	1.414(2)
C(3) – C(8)	1.421(3)	C(13) – C(14)	1.367(3)
C(4) – C(5)	1.343(4)	C(14) – C(15)	1.401(3)
C(5) – C(6)	1.380(4)	C(15) – C(16)	1.355(3)
C(6) – C(7)	1.381(3)	C(16) – C(17)	1.420(3)
C(7) – C(8)	1.412(3)	C(17) – C(18)	1.413(3)
C(8) – C(9)	1.447(2)	C(18) – C(19)	1.371(3)
C(9) – C(10)	1.380(3)	C(19) – C(20)	1.425(3)
O(1) – C(10) – C(1)	113.1(2)	O(1) – C(13) – C(12)	120.0(2)
O(1) – C(13) – C(14)	117.5(2)	O(2) – C(20) – C(11)	124.6(2)
O(2) – C(20) – C(19)	112.9(2)	Si(1) – C(19) – C(18)	122.8(2)
Si(1) – C(19) – C(20)	119.2(2)	Si(2) – C(1) – C(2)	122.8(2)
Si(2) – C(1) – C(10)	121.1(2)	C(10) – C(1) – C(2)	116.0(2)
C(1) – C(2) – C(3)	122.8(2)	C(10) – C(9) – C(11)	118.4(2)
C(2) – C(3) – C(4)	121.4(2)	C(11) – C(12) – C(13)	120.1(2)
C(2) – C(3) – C(8)	119.4(2)	C(11) – C(12) – C(17)	121.9(2)
C(3) – C(4) – C(5)	121.6(2)	C(12) – C(13) – C(14)	122.3(2)
C(3) – C(8) – C(9)	118.9(2)	C(12) – C(17) – C(16)	119.1(2)
C(4) – C(5) – C(6)	119.9(2)	C(12) – C(17) – C(18)	117.4(2)
C(5) – C(6) – C(7)	121.1(2)	C(13) – O(1) – C(10)	119.6(2)
C(6) – C(7) – C(8)	120.5(2)	C(13) – C(12) – C(17)	117.8(2)
C(7) – C(8) – C(8)	117.5(2)	C(13) – C(14) – C(15)	119.3(2)
C(7) – C(8) – C(3)	123.4(2)	C(14) – C(15) – C(16)	120.7(2)
C(8) – C(3) – C(4)	119.1(2)	C(15) – C(16) – C(17)	120.7(2)
C(8) – C(9) – C(10)	116.5(2)	C(16) – C(17) – C(18)	123.4(2)
C(8) – C(9) – C(11)	124.8(2)	C(17) – C(18) – C(19)	122.3(2)
C(9) – C(10) – C(1)	125.2(2)	C(18) – C(19) – C(20)	118.0(2)
C(9) – C(10) – O(1)	121.7(2)	C(19) – C(20) – C(11)	122.6(2)
C(9) – C(11) – C(12)	116.1(2)	C(20) – C(11) – C(12)	116.0(2)
C(9) – C(11) – C(20)	127.7(2)		

Further recrystalization attempts resulted in the formation of cubic-shaped crystals that differed in appearance from the rod-shaped crystals which were identified as the pentacyclic compound **3a**. X-ray crystallography confirmed that the identity of this second material was the highly symmetric hexacyclic compound **4a**. The two halves of of the molecule **4a** are related through a center of inversion located in the center of the C(9)-C(9′) inneranular bond. Other symmetry elements include a C_2 axis and a σ_h mirror plane, leading to the assignment of the C_{2h} point group for this molecule. An ORTEP diagram is shown **Figure 3.2** and selected bond distances and angles are collected in **Table 3.2**. The C-O bond distances in **4a** were found to be 1.393(3) Å, which is significantly elongated relative to the distances of 1.383(2) Å and 1.380(2) Å observed in compound **3a**. In contrast to the pentacyclic compound **3a**, the hexacyclic compound **4a** was shown to be completely planar.

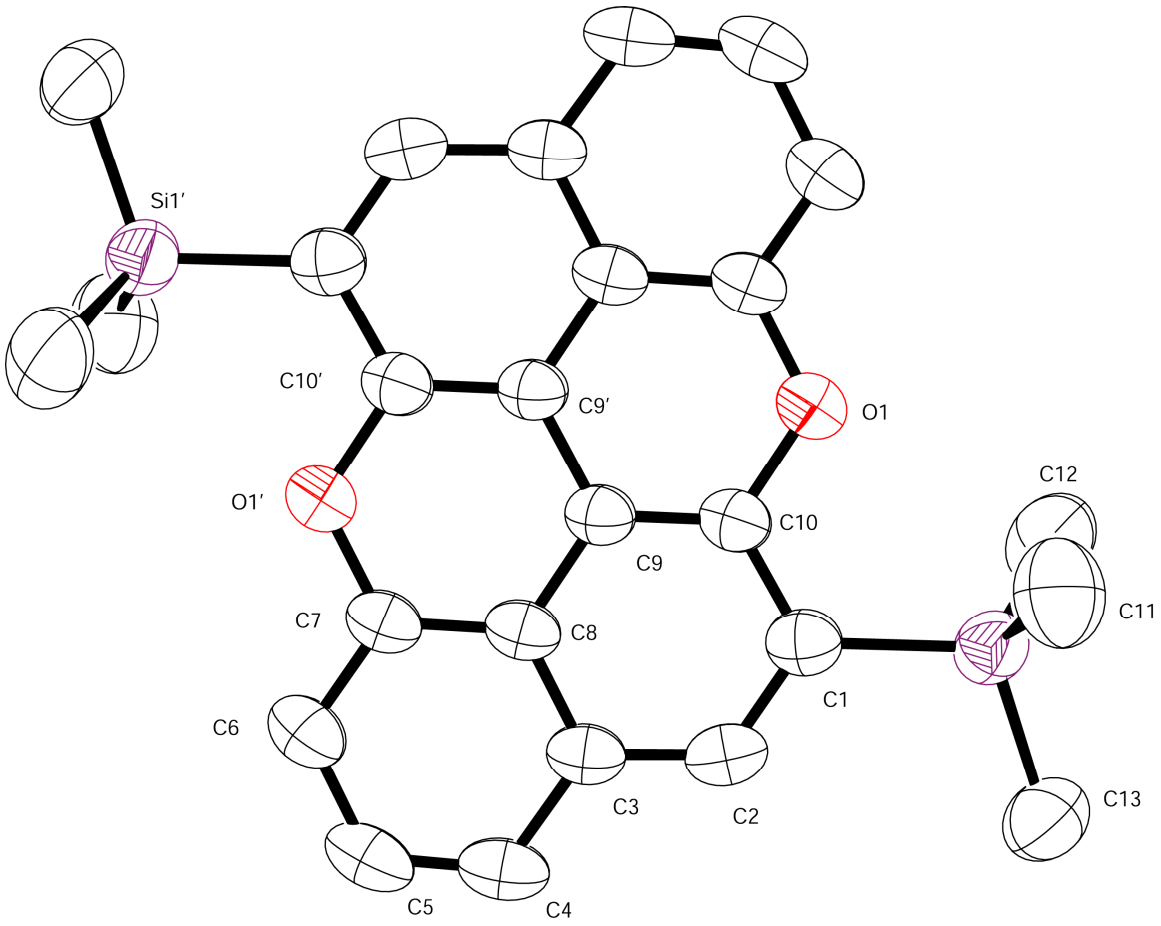

Fig. 3.2: ORTEP diagram of compound **4a**. Thermal ellipsoids are drawn at 50% probability.

Table 3.2. Selected bond distances (Å) and angles (°) for compounds **4a**.

Selected Bonds in 4a	**4a Bond Distances (Å)**
O(1) – C(10)	1.394(3)
O(1′) – C(7)	1.393(3)
Si(1) – C(1)	1.888(3)
C(1) – C(2)	1.386(4)
C(1) – C(10)	1.419(4)
C(2) – C(3)	1.419(4)
C(3) – C(4)	1.417(4)
C(3) – C(8)	1.417(4)
C(4) – C(5)	1.358(5)
C(5) – C(6)	1.407(5)
C(6) – C(7)	1.358(4)
C(7) – C(8)	1.404(4)
C(8) – C(9)	1.404(4)
C(9) – C(9′)	1.439(5)
C(9) – C(10)	1.366(4)
Selected Bonds in 4a	**4a Bond Angles (°)**
O(1) – C(10) – C(1)	116.9(3)
O(1) – C(10) – C(9)	121.2(2)
O(1′) – C(7) – C(6)	118.0(3)
O(1′) – C(7) – C(8)	120.8(2)
Si(1) – C(1) – C(2)	123.0(2)
Si(1) – C(1) – C(10)	120.8(2)
C(1) – C(2) – C(3)	124.3(3)
C(2) – C(3) – C(4)	125.8(3)
C(2) – C(3) – C(8)	117.1(3)
C(3) – C(4) – C(5)	120.8(3)
C(3) – C(8) – C(7)	120.6(3)
C(3) – C(8) – C(9)	119.2(3)
C(4) – C(5) – C(6)	121.9(3)
C(4) – C(3) – C(8)	117.0(3)
C(5) – C(6) – C(7)	118.5(3)
C(6) – C(7) – C(8)	121.2(3)
C(7) – C(8) – C(9)	120.2(3)
C(8) – C(9) – C(10)	121.4(3)
C(8) – C(9) – C(9′)	117.8(3)
C(9) – C(10) – C(1)	121.9(3)
C(10) – C(1) – C(2)	116.0(3)
C(10) – C(9) – C(9′)	120.8(3)
C(10) – O(1′) – C(7′)	119.2(2)

The reaction of the pentacyclic species **3a** with an additional equivalent of $Hg[N(SiMe_3)_2]_2$ at 85°C resulted in quantitative conversion to **4a** after a reaction time of 18 hrs as shown by ^{1}H-NMR spectroscopy. A preparative scale reaction under the same reaction conditions furnished **4a** from **3a** in 85% yield according to **Scheme 3.3**

.

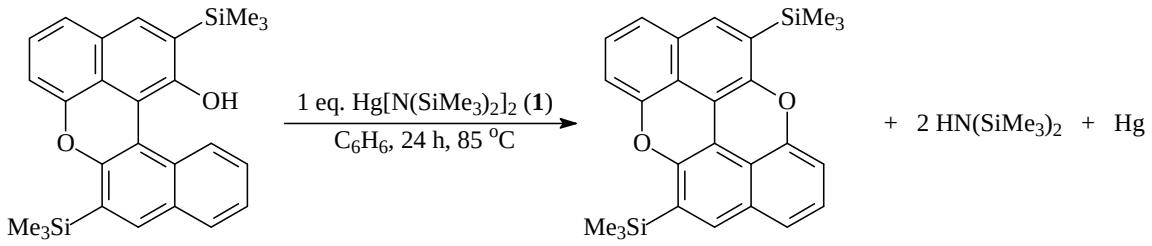

3a **4a**

85 %

Scheme 3.3: Reaction of the pentacyclic compound **3a** with a second equivalent of $Hg[N(SiMe_3)_2]_2$.

Compounds **3a** and **4a** were further characterized by NMR (^{1}H and ^{13}C) spectroscopy and elemental analysis. The ^{1}H-NMR spectrum of **3a (Figure 3.3)** displayed a resonance at δ 4.20 ppm corresponding to the single hydroxyl group present in the molecule, while two features at δ 0.54 ppm and δ 0.51 ppm correspond to the two non-equivalent –$SiMe_3$ groups. The ^{13}C-NMR of **3a** exhibited the expected 22 resonances with signals at δ -0.6 and δ -0.7 ppm corresponding to the two trimethylsilyl groups, and a peak at δ 120.4 ppm arising from the carbon atom directly attached to the single hydroxyl group. Both the ^{1}H and ^{13}C NMR spectra for compound **4a** (**Figures 3.4** and **3.5**, respectively) exhibited single resonances for the symmetrically related trimethylsilyl groups at chemical shifts of 0.44 ppm and -0.9 ppm (respectively). Ten

additional features ranging from δ 1.3 to 153.0 ppm were observed in the ^{13}C-NMR for the carbons present in the rings, with two distinct peaks being observed at δ 153.0 ppm and δ 111.0 ppm arising from the oxygen-bound C(7) and C(10) atoms, respectively.

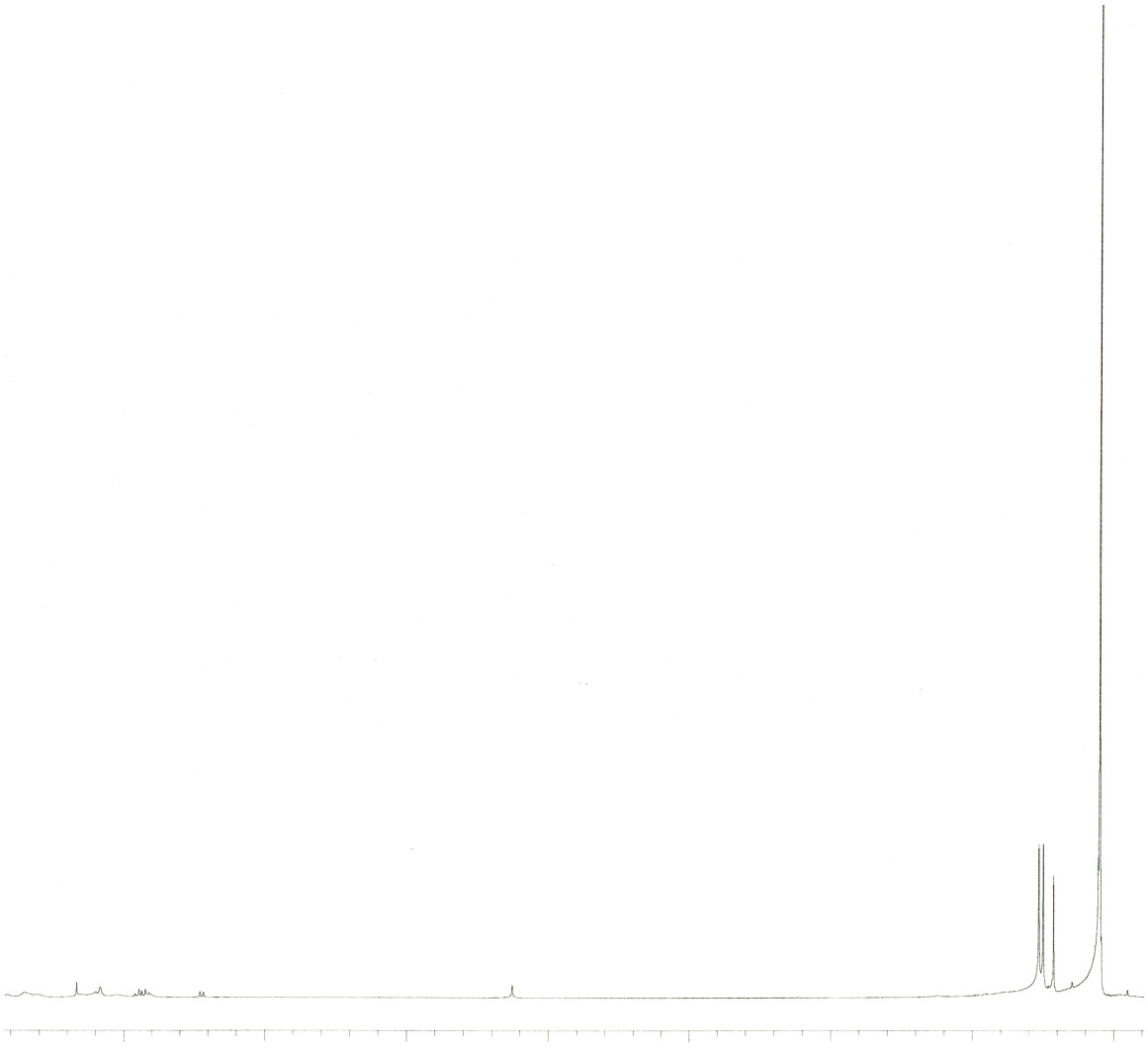

a)

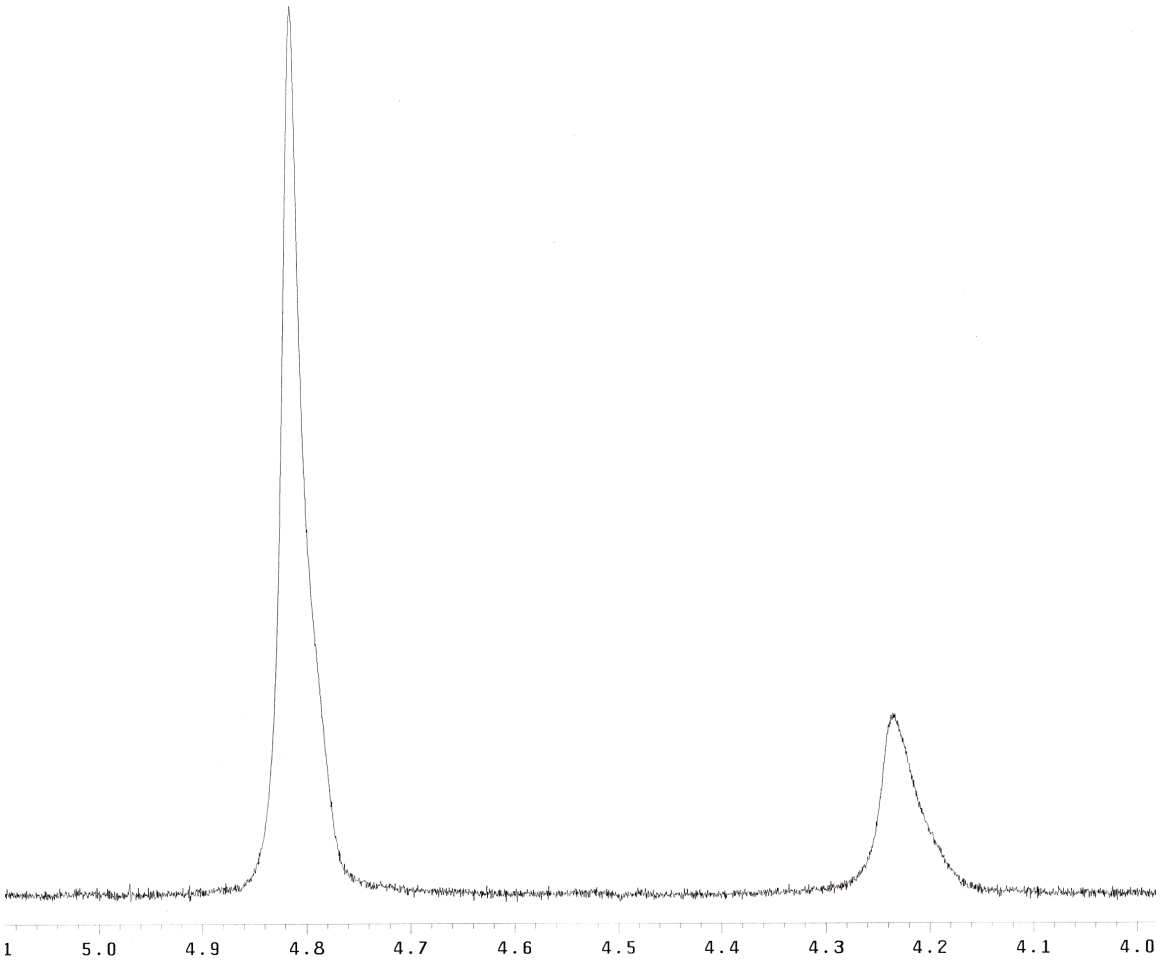

b)

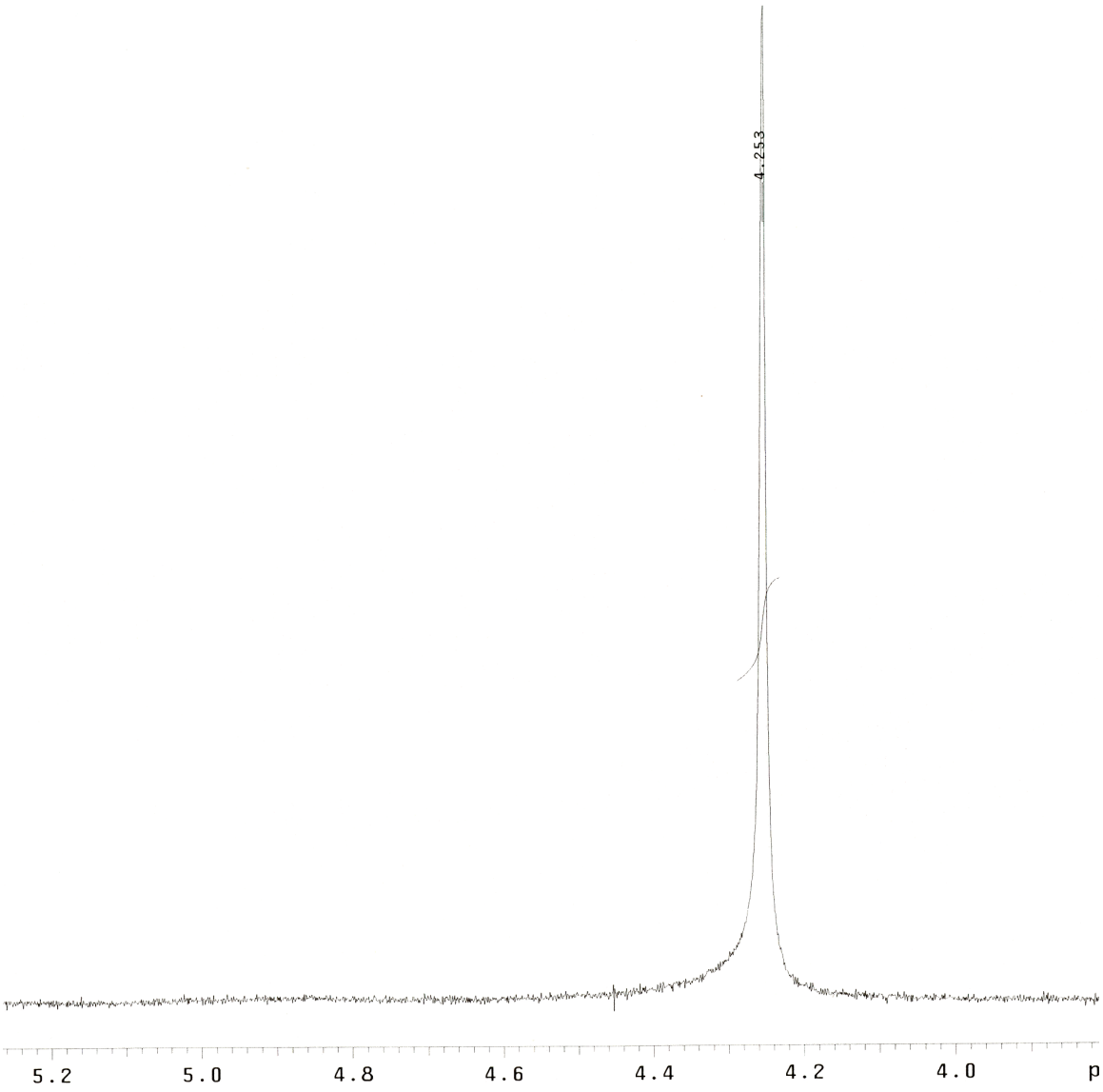

c)

Figure 3.3: Full ^{1}H-NMR of compound 3a *(a)* as well as 2 expanded hydroxyl proton regions showing intermediates/products *(b)* and a completed reaction with evidence of only product formation *(c).*

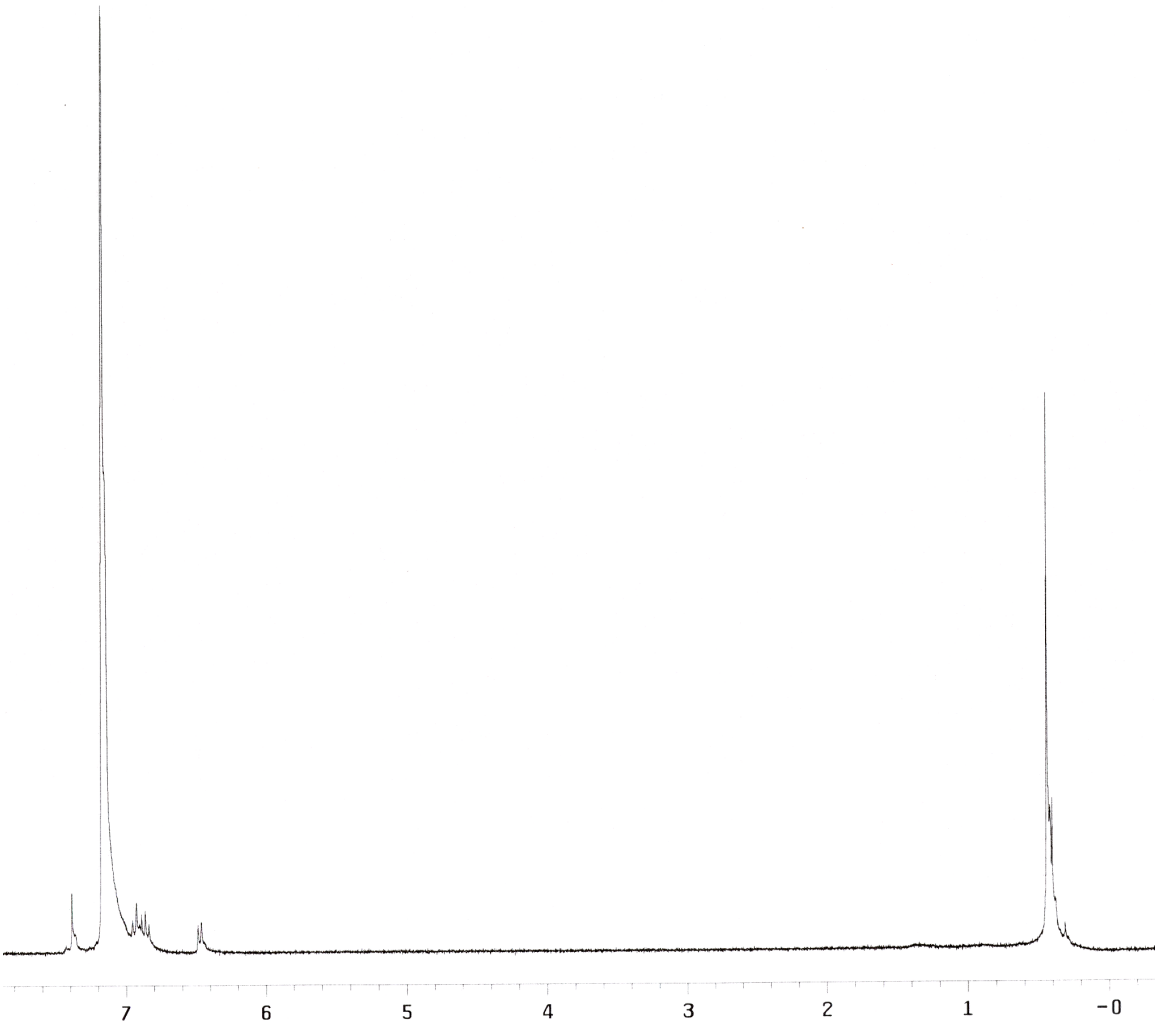

Figure 3.4: ^{1}H-NMR of compound 4a crystals. No observed peaks in the hydroxyl proton region of the spectrum.

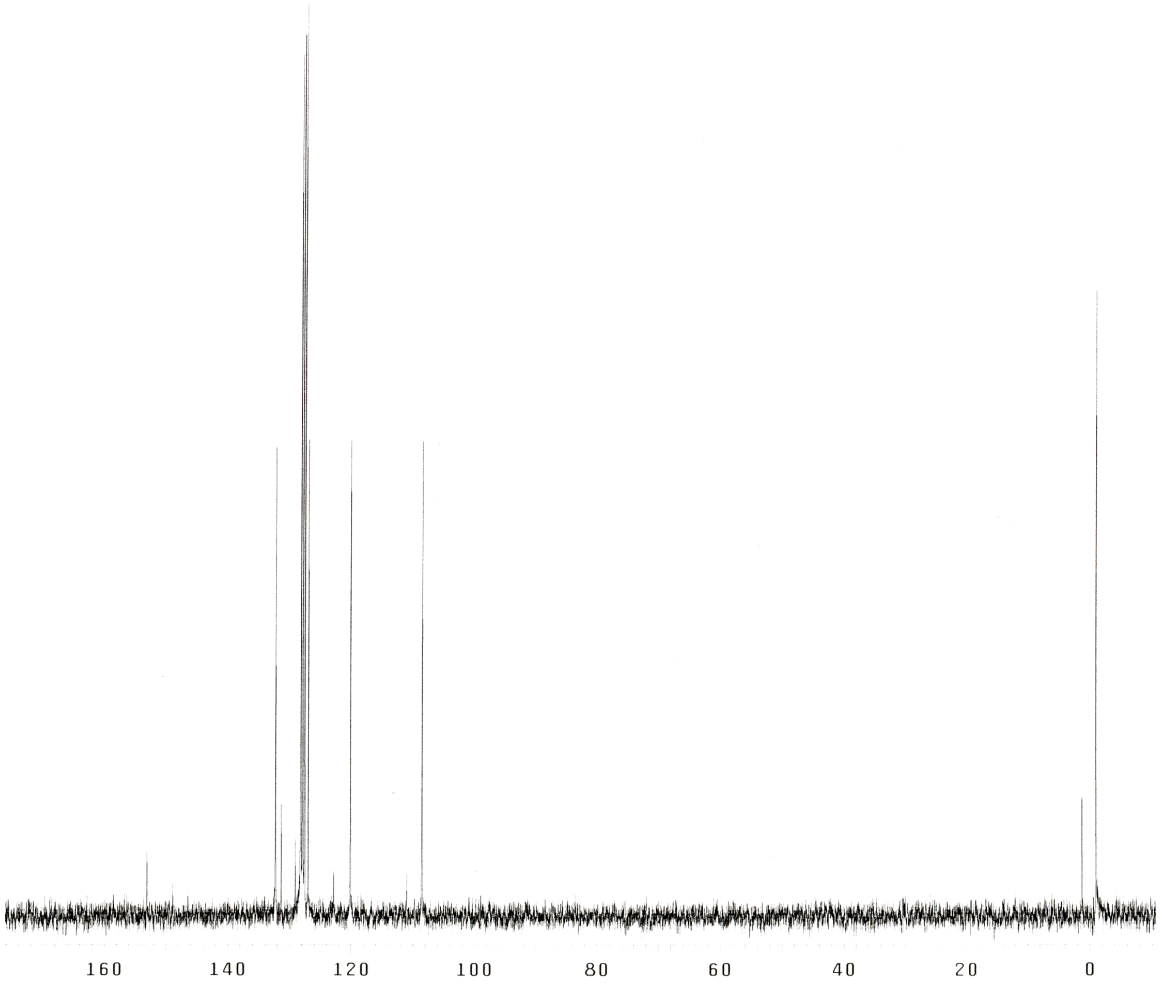

a)

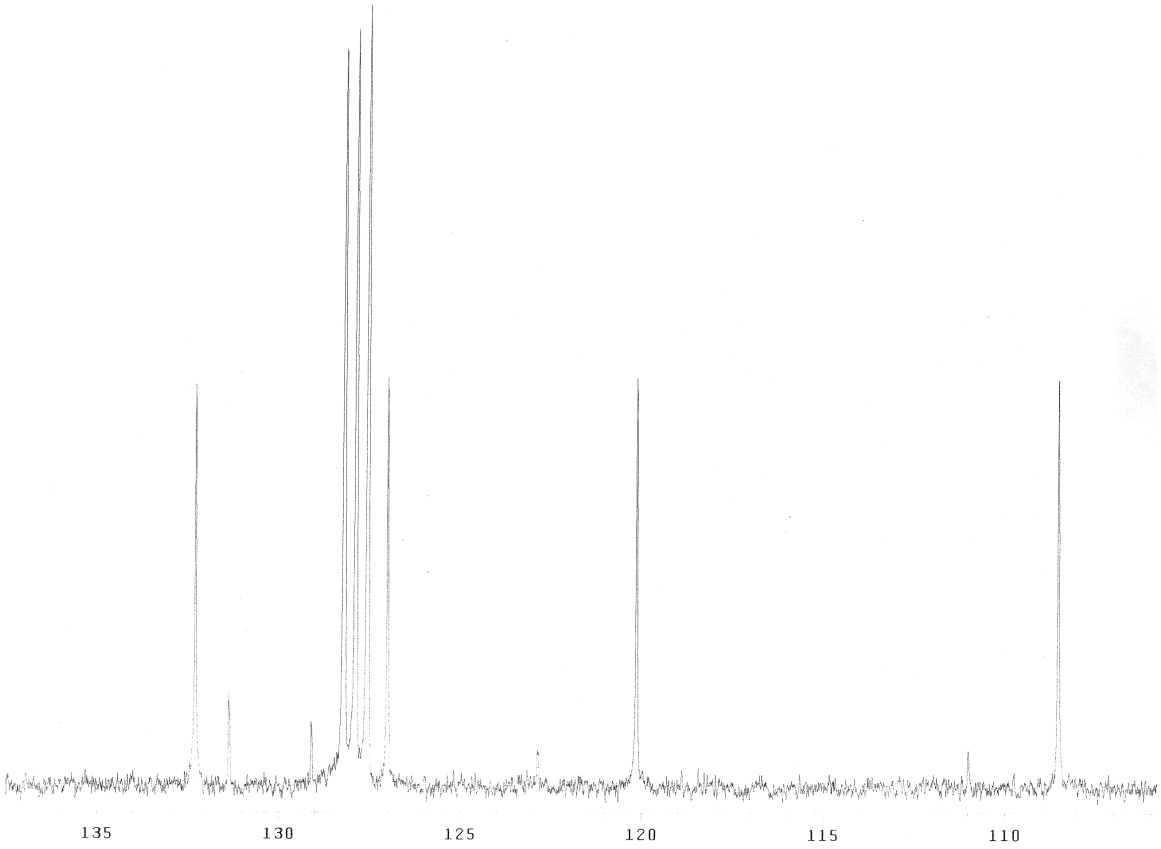

b)

Figure 3.5: ^{13}C-NMR of compound 4a. Spectrum *(a)* shows a full spectrum, *(b)* is an expanded region form δ 100.0 to 140.0 ppm provided for clarity.

The formation of **3a** and **4a** was also confirmed using Gas Chromatography/ Mass Spectrometry (GCMS) with a column temperature of 250 °C. Analysis of a crude product obtained from the reaction of **2a** with two equivalents of $Hg[N(SiMe_3)_2]_2$ revealed a single peak with a retention time of 95.5 minutes. The mass spectrum displayed a base peak at m/z = 426, with a feature corresponding to the parent molecule **4a** also being visible at an m/z of 428. The fragmentation pattern observed corresponded

to the sequential loss of all six methyl groups of **4a**. The chromatograph of the product mixture isolated from the reaction of one equivalent of $Hg[N(SiMe_3)_2]_2$ and **2a** exhibited two peaks with retention times of 29.8 and 95.2 minutes. The mass spectrum of the first material eluted exhibited a base peak at m/z = 430 corresponding to the parent compound **3a**. A second peak at m/z = 398 arising from the loss of two oxygen atoms was observed, as well as a fragmentation pattern resulting from the sequential loss of all six methyl groups. The second material eluted (t_r = 95.2 min) was shown to be identical to that obtained for **4a**. Analysis of the product obtained according to **Scheme 3.4** also indicated the presence of only compound **4a**.

To probe the reaction pathway leading to the formation of **3a** and **4a**, an NMR scale reaction was conducted by combining $Hg[N(SiMe_3)_2]_2$ with **2a** in C_6D_6 using a 1:1 stoichiometric ratio. The reaction was monitored via ^{1}H-NMR spectroscopy at 25^{o}C, and the resulting observations can be correlated to the species present in the proposed pathway shown in **Schemes 3.4** and **3.5**.

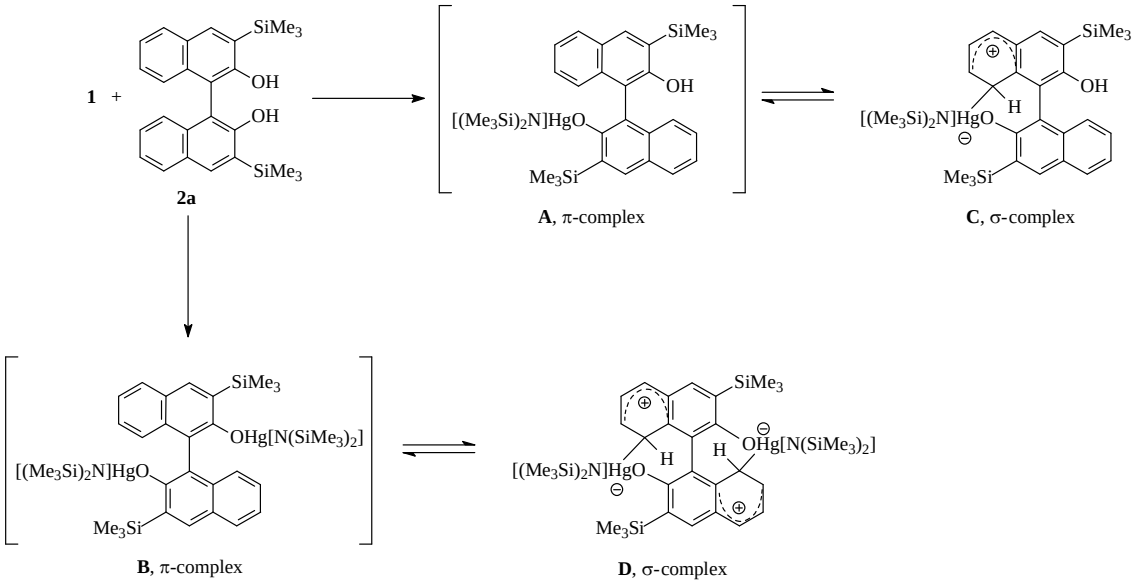

Scheme 3.4: Proposed pathway for the formation of the mercurated π and σ complexes.

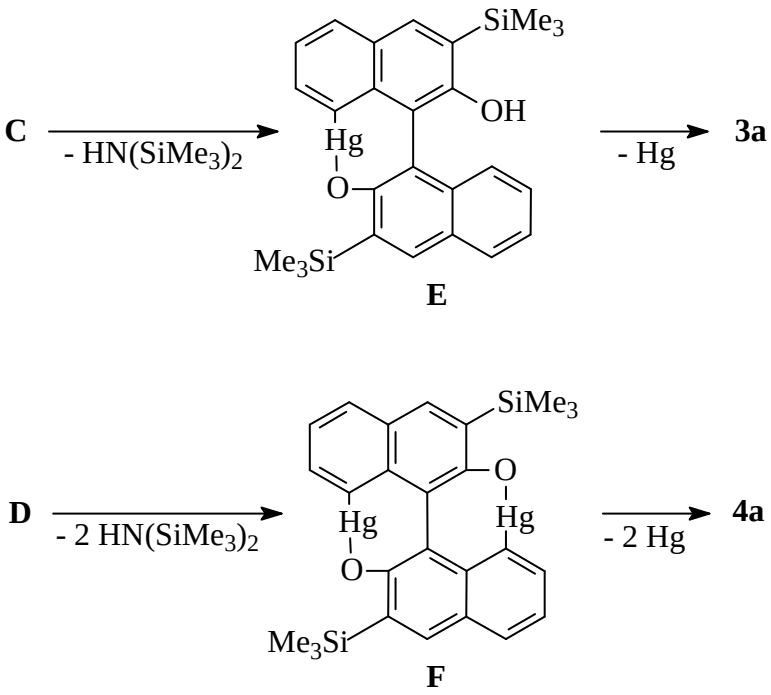

Scheme 3.5: Proposed pathway for the formation of compounds **3a** and **4a** from the mercurated σ complexes **C** and **D**.

After the first 5 minutes of reaction, the mixture had become intensely yellow in color with a resonance becoming clearly visible at δ 5.41 ppm, that is shifted downfield form the original hydroxyl resonance for **2a** (δ 4.81 ppm). The integrated intensity of the new resonance was approximately one third of that for the initial hydroxyl feature corresponding to compound **2a**, and this new feature is attributed to the formation of the intermediate π-complex **A**, resulting from the displacement of one $–N(SiMe_3)_2$ ligand from $Hg[N(SiMe_3)_2]_2$ upon reaction with a single –OH group. The intense color observed is likely a result of the donation of electron density from the aromatic ring

system to the neighboring –OHg[$N(SiMe_3)_2$] moiety in the intermediate π-complex **A** at the beginning of the intramolecular electrophilic aromatic substitution reaction. At this time the alkyl region of the spectrum contained three features at δ 0.24, 0.46 and 0.10 ppm arising from the –$SiMe_3$ groups of the mercury(II) amide, compound **2a** and $HN(SiMe_3)_2$ respectively, with the integrated intensities for the resonances of -OHg[$N(SiMe_3)_3]_2$ moiety and $HN(SiMe_3)_2$ being approximately 2:1. Three less intense peaks were also present in the alkyl region of the spectrum. Two of these resonances at δ 0.61 and -0.04 corresponding to the magnetically inequivalent –$SiMe_3$ of intermediate π-complex **A** with the third resonance being observed at -0.15 ppm corresponding to the equivalent –$SiMe_3$ groups of intermediate π-complex **B** (relative intensities of 1:1:2).

After 3 hours of reaction time at 25°C the solution had become dark purple/red in color with the two resonances at δ 0.24 and 0.10 ppm now present in a ratio of 1:1, indicating that approximately half of the initial mercury(II) amide had been converted to $HN(SiMe_3)_2$. Also at this time, the resonance at δ 5.41 ppm was absent. After 12 hours of reaction at 25°C the intense color had faded to a dark yellow and small beads of mercury metal were present in the bottom of the NMR tube. Analysis of the ^{1}H-NMR spectrum at this time revealed that the remaining solution contained a mixture of the pentacyclic species **3a**, hexacyclic species **4a** and starting binaphthol **2a**. Peaks corresponding to the presence of starting binaphthol **2a** were observed at δ 4.81 and 0.46 ppm due to the two equivalent hydroxyl groups and the two equivalent trimethylsilyl groups, respectively. Resonances for compound **3a** appeared in the spectrum at δ 4.20, 0.54 and 0.51 ppm, arising from the single hydroxyl group and the two magnetically non-equivalent –$SiMe_3$ groups (respectively). The presence of compound **4a** resulted in the

appearance of a resonance at δ 0.43 ppm corresponding to its two equivalent –$SiMe_3$ groups. Integration of the peaks attributed to the three components of the mixture indicated that **2a**, **3a** and **4a** were present in approximately a 2:2:1 ratio.

To further investigate the reaction pathway, the reaction of 2 equivalents of mercury(II) amide with 1 equivalent of **2a** in C_6D_6 at 25°C was monitored by ^{199}Hg-NMR spectroscopy. The ^{199}Hg spectrum of the $Hg[N(SiMe_3)_3]_2$ starting material contained a single resonance at δ -992.4 ppm (relative to $Hg(CH_3)_2$) with a half-height line width($\Delta\nu_{1/2}$) of 242 Hz resulting from coupling of the ^{199}Hg nucleus (I = ½) to the quadrupolar ^{14}N nucleus (I = 1). Peak values were referenced to $Hg(CH_3)_2$ by first obtaining a spectrum of $Hg(NO_3)_2$ in D_2O and then setting its resonance to -2400 ppm relative to neat $Hg(CH_3)_2$ at δ 0 ppm After 20 minutes, the ^{199}Hg-NMR spectrum of the reaction mixture exhibited a peak for $Hg[N(SiMe_3)_3]_2$ as well as two sharper features at δ -1408 ppm ($\Delta\nu_{1/2}$ = 92 Hz) and δ -1452 ppm ($\Delta\nu_{1/2}$ = 95 Hz) with approximately equal intensities. After a reaction time of 2 hours, both resonances had decreased in intensity significantly, and after 3 hours the two peaks were only slightly visible relative to the baseline. The peaks were absent after a total reaction time of 4 hours.

A similar ^{199}Hg-NMR study involving the reaction of $Hg[N(SiMe_3)_3]_2$ with compound **2a** in a 1:1 ratio (in C_6D_6 at 25^{o}C) resulted in a spectrum with the same two sharp resonances appearing at δ -1408 ppm ($\Delta\nu_{1/2}$ = 102 Hz) and δ -1452 ppm ($\Delta\nu_{1/2}$ = 100 Hz) after 20 minutes. In this case however, the peak intensity of the upfield peak at -1452 ppm was twice that of the resonance at δ -1408 ppm, indicating that the former feature arises as a result of the formation of the monomercurated intermediate **A**. After 4 hours of reaction time, both resonances were absent. Subsequent spectra acquired in

regular 1 hour intervals over the course of a 24 hour period for the reaction of **2a** with both one and two equivalents of $Hg[N(SiMe_3)_2]_2$ resulted in no additional features.

The proposed intermediates **A-D** shown in scheme 3 are presumed to be generated via an intramolecular reaction between the $–OHg[N(SiMe_3)_2]$ moiety and the carbon atom at the 9-position of the adjacent naphthyl ring, with precedence for these reactions having been observed for several related systems.[101-103] The first step in the intramolecular electrophilic aromatic substitution reactions involves the formation of the two donor-acceptor π-complexes A and B, resulting in intensely colored solutions observed throughout the initial phases of the reactions. Our spectroscopic studies suggest that these intermediates are present for several hours, as the reactions slowly undergo conversion to their corresponding Wheland intermediates (σ-complexes,C and D), which is consistent with other electrophilic aromatic substitution reactions where the conversion of π-complexes to σ-complexes has been shown to be a slow process.[104-106] The conversion of π – to σ-complexes in electrophilic aromatic substitution reactions are known to occur in a stepwise fashion[105-109] and the charge transfer π-complexes involving mercury(II) have been shown to be colored species.[101,102] Another possible reaction pathway involves the formation of radical species, but this does not appear to occur in this system since irradiation by UV light is not required for the reactions to occur[103] and no magnetic anomalies were observed when probing these reactions by ^1H NMR spectroscopy.

Absorbance spectra of the reaction mixtures of **2a-d** with 2 equivalents of $Hg[N(SiMe_3)_2]_2$ were acquired after a reaction time of 1.5 hours. At this point, the reaction solutions were intensely colored, and for each reaction a peak was observed at

342 nm, 345 nm, 347 nm and 348 nm for **2a-d** respectively, due to the presence of the π-complexes **A** and **B**. The observed bathochromic shift among the absorbance maxima is attributed to the increasing number of phenyl groups attached to the silicon atom throughout the reaction series **2a-d**, which makes the π-system more delocalized. Upon their formation, the Wheland intermediates **C** and **D** presumably eliminate $HN(SiMe_3)_2$ in a rapid reaction to give the C-Hg-O fused species **E** and **F**. Mercury metal is then extruded from the reaction leading to the formation of the interannular C-O bonds of **3a** and **4a** as shown in **Scheme 3.5**. Similar examples of this process have been reported for several phenolic systems bearing O-vinylmercury substituents,[110] as well as systems employing fluorinated benzene[111] or alkenyl acetates[112] as reagents. In these examples the application of heat led to the cleavage of the Hg-O bond and the formation of a new C-O bond resulting in the non-mercurated final products and mercury metal as a by-product.

The reaction of $Hg[N(SiMe_3)_2]_2$ with the more sterically encumbered Binaphthols **2b** (R = $SiMe_2Ph$), **2c** (R = $SiMePh_2$), and **2d** (R = $SiPh_3$) proceeded in an identical fashion to that of the reaction involving **2a,** as shown in **Schemes 3.1** and **3.2**. Analysis of the crude products of the reaction between **2b-d** and 1 equivalent of $Hg[N(SiMe_3)_2]_2$ using ^{1}H-NMR spectroscopy indicated the presence of both the pentacyclic (3b-d) and the hexacylic species (**4b-d**), as well as the starting materials (2b-d) in all three cases, with the hydroxyl resonances for **3b-d** being observed at δ 4.19, 4.15, and 4.36 ppm (respectively). The reaction of binaphthols **2b-d** with 2 equivalents of $Hg[N(SiMe_3)_2]_2$ cleanly furnished the hexacyclic derivatives **4b-d** with no evidence of the pentacyclic species and complete consumption of the starting materials as observed by ^{1}H-NMR

spectroscopy. Isolation of the hexacyclic derivatives **4b-d** resulted in yields of 84% (**4b**), 85% (**4c**) and 49% (**4d**).

Recrystallization of the three crude product mixtures from hot benzene resulted in X-ray quality crystals for both **4b** and **4c**, but not **4d**, as only an amorphous powder was obtained in this case. The ORTEP diagrams of **4b** and **4c** are shown below in **Figures 3.6** and **3.8** (respectively) and bond angles and distances are collected in **Tables 3.3** and **3.4**.

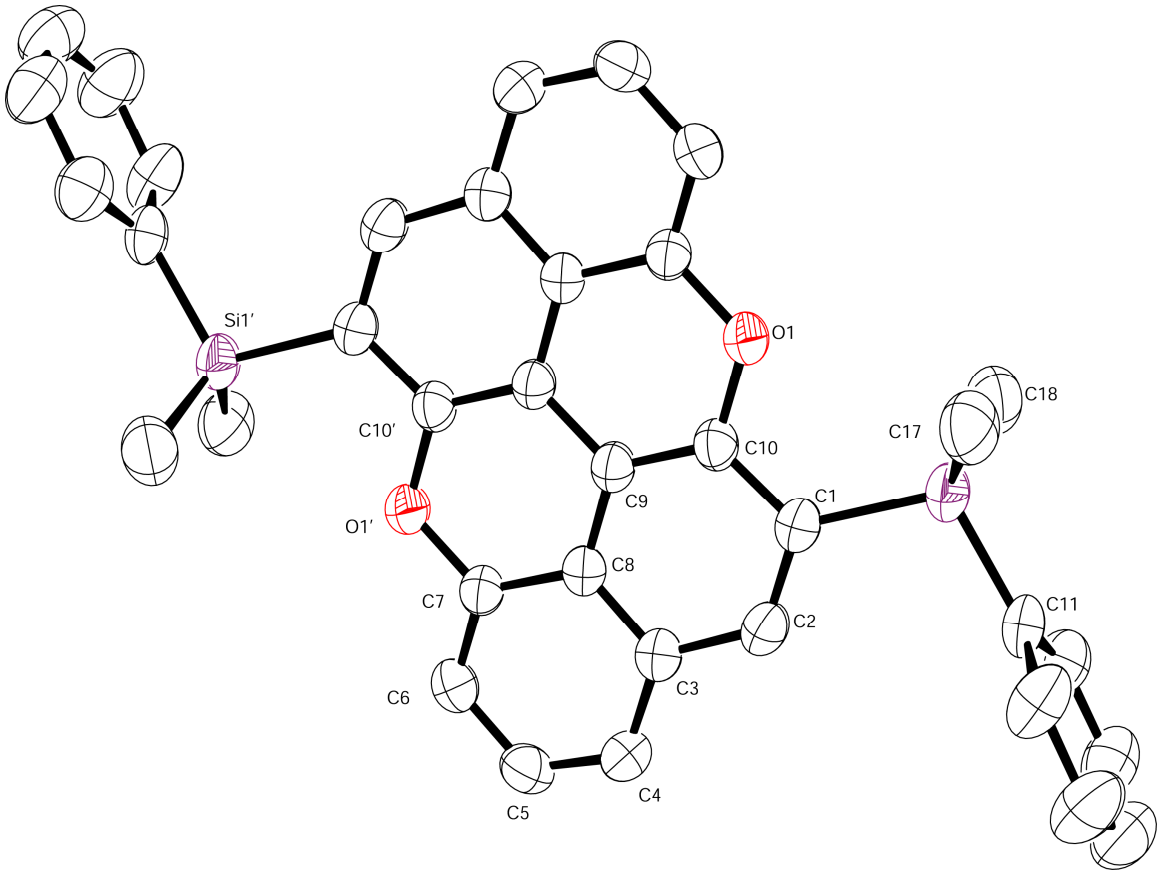

Fig. 3.6: ORTEP diagram of compound 4b. Thermal ellipsoids are drawn at 50% probability.

Table 3.3. Selected bond distances (Å) and angles (°) for compound **4b**.

Selected Bonds in 4b	**4b Bond Distances (Å)**
O(1) – C(10)	1.416(2)
O(1′) – C(7)	1.402(2)
Si(1) – C(1)	1.896(2)
C(1) – C(2)	1.384(2)
C(1) – C(10)	1.416(2)
C(2) – C(3)	1.427(2)
C(3) – C(4)	1.408(2)
C(3) – C(8)	1.411(2)
C(4) – C(5)	1.365(2)
C(5) – C(6)	1.401(2)
C(6) – C(7)	1.344(2)
C(7) – C(8)	1.417(2)
C(8) – C(9)	1.398(2)
C(9) – C(9′)	1.440(3)
C(9) – C(10)	1.372(2)
Selected Bonds in 4b	**4b Bond Angles (°)**
O(1) – C(10) – C(1)	117.3(2)
O(1) – C(10) – C(9)	120.4(2)
O(1′) – C(7) – C(6)	120.7(2)
O(1′) – C(7) – C(8)	118.5(2)
Si(1) – C(1) – C(2)	121.9(2)
Si(1) – C(1) – C(10)	122.2(2)
C(1) – C(2) – C(3)	124.5(2)
C(2) – C(3) – C(4)	125.2(2)
C(2) – C(3) – C(8)	116.3(2)
C(3) – C(4) – C(5)	119.9(2)
C(3) – C(8) – C(7)	119.6(2)
C(3) – C(8) – C(9)	120.5(2)
C(4) – C(5) – C(6)	121.7(2)
C(4) – C(3) – C(8)	118.4(2)
C(5) – C(6) – C(7)	119.5(2)
C(6) – C(7) – C(8)	120.8(2)
C(7) – C(8) – C(9)	119.9(2)
C(8) – C(9) – C(10)	120.5(2)
C(8) – C(9) – C(9′)	118.1(2)
C(9) – C(10) – C(1)	122.3(2)
C(10) – C(1) – C(2)	115.9(2)
C(10) – C(9) – C(9′)	121.4(2)
C(10) – O(1′) – C(7′)	119.6(2)

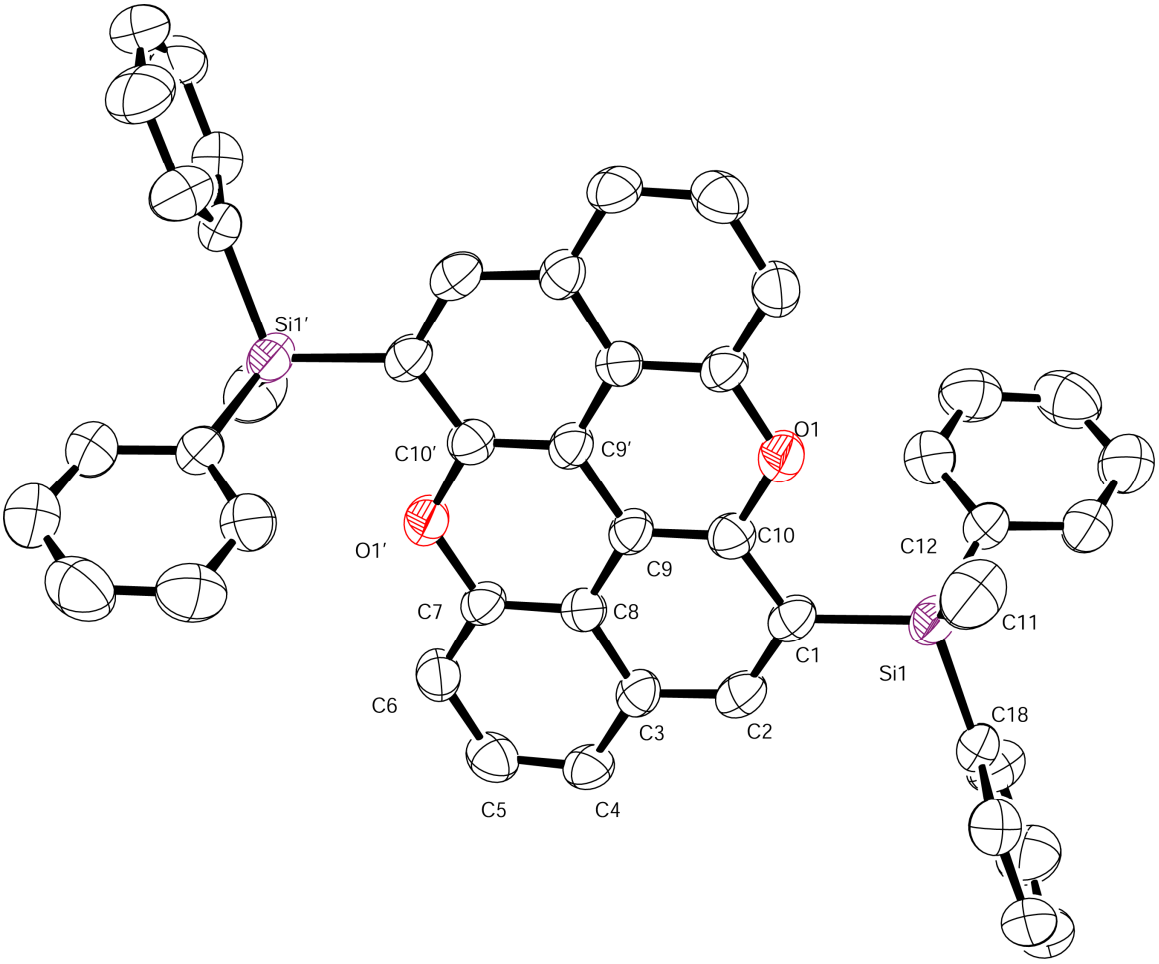

Fig. 3.7: ORTEP diagram of compound 4c. Thermal ellipsoids are drawn at 50% probability.

Table 3.4. Selected bond distances (Å) and angles (°) for compounds **4c**.

Selected Bonds in 4c	**4c Bond Distances (Å)**
O(1) – C(10)	1.399(3)
O(1′) – C(7)	1.402(3)
Si(1) – C(1)	1.879(3)
C(1) – C(2)	1.394(3)
C(1) – C(10)	1.416(3)
C(2) – C(3)	1.422(3)
C(3) – C(4)	1.408(3)
C(3) – C(8)	1.415(3)
C(4) – C(5)	1.363(4)
C(5) – C(6)	1.407(3)
C(6) – C(7)	1.356(3)
C(7) – C(8)	1.395(3)
C(8) – C(9)	1.405(3)
C(9) – C(9′)	1.439(5)
C(9) – C(10)	1.362(3)
Selected Bonds in 4c	**4c Bond Angles (°)**
O(1) – C(10) – C(1)	116.6(2)
O(1) – C(10) – C(9)	120.6(2)
O(1′) – C(7) – C(6)	117.6(2)
O(1′) – C(7) – C(8)	121.1(2)
Si(1) – C(1) – C(2)	122.7(2)
Si(1) – C(1) – C(10)	121.9(2)
C(1) – C(2) – C(3)	124.4(2)
C(2) – C(3) – C(4)	125.3(2)
C(2) – C(3) – C(8)	116.8(2)
C(3) – C(4) – C(5)	120.0(2)
C(3) – C(8) – C(7)	120.2(2)
C(3) – C(8) – C(9)	119.7(2)
C(4) – C(5) – C(6)	121.9(3)
C(4) – C(3) – C(8)	118.0(2)
C(5) – C(6) – C(7)	118.6(3)
C(6) – C(7) – C(8)	121.3(2)
C(7) – C(8) – C(9)	120.1(2)
C(8) – C(9) – C(10)	120.9(2)
C(8) – C(9) – C(9′)	117.7(3)
C(9) – C(10) – C(1)	122.8(2)
C(10) – C(1) – C(2)	115.4(2)
C(10) – C(9) – C(9′)	121.4(3)
C(10) – O(1′) – C(7′)	119.1(2)

As found in the structure of **4a,** the hexacyclic ring systems of **4b** and **4c** are planar with C_{2h} symmetry and similar bond lengths and angles to compound **4a**, indicating that an increase in the steric nature of the $-SiR_3$ group has little effect on the overall hexacyclic ring structure. The C-O bonds of **4a-c** are substantially longer than the two intracyclic C-O bonds of **3a** (1.383(2) and 1.380(2) Å) due to the planarity of the hexacyclic ring systems, which enforces an elongated carbon-oxygen contact. The presence of bulky trialkylsilyl substituents also results in longer C-O bonds in **4a-c** than are seen in the unsubstituted parent compound PXX (1.381(9) Å), due to their electron donating nature which results in an even more electron enriched aromatic environment.[87] Each of the three structures of **4a-c** contains individual molecules that are alligned via π-stacking interactions, such that there are they are arranged into columns along each of the three crystallographic axes **(see figures 3.8 and 3.9 shown below)**.

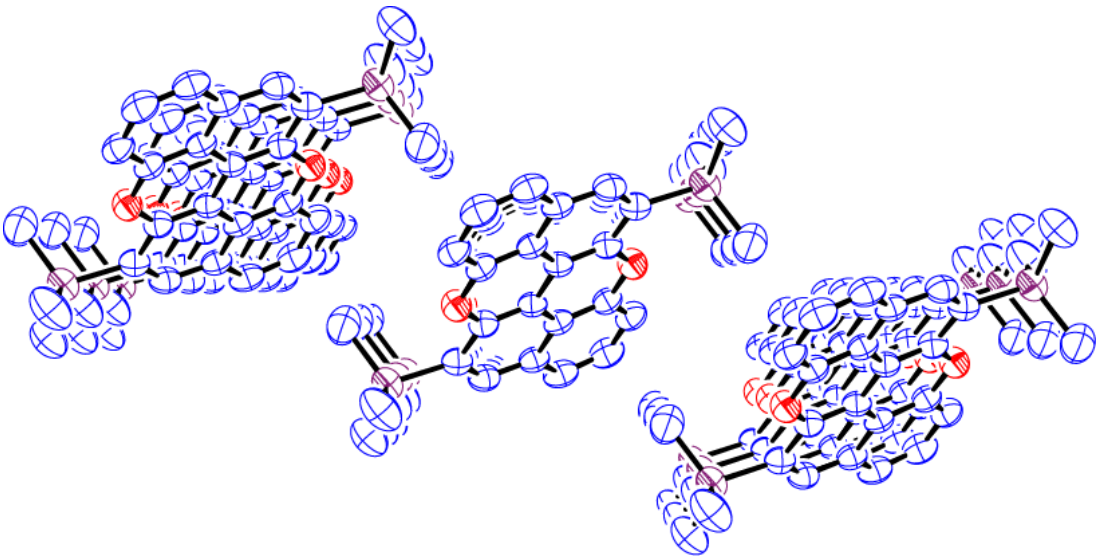

Fig. 3.8: ORTEP Stacking diagram of compound 4a (b-axis). Thermal ellipsoids are drawn at 50% probability.

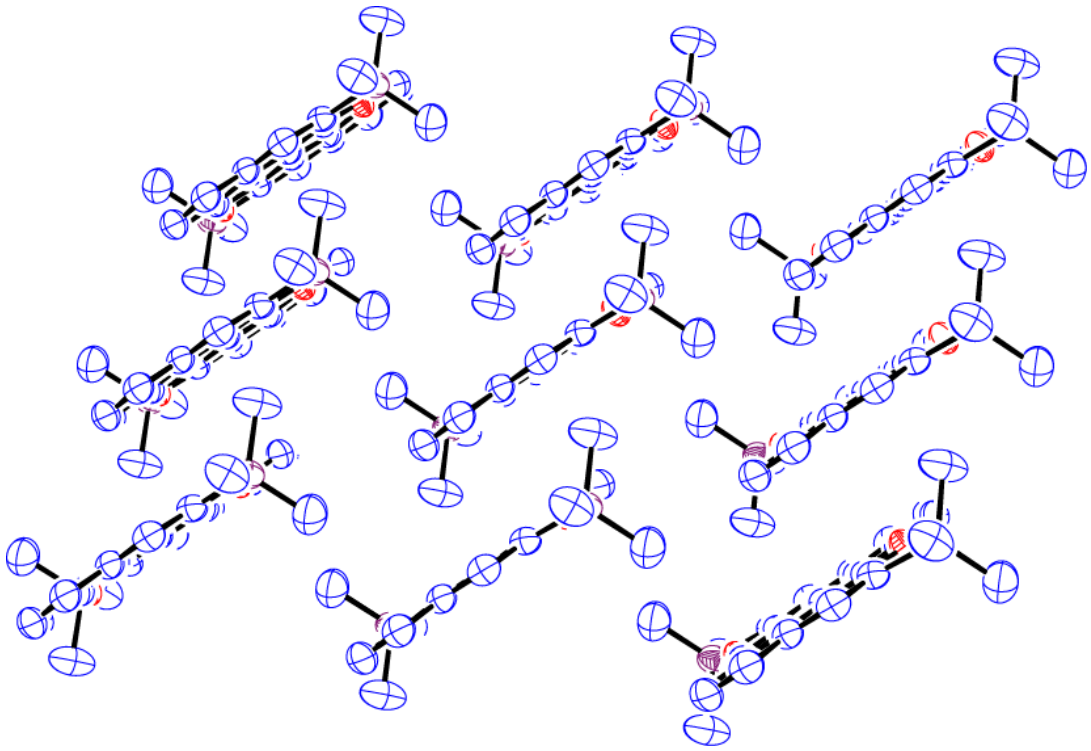

Fig. 3.9: ORTEP Stacking diagram of compound 4a (a-axis). Thermal ellipsoids are drawn at 50% probability.

Reaction of the unsubstituted binaphthol **2e** with 2 equivalents of $Hg[N(SiMe_3)_2]_2$ furnishes *peri*-xanthenoxanthene (6,12-dioxaanthanthrene, PXX), as confirmed by both ^{1}H-NMR and UV-Visible spectroscopy, in 79 % yield.[113] This is a significant improvement over the previous method of synthesis which consisted of reacting 1,1´-Bi-2,2´-Naphthol with $Cu(O_2CCH_3)$ to obtain a 52% yield.[100] A collection of absorbance data for PXX[113] and its 1,7-disubstituted derivatives (**4a-d**) are provided in **Table 3.5**.

Table 3.5 UV/visible data for PXX and **4a**-d (in C_6H_6 solution).

	λ_{max} (nm)	log ε		λ_{max} (nm)	log ε
PPX	313	3.67	**4a**	282	4.28
	327	3.83		293	4.26
	371	3.38		319	3.72
	392	3.71		334	3.92
	416	4.05		400	3.83
	443	4.17		425	4.20
				454	4.33
4b	281	4.25	**4c**	278	4.15
	293	4.17		293	4.06
	321	3.74		322	3.63
	335	3.92		337	3.83
	404	3.72		406	3.58
	428	4.09		431	3.96
	457	4.22		460	4.10
4d	279	4.21			
	293	4.07			
	323	3.67			
	337	3.70			
	407	3.29			
	432	3.38			
	462	3.36			

As anticipated the structurally similar compounds of **4a-d** have very similar absorbance spectra which contain several pronounced absorbance bands **(shown below in figure 3.10)** resulting from $\pi \rightarrow \pi^*$ transitions. These spectra are also similar to that of the spectrum for parent PXX molecule, with the main differences being that a slight bathochromatic shift is observed as the steric bulk at the silicon atom increases.

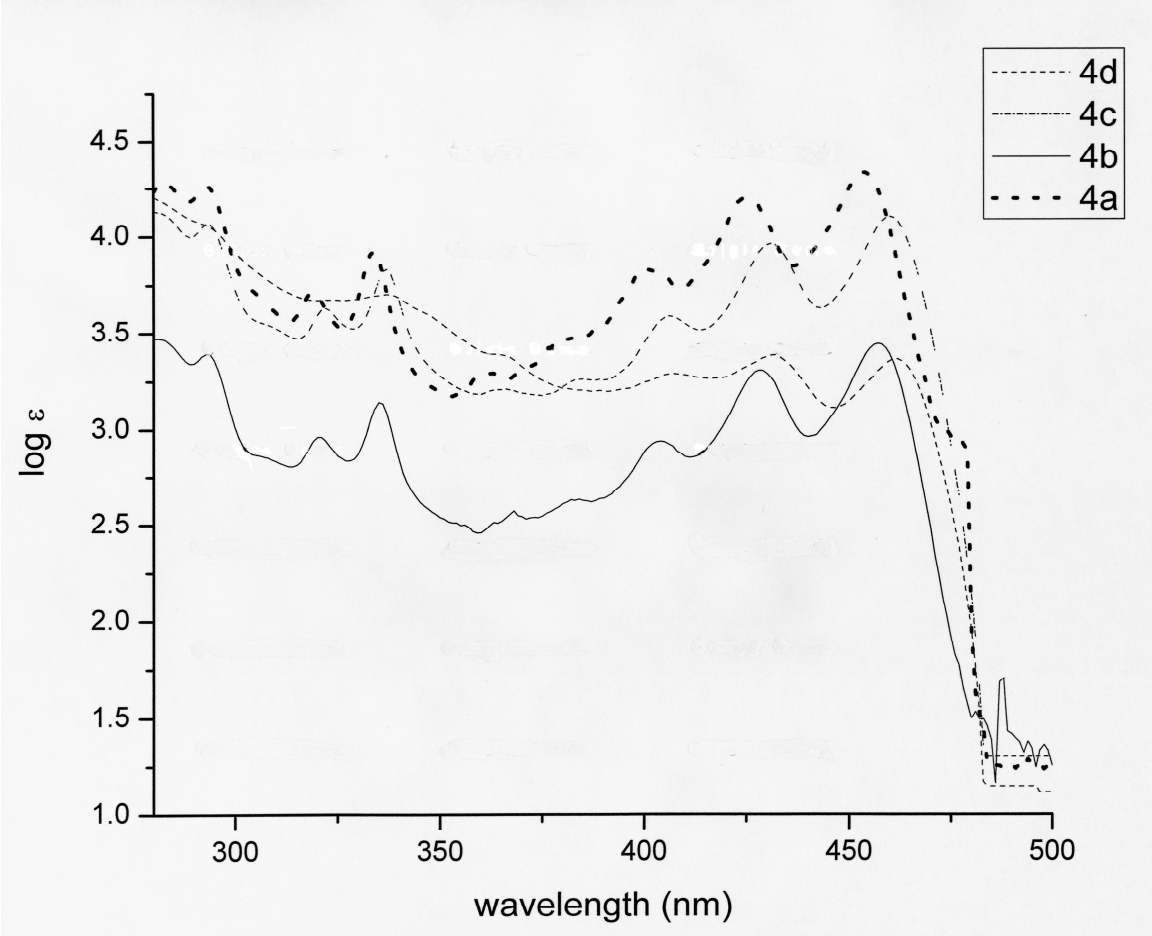

Figure 3.10: Absorbance sperctra for compounds **4a-d**.

Compounds **4a-d** were also observed to fluoresce in both solution (C_6H_6) and crystalline form. The solution emission data for **4a-d** in benzene are collected in **Table 3.6**, given below.

Table 3.6 Fluorescence data for compounds **4a-**d (in C_6H_6 solution).

Compound	$\lambda_{excitation}$	$\lambda_{emission}$	Compound	$\lambda_{excitation}$	$\lambda_{emission}$
4a	334	452	**4b**	335	452
		471			482
		483			515
		500			534
		529			573 (sh)
		566 (sh)			
4c	337	452	**4d**	338	459
		485			490
		527			519
		557 (sh)			538 (sh)
		585 (sh)			583 (sh)

Compound **4a** exhibited four well defined emission maxima between 450-500nm with an additional feature being observed at 529nm. The emission spectra obtained from compounds **4b-d** exhibit similar features to that of **4a** with the main differences being a slight red shift and the lack of defined bands at 500 and 529nm. Benzene solutions of all four species appear yellow-green in color when irradiated with a shortwave UVP lamp. Species **4c** and **4d** appeared more intensely yellow in color, which is attributed to the greater number of phenyl substituents, resulting in an increase in the possible number of $\pi \rightarrow \pi^*$ transitions.

The lighter congeners of $Hg[N(SiMe_3)_2]_2$, containing either zinc or cadmium, also react with the binaphthol **2a**. The reaction of 1 equivalent of $Cd[N(SiMe_3)_2]_2$ with **2a** exhibited similar behavior to that of the mercury(II) amide case, resulting in the formation of both compounds **3a** and **4a** as observed by ^{1}H-NMR. The spectrum also contains a resonance at δ 5.16 ppm corresponding to the cadmium analog of intermediate species **A** after heating at 85ºC for 48 h (scheme 1), indicating that this species remains in solution. The reaction also generated a gelatinous precipitate which is likely a polymeric

cadmium-binaphthol product. The reaction of $Cd[N(SiMe_3)_2]_2$ with 2 equivalents of **2a** also formed the gelatinous species as well as compound **4a**, the presence of which was indicated by ^{1}H-NMR.

The reaction of $Zn[N(SiMe_3)_2]_2$ with compound **2a** exhibited a drastically different outcome from that which was observed in the mercury and cadmium cases. Regardless of the stoichiometry employed, the reaction proceeds to furnish $HOC_{20}H_{10}(OSiMe_3)$-2′-$(SiMe_3)_2$-3,3′, were the source of the $–SiMe_3$ group is the $–N(SiMe_3)_2$ ligands of $Zn[N(SiMe_3)_2]_2$. Other metal(II) amides have shown similar reactivity with **2a** including the germanium derivative ($Ge[N(SiMe_3)_2]_2$)[70] and the group 2 and 14 compounds $M[N(SiMe_3)_2]_2$ (M = Be, Mg, Ca, Sn, Pb).[55]

Conclusions

The mercury(II) amide $Hg[N(SiMe_3)_2]_2$ has been employed to promote both single and double cyclization reactions of 3,3′-disubstitituted-1,1′-bi-2,2′-naphthols, resulting in the formation of five new compounds as well as the conversion of 1′1-bi-2,2′-napththol to the known species *peri*-xanthenoxanthene (PXX). The structures of the three 1,7-disubstituted PXX derivatives were obtained, and the pathway of the reactions was investigated, indicating that the cyclization reactions proceed via an intermolecular electrophilic aromatic substitution reaction. Reactions involving $Cd[N(SiMe_3)_2]_2$ proceed in a similar manner, furnishing similar products, while reactions using the zinc congener afford silyl ethers.

Experimental

General Considerations: *Caution! All compounds containing mercury or cadmium should be regarded as extremely toxic. Proper personal protective equipment is essential when handling these materials.* All air-sensitive compounds were manipulated using standard Schlenk line, syringe, and glovebox techniques.[72] The starting materials $Hg[N(SiMe_3)_2]_2$[79] and **2a-d**[73] were prepared according to literature methods or slight variations thereof. All solvents were dried and purified using a Glass Contour solvent purification system. ^1H and ^{13}C NMR spectra were recorded using a Varian Gemini 2000 instrument operating at 300 MHz (^1H) or 75.5 MHz (^{13}C). Spectral assignments for the ^1H NMR spectra of **4a-d** were made based on the numbering scheme shown below in **Figure 3.11**.

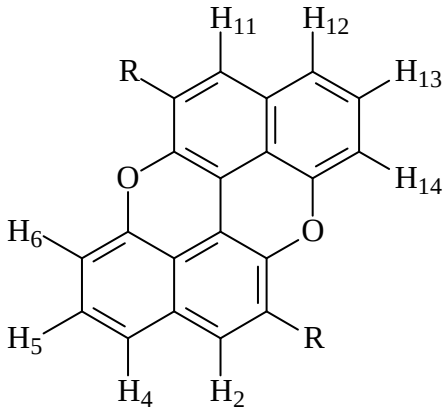

Figure 3.11: Numbering scheme for the ^1H-NMR spectra of **4a-d**

The ^{199}Hg spectra were recorded using a Varian Inova 400 instrument operating at 71.5 MHz and were referenced to a 1.0 M solution of $Hg(NO_3)_2$ in D_2O set at δ – 2400 ppm (relative to neat $Hg(CH_3)_2$ at δ 0 ppm).[114,115] UV-Visible spectra were obtained

using a Perkin Elmer Agilent UV/visible spectroscopy system with a benzene blank. Fluorescence spectra were acquired employing blank benzene solutions using a Horaba Fluorolog-3 instrument. Samples analyzed by GC/MS were run on a Shimadzu QP2010S instrument operating at 250 °C. Elemental analyses were conducted by Desert Analytics (Tucson, AZ).

Preparation of Compound 3a

To a solution of **1** (0.310 g, 0.594 mmol) in benzene (10 ml) in a Schlenk tube was added a solution of **2a** (0.258 g, 0.599 mmol) in benzene (10 ml) under N_2. The reaction mixture became dark yellow in color and turned dark purple/red after stirring for 2 h at 85 ºC. Heating was continued for 12 h after which time the reaction mixture had become yellow in color and beads of mercury metal were visible in the reaction vessel. The Schlenk tube was opened in air, the reaction mixture was filtered through Celite and the volatiles were removed *in vacuo* to yield an orange/yellow solid. Recrystallization of the crude product from hot benzene (5 ml) furnished **3a** (0.117 g, 45%) as transparent yellow crystals. ^{1}H-NMR(C_6D_6, 25 °C) δ 7.87 (s, 1H, C18-*H*), 7.76 (s, 1H, C2-*H*), 7.63 (d, *J* = 8.4 Hz, 1H, C14-*H*), 7.38 – 7.19 (m, 4H, aromatics), 7.06 (t, *J* = 7.5 Hz, 1H, C15-*H*), 6.85 (d, *J* = 7.5 Hz, 1H, C16-*H*), 4.20 (s, 1H, -O*H*), 0.54 (s, 9H, -Si(CH_3)$_3$), 0.52 (s, 9H, -Si(CH_3)$_3$) ppm. ^{13}C-NMR (C_6D_6, 25 °C) δ 136.9, 133.9, 130.5, 129.3, 128.2, 128.1, 127.9, 127.8, 127.5, 127.4, 127.3, 127.1, 124.7, 124.5, 124.2, 120.4, 119.6, 108.1, 10.1, 7.2, -0.6, -0.7 ppm. UV-Vis (C_6H_6, 25 °C): λ_{max} 282, 293, 319, 334, 400, 425, 454 nm. Anal. Calc. for $C_{26}H_{29}O_2Si_2$: C, 72.70; H, 6.81. Found: C, 72.62; H, 6.69%.

Preparation of Compound 4a

To a solution of **1** (0.242 g, 0.465 mmol) in benzene (10 ml) was added a solution of **2a** (0.100 g, 0.233 mmol) in benzene (10 ml) in a Schlenk tube under N_2. The solution became dark yellow in color and was dark purple/red after stirring for 1 h at 85 ºC. Heating was continued for an additional 24 h after which time the solution was green/yellow in color. The tube was opened in air, the reaction mixture was filtered through Celite, and the volatiles were removed *in vacuo* to yield a yellow solid which was recrystallized from hot benzene (5 ml) to furnish **4a** (0.0967 g, 97%) as transparent yellow crystals. ^{1}H-NMR spectra (C_6D_6, 25 °C) δ 7.38 (s, 2H, 2,11-*H*), 6.89 (m, 4H, 4,12-*H* and 5,13-*H*), 6.47 (d, *J* = 7.2 Hz, 2H, 6,14-*H*), 0.44 (s, 18H, -Si(CH_3)$_3$) ppm. ^{13}C-NMR (C_6D_6, 25 °C) δ 153.0, 132.3, 131.4, 129.1, 127.0, 122.9, 120.1, 111.0, 108.5, 1.3, -0.9 ppm. Anal. Calc. for $C_{26}H_{26}O_2Si_2$: C, 73.21; H, 6.15. Found: C, 73.33; H, 6.21%.

Reaction of 3a with an Additional Equivalent of $Hg[N(SiMe_3)_2]_2$

To a solution of **3a** (0.037 mg, 0.086 mmol) in benzene (5 mL) in a Schlenk tube was added a solution of **1** (0.045 g, 0.086 mmol) in benzene (5 mL) under N_2. The Schlenk tube was sealed and heated for 18 hours at 85 ºC. The tube was opened in air, the solution was filtered through Celite, and the volatiles were removed *in vacuo* to yield **4a** (0.032 g, 86%).

Preparation of 3b/4b

Compound **2b** was reacted with **1** in an identical fashion as for **2a**, using **2b** (0.100 g, 0.180 mmol) and **1** (0.094 g, 0.180 mmol) resulting in a mixture of **3b** and **4b** as shown by ^{1}H NMR spectroscopy.

Preparation of 3c/4c

Compound **2c** was reacted with **1** in an identical fashion as for **2a**, using **2c** (0.100 g, 0.147 mmol) and **1** (0.077 g, 0.148 mmol) resulting in a mixture of **3c** and **4c** as shown by ^{1}H NMR spectroscopy.

Preparation of 3d/4d

Compound **2d** was reacted with **1** in an identical fashion as for **2a**, using **2d** (0.100 g, 0.125 mmol) and **1** (0.065 g, 0.125 mmol) resulting in a mixture of **3d** and **4d** as shown by ^{1}H NMR spectroscopy.

Preparation of 4b

Compound **4b** was prepared in an analogous fashion as for **4a** using **2b** (0.254 g, 0.368 mmol) and **1** (0.477 g, 0.737 mmol). Yield of **4c**: 0.131g (84%). ^{1}H-NMR (C_6D_6, 25 °C) δ 7.65 – 7.63 (m, 4H, (*m*-C_6H_5)$SiMe_2$), 7.34 (s, 2H, 2,11-*H*), 7.32 – 7.20 (m, 8H, (*o*-C_6H_5)$SiMe_2$, (*p*-C_6H_5)$SiMe_2$, and 4,12-*H*), 6.77 (d, J = 4.8 Hz, 2H, 6,14-*H*), 6.38 (t, J = 4.8 Hz, 2H, 5,13-*H*), 0.68 (s, 12H, -SiPh(CH_3)$_2$) ppm. ^{13}C-NMR (C_6D_6, 25 °C) exhibited resonances at δ 137.8, 134.5, 133.4, 131.3, 129.4, 128.1, 127.6, 127.0, 123.0, 120.2, 111.1, 108.6, 102.6, 1.3, -2.1 ppm.

Preparation of 4c

Compound **4c** was prepared in an analogous fashion as for **4a** using **2c** (0.250 g, 0.368 mmol) and **1** (0.384 g, 0.737 mmol). Yield of **4c:** 0.213g (85%). ^{1}H-NMR (C_6D_6, 25 °C) δ 7.66 – 7.63 (m, 8H, -$SiMePh_2$ *meta*-H), 7.47 – 7.30 (m, 18H. aromatics), 6.98 (s,

2H, 2,11-*H*), 1.01 (s, 6H, Si*Me*Ph_2). ^{13}C NMR ($CDCl_3$, 25 °C) δ 135.5, 135.2, 134.6, 134.3, 134.2, 129.9, 129.7, 128.1, 127.9, 127.8, 127.2, 120.4, 109.0, 1.3, -2.6 ppm. UV-Vis (C_6H_6, 25 ºC): λ_{max} 278, 293, 322, 337, 406, 431, 460 nm. Anal. Calc. for $C_{46}H_{34}O_2Si_2$: C, 81.87; H, 5.08. Found: C, 81.60; H, 5.54%.

Preparation of 4d

Compound **4d** was prepared in an analogous fashion to **4a** using **2d** (0.250 g, 0.312 mmol) and **1** (0.325 g, 0.624 mmol). Yield of **4d**: 0.121g (49%). ^{1}H NMR ($CDCl_3$, 25 °C) δ 7.85 – 7.63 (m, 12H, -$SiPh_3$ *meta*-H), 7.61 – 7.10 (m, 26H, aromatics). ^{13}C NMR ($CDCl_3$, 25 °C) δ 136.7, 136.0, 125.8, 135.7, 135.6, 135.4, 130.5, 130.3, 129.9, 129.6, 128.4, 128.2, 128.0, 1.4 ppm. UV-Vis (C_6H_6, 25 °C): λ_{max} 279, 293, 323, 337, 407, 432, 462 nm.

Reaction of 1 with 2e

As for **4a,** compound **1** (0.728 g, 1.40 mmol) and 1,1′-Bi-2,2′-Naphthol **2e** (0.200 g, 0.699 mmol) were reacted to furnish *peri*- xanthenoxanthene (PXX, 0.156 g, 79%). ^{1}H-NMR (C_6D_6, 25 °C) δ 6.88 (d, J = 9.0 Hz), 2H, H_1), 6.81 (d, J = 4.8 Hz, 2H, H_6), 6.80 (d, J = 3.6 Hz, 2H, H_4), 6.69 (d, J = 9.0 Hz, 2H, H_2), 6.56 (dd, J = 3.6 Hz, J = 4.8 Hz, 2H, H_5) ppm. UV-Vis (C_6H_6, 25 °C): λ_{max} 290, 313, 327, 392, 416, 443 nm.

Reaction of 2a with 1 Equivalent of $Cd[N(SiMe_3)_2]_2$

A solution of $Cd[N(SiMe_3)_2]_2$ (0.025 g, 0.0578 mmol) in C_6D_6 (0.3 mL) was added to a solution of **2a** (0.025 g, 0.0580 mmol) in C_6D_6 (0.3 mL) and the progress of the reaction was monitored by ^1H NMR spectroscopy.

Reaction of 2a with 2 Equivalent of $Cd[N(SiMe_3)_2]_2$

A solution of $Cd[N(SiMe_3)_2]_2$ (0.201 g, 0.464 mmol) in C_6D_6 (0.5 mL) was added to a solution of **2a** (0.100 g, 0.232 mmol) in C_6D_6 (0.3 mL) and the progress of the reaction was monitored by ^1H NMR spectroscopy.

X-ray Structure Determination

Diffraction intensity data were collected with a Bruker SMART APEX II diffractometer. Crystallographic data and details of X-ray studies are shown in **Table 3.7**. Absorption corrections were applied for all data by SADABS. The structures were solved using direct methods, completed by difference Fourier syntheses, and refined by full matrix least squares procedures on F^2. All non-hydrogen atoms were refined with anisotropic displacement coefficients and hydrogen atoms were treated as idealized contributions. All software and sources of scattering factors are contained in the SHEXTL (6.1) program package (G. Sheldrick, Bruker AXS, Madison, WI). ORTEP diagrams were drawn using the ORTEP3 program (L. J. Farrugia, Glasgow).

Table 3.7 Crystallographic data for compounds **3a** and **4a-c**.

	3a	**4a**	**4b**	**4c**
Formula	$C_{26}H_{28}O_2Si_2$	$C_{26}H_{26}O_2Si_2$	$C_{36}H_{30}O_2Si_2$	$C_{46}H_{34}O_2Si_2$
Space group	$P2_1/c$	$P2_1/c$	P-1	$Pbca$
a (Å)	14.821(3)	6.6114(7)	8.3392(6)	16.751(4)
b (Å)	12.578(3)	8.5488(9)	9.3961(7)	12.492(3)
c (Å)	14.290(4)	20.676(2)	10.1356(6)	17.074(3)
α (°)	90	90	70.071(4)	90
B (°)	115.47(1)	94.993(8)	71.293(4)	90
γ (°)	90	90	73.480(4)	90
V (Å^3)	2404.9(1)	1164.2(2)	716.93(9)	3572.9(1)
Z	4	2	1	4
ρ_{calc} (g cm^{-3})	1.184	1.217	1.276	1.258
Temperature (K)	293	293	293	293
Radiation	Mo Kα	Mo Kα	Mo Kα	Mo Kα
Wavelength (Å)	0.71073	0.71073	0.71073	0.71073
R	0.0473	0.0513	0.0531	0.059
R_w	0.1126	0.1504	0.1078	0.1110

CHAPTER IV

SYNTHESIS AND STRUCTURE OF AN UNUSUAL GERMANIUM(II) CALIX[4]ARENE COMPLEX AND THE FIRST GERMANIUM(II) CALIX[8]ARENE COMPLEX AND THEIR REACTIVITY WITH DIIRON NONACARBONYL

Introduction

Calixarenes are highly useful macrocyclic compounds which have a variable cavity size and have a variety of applications in the areas of molecular self-assembly, ionic and molecular recognition and catalysis.[116-122] A number of transition-metal and main-group complexes using these species as ligands have been prepared.[123-143] These species include examples such as W(*t*-Bucalix[4]arene)Cl_2[123] and the bis(calix[4]arene-11,23-dicarboxylato) dirhodium complex **(Figure 4.1)**[140] for transition metals and phosphorous[131] and arsenic **(Figure 4.2)**[144] containing compounds for main group metals.

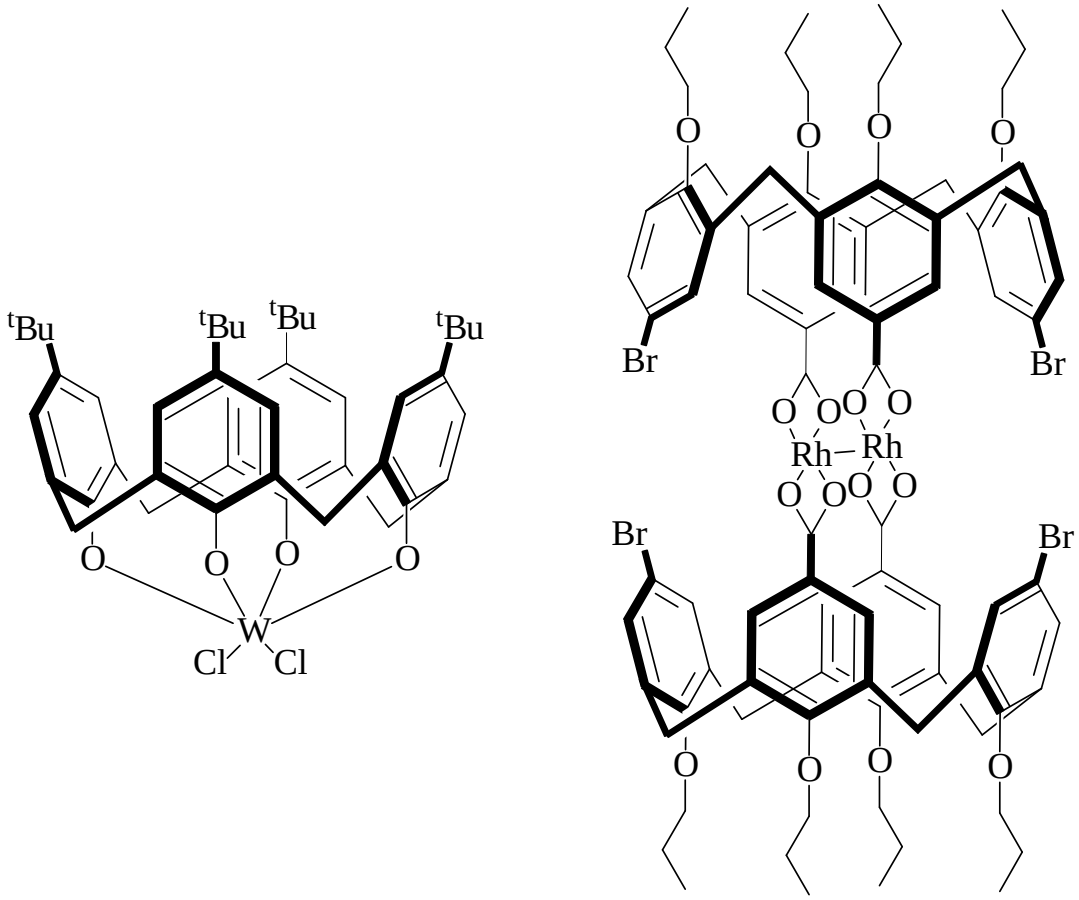

Figure 4.1: Structure of W(*t*-Bucalix[4]arene)Cl_2 and bis(calix[4]arene-11,23-dicarboxylato) dirhodium complex

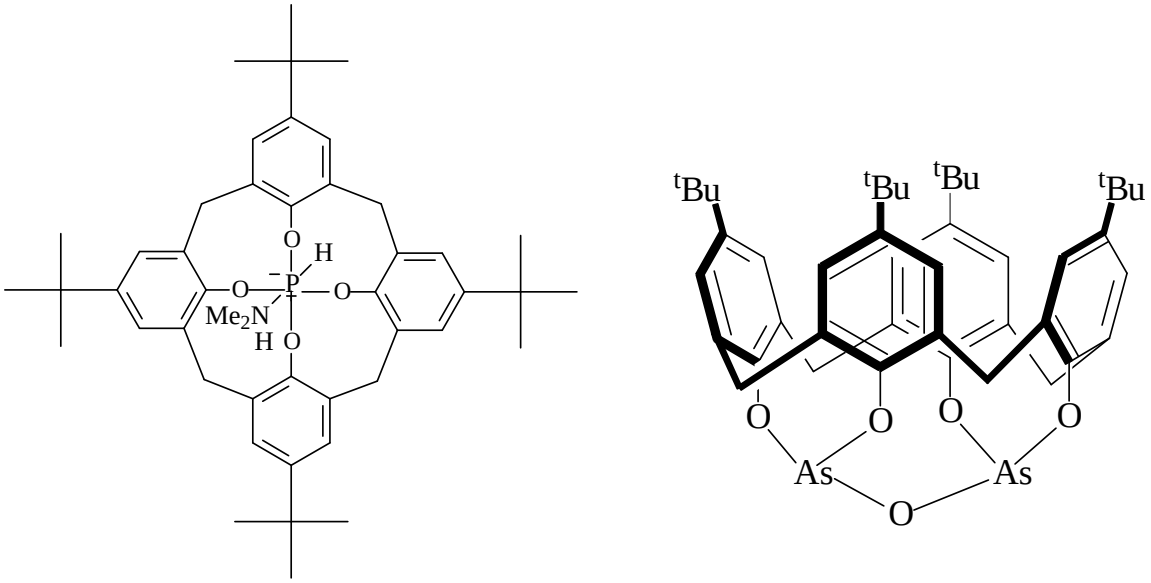

Figure 4.2: Structure of phosphorus containing ^{t}Bucalix[4]arene and arsenic containing ^{t}Bucalix[4]arene

Calixarene complexes containing germanium are rare[145-151] and prior to our investigations, only three materials having germanium bound directly to the calixarene oxygen atoms have been synthesized and structurally characterized.[145,147] These include the calix[4]arene complex [Bu^{t}calix]Ge_2, shown below if **Figure 4.3**, [147] and the two structural isomers of [Bu^{t}calix$^{(TMS)2}$]Ge shown if **Figure 4.4**.[145]

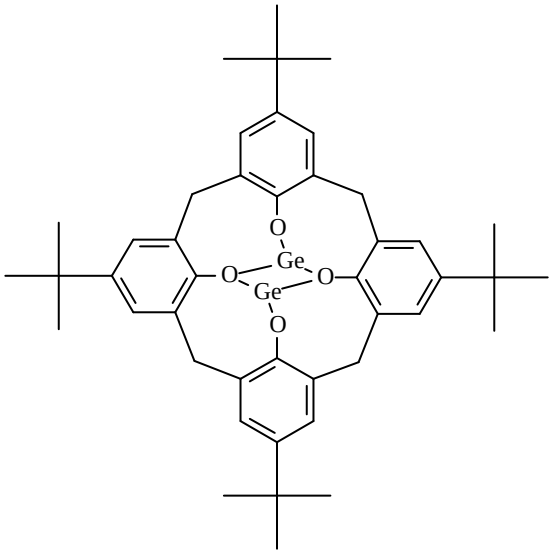

Figure 4.3: Structure of [Bu^{t}calix]Ge_2.

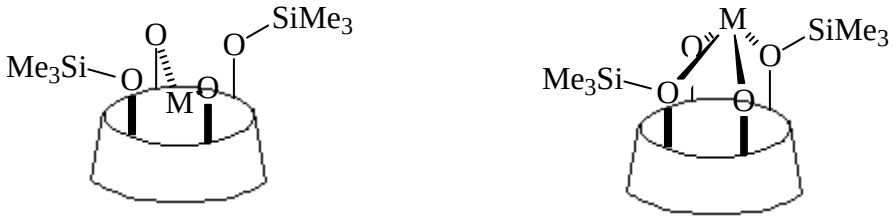

endo (M = Ge)

exo (M = Ge)

Figure 4.4: Structural isomers of [Bu^{t}calix$^{(TMS)2}$]Ge.

As part of an ongoing investigation of germanium aryloxide chemistry we have prepared the related unsubstituted germanium(II) calix[4]arene complex and also the first germanium calix[8]arene complex and have also determined the X-ray crystal structures of each.[54] All of the germanium(II) centers in both of these complexes have a lone pair of electrons available for donation to other metal centers, and thus these species could be

useful platforms for the support of multiple main-group or transition-metal fragments. We have investigated the reaction of both complexes with $Fe_2(CO)_9$, resulting in the formation of a germanium iron macrocycle containing eight iron atoms in the case of the germanium calix[8]arene compound.

Results and Discussion

Reaction of calix[4]arene with 2 equivalents of $Ge[N(SiMe_3)_2]_2$ furnishes the complex {calix[4]}Ge_2 **(1)** in 56% yield. The formation of **1** proceeds via a protonolysis reaction resulting the liberation of four equivalents of free $HN(SiMe_3)_2$. The structure of **1** has been determined and a reaction scheme and ORTEP diagram are shown below in **Scheme 4.1** and **Figure 4.5** respectively, while selected bond distances and angles are collected in **Table 4.1**.

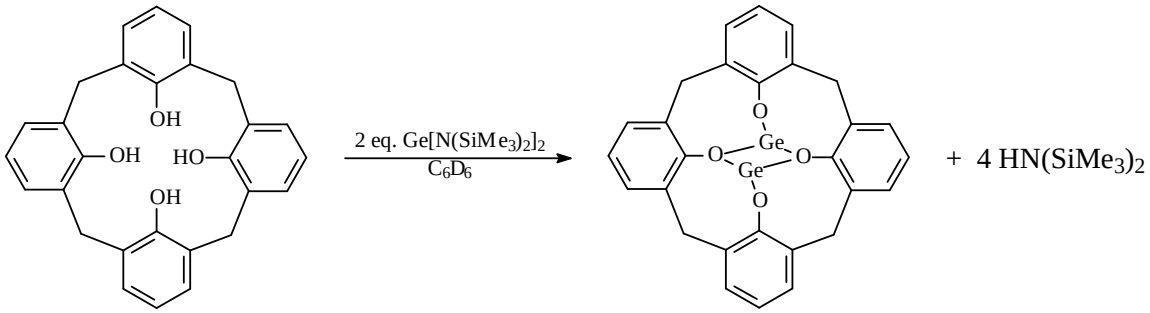

1

Scheme 4.1: Reaction of calix[4]arene with 2 equivalents of $Ge[N(SiMe_3)_2]_2$.

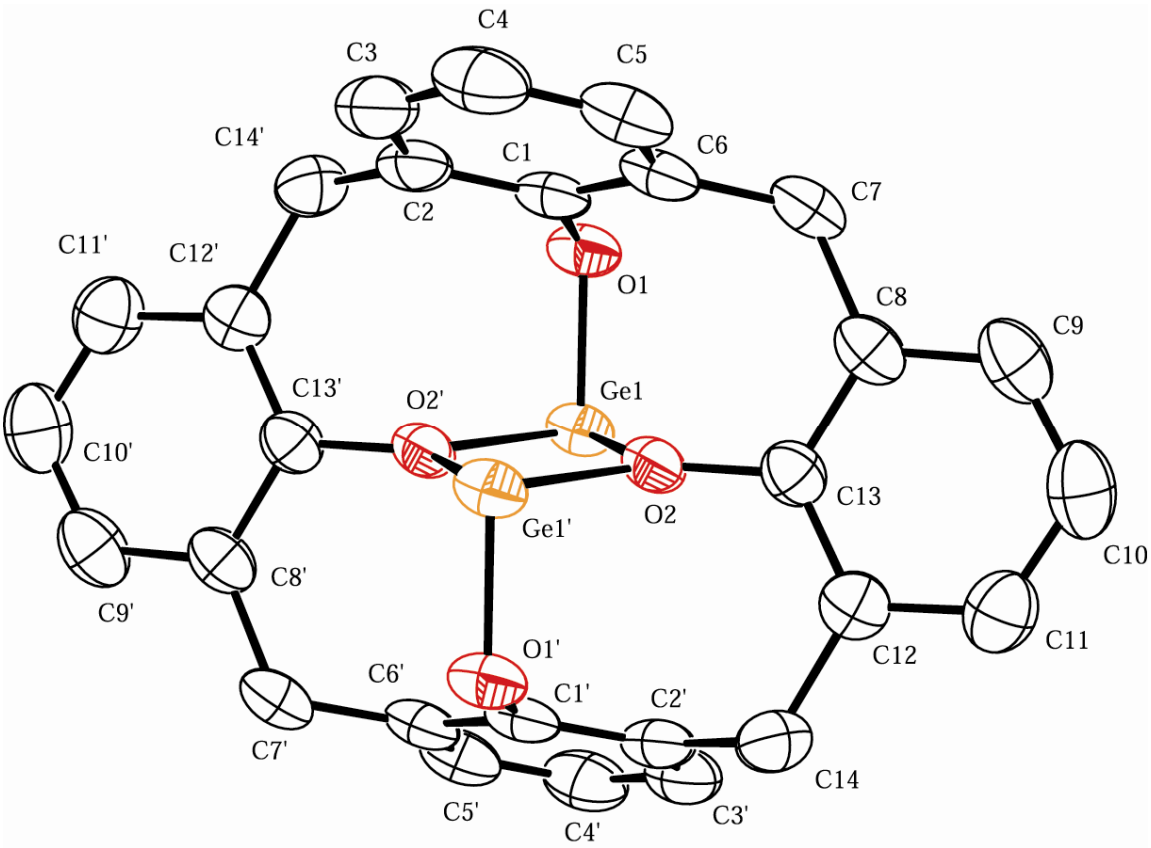

Figure 4.5. ORTEP diagram of **1**. Thermal ellipsoids are drawn at 50 % probability.

Table 4.1. Selected bond distances (Å) and angles (°) for compound **1**.

Ge(1) – O(1)	1.845(1)	Ge(1) – O(2) – Ge(1´)	107.89(6)
Ge(1) – O(2)	1.989(1)	O(1) – Ge(1) – O(2)	91.72(6)
Ge(1) – O(2´)	1.987(1)	O(2) – Ge(1) – O(2´)	72.11(6)
C(1) – O(1)	1.373(3)	Ge(1) – O(1) – C(1)	117.9(1)
C(13) – O(2)	1.385(2)	Ge(1) – O(2) – C(13)	126.5(1)

The two germanium centers are related by C_2 symetry, and each is bound to three different oxygen atoms. The shorter Ge(1)-O(1) distance is representative of a typical germanium(II)-phenolic oxygen bond whereas the elongated Ge(1)-O(2) and Ge(1)-O(2´)distance can be regarded as two dative O→ Ge(II) bonds which arise from donation of a lone pair of electrons on oxygen to the vacant p-orbital on germanium.[70,152-154] The germanium centers in **1** are formally in the +2 oxidation state, and the lone pairs of electrons present are stereochemically active and point out and away from the central Ge_2O_2 rhombus. The O_{term}-Ge-O_{br} and bond angles in **1** are close to the expected value of 90º, while the angles inside the central rhombus are 107.89(6)º for Ge(1)-O(2)-Ge(1´) and 72.11(6)º for O(2)-Ge(1)-O(2´). The aromatic rings attached to the O(1) and O(1´) atoms are bent back, such that they lie above Ge(1´) on the opposite side of the Ge_2O_2rhombus, and the closest contact between the ring carbons and the germanium atoms is 3.28 Å, indicating the absence of any Ge-C π-type interactions.

The bonding environment in the Ge_2O_2 rhombus (**Figure 4.6**) closely resembles that of the germanium(II) aryloxide compounds $[Ge(OC_6H_3(Pr^i)_2\text{-}2,6)_2]_2$ and $[Ge(OC_6H_2(Me)_32,4,6)_2]_2$, **Figure 4.7**, both of which contain bridging aryloxide groups.[154] The bond distances and angles for the Ge_2O_2 rhombi in these compounds are similar to that of compound **1** averaging 1.824(5)Å for the Ge-O_{term} bonds, 1.990(8)Å for the Ge-O_{br} bond lengths and 72.19(5)º for the average O_{br}-Ge-O_{br} angle.

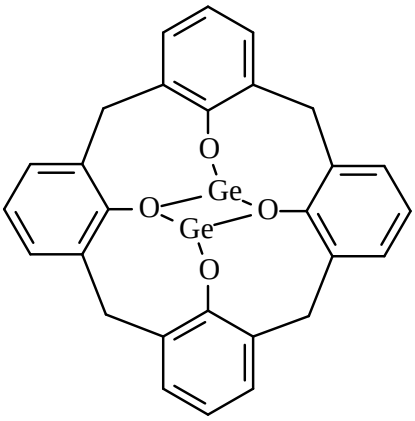

1

Figure 4.6: Structure of {calix[4]}Ge_2.

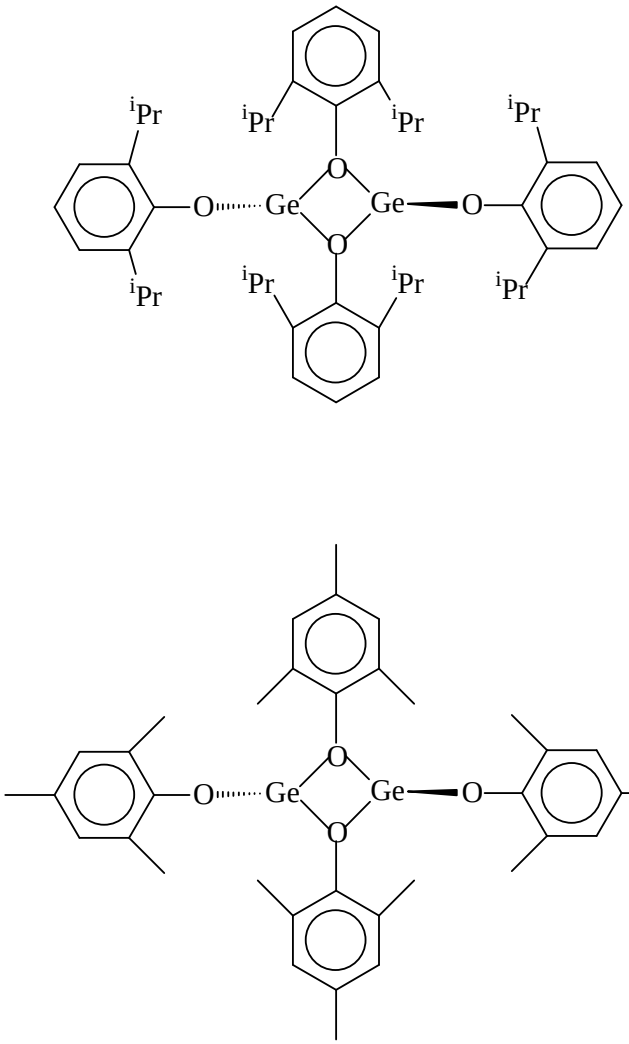

Figure 4.7: Structure of $[Ge(OC_6H_3(Pr^i)_2\text{-}2,6)_2]_2$ and $[Ge(OC_6H_2(Me)_32,4,6)_2]_2$.

Furthermore, the structure of **1** and the *tert*-butyl calix[4]arene ([Bu^{t}calix]Ge_2) **(2)**[147] are nearly identical, with these two species having the same Ge-O_{term} and Ge-O_{br} bond distances within experimental error averaging 1.833(1)Å and 1.999(8)Å respectively as well as the same O_{term}-Ge-O_{br} and O_{br}-Ge-O_{br} bond angles within experimental error averaging 92.1(8)° and 73.08° respectively. The structures of the two possible isomers of the only other crystallographically characterized germanium(II) calixarene [Bu^{t}calix$^{(TMS)2}$]Ge **(3)** differ considerably from **1** and **2** in that **3** contains only one germanium atom and can adopt either an *exo* or an *endo* isomeric form.[145] In the *exo* isomer, the germanium atom is formally bound to the two unsubstituted oxygen atoms with Ge-O distances of 1.765(6) and 1.842(6) Å, and also exhibits long dative interactions with the oxygen atoms of the two –$OSiMe_3$ groups measuring 2.421(5) and 2.486(5) Å. In the *endo* isomer, the Ge-O distances are 1.841(5) and 1.853(5) Å and there are no dative interactions with the oxygen atoms of the trimethylsiloxy groups. The formal Ge-O single bonds in the *endo* isomer are similar to those of **1**, while the absence of elongated dative interactions are a result of the steric crowding of the –$OSiMe_3$ groups which point outward from the center of the macrocycle in **3**.

While free calix[4]arene undergoes a rapid exchange between cone and inverted cone configurations in solution,[155] the presence of the bridging oxygen atoms attached to the two germanium centers enforces structural rigidity in **1**. The ^{1}H-NMR spectrum obtained for **1 (Figure 4.8)** correlates with its solid-state structure, where resonances for protons directed toward the central Ge_2O_2 rhombus are shifted downfield versus those pointing away from this moiety, which are observed for both the *meta* and *para* protons of the aromatic rings. The two sets of bridging methylene units of the calix[4]arene

ligand system are also magnetically non-equivalent, where the protons attached to C(7) and C(14) directed toward the Ge_2O_2 rhombus give rise to a doublet at δ 4.41 ppm (J = 12.9 Hz), and those attached to these two carbon atoms and directed away from the Ge_2O_2 fragment appear as a doublet at δ 3.23 ppm (J = 12.9 Hz). The down field resonances associated with the protons directed towards the rhombus are a result of the magnetic anisotropy from both the π-systems of the aromatic rings and the germanium atoms.

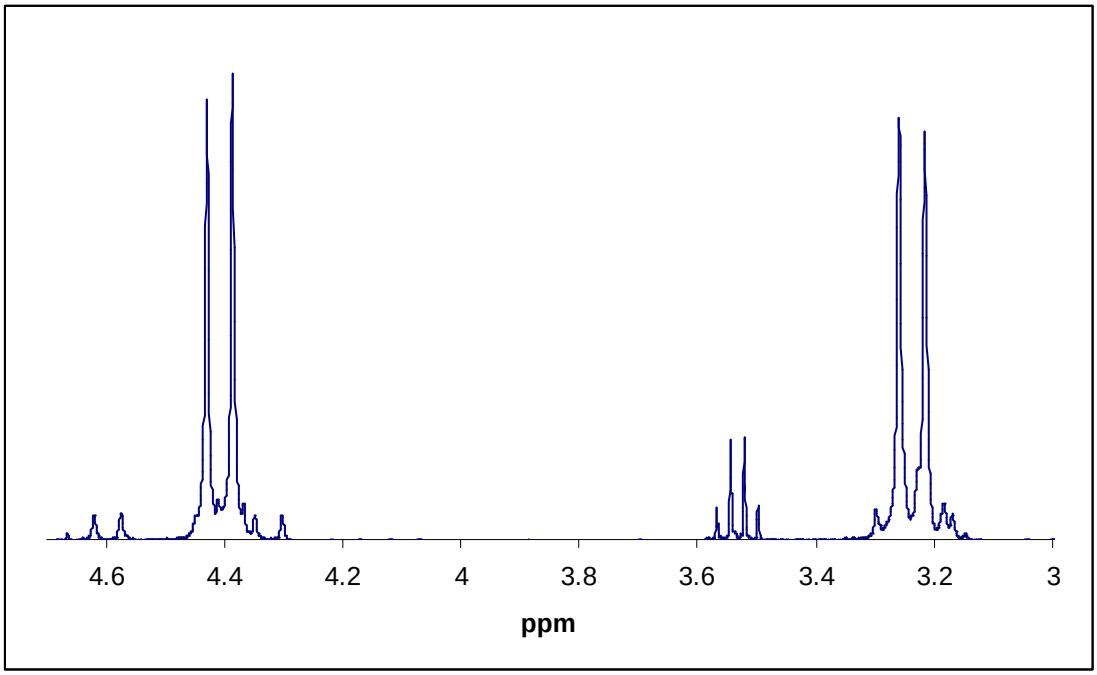

Figure 4.8: ^{1}H-NMR of expanded methylene region for compound **1**.

The pathway for the formation of **1** was determined to occur in a stepwise manner and was monitored using ^{1}H-NMR spectroscopy by the introduction of sequential aliquots of $Ge[N(SiMe_3)_2]_2$ to a solution of calix[4]arene in C_6D_6. The diagnostic resonances for this investigation were those of the bridging methylene units as well as the hydroxyl resonances of the calix[4]arene system. Calix[4]arene exhibits a singlet at δ

10.21 ppm in C_6D_6 arising from the four equivalent hydroxyl protons, and the methylene resonances for this compound appear as two broad features centered at δ 4.12 and 3.28 ppm due to the rapid interconversion of the macrocyclic ring system from a cone to an inverted cone configuration.[155] These correspond to the axial and equatorial $–CH_2$- groups, respectively.

Addition of 1 equivalent of $Ge[N(SiMe_3)_2]_2$ to a C_6D_6 solution of calix[4]arene results in the formation of two intermediate species **4** and **5** as well as the final product **1** **(Scheme 4.2)**.

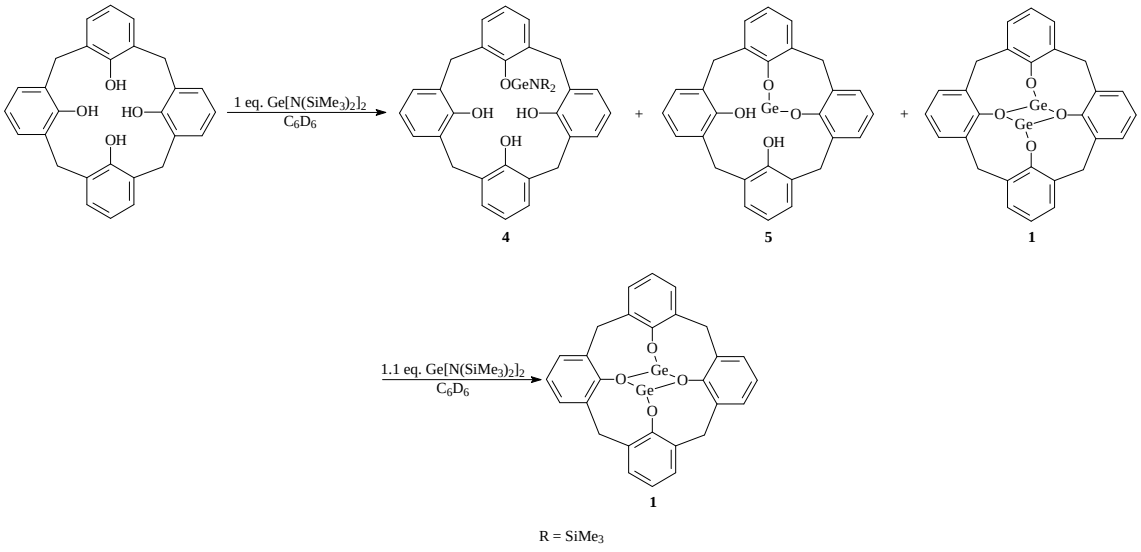

Scheme 4.2: Proposed pathway for the reaction of calix[4]arene with 1 and 2 equivalents of $Ge[N(SiMe_3)_2]_2$.

Two singlets for the nonequivalent –OH groups of **4** were visible at δ 9.50 and 9.18 ppm (intensity ratio 1:2) , while a third singlet at δ 7.74 ppm arises from the two equivalent –OH groups of **5**. The integrated intensity of the feature for **5** was approximately half of that of the two resonances observed for **4**. The feature at δ 10.21 ppm for the calix[4]arene starting material was also still present. The formation of **4** and **5** was also reflected in the signals for the methylene groups of the calix[4]arene system as there were six sets of doublets visible in the methylene region of the ^{1}H-NMR spectrum at this time. The signals at δ 4.41 and 3.23 ppm correspond to **1**, those at δ 4.38 (J = 12.9 Hz) and 3.26 (J = 13.8 Hz) ppm correspond to **4**, and those at δ 4.33 (J = 13.8 Hz) and 3.18 (J = 13.5 Hz) ppm correspond to **5**, where the assignments for **4** and **5** are based on the integrated intensities of the respective peaks. A singlet at δ 0.90 ppm was also visible due to the formation of $HN(SiMe_3)_2$, and a singlet at δ 0.28 ppm can be attributed to the trimethylsilyl groups of **4**. Addition of a further 0.5 equivalent of $Ge[N(SiMe_3)_2]_2$ to the NMR tube resulted in an increase in intensity of the hydroxyl resonance at δ 7.74 ppm for **5**, while the hydroxyl resonance for **4** and calix[4]arene were much less intense. The methylene resonances for **4** had also diminished, while those for **1** and **5** had increased in intensity. Increasing the amount of $Ge[N(SiMe_3)_2]_2$ to a slight excess of 2.2 equivalents resulted in the consumption of the remaining calix[4]arene starting material and complete conversion of **4** and **5** to compound **1 (Figure 4.9)**.

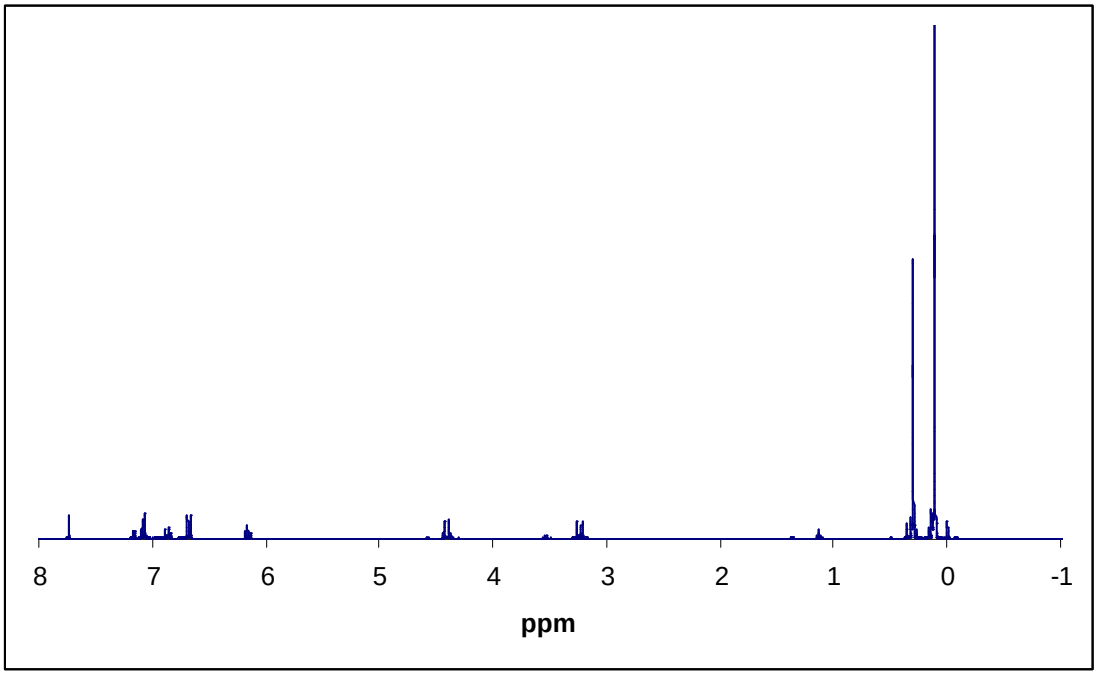

Figure 4.9: ^{1}H-NMR of compound **1**.

The reaction of calix[8]arene with 4 equivalents of $Ge[N(SiMe_3)_2]_2$ also proceeded via a protonolysis reaction that liberates $HN(SiMe_3)_2$, resulting in the formation of the tetragermanium species {calix[8]}Ge_4 **(6)** in excellent yield (89%) **(Scheme 4.3)**.

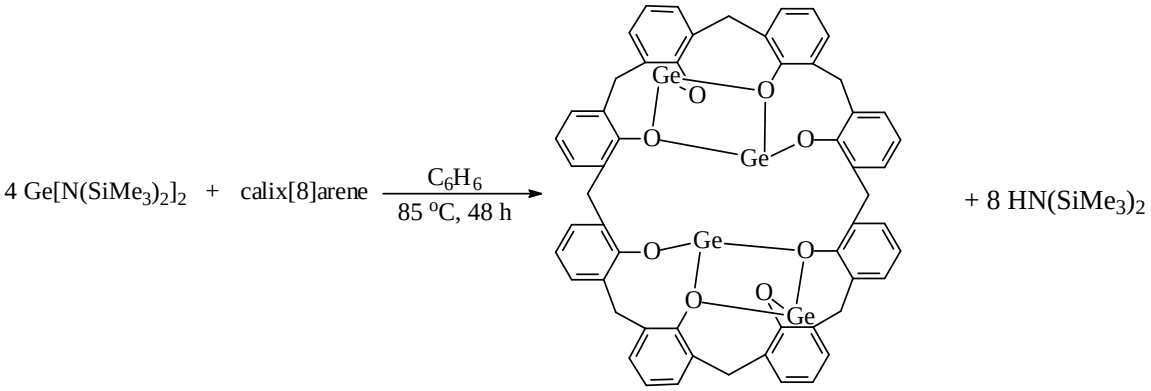

6

Scheme 4.3: Reaction of calix[8]arene with 4 equivalents of $Ge[N(SiMe_3)_2]_2$.

The structure of **6**·C_6H_6 was determined and an ORTEP diagram is shown in **Figure 4.10**, while selected bond distances and angles are collected in **Table 4.2**.

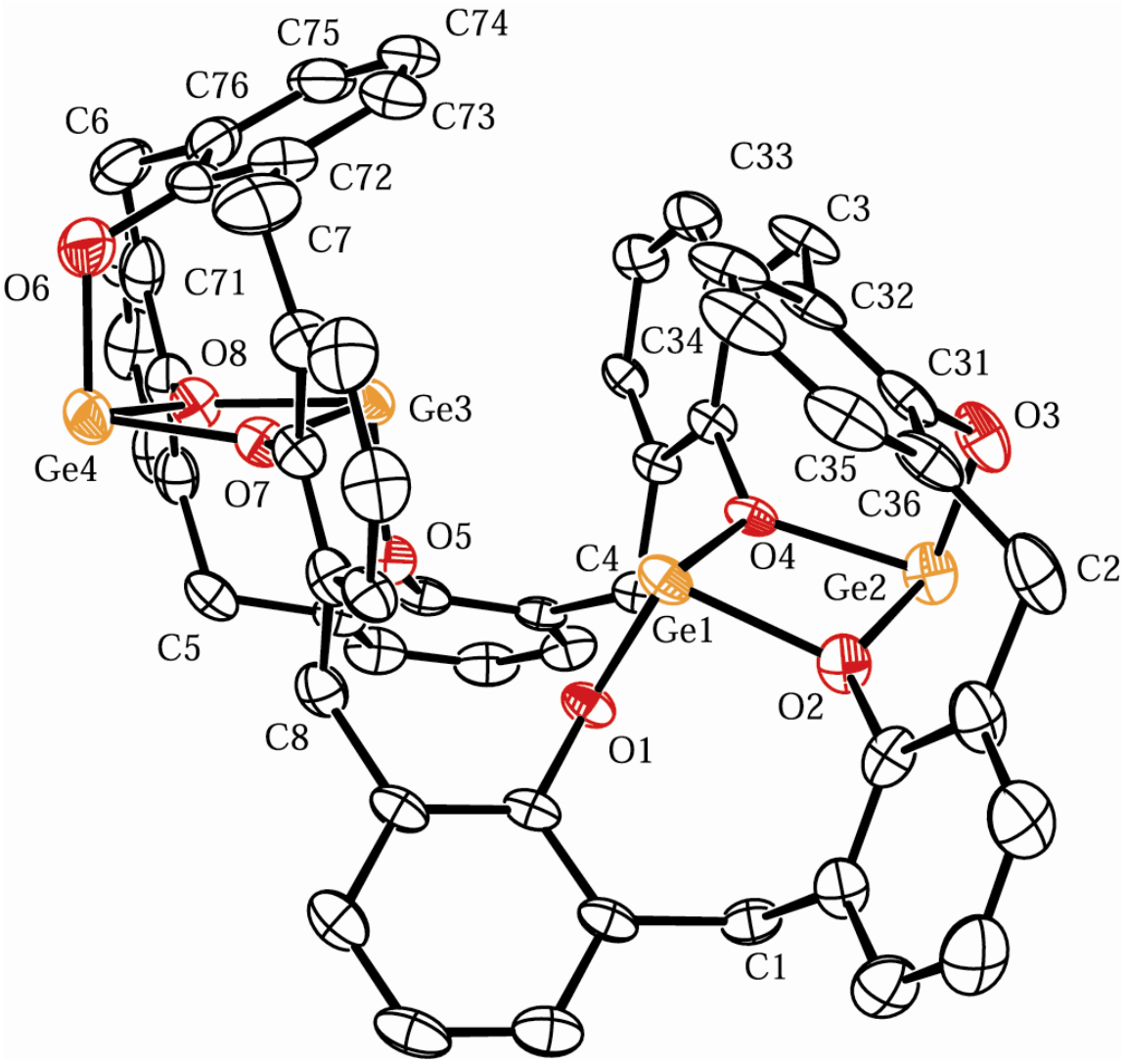

Figure 4.10. ORTEP diagram of **6**·C_6H_6. The benzene molecule is not shown, and thermal ellipsoids are drawn at 50 % probability.

Table 4.2 Selected bond distances (Å) and angles (°) for compound **6**·C_6H_6.

Ge(1) – O(1)	1.834(4)	O(1) – Ge(1) – O(2)	93.7(2)
Ge(1) – O(2)	2.036(3)	O(1) – Ge(1) – O(4)	90.9(1)
Ge(1) – O(4)	2.012(3)	O(2) – Ge(1) – O(4)	72.0(1)
Ge(2) – O(2)	1.970(3)	O(2) – Ge(2) – O(3)	94.4(2)
Ge(2) – O(3)	1.833(4)	O(3) – Ge(2) – O(4)	92.3(2)
Ge(2) – O(4)	2.000(3)	O(2) – Ge(2) – O(4)	73.6(1)
Ge(3) – O(5)	1.837(4)	O(5) – Ge(3) – O(7)	93.0(2)
Ge(3) – O(7)	2.019(3)	O(5) – Ge(3) – O(8)	92.1(2)
Ge(3) – O(8)	2.030(3)	O(7) – Ge(3) – O(8)	71.7(1)
Ge(4) – O(6)	1.828(4)	O(6) – Ge(4) – O(7)	95.2(2)
Ge(4) – O(7)	1.980(3)	O(6) – Ge(4) – O(8)	93.1(2)
Ge(4) – O(8)	1.953(4)	O(7) – Ge(4) – O(8)	74.2(1)
O(1) – C_{ipso}(11)	1.379(5)	Ge(1) – O(2) – Ge(2)	106.5(1)
O(2) – C_{ipso}(21)	1.401(5)	Ge(1) – O(4) – Ge(2)	106.3(1)
O(3) – C_{ipso}(31)	1.374(7)	Ge(3) – O(7) – Ge(4)	106.1(1)
O(4) – C_{ipso}(41)	1.401(5)	Ge(3) – O(8) – Ge(4)	106.7(1)
O(5) – C_{ipso}(51)	1.379(6)		
O(6) – C_{ipso}(71)	1.386(6)		
O(7) – C_{ipso}(81)	1.408(6)		
O(8) – C_{ipso}(61)	1.409(6)		

The four germanium atoms in **6** are assembled in pairs on opposite sides of the molecule, and each germanium is bound to three oxygen atoms to form rhombi in a similar fashion to **1**. The Ge-O bonds to the terminal oxygen atoms are all shorter than those to the bridging oxygens, which have an average distance of 1.833(4) Å that is considerably shorter than the corresponding distances in **1**.

Both of the Ge_2O_2 rhombi in **6** have essentially the same geometry, where the individual fragments are skewed such that one Ge-O_{br} distance is shorter than the other for each of the four germanium atoms **(Table 4.2)**. The O_{term}-Ge-O_{br} bond angles deviate significantly from 90º with an average value of 93.1(2)º while the O_{br}-Ge-O_{br} angles within the Ge_2O_2 rhombi have an average value of 72.9(2)º. The average Ge-O_{br}-Ge bond angle within the Ge_2O_2 fragments is 106.4(1)º. The Ge(1)-O(2)-Ge(2)-O(4) rhombus is puckered by 8.2º while the other fragment containing Ge(3)-O(7)-Ge(4)-O(8) is puckered by 7.3º, and this contrasts with the structure of **1** where the Ge_2O_2 moiety is completely planar. The overall shape of the molecule resembles a deep U-shaped bowl with two of the aromatic rings, containing C(31)-C(36) and C(71)-C(76) bent inward toward the center of the molecule. The distance between C(34) and C(74) at the smallest part of the top of the bowl measures 6.878Å. A wireframe diagram illustrating the structure of **6** is shown in **Figure 4.11**.

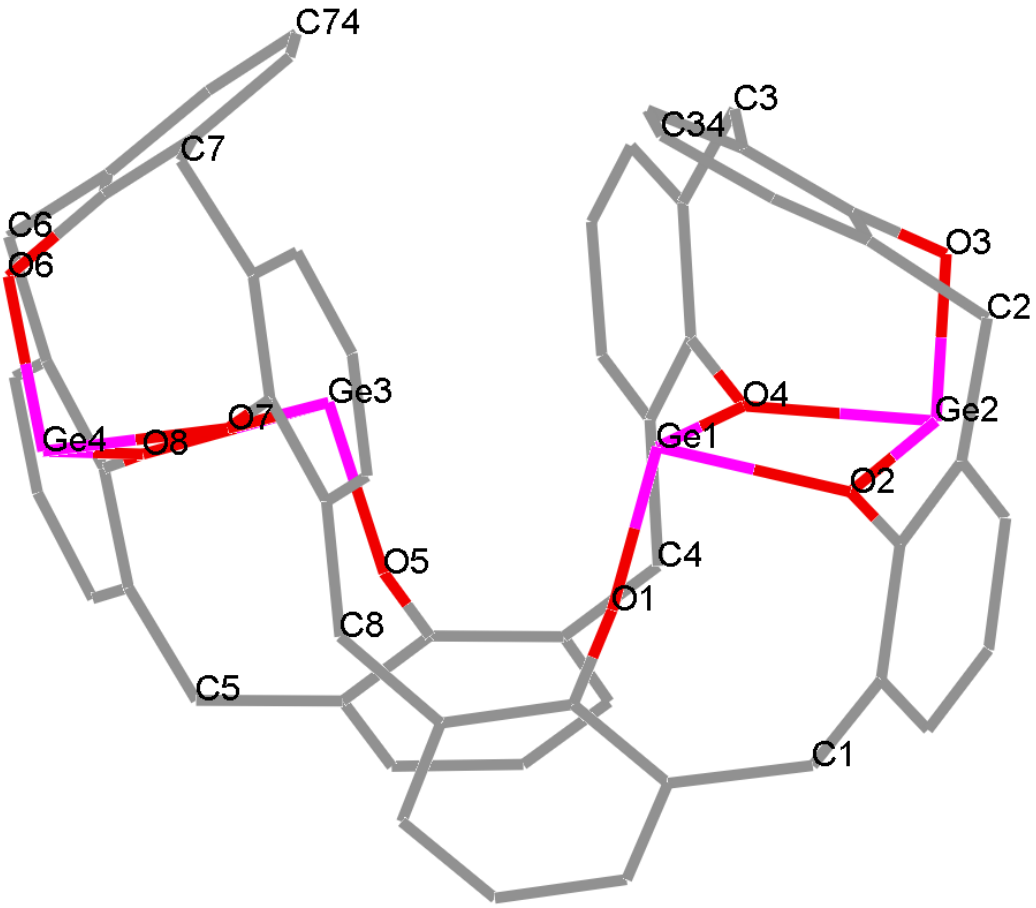

Figure 4.11. Wireframe drawing of **6**. The germanium atoms are drawn in blue, the oxygen atoms in red, and the carbon atoms in grey.

As found for **1**, the individual protons of the eight methylene groups in the calix[8]arene macrocycle are magnetically nonequivalent. Each methylene carbon contains 2 hydrogen atoms, labeled **A** and **B** corresponding to the hydrogen atom directed inwards towards the center of the molecule and away from the center of the molecule respectively. The presence of a C_2 axis of symmetry in solution results in the appearance of eight doublets for these protons in the ^{1}H-NMR spectrum **(Figure 4.12)** of **6**.

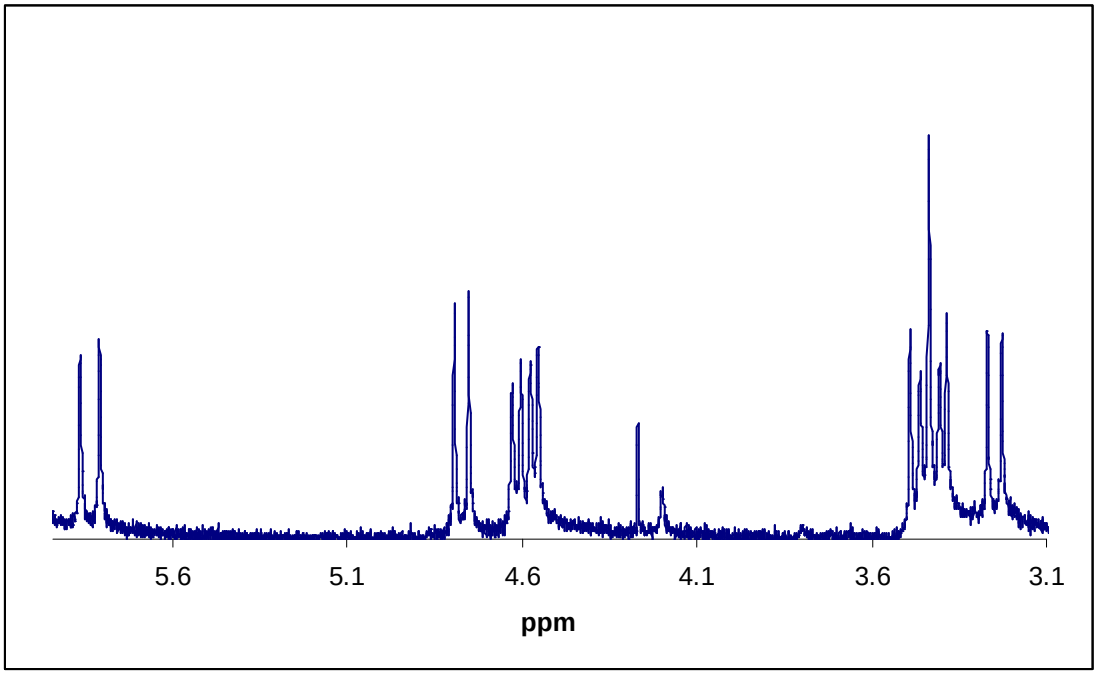

Figure 4.12: ^{1}H-NMR of methylene region for compound **6**.

One resonance appears far downfield at δ 5.73 ppm (J = 16.8 Hz) that can be attributed to the hydrogen atoms H(4a) and H(8a) bound to C(4) and C(8), which are located at the bottom of the bowl-shaped geometry of the molecule and point inward toward each of the

two Ge_2O_2 rhombi. In the solid-state structure of **6**, H(8a) has two close contacts with O(1) and O(5) measuring at 2.32(1) and 2.52(1) Å, respectively, while H(4a) has two similar close contacts O(1) and O(4) measuring 2.32(1) and 2.46(1) Å, respectively, all of which are within the sum of the van der Waals radii of hydrogen and oxygen (2.60 Å).[156] There are two additional close contacts between H(4a)-O(5) and H(8a)-O(1) measuring 2.67(1) and 2.60(1) Å, respectively. The proximity of these H´s to the Ge_2O_2 rhombi again led to a downfield shift resulting from anisotropic effects.

The hydrogen atom H(1a) has two close contacts with O(1) (2.48(1) Å) and O(2) (2.47(1) Å), and H(5a) has close contacts with O(5) and O(8) measuring 2.52(1) and 2.50(1) Å, respectively. These two protons, which are directed inward toward the Ge_2O_2 rhombi, result in the appearance of a doublet at δ 4.77 ppm (J = 12.6 Hz) in the ^{1}H-NMR of **6**, and a second set of closely spaced doublets at δ 4.60 ppm (J = 15.8 Hz) and 4.57 (J =15.0 Hz) ppm can be attributed to the four protons attached to C(2) and C(3) and C(6) and C(7), respectively, which are directed inward toward the two Ge_2O_2 rhombi. The remaining eight hydrogen atoms on each of the methylene groups are directed outward from the two Ge_2O_2rhombi and have chemical shifts in the range of δ 3.48-3.22 ppm. One feature appears upfield at δ 3.24 ppm (J = 12.6 Hz) arising from the two protons attached to C(1) and C(5) which are located at distances of 4.46 and 4.47 Å, respectively, from the centroids of the two Ge_2O_2 rhombi in **6**.

The presence of lone pairs of electrons on the four germanium(II) atoms in **6** renders this molecule a potentially useful platform for the support of multiple coordinatively unsaturated transition-metal centers. In order to investigate this postulate,

compound **6** was reacted with 4 equivalents of $Fe_2(CO)_9$, resulting in the isolation of a ruby-red solid in good yield (73%) **(Scheme 4.4)**.

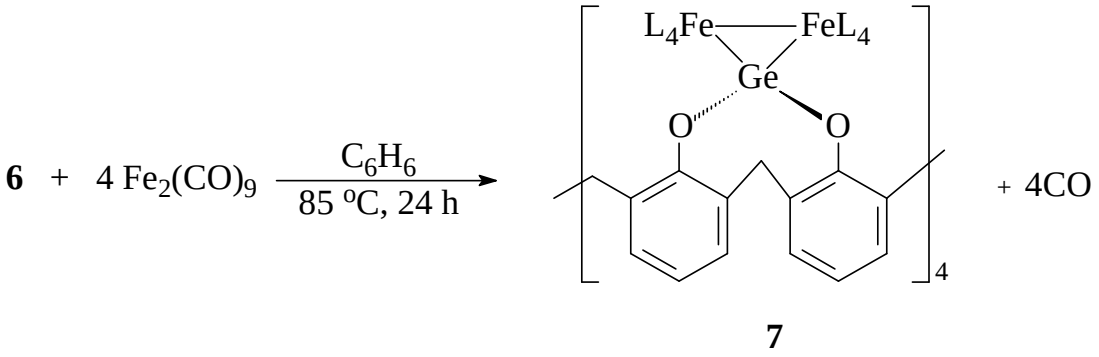

7

Scheme 4.4: Reaction of {calix[8]}Ge_4 with 4 equivalents of $Fe_2(CO)_9$.

The product was isolated and identified to be the octairon complex **7** upon obtaining its X-ray crystal structure. Compound **7** crystallizes with one molecule of benzene in the unit cell and an ORTEP diagram of **7** is shown in **Figure 4.13**, while selected bond distances and angles are collected in **Table 4.3**.

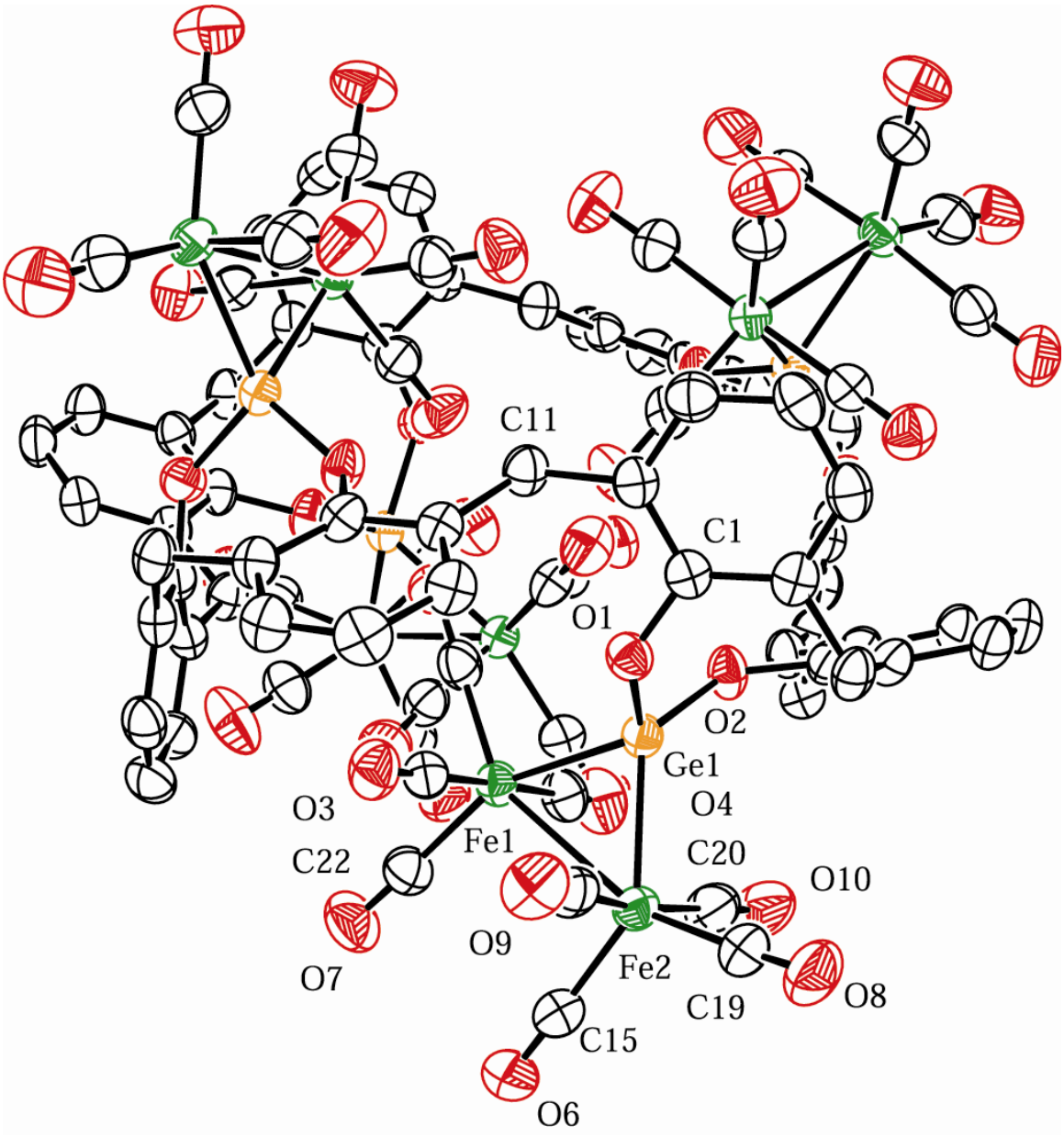

Figure 4.13. ORTEP diagram of the complete molecule of **7**·C_6H_6. The benzene molecule is not shown, and thermal ellipsoids are drawn at 50 % probability.

Table 4.3 Selected bond distances (Å) and angles (°) for compound **7**·C_6H_6

Ge(1) – O(1)	1.788(2)	O(1) – Ge(1) – O(2)	103.7(1)
Ge(1) – O(2)	1.772(2)	O(1) – Ge(1) – Fe(1)	116.77(7)
Ge(1) – Fe(1)	2.3543(5)	O(1) – Ge(1) – Fe(2)	119.70(7)
Ge(1) – Fe(2)	2.3244(6)	O(2) – Ge(1) – Fe(1)	115.91(7)
Fe(1) – Fe(2)	2.8407(6)	O(2) – Ge(1) – Fe(2)	124.55(8)
Fe(1) – C(16)	1.812(3)	Fe(1) – Ge(1) – Fe(2)	74.77(2)
Fe(1) – C(17)	1.810(4)	Ge(1) – Fe(1) – Fe(2)	52.14(2)
Fe(1) – C(18)	1.778(4)	Ge(1) – Fe(2) – Fe(1)	53.10(2)
Fe(1) – C(22)	1.826(4)	Ge(1) – Fe(1) – C(16)	90.6(1)
Fe(2) – C(15)	1.837(4)	Ge(1) – Fe(1) – C(17)	90.0(1)
Fe(2) – C(19)	1.791(4)	Ge(1) – Fe(1) – C(18)	96.3(1)
Fe(2) – C(20)	1.808(4)	Ge(1) – Fe(1) – C(22)	154.5(1)
Fe(2) – C(21)	1.806(4)	Ge(1) – Fe(2) – C(15)	140.5(1)
C(15) – O(6)	1.120(5)	Ge(1) – Fe(2) – C(19)	108.0(1)
C(16) – O(3)	1.131(4)	Ge(1) – Fe(2) – C(20)	85.9(1)
C(17) – O(4)	1.129(5)	Ge(1) – Fe(2) – C(21)	87.6(1)
C(18) – O(5)	1.150(4)		
C(19) – O(8)	1.125(5)		
C(20) – O(10)	1.140(5)		
C(21) – O(9)	1.139(5)		
C(22) – O(7)	1.121(4)		

The overall complex has fourfold symmetry, and the entire structure can be generated from the asymmetric unit which consists of a germanium atom, a $Fe_2(CO)_8$ moiety, two phenyl rings, and two methylene groups. The structure of this fragment is shown in **Figure 4.14**.

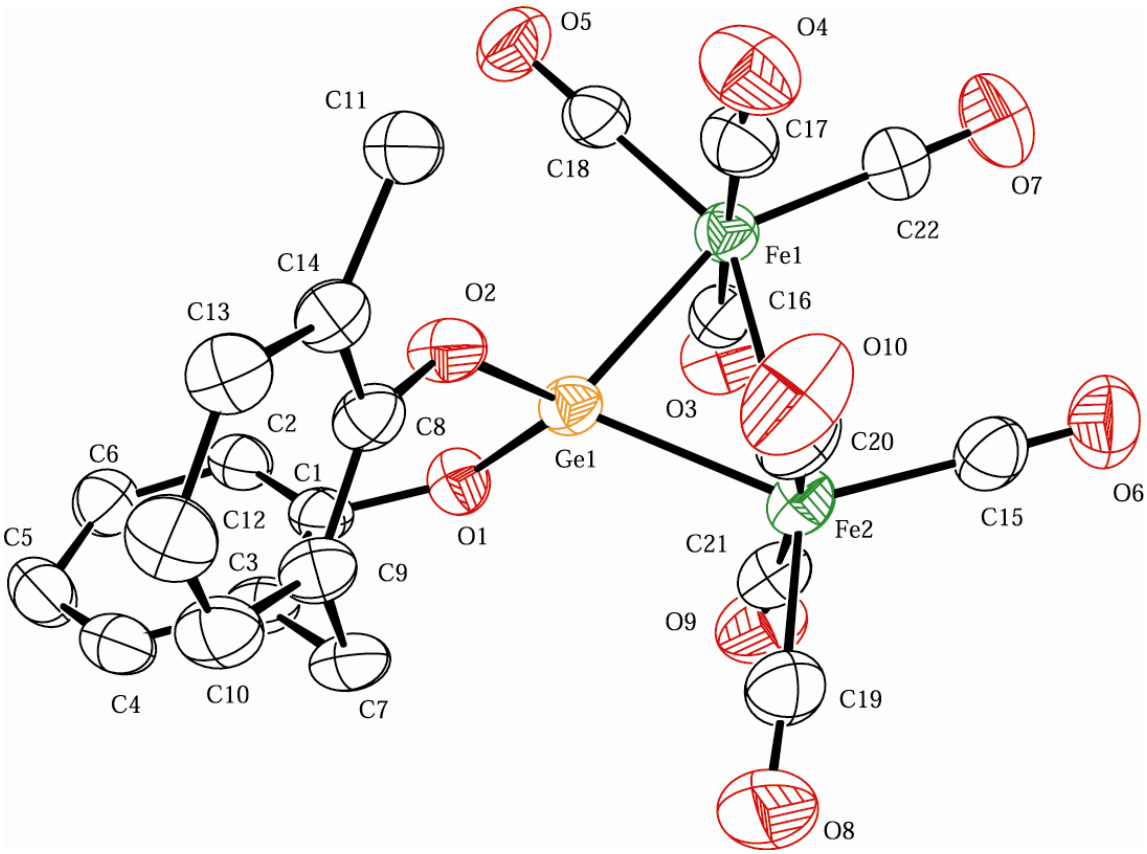

Figure 4.14. ORTEP diagram of the asymmetric unit of **7**·C_6H_6. Thermal ellipsoids are drawn at 50 % probability.

Initially, we expected the reaction of **6** with $Fe_2(CO)_9$ to affect cleavage of the Fe-Fe bond leading to the coordination of a $Fe(CO)_4$ moiety to each of the germanium centers with concomitant formation of free $Fe(CO)_5$, which was observed in the reaction of $(Bu^t_2$-2,6-Me-4-$C_6H_2O)_2Ge$ with $Fe_2(CO)_9$ resulting in the formation of **8 (Scheme 4.5)**.[157] A similar reaction was also observed in the reaction of {p-Bu^t_8calix[8]arene}Ge_4 with $Fe_2(CO)_9$, which yielded {p-Bu^t_8calix[8]arene}$Ge_4[Fe(CO)_4]_2$ (**9**) **(Scheme 4.6)**.[158]

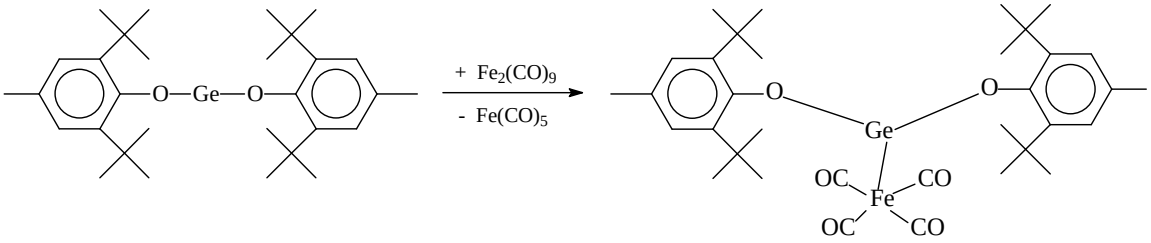

Scheme 4.5: Reaction of $(Bu^t_2$-2,6-Me-4-$C_6H_2O)_2Ge$ with $Fe_2(CO)_9$.

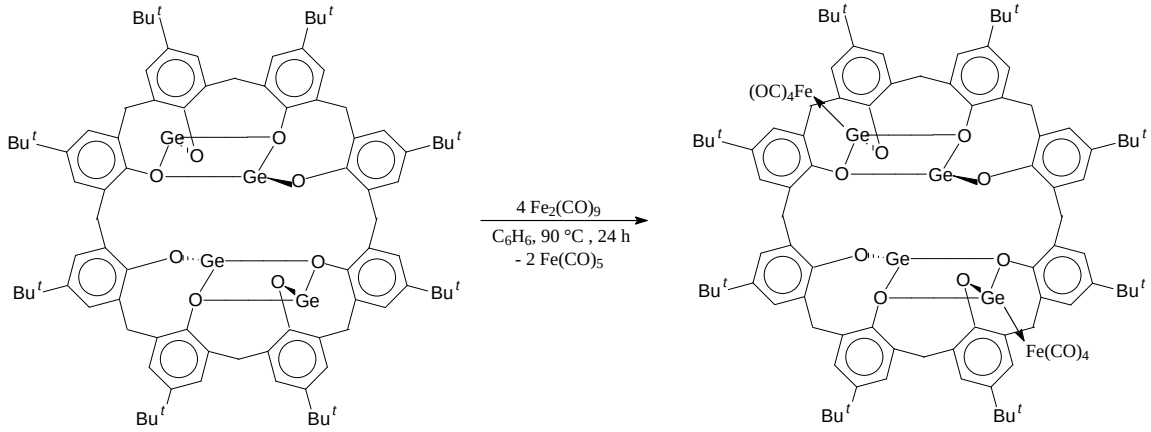

Scheme 4.6: Reaction of {p-Bu^t_8calix[8]arene}Ge_4 with $Fe_2(CO)_9$.

Instead, reductive decarbonylation involving extrusion of one bridging CO group from $Fe_2(CO)_9$ and formation of four triangular $GeFe_2$ three-membered rings was observed. The reaction involves formal oxidation of the Ge atoms from the +2 to the +4 oxidation state as the diiron fragments are regarded as $Fe_2(CO)_8^{2-}$ anions. The difference in the reactivity between **6** and the germylene complex **8** with $Fe_2(CO)_9$ likely stems from the electronic attributes of the Ge_2O_2 moieties versus a discrete germanium(II) atom in (Bu^t_2-2,6-Me-4-$C_6H_2O)_2Ge$. The oxidation state of germanium is clearly indicated by the Ge-O distances in **7**, which measure 1.772(2) and 1.788(2) Å and are representative of Ge(IV)-O single bonds. Each germanium center is, thus, formally bound to two oxygen atoms and any dative-type bridging interactions are absent, which is expected since germanium(IV) does not have a vacant p-orbital that can accommodate electron density from donor atoms or molecules; the p-orbital is available when it is in the +2 oxidation state.

Formation of **7** also results in the reduction of each of the formally zero valent iron atoms of $Fe_2(CO)_9$ to the -1 formal oxidation state with loss of one carbonyl ligand. Thus, the reaction of $Fe_2(CO)_9$ with the germanium atoms of the calix[8]arene complex can be regarded as a two-electron transfer from each of the four germanium centers to a bonded pair of iron atoms to generate the di-ferrate moiety. The $GeFe_2$ triangles are planar, and each of the iron atoms in these groups has approximate C_s symmetry. The iron-iron bond length in **7** is 2.8407(6) Å while the two Ge-Fe distances measure 2.3543(5) and 2.3244(6) Å. The Fe-Fe distance in the dianion of $[(Ph_3P)_2N]_2[Fe_2(CO)_8]\cdot 2CH_3CN$ is 2.787(2) Å,[159] which like **7** has no bridging carbonyl ligands. The introduction of μ_2-bridging germanium(IV) atoms results in an elongation

of the Fe-Fe bond due to electron donation from the $Fe_2(CO)_8^{2-}$ anion to the germanium(IV) metal center.

The germanium atoms of **7** are in a highly disordered tetrahedral environment enforced by the presence of the $GeFe_2$ moieties. The O(1)-Ge(1)-O(2) angle is compressed to 103.7(1)º from the ideal value of 109.5º , and the two O-Ge-Fe angles are widened to 119.70(7)º and 124.55(8)º. The Fe(1)-Ge(1)-Fe(2) angle is highly distorted from the ideal value measuring 74.77(2)º. The geometry at the germanium centers is a result of the presence of the strained $GeFe_2$ triangles, and the bond angles within these groups are also significantly distorted from their ideal values of 60º. The internal angles in the $GeFe_2$ triangles measure 52.14(2)º, 53.10(2)º, and 74.77(2)º for the Ge(1)-Fe(1)-Fe(2), Ge(1)-Fe(2)-Fe(1), and Fe(1)-Ge(1)-Fe(2) angles, (respectively), indicating the presence of significant angle strain in these moieties.

The spirocyclic complex $Ge[Fe_2(CO)_8]_2$ **(10)**[160-162] contains two $Fe_2(CO)_8^{2-}$ groups bridged by a bare germanium(IV) atom, and the structure of **10** has been reported on two separate occasions.[161,162] The two reported structures that were determined are nearly identical, with one having an average Ge-Fe distance of 2.40(1) Å and an average Fe-Fe bond length of 2.823(2) Å[161] and the other having average Ge-Fe and Fe-Fe distances of 2.407(2) and 2.823(3) Å, respectively.[162] The longer Ge-Fe and shorter Fe-Fe distances in **10** versus those in **7** are likely a result of the attachment of the two germanium atoms in **7** to electron-withdrawing phenolic oxygen atoms versus a second $Fe_2(CO)_8^{2-}$ moiety in **10.** The average Fe-Ge-Fe bond angle in **10** (among the two structure reports) is 71.9(1)º while the average Ge-Fe-Fe bond angle is 54.0(1)º,[161,162] both of which are more acute than the corresponding angles in **7** due to the spirocyclic geometry in **10**.

The geometries at the iron atom in **7** and **10** are identical but the C-O bond lengths in **7** are shorter than the corresponding distances in **10**,[161] again resulting from the germanium atoms in **7** being bond to electron-withdrawing phenolic oxygen atoms. The average bond distances for the C-O groups pointing outward from the $GeFe_2$ triangle (C(15)-O(6) and C(22)-O(7)) in **7** is 1.120(4) Å while the corresponding C-O groups for **10** have an average distance of 1.134(7) Å.[161] The three sets of C-O distances remaining in **7** average 1.135(4), 1.140(4), and 1.132(4) Å while the corresponding distances in **10** are 1.140(7), 1.138(7), and 1.148(7) Å.[161]

These differences are manifested in the infrared spectrum of **7** in CH_2Cl_2, which contains four carbonyl stretching bands at 2109, 2059, 2044, and 2020 cm^{-1}. This differs from the expected two bands that would be observed for the axial and equatorial CO ligands if the molecule where to have idealized C_{2v} symmetry. The presence of the large calix[8]areneGe_4 "ligand" however results in a reduction in symmetry from C_{2v} to C_s at each of the iron atoms, which leads to the four observable bands. Each of these bands appear at higher energy than the corresponding IR features for **10** in CH_2Cl_2 (2076, 2050, 2033, and 2011 cm^{-1}).[162] These structural and spectroscopic differences indicate that the C-O bonds in **7** are stronger than those in **10** since the $Fe_2(CO)_8^{2-}$ groups in **7** are more strongly bound to the germanium atoms than those in **10**, which results in less electron density for Fe-CO backbonding to the carbonyl groups.

The ^{1}H-NMR spectrum of **7** recorded in CD_3CN indicates that the molecule retains its rigid structure in solution. There are four doublets for each of the magnetically nonequivalent methylene protons **(Figure 4.15)** of **7**, as also found in the ^{1}H-NMR spectra of compounds **1** and **6**.

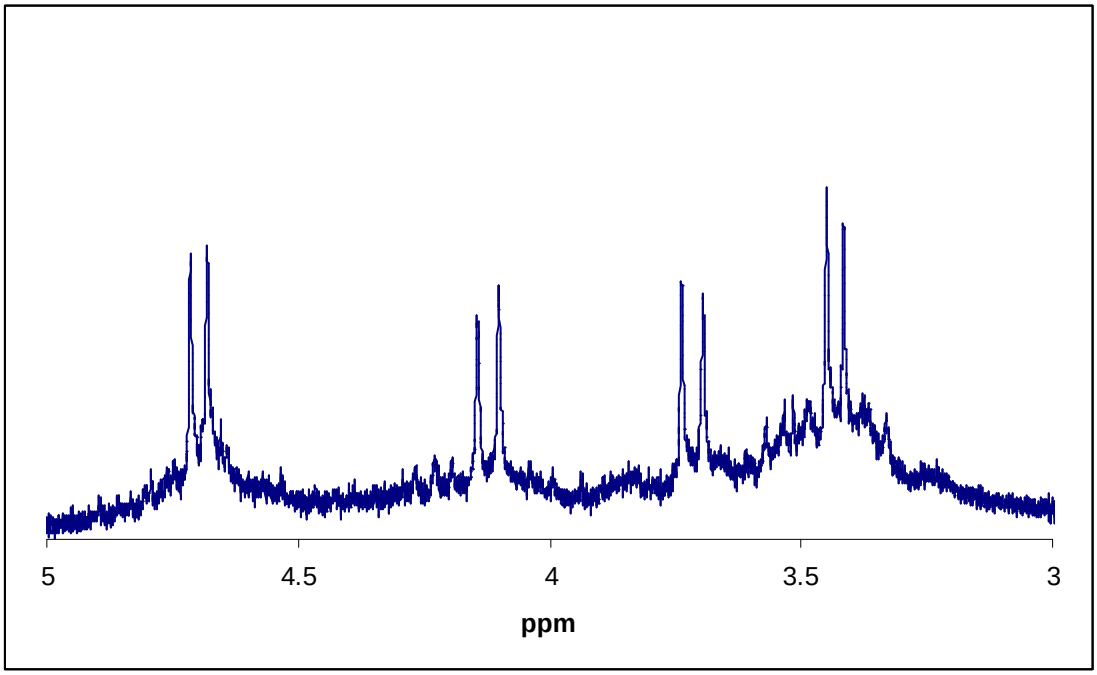

Figure 4.15: ^{1}H-NMR of expanded methylene region for compound **7**.

A resonance at δ 4.70 ppm (J = 10.2 Hz) arises from the protons attached to C(7) which are directed toward the $GeFe_2$ triangles while that at δ 3.42 ppm (J = 10.2 Hz) corresponds to the protons on C(7) which are directed away from this fragment. The other two doublets at δ 4.12 (J = 12.9 Hz) and 3.72 ppm (J = 12.9 Hz) are assigned to the protons attached to C(11), which are directed toward and away from the $GeFe_2$ triangles, respectively.

Several other carbonyl compounds containing the $GeFe_2$ structural motif have been reported and characterized[163-168] as have complexes containing $GeCo_2$ triangles.[169-175] In addition, a number of higher nuclearity clusters containing μ_3-[176-179] or μ_4-germanium atoms,[169,170,174,180-184] Ge_2Fe_2 arrays,[185-187] or rings containing germanium, iron, and cobalt[176,188-191] are also well known. The synthesis of these species typically

involve using germanium(IV), while preparative routes involving the oxidation of germanium(II) precursors such as that employed for the synthesis of **7** are more uncommon. One notable exception is the synthesis of $[Et_4N]_2[Fe(CO)_9(\mu_3\text{-}CO)(\mu_3\text{-}Ge\{Fe(CO)_4\}]$ from $[Et_4N]_2[Fe_2(CO)_8]$ and GeI_2.[179] Reaction of **1** with 2 equivalents of $Fe_2(CO)_9$ neither furnished a complex similar to **7** nor resulted in the formation of Ge-$Fe(CO)_4$ fragments. Although a reaction did occur, the products were identified as **1** and fine particles of iron metal. Presumably, the decarbonylation of $Fe_2(CO)_9$ by complex **1** results in an unstable species, which releases all of the remaining carbonyl ligands to furnish the iron metal.

Conclusions

We have prepared and structurally characterized two unusual germanium(II) calixarene complexes via the protonolysis reaction between the bulky germanium(II) amide $Ge[N(SiMe_3)_2]_2$ and calix[4]arene or calix[8]arene. The former complex is highly symmetric and contains two germanium atoms arranged in a central Ge_2O_2 rhombus, while the latter species represents the first germanium(II)-calix[8]arene complex and contains two of these Ge_2O_2 rhombi located inside a bowl-shaped macrocycle. The latter complex reacts with $Fe_2(CO)_9$ via a redox process involving the elimination of CO and the oxidation of Ge(II) to Ge(IV) to give a highly symmetric octairon complex containing four $GeFe_2$ triangles attached to the macrocyclic calix[8]arene framework. This process indicates that these germanium(II) calixarenes can serve as platforms for the support of multiple transition-metal centers.

Experimental

General Considerations: All manipulations were carried out under an inert N_2 atmosphere using standard glovebox, Schlenk, and syringe techniques.[72] Solvents were dried and purified using a Glass Contour solvent purification system. Calix[4]arene, calix[8]arene, and $Fe_2(CO)_9$ were purchased from Aldrich and used without further purification, and $Ge[N(SiMe_3)_2]_2$ was prepared according to the literature method.[192-194] Infrared spectra were obtained using a Hewlett-Packard FT-IR spectrometer, and NMR spectra were recorded on either a Varian Gemini 2000 or a Varian Unity INOVA 400 operating at 300 or 400 MHz, respectively, and were referenced to residual protio solvent. The numbering system used below refers to that in the crystal structures of **1**, **6**, and **7**.

Synthesis of {Calix[4]}Ge_2 (1).

To a solution of calix[4]arene (0.404 g, 0.952 mmol) in benzene (25 ml) in a Schlenk tube was added a solution of $Ge[N(SiMe_3)_2]_2$ (0.750 g, 1.91 mmol) in benzene (5 ml). The tube was sealed with a Teflon plug, and the reaction was heated at 85 ºC in an oil bath for 24 hours. The volatiles were removed in vacou to yield an off-white solid, which was washed with hexane (3 x 5 ml) and subsequently recrystallized from hot benzene (10 ml) to yield **1** (0.301g, 56%) as colorless crystals. ^{1}H NMR (C_6D_6, 25 °C) δ 7.07 (d, *J* = 7.5 Hz, 4H, *meta*-H C(1) – C(6)), 6.86 (t, *J* = 7.5 Hz, 2H, *para*-H C(1) – C(6)), 6.68 (d, *J* = 7.5 Hz, 4H, *meta*-H C(8) – C(13)), 6.16 (d, *J* = 7.5 Hz, 2H, *para*-H

C(8) – C(13)), 4.41 (d, *J* = 13.2 Hz, 4H, -C(7)H_2-), 3.23 (d, *J* = 12.9 Hz, 4H, -C(14)H_2-) ppm.

Stepwise Reaction of $Ge[N(SiMe_3)_2]_2$ with Calix[4]arene.

To a solution of calix[4]arene (0.095 g, 0.22 mmol) in benzene-d_6 (0.50 ml) in a screw top NMR tube was added a solution of $Ge[N(SiMe_3)_2]_2$ (0.088 g, 0.22 mmol) in benzene-d_6 (0.25 ml). The ^{1}H-NMR spectrum was recorded 30 minutes after mixing the sample. The NMR tube was subsequently opened in the glovebox and an additional solution of $Ge[N(SiMe_3)_2]_2$ (0.043 g, 0.11 mmol) in benzene-d_6 (0.15 ml) was added. After the reaction mixture was mixed, the ^{1}H-NMR spectrum of the sample was recorded. This process was repeated with further addition of $Ge[N(SiMe_3)_2]_2$ (0.051 g, 0.013 mmol) to the tube.

Synthesis of {Calix[8]}Ge_4 (6).

To a solution of calix[8]arene (0.252 g, 0.297 mmol) in benzene (20 ml) in a Schlenk tube was added a solution of $Ge[N(SiMe_3)_2]_2$ (0.514 g, 1.31 mmol) in benzene (10 ml). The tube was sealed with a Teflon plug, and the reaction was heated at 85 ºC in an oil bath for 48 hours. The volatiles were removed in vacuo to yield an off-white solid, which was washed with hexane (3 x 5 ml) and subsequently recrystallized from hot benzene (10 ml) to yield **6** (0.298 g, 89%) as colorless crystals. ^{1}H NMR (C_6D_6, 25 °C) δ 7.26 (d, *J* = 7.5 Hz, 1H, *meta*-H C(55)), 7.25 (d, *J* = 7.5 Hz, 1H, *meta*-H C(15)), 7.09 (d, *J* = 7.5 Hz, 1H, *meta*-H C(43)), 7.08 (d, *J* = 7.5 Hz, 1H, *meta*-H C(85)), 6.95 – 6.85 (m, aromatics, 9 H), 6.79 – 6.91 (m, aromatics, 8 H), 6.66 (d, *J* = 7.5 Hz, 1 H, *meta*-H C(35)),

6.11 (t, *J* = 7.8 Hz, 1H, *para*-H C(24)), 5.97 (d, *J* = 7.8 Hz, 1H, *meta*-H C(25)), 5.83 (d, *J* = 16.8 Hz, 2H, H(4a) and H(8a)), 4.77 (d, *J* = 12.6 Hz, 2H, H(1b) and H(5b)), 4.60 (d, *J* = 15.8 Hz, 2H, H(2b) and H(3b)), 4.57 (d, *J* = 15.0 Hz, 2H, H(6b) and H(7b)), 3.46 (d, *J* = 15.8 Hz, 2H, H(2a) and H(3a)), 3.43 (d, *J* = 16.8 Hz, 2H, H(4b) and H(8b)), 3.41 (d, *J* = 15.0 Hz, 2H, H(6a) and H(7a)), 3.24 (d, *J* = 12.6 Hz, 2H, H(1a) and H(5a)) ppm.

Synthesis of {Calix[8]}$Ge_4[Fe_2(CO)_8]_4$ (7).

To a solution of **6** (0.150 g, 0.132 mmol) in benzene (15 ml) in a Schlenk tube was added a suspension of $Fe_2(CO)_9$ (0.212 g, 0.583 mmol) in benzene (20 ml). The tube was sealed with a Teflon plug, and the mixture was heated at 85 ºC for 24 hours. The reaction mixture was filtered, and the solid was washed with benzene (4 x 10 ml) to yield a dark red filtrate. The volatiles were removed in vacuo to yield **7** as a dark-red solid (0.240 g, 73%). ^{1}H NMR (CD_3CN, 25 °C) δ 7.13 – 6.97 (m, aromatics, 8 H), 6.84 – 6.57 (m, aromatics, 18 H), 4.70 (d, *J* = 10.2 Hz, 8H, H(7b)), 4.12 (d, *J* = 12.9 Hz, 8H, H(11a)), 3.72 (d, *J* = 12.9 Hz, 8H, H(11b)), 3.43 (d, *J* = 10.2 Hz, 8H, H(7a)) ppm. IR (CH_2Cl_2): 2109(w), 2059(s), 2044(m), and 2020(s) cm^{-1}. UV/visible (CH_3CN): λ_{max} 327 nm (ε = 3.32 x 10^4 L mol^{-1} cm^{-1}).

X-ray Structure Determinations.

Diffraction intensity data were collected with a Siemens P4/CCD diffractometer. Crystallographic data and details of the X-ray study are shown in **Table 4.4**.

Table 4.4. Crystallographic data for compounds **1**, **6**·C_6H_6, and **7**·C_6H_6.

	1	**6**·C_6H_6	**7**·C_6H_6
formula	$C_{28}H_{20}Ge_2O_4$	$C_{62}H_{45}Ge_4O_8$	$C_{50}H_{24}Fe_4Ge_4O_{20}$
space group	*Pbca*	*P*-1	*P*4(2)/*n*
a (Å)	16.988(1)	12.923(4)	18.4671(6)
b (Å)	8.8914(7)	13.690(4)	18.4671(6)
c (Å)	14.630(1)	14.589(4)	15.956(1)
α (°)	90	92.868(6)	90
β (°)	90	96.527(6)	90
γ (°)	90	93.774(6)	90
V (Å^3)	2209.9(3)	2554(1)	5441.5(4)
Z	4	2	4
ρ_{calc} (g cm^{-1})	1.700	1.571	1.603
temperature (K)	100(2)	198(2)	203(2)
radiation	MoKα	MoKα	MoKα
wavelength (Å)	0.71073	0.71073	0.71073
R	0.0290	0.0654	0.0476
R_w	0.0483	0.0815	0.0577

Absorption corrections were applied for all data by SADABS. The structures were solved using direct methods, completed by Fourier sytheses, and refined by full-matrix least-squares procedures on F^2. All non-hydrogen atoms were refined with anisotropic displacement coefficients, and hydrogen atoms were treated as idealized contributions. All software and sources of scattering factors are contained in the SHELXTL (5.10) program package (G. Sheldrick, Bruker XRD, Madison, WI). ORTEP diagrams were drawn using the ORTEP3 program (L. J. Farrugia, Glasgow).

CHAPTER V

SYNTHESIS AND CRYSTAL STRUCTURE OF A GERMANIUM(II) CALIX[6]ARENE CONTAINING UNUSUAL DIAMIDOSILYL ETHER GROUPS

Introduction

Calix[n]arenes are an important class of macrocycles that contain four or more phenol moieties connected together by methylene bridges. These species have applications in the areas of catalysis, self-assembly, and molecular or ionic recognition, and can also serve as platforms for the support of single or multiple transition- or main group-metal centers[116-122,130,131,144,195-208], including silicon[195,196,205,208], phosphorus[130,131,195,197-202,206,207], and arsenic[144]. Variation of the number of phenolic subunits present in the molecule allows control over the cavity size in these systems, which in turn has a profound effect on their properties and reactivity. The presence or absence of conformational rigidity, which is typically influenced by the attachment of peripheral substituents to the *para*-positions (or upper rim) of the aromatic rings, is also important in this regard.[116,117,119,209-211]

Calix[6]arenes have been shown to be more flexible than calix[4]- and calix[8]arenes bearing identical *para*-substituents by variable temperature NMR spectral studies.[212,213] Several oxygen-functionalized calix[6]arenes have been employed for the

complexation of metal ions[133,214-226] and some bimetallic complexes containing group 2 or 4 metals[227-229] bound directly to the oxygen atoms have been prepared. These bimetallic complexes containing group 2 or 4 metals are uncommon, presumably due to the high conformational mobility of the hexamers versus the related tetramers and octamers. We have described the synthesis and structures of calix[4]- and calix[8]arene complexes containing two or four germanium(II) sites (respectively) bound to the oxygen atoms of the macrocycles which were prepared via the protonolysis reaction of $Ge[N(SiMe_3)_2]_2$ with the *para*-unsubstituted parent calixarenes.[54] The structure of these two compounds were similar in that the germanium atoms were incorporated into Ge_2O_2 rhombi each having one terminal and two bridging Ge-O attachments. The calix[8]arene species was also shown to undergo a redox reaction with $Fe_2(CO)_9$ resulting in an octa-iron compound containing four $GeFe_2$ triangles, where Ge(II) is oxidized to Ge(IV).

In light of these results, we attempted to prepare a similar complex by treatment of the *para*-unsubstituted calix[6]arene with three equivalents of $Ge[N(SiMe_3)_2]_2$. Instead of forming a complex containing a Ge_2O_2 rhombus as observed in the reactions of $Ge[N(SiMe_3)_2]_2$ with calix[4]- and calix[8]arene, the reaction of the germanium amide with the calix[6]arene substrate furnished a complex having a Ge_2NO rhombus which contains a bridging amide group and has two germanium atoms bound to three of six oxygen atoms present in the macrocycle. One of the remaining three oxygen atoms has been incorporated into a $–OSiMe_3$ moiety while the other two have been incorporated into structurally unprecedented $–OSi(H)(NH_2)_2$ groups.

Results and Discussion

Treatment of calix[6]arene with three equivalents of $Ge[N(SiMe_3)_2]_2$ yielded complex **1** in 41% yield as shown in **Scheme 5.1**.

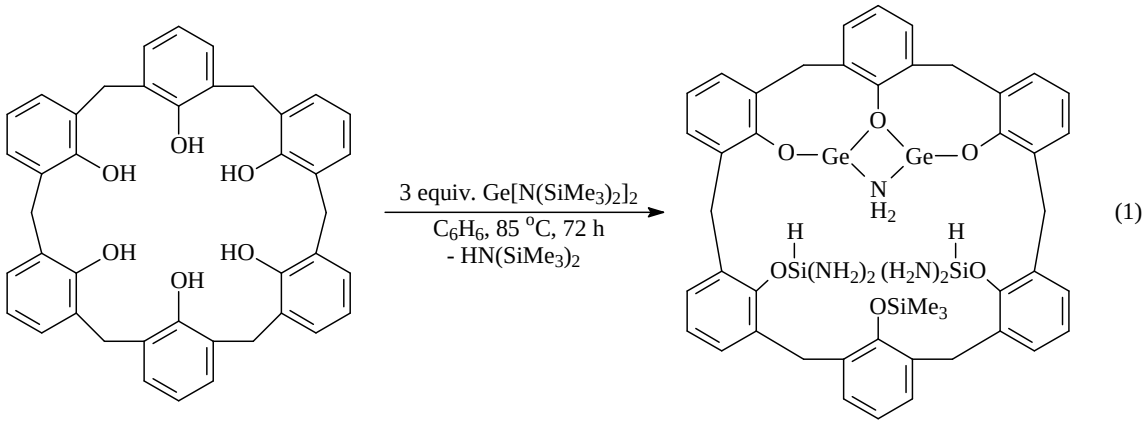

(1)

Scheme 5.1: Reaction of calix[6]arene with 3 equivalents of $Ge[N(SiMe_3)_2]_2$.

The identity of **1** was ascertained by obtaining its X-ray crystal structure, and an ORTEP diagram of **1** is shown in **Figure 5.1** while selected bond distances and angles are collected in **Table 5.1**. The presence of larger than normal thermal ellipsoids for the nitrogen atoms of **Figure 5.1** is indicative of the fact that the two silicon atoms to which the $–NH_2$ groups are bond are disordered over two positions.

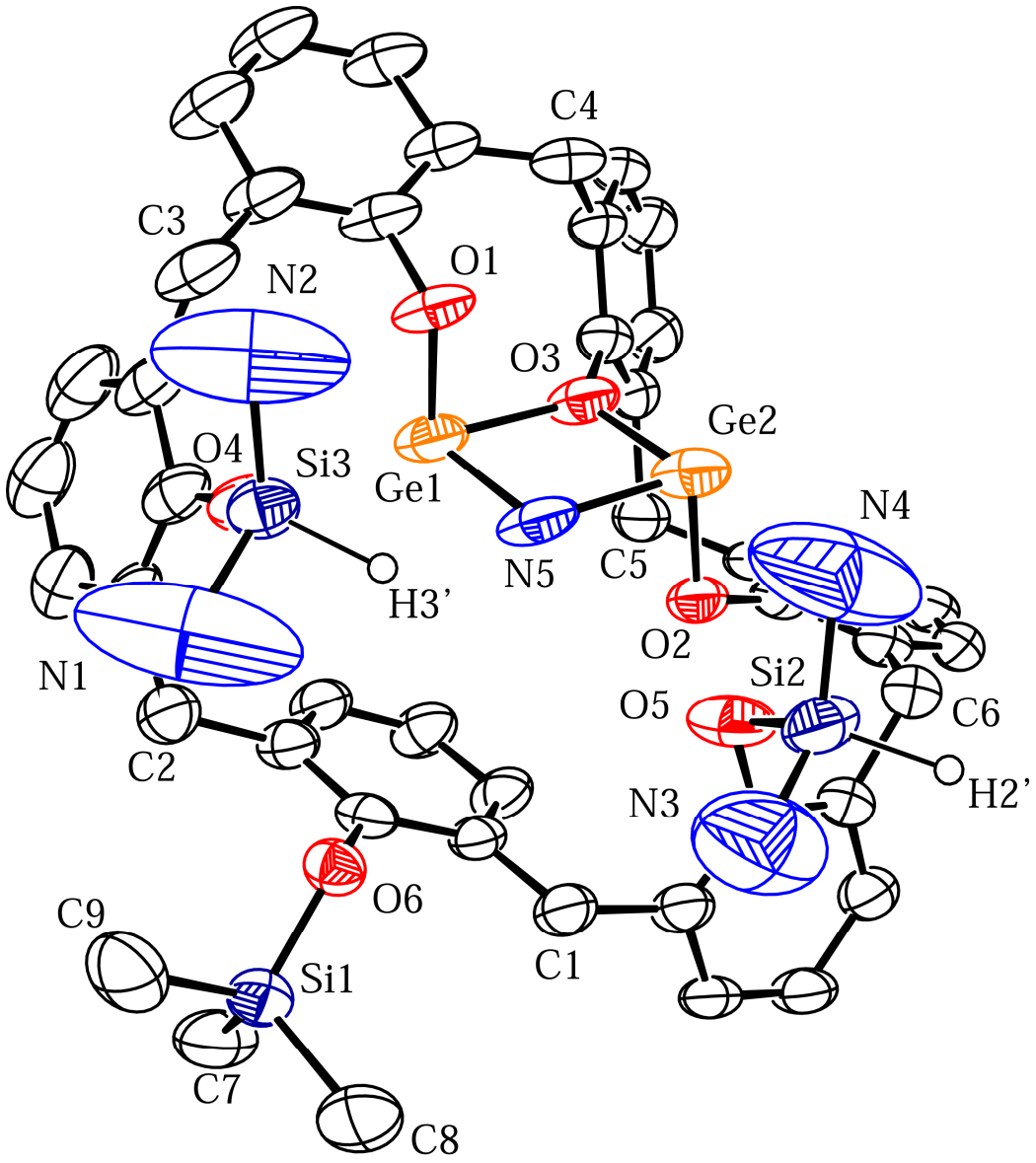

Figure 5.1. ORTEP diagram of compound **1**. Thermal ellipsoids are drawn at 50% probability.

Table 5.1 Selected bond distances (Å) and angles (deg) for compound **1**

Ge(1) – O(1)	1.860(3)	O(1) – Ge(1) – O(3)	91.4(1)
Ge(1) – O(3)	1.992(3)	O(1) – Ge(1) – N(5)	89.7(1)
Ge(1) – N(5)	2.011(4)	O(2) – Ge(2) – O(3)	91.6(1)
Ge(2) – O(2)	1.835(3)	O(2) – Ge(2) – N(5)	91.4(1)
Ge(2) – O(3)	1.993(3)	O(3) – Ge(1) – N(5)	77.1(1)
Ge(2) – N(5)	1.995(4)	O(3) – Ge(2) – N(5)	77.4(1)
Si(1) – O(6)	1.664(3)	Ge(1) – O(3) – Ge(2)	103.0(1)
Si(2) – O(5) ‡	1.696(5)	Ge(1) – N(5) – Ge(2)	102.3(2)
Si(2) – N(3) ‡	1.816(8)	O(5) – Si(2) – N(3) ‡	111.6(3)
Si(2) – N(4) ‡	1.715(8)	O(5) – Si(2) – N(4) ‡	108.2(3)
Si(3) – O(4) ‡	1.712(4)	N(3) – Si(2) – N(4) ‡	122.8(5)
Si(3) – N(1) ‡	1.700(8)	O(4) – Si(3) – N(1) ‡	112.4(4)
Si(3) – N(2) ‡	1.806(9)	O(4) – Si(3) – N(2) ‡	108.8(4)
		N(1) – Si(3) – N(2) ‡	119.6(4)

‡ The atoms of Si(2) and Si(3) are disordered over two positions. The tabulated values are an average for the two positions.

Of the six phenolic oxygen atoms present in **1**, three are bound to the two Ge atoms in either a terminal or bridging fashion while the remaining three oxygen atoms have been incorporated into either $–OSiMe_3$ or $–OSi(H)(NH_2)_2$ groups. We have previously observed the transformation of hydroxyl groups to trimethylsiloxy groups in the reactions

of 3,3´-disubstituted binaphthols with metal(II) amides $M[N(SiMe_3)_2]_2$ (M = Be, Zn, Ge, Sn)[55]; however, the conversion of –OH groups to silylamides has not been previously described.

Compound **1** contains an unusual bridging $–NH_2-$ group between the two germanium centers, and the structure of **1** can be compared to the two related calixarene complexes {calix[4]}Ge_2 **(2)** and {calix[8]}Ge_4 **(3)**[54] as well as the dimeric species $[(C_6H_3\{C_6H_3Pr^i_2\text{-}2,6\}_2\text{-}2,6)GeNH_2]_2$ **(4)**, shown in **Figure 5.2**, which also contains bridging $–NH_2-$ moieties.[230]

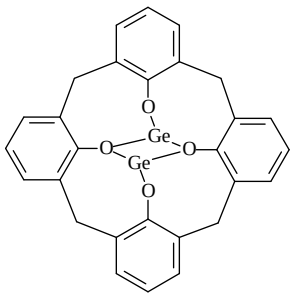

2

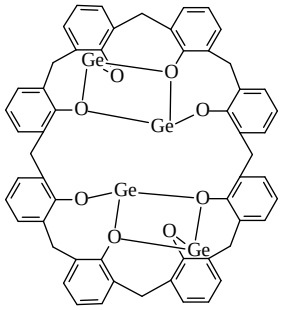

3

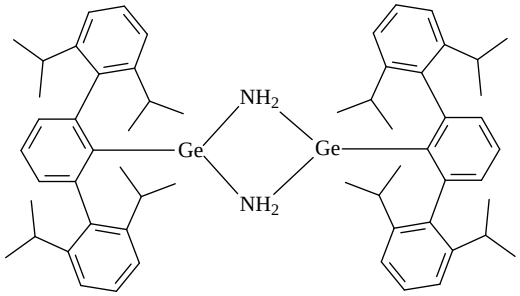

4

Figure 5.2: Structures of {calix[4]}Ge_2 **(2)**, {calix[8]}Ge_4 **(3)** and $[(C_6H_3\{C_6H_3Pr^i_2\text{-}2,6\}_2\text{-}2,6)GeNH_2]_2$ **(4)**.

Similar to the Ge_2O_2 rhombus in compound **2**, the Ge_2NO rhombus adopts a planar geometry. The Ge(1)-O(3)-Ge(2) angle of 103.0(1)º is significantly more acute than the Ge-O_{br}-Ge angles in **2** and **3** which range from 106.1(1) to 107.89(6)º.[54] Furthermore, the Ge(1)-N(5)-Ge(2) angle measures 102.3(2)º, which is more obtuse than the average Ge-N_{br}-Ge angles in **4** (100.0(1)º).[230] The O(3)-Ge(1)-N(5) and O(3)-Ge(2)-N(5) angles average 77.3(1)º which are wider than the O_{br}-Ge-O_{br} angles in **2** and **3** but more acute thaan the N_{br}-Ge-N_{br} ligand angles in **4**. These structural differences can be attributed to the presence of two different types of bridging atoms in **1,** and the internal angles in the Ge_2NO rhombus can be regarded as being intermediate between the Ge_2O_2 rhombi of **2** and **3** and the Ge_2N_2 rhombus of **4**.

The terminal Ge(1)-O(1) and Ge(2)-O(2) bond lengths in **1** are typical for germanium(II)-oxygen distances and are comparable to those in compounds **2** and **3**[54] as well as in other Ge(II) aryloxides[70,145,147,231,232]. The bridging Ge(1)-O(3) and Ge(2)-O(3) bond lengths in **1** are 1.992(3) and 1.993(3) Å (respectively) which fall between the average Ge-O_{br} bond distances in **2** (1.988 Å) and **3** (2.000 Å)[54]. The bridging N atom is not symmetrically disposed between the two germanium atoms in **1** as indicated by the two different Ge-N bond lengths measuring 2.011(4) and 1.995(4) Å. These distances are shorter than those found in the structure of **4** which has an average Ge-N distance of 2.013(3) Å[230]. The Ge-N distances in **1** are longer than those in germanium(II) compounds bearing ligands with terminal Ge-N bonds, including the well-known bulky bisamide $Ge[N(SiMe_3)_2]_2$ which has Ge-N bond lengths of 1.873(5) and 1.878(5) Å[233] and the bis(piperidinato) complex $Ge[NC_5H_6Me_4\text{-}2,2,6,6]_2$ which has distances of 1.87(1) and 1.90(1) Å.[234] However, the Ge-N distances in **1** are considerably shorter than those in

divalent germanium compounds having dative N → Ge bonds including those in [Ge(2-{$(Me_3Si)_2C$}-C_5H_4N)R] which measure 2.082(4) or 2.089(7) Å (R = Cl or $CH(PPh_2)_2$, respectively).[235] These distances are also shorter than those in the divalent binhapthoxide complex (*R*)-[Ge{$O_2C_{20}H_{10}(SiMe_2Ph)_2$-3, 3´}{$NH_3$} (*d* Ge-N = 2.093(4) Å) which contains a coordinated NH_3 molecule[70] and also in [Ge{$OCH(CF_3)_2$}$_2${NH_2Ph}] (d Ge-N = 2.092(3) Å) which contains a coordinated aniline molecule.[236]

The three remaining oxygen atoms in **1** are each attached to a silicon atom. One of these is incorporated into a $–OSiMe_3$ silyl ether group which arises from the transfer of the $–SiMe_3$ moiety from a $–N(SiMe_3)_2$ ligand in $Ge[N(SiMe_3)_2]_2$ to the phenolic oxygen atom.[55] The geometry of the silyl ether moiety is normal with an approximant tetrahedral environment at silicon and a typical Si-O bond distance of 1.664(3) Å. The Si-O-C_{ipso} angle is 123.7(2)º and the $–SiMe_3$ group is directed outward from the central cavity of the molecule. The other two oxygen atoms have been incorporated into unusual $–OSi(H)(NH_2)_2$ groups. The silicon atoms in both of these groups are disordered over two positions (50% occupancy) which also result in each of the nitrogen atoms of the four attached $–NH_2$ groups also being disordered over two positions. The four nitrogen atoms were also disordered with very small positional differences over the two individual positions, and these were refined with a broad thermal parameter which resulted in large ellipsoids present in the ORTEP plot of **1 (Figure 5.1)**.

The Si-N bond distances (when taking into consideration the disorder of the silicon atoms) are 1.816(8), 1.715(8), 1.700(8), and 1.806(9) Å while, the N-Si-N angles are 122.8(5) and 199.6(4)º at Si(2) and Si(3), respectively. Diaminosilyl ether groups similar to those attached to O(4) and O(5) in **1** have not been described previously and

thus a direct comparison to other structurally characterized species is not possible. However, a few small molecules containing $–NH_2$ groups bound to silicon and having $–NH_2$ and –OH groups attached to the same silicon atom have been reported.[237,238] The structure of $Mes_2Si(NH_2)_2$ has Si-N bond distances of 1.713(2) and 1.717(2) Å and a N-Si-N angle of 106.89(5)° [238] while that of $Bu^t_2Si(OH)NH_2$ exhibits a Si-N bond distance of 1.746(4) Å.[237]

The average of the four Si-N bond distances is 1.759(8) Å in **1** which is longer than the corresponding bond distance in $Bu^t_2Si(OH)NH_2$. [237] This can be attributed to the attachment of the $–Si(H)(NH_2)$ moieties in **1** to a phenolic oxygen atom which is electron withdrawing and leads to a stronger O-Si bond, resulting in a weaker/longer Si-N bond. The two N-Si-N angles in **1** average 121.2(5)° which is significantly more obtuse than the N-Si-N angle in $Mes_2Si(NH_2)_2$.[238] This structural difference is expected since the latter compound contains two sterically encumbering mesityl groups, while compound **1** instead has only a proton and an oxygen atom bound to silicon.

Spectroscopic (^1H, ^{13}C and ^{29}Si NMR) data in benzene-d_6 are consistent with the solid-state structure of **1**. Similar to compounds **2** and **3**, the conformational flexibility of **1** is restricted versus the calix[6]arene starting material due to the presence of the Ge_2NO rhombus and the relatively large $–OSiMe_3$ and $–OSi(H)(NH_2)_2$ groups. This renders all of the individual protons of the six methylene units in **1** magnetically non-equivalent, resulting in twelve distinct doublets in the ^1H-NMR spectrum in the chemical shift range δ 3.1-4.8 ppm which are divided into two sets of six features **(Figure 5.3)**.

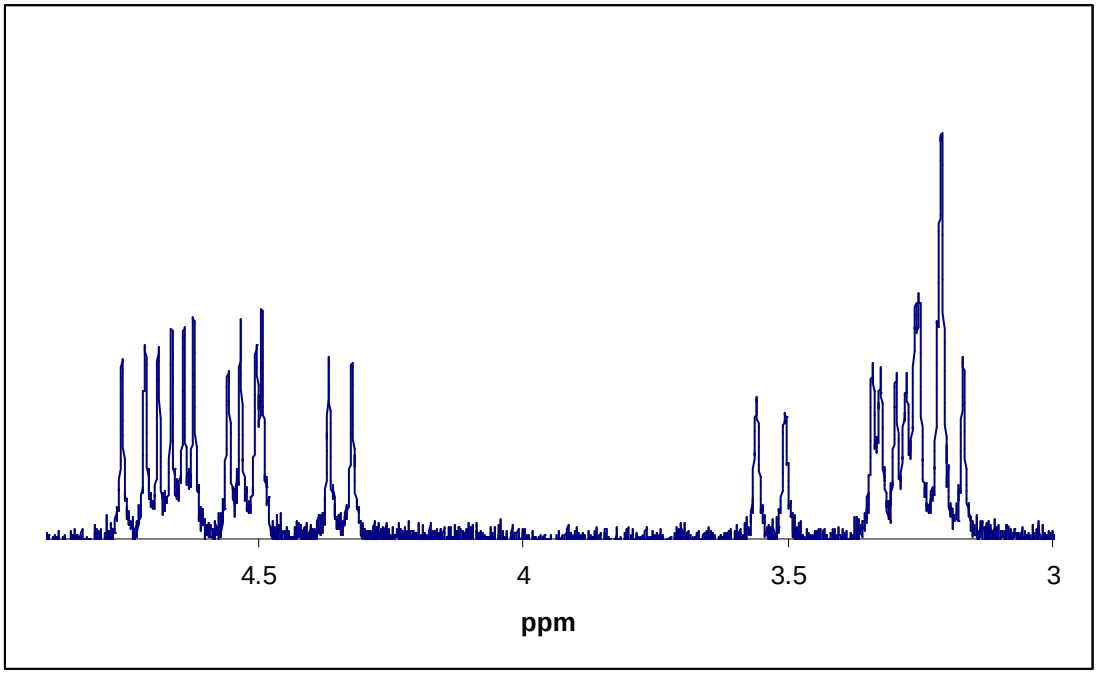

Figure 5.3: Expanded methylene region of the ^{1}H-NMR spectrum for compound **1**.

The downfield grouping of resonances correspond to the methlylene protons directed inward toward the Ge_2NO rhombus while the upfield features are attributed to those directed away. This is due to the anisotropic effects of the aromatic π-systems and the presence of the germanium atoms.

In the downfield grouping of resonances, the doublet at δ 4.74 (J = 13.2 Hz) ppm is assigned to the proton attached to C(5) which has two close contacts with O(2) and O(3) measuring 2.498 and 2.549 Å (respectively). The two sets of closely grouped doublets at δ 4.66 (J = 14.7 Hz) and 4.64 (J = 12.6 Hz) ppm correspond to the protons bound to C(4) and C(3) (respectively) due to their relative proximity to O(3) and O(1), and the features at δ 4.53 (J = 16.2 Hz) and 4.51 (J = 11.7 Hz) ppm are assigned to the protons attached to C(6) and C(2) (respectively) due to their proximity to the silylated

oxygen atoms O(4) and O(5). The remaining doublet at δ 4.34 (J = 13.5 Hz) ppm arrises from the proton attached to C(1) which only has long (>2.6 Å) contacts with the neighboring oxygen atoms.

Assignments for the upfield group of six doublets are based on a COSY NMR in **Figure 5.4**.

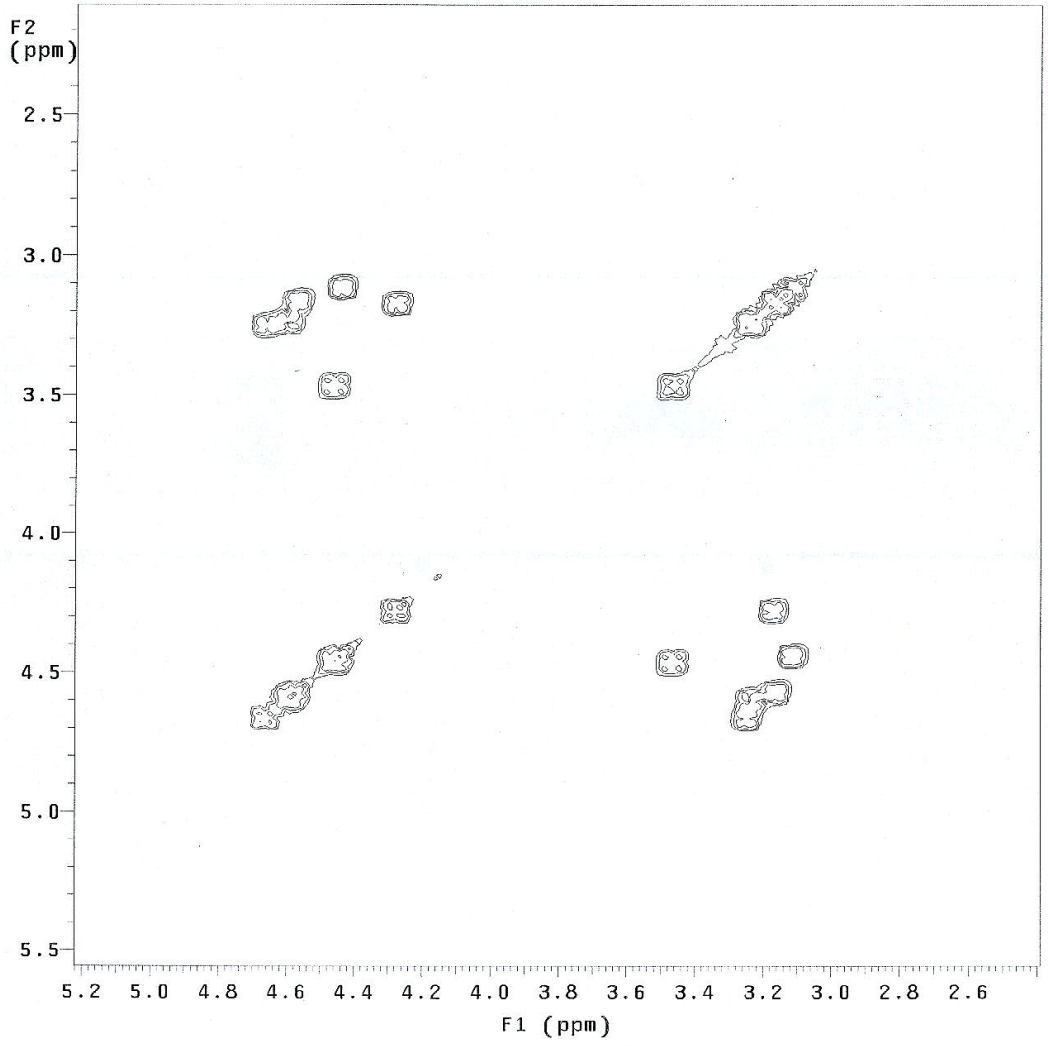

Figure 5.4: 2D COSY NMR spectrum for compound **1**.

The doublet at δ 3.53 (J = 16.2 Hz) ppm corresponds to the second proton bound to C(6), while the four closely spaced features at δ 3.32 (J = 13.2 Hz), 3.30 (J = 14.7 Hz), 3.24 (J = 13.5 Hz), and 3.23 (J = 12.6 Hz) ppm arise from the remaining protons attached to C(5), C(4), C(1) and C(3) (respectively). The resonance at δ 3.19 (J = 11.7 Hz) ppm results from the second proton bound to C(2). Due to the rigidity in the Ge_2NO rhombus, the protons in the bridging -NH_2 group also are magnetically non-equivalent, appearing as two broad but clearly resolved doublets at δ 1.66 (J = 9.6 Hz) and 1.04 (J = 9.6 Hz) ppm. The two Si-H protons are also non-equivalent and appear as two singlets in the ^{1}H-NMR spectrum at δ 6.34 and 6.32 ppm, while the –$Si(NH_2)_2$ protons appear as two upfield singlets at δ 0.27 and 0.24 ppm and the protons of the –$OSiMe_3$ moiety appear as a singlet at δ 0.42 ppm. The ^{13}C-NMR spectrum of **1** also is consistent with its solid-state structure and exhibits six distinct lines for each of the magnetically non-equivalent *ipso*- and *para*-carbon atoms as well as twelve lines for both the *ortho*- and *meta*-carbons. Signals for the carbon atoms of the six methylene groups as six peaks between δ 31-35 ppm and there is only one resonance in the -SiR_3 region of the spectrum at δ 1.6 ppm corresponding to the carbon atoms of the –$OSi(CH_3)_3$ group.

The ^{29}Si{^{1}H} NMR (119.2MHz) spectrum of **1** contains three singlets at δ 20.79, 20.33, and 20.23 ppm, where the downfield resonance arises from the silicon atom in the –$OSiMe_3$ group and the two upfield resonances correspond to the silicon atoms in the two –$Si(H)(NH_2)_2$ groups **(Figure 5.5)**. The chemical shift for the silyl ether feature is similar to that of $C_6H_5OSiMe_3$ which appears at δ 19.46ppm.[239] The proton coupled ^{29}Si-NMR spectrum of **1** was also recorded at 119.2 MHz, and the singlet at δ 20.23 in the ^{1}H-

decoupled spectrum splits into a multiplet with eight of ten expected lines being clearly discernable **(Figure 5.6)**. This arises from the two-bond coupling between the silicon atom and the protons of the methyl groups, with a coupling constant of 6.43 Hz. The two features for the $-Si(H)(NH_2)_2$ groups are more complex due to the presence of both one-bond Si-H and three bond Si-NH_2 coupling. Each of these features are expected to appear as a doublet of quintets but their proximity in chemical shifts resulted in overlap with one another such that the expected one-bond Si-H coupling could not be clearly observed.

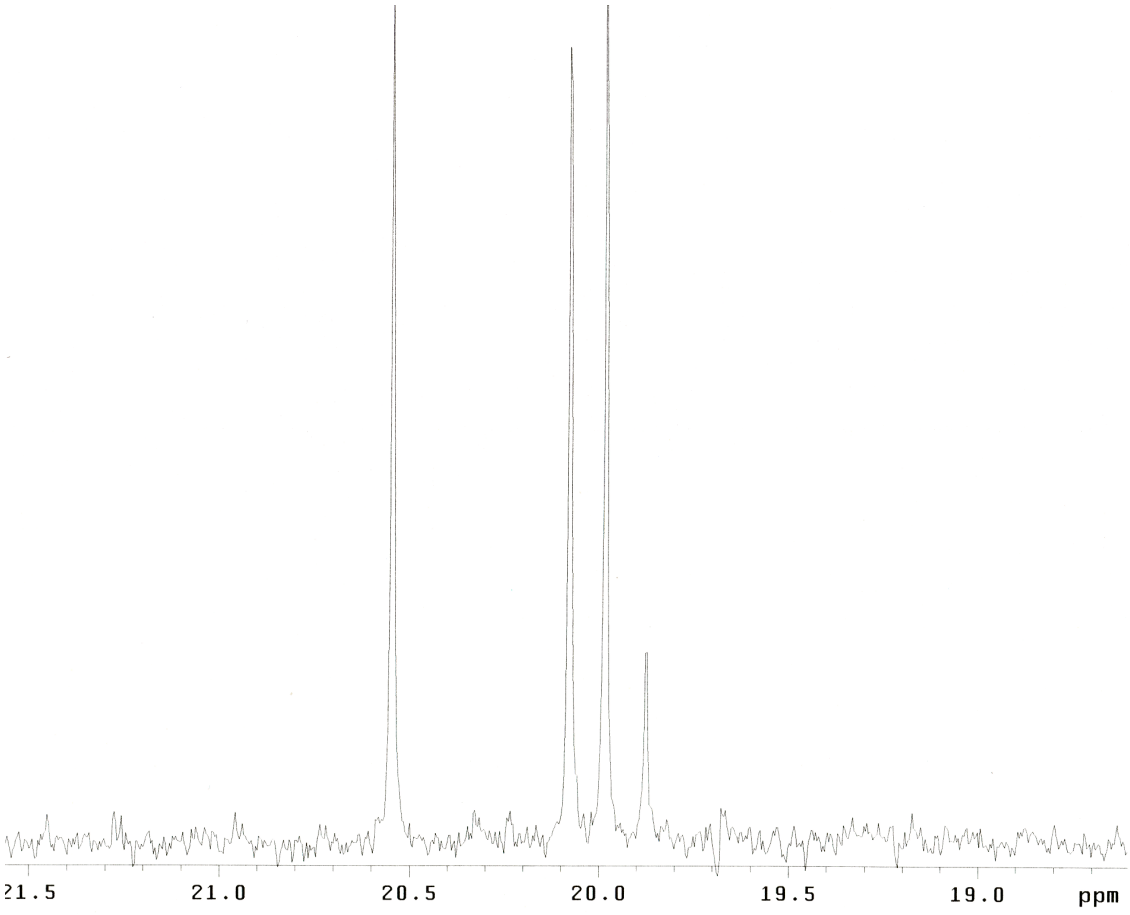

Figure 5.5: ^{1}H decoupled ^{29}Si NMR

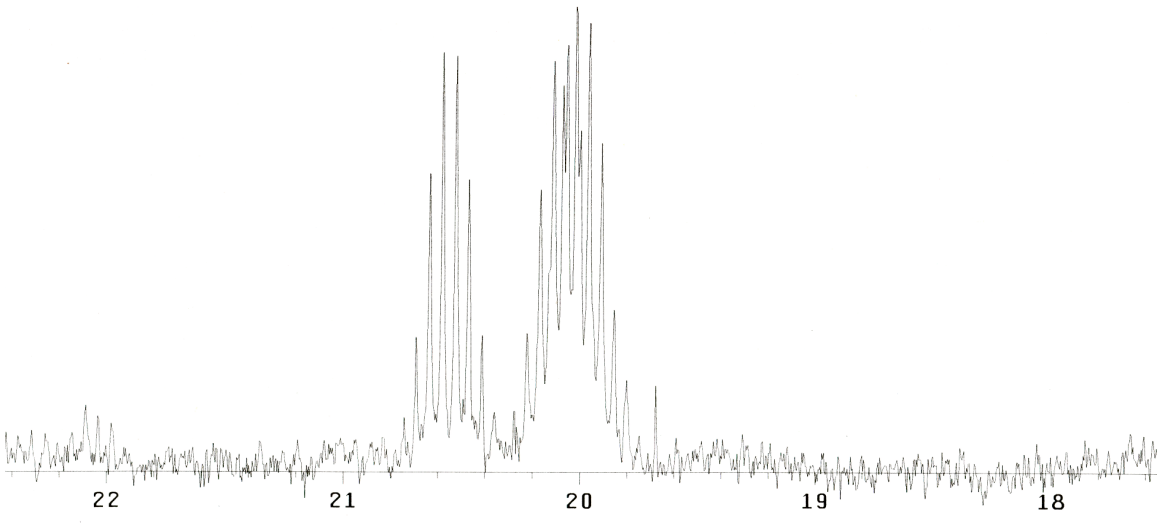

Figure 5.6: ^{1}H coupled ^{29}Si NMR

The mass spectrum of compound **1** was also acquired using electrospray mass spectrometry (positive ion mode), and exhibited a clear fragmentation pattern having nine well-defined peaks which are listed and assigned in **Table 5.2**. The proposed fragmentation pattern is illustrated in **Scheme 5.2**.

Table 5.2 Electrospray mass spectrometry data for compound **1**.

Ion	*m/z*	Formula	Relative Intensity (%)
1a	988.5	$[(C_6H_3)_6(CH_2)_6O_3Ge_2(NH_2)\{OSi(H)(NH_2)_2\}_2OSiMe_3]H^+$	n/a
1b	927.5	$[(C_6H_3)_6(CH_2)_6O_3Ge_2(NH_2)OSi(H)(NH_2)_2OSiMe_3O]H^+$	2
1c	898.5	$[(C_6H_3)_6(CH_2)_6O_3Ge_2(NH_2)OSiH_3OSiMe_3OH]H^+$	29
1d	826.4	$[(C_6H_3)_6(CH_2)_6O_3Ge_2(NH_2)OSiH_3(OH)_2]H^+$	72
1e	798.4	$[(C_6H_3)_6(CH_2)_6O_2Ge_2(NH_3)(OH)_4]H^+$	100
1f	754.4	$[(C_6H_3)_6(CH_2)_6O_2Ge(NH_2)OSiH_3(OH)_3]H^+$	8
1g	726.4	$[(C_6H_3)_6(CH_2)_6OGe(NH_3)(OH)_5]H^+$	12
1h	682.4	$[(C_6H_3)_6(CH_2)_6O(NH_2)OSiH_3(OH)_4]H^+$	16
1i	654.4	$[(C_6H_3)_6(CH_2)_6(NH_3)(OH)_6]H^+$	28
1j	637.3	$[(C_6H_3)_6(CH_2)_6(OH)_6]H^+$	4

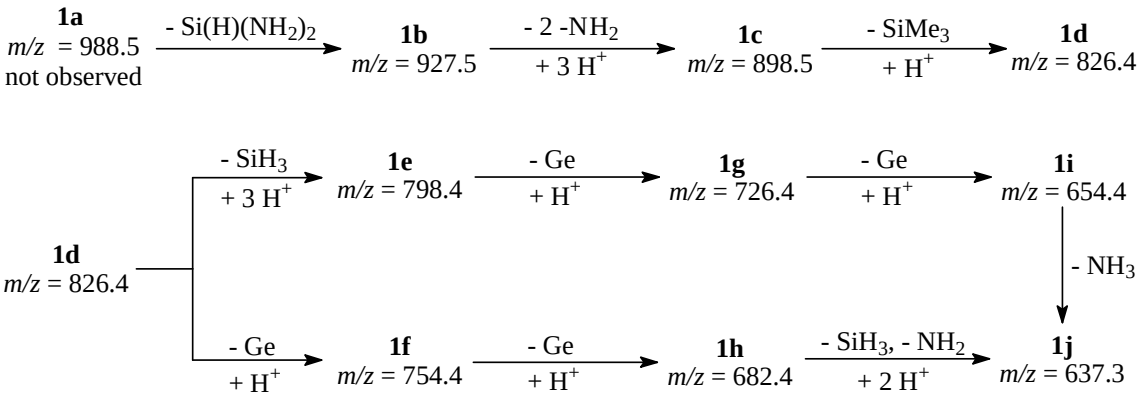

Scheme 5.2: Proposed fragmentation pattern.

Although the parent molecular ion at m/z = 988.5 was not observed a feature at m/z = 927.5 corresponding to the loss of one $–Si(H)(NH_2)_2$ fragment and monoprotonation of the remaining molecule was present in the spectrum. Subsequent fragmentations involve the loss of the $–SiMe_3$ group, the two germanium atoms, the oxygen atoms, and the bridging $–NH_2$- group. The –O and $–NH_2$ groups to which these fragments were bound appear to be protonated during the course of this process to yield –OH or NH_3 groups (respectively). Ultimately, all of the substituents in compound **1** udergo fragmentation to produce the parent calix[6]arene in protonated form.

The pathway for the formation of **1** is likely complex, but two key aspects for the generation of this species are evident. First, compound **1** contains twelve protons distributed among single bridging $–NH_2$- and the two $–Si(H)(NH_2)_2$ groups. Since calix[6]arene is the only proton source present in the reaction, all of these must originate from this starting material. Furthermore, 2 equivalents of calix[6]arene must be

consumed for every one equivalent of **1** generated in the reaction since calix[6]arene contains only six phenolic protons. This dictates a maximum theoretical yield of 50% for **1** with the concomitant formation of one or more other products, and this postulate is further supported by the complete consumption of calix[6]arene in the reaction. Compound **1** has been isolated in a maximum of 41% during the course of these studies.

Second, the $-N(SiMe_3)_2$ ligands of $Ge[N(SiMe_3)_2]_2$ are the source of both the bridging $-NH_2-$ group and the two $-Si(H)(NH_2)_2$ groups in **1**. We have demonstrated that $Ge[N(SiMe_3)_2]_2$ reacts with binaphthols via formation of an intermediate bearing a $-OGe[N(SiMe_3)_2]$ moiety which subsequently transfers a $-SiMe_3$ fragment to the oxygen atom of one –OH substituent of the binaphthol.[55] This results in the generation of a $-OGe[NH(SiMe_3)]$ group and this process can occur a second time to yield a $-OGe[NH_2]$ moiety which could then serve as the source of the bridging amide in **1**. The $-Si(H)(NH_2)_2$ groups, however must ultimately result from the demethylation of a $-SiMe_3$ group during the course of the reaction. The transfer of a methyl group to gallium in the reaction of $GaCl_3$ with $Li[N(SiMe_3)_2]$ has been reported[240], and similar methyl group migrations have been found upon treatment of $GaCl_3$ with $N(SiMe_3)_3$ [241] or $SiMe_4$ [242]. The germanium atoms present in **1** clearly are not methylated, but the generation of Me_4Ge or CH_4 might be expected to occur during the course of this reaction.

In order to probe the pathway for the formation of **1**, the progress of the reaction of one, two and three equivalents of $Ge[N(SiMe_3)_2]_2$ with calix[6]arene was monitored over time using ^{1}H-NMR spectroscopy in benzene-d_6 in three separate experiments. The methylene (δ 5.2-3.0 ppm) and alkylsilyl (δ 0.4-0.0 ppm) regions of these spectra contained diagnostic features which were compared over a reaction period of 120 h in

each case. Upon treatment of calix[6]arene with 3 equivalents of $Ge[N(SiMe_3)_2]_2$, a resonance for the formation of free $HN(SiMe_3)_2$ at δ 0.09 ppm was observed after 10 minutes at room temperature and $Ge[N(SiMe_3)_2]_2$ and a trace amount of calix[6]arene were still present in solution. After heating the sample at 85 ºC for 1 hour, the aromatic and methylene regions of the spectrum were complex, but the appearance of peaks at δ 0.42, 0.29 and 0.25 ppm indicated that compound **1** was already present in solution. The absence of a resonance at δ 10.50 ppm attributable to the six phenolic protons of the calix[6]arene starting material also indicated all of this substrate had been consumed at this time.

After heating the sample at 85 ºC for a total of 6 hours, the overall appearance of the spectrum had simplified and suggested that compound **1** was present in solution along with a second intermediate species. The methylene region of the spectrum contained 24 distinct doublets divided into an upfield and downfield grouping of 12 features each. Some overlap of these resonances was observed but four distinct peaks at δ 5.08 (J = 15.0 Hz), 4.43 (J = 13.5 Hz), 3.15 (J = 12.3 Hz) and 3.13 (J = 12.9 Hz) ppm were visible, which clearly are not attributed to **1** but arise from a second compound present in solution. Similarly, two additional peaks at δ 0.36 and 0.30 ppm in the alkylsilyl region were observed at this time, as were two additional downfield singlets at δ 6.32 and 6.30 ppm, each arising from a Si-H proton.

The presence of the four features at δ 6.32, 6.30, 0.36 and 0.30 ppm along with the structural rigidity evident in the intermediate species suggest that all or part of the Ge_2NO rhombus and the two $–Si(H)(NH_2)_2$ groups are generated prior to silylation of the remaining hydroxyl group to generate the silyl ether moiety. Further evidence for this

results from the presence of a broad singlet at δ 5.92 ppm which suggests the presence of a single hydroxyl group in the intermediate species. Similar ^{1}H-NMR –OH features were observed for the main group calixarenes {(OH)(calix[4]arene)P} (δ 5.4 ppm)[201], {(OH)(p-*tert*-butylcalix[4]arene)SiMe} (δ 4.59 ppm)[205], {(OH)(calix[4]arene)As} (δ 4.90 ppm)[144], and {(OH)(p-*tert*-butylcalix[4]areneAs} (δ 4.74 ppm)[144], (see structures in **Figure 5.7**) all of which have a single unbound –OH group and three oxygen atoms bound to the main group element.

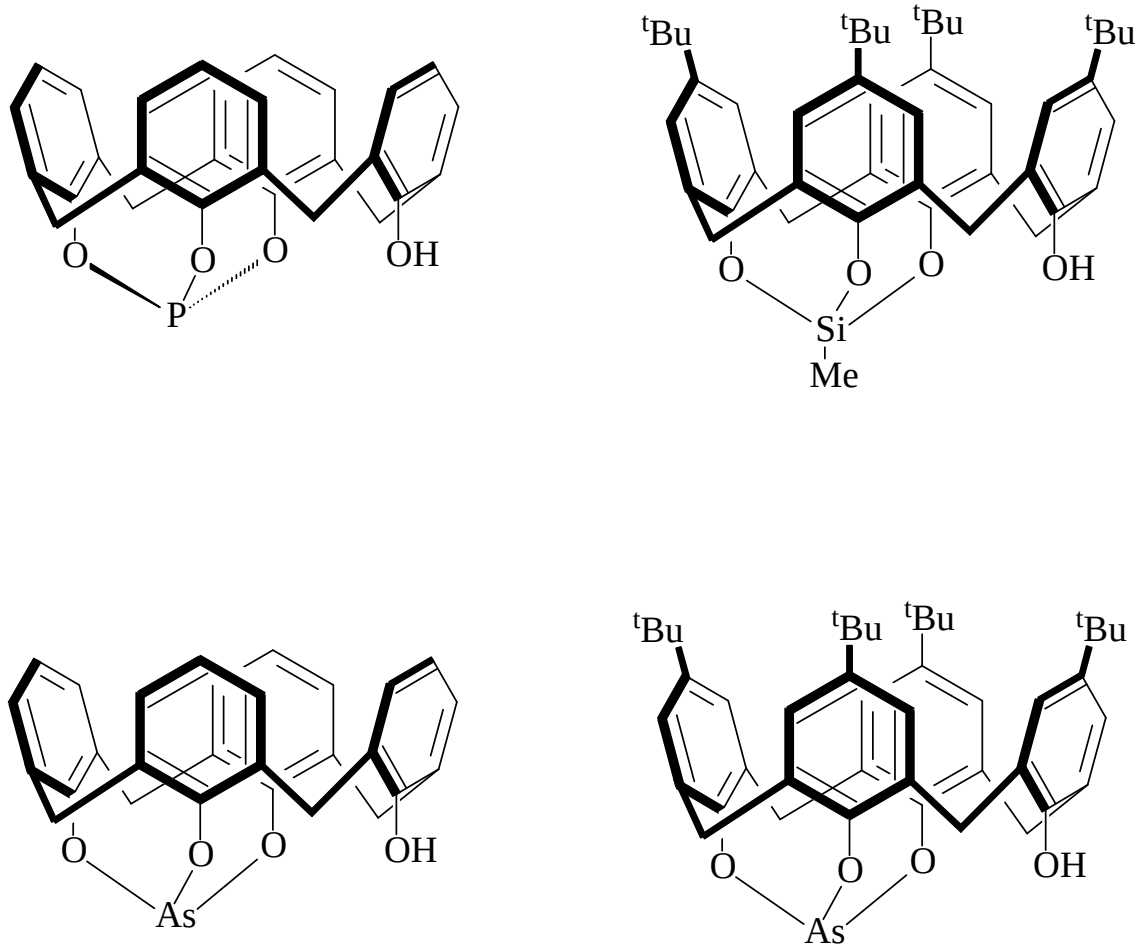

Figure 5.7: Structures of {(OH)(calix[4]arene)P}, {(OH)(p-*tert*-butylcalix[4]arene)SiMe}, {(OH)(calix[4]arene)As}, and {(OH)(p-*tert*-butylcalix[4]areneAs}.

The resonance at δ 5.92 ppm had significantly reduced in intensity after heating the sample for a total of 48 hours, as had the two features at δ 6.32 and 6.30 ppm and the upfield peaks at δ 0.36 and 0.30 ppm. We therefore postulate that the structure of the intermediate detected by ^{1}H-NMR spectroscopy is that of **2** illustrated **Scheme 5.3**, which undergoes an exchange of the –$SiMe_3$ group attached to the nitrogen with the remaining hydroxyl proton followed by closure of the Ge_2NO rhombus.

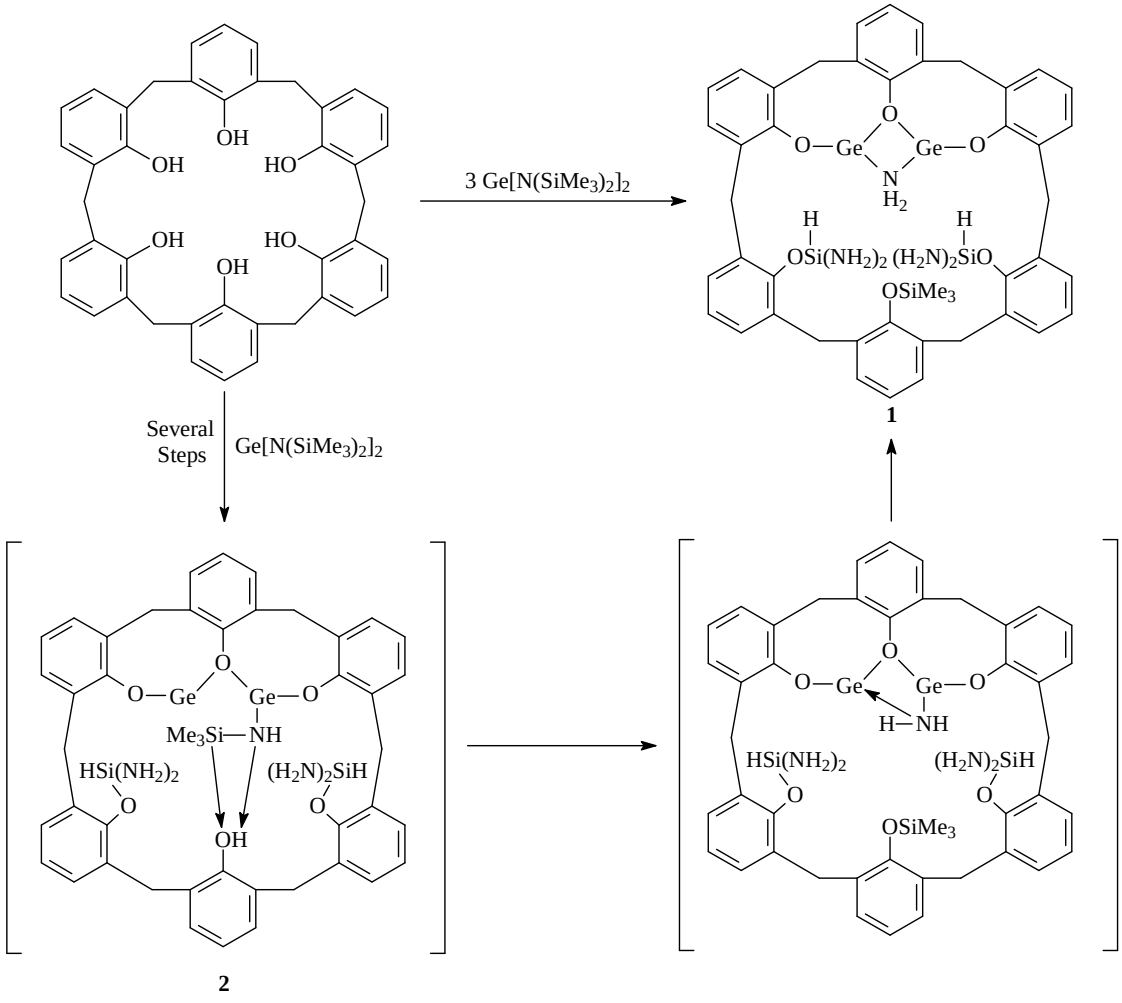

Scheme 5.3: Proposed pathway for the reaction of calix[6]arene with 3 equivalents of $Ge[N(SiMe_3)_2]_2$.

After heating the sample for an additional 12 h resonances corresponding only to **1**, free $HN(SiMe_3)_2$, and unreacted $Ge[N(SiMe_3)_2]_2$ remained. The appearance of the spectrum remained unchanged with up to 120 hours of heating at 85 ºC. Nearly identical results were obtained when calix[6]arene was treated with 2 equivalents of $Ge[N(SiMe_3)_2]_2$ under the same reaction conditions except that $Ge[N(SiMe_3)_2]_2$ was absent after the reaction had gone to completion. The outcome of this process is consistent with the overall reaction stoichiometry since two germanium atoms are present in the framework of **1**. The ^{1}H-NMR spectra of the reaction of calix[6]arene with 1 equivalent of $Ge[N(SiMe_3)_2]_2$ in benzene-d_6 indicated the formation of a complex mixture of species which include **1** and the intermediate **2** which remained present in solution even after heating the reaction mixture for 120 hours.

In the course of these studies, no conclusive evidence for the formation of $GeMe_4$ or CH_4 was found which exhibit similar ^{1}H-NMR resonances at δ 0.14 and 0.15 ppm in benzene-d_6. However, identification of calix[6]arene as the source of all of the protons in the two $–Si(H)(NH_2)_2$ groups and in the bridging $-NH_2-$ group was confirmed by the reaction of three equivalents of $Ge[N(SiMe_3)_2]_2$ with calix[6]arene-d_6 (prepared via the reaction of calix[6]arene with a solution of 2.5M Bu^nLi in hexanes followed by quenching with D_2O) which contained six dueterated hydroxyl groups. The ^{1}H-NMR spectrum of the resulting product contained only a single line at δ 0.42 ppm arising from the $–OSiMe_3$ moiety as well as a feature corresponding to unreacted germanium amide.

Conclusions

In conclusion the reactivity of calix[6]arene with $Ge[N(SiMe_3)_2]_2$ differs considerably from that found in reactions involving calix[4]arene and calix[8]arene. Instead of forming complexes containing Ge_2O_2 rhombi, the germanium calix[6]arene complex **1** contains a central Ge_2NO rhombus incorporating three of six oxygen atoms of the macrocycle. The remaining three oxygen atoms have been converted to two $–OSi(H)(NH_2)_2$ moieties and one $–OSiMe_3$ group. The pathway for the formation of **1** is likely complex, but involves the consumption of two equivalents of calix[6]arene for each equivalent of **1** produced in the reaction.

Experimental

All manipulations were carried out using standard Schlenk, syringe and glovebox techniques.[72] Calix[6]arene was purchased from Alfa Aesar and $Ge[N(SiMe_3)_2]_2$ was synthesized according to the published procedure.[13,74,193] Solvents were dried using a Glass Contour Solvent Purification System. One and two-dimensional ^{1}H-NMR spectra were recorded at 400 MHz on a Varian Unity INOVA 400 spectrometer and referenced to residual protio solvent. For the ^{1}H-NMR assignments in **1**, the numbering scheme of the carbon atoms corresponds to the crystal structure of **1**, *i.e.* $–C(5)H_2-$ refers to a proton bound to C(5). ^{13}C-NMR spectra were recorded at a frequency of 100.6 MHz on a Varian Unity INOVA 400 and referenced to the solvent while ^{29}Si-NMR were acquired using a Varian Unity INOVA 600 operating at 119.2 MHz and were referenced to external $SiMe_4$. Mass spectra were acquired using a Bruker Agilent 1100 LC/MSD

System in acetonitrile solvent. Elemental analysis was performed by Midwest Microlab, LLC (Indianapolis, IN).

Synthesis of compound 1

To a solution of calix[6]arene (0.458 g, 0.719 mmol) in benzene (10ml) was added a solution of $Ge[N(SiMe_3)_2]_2$ (0.852 g, 2.17 mmol) in benzene (4ml). The mixture was sealed in a Schlenk tube and heated at 85 ºC for 72 h. The solvent was removed *in vacuo* to yield a white solid which was recrystallized from hot benzene (5ml) to yield **1** as colorless crystals which were washed with hexane (3 x 15ml) and dried *in vacuo*. Yield: 0.292 g (41 %). ^{1}H NMR (C_6D_6, 25 °C): δ 7.29 – 6.75 (m, 18 H, aromatics), 6.34 (s, 1H, -Si(*H*)$(NH_2)_2$), 6.32 (s, 1H, -Si(*H*)$(NH_2)_2$), 4.74 (d, *J* = 13.2 Hz, 1H –C(5)H_2-), 4.66 (d, *J* = 14.7 Hz, 1H, -C(4)H_2-), 4.64 (d, *J* = 12.6 Hz, 1H, -C(3)H_2-), 4.53 (d, *J* = 16.2 Hz, 1H, -C(6)H_2-), 4.51 (d, *J* = 11.7 Hz, 1H, -C(2)H_2-), 4.34 (d, *J* = 13.5 Hz, 1H, -C(1)H_2-), 3.53 (d, *J* = 16.2 Hz, 1H, -C(6)H_2-), 3.32 (d, *J* = 13.2 Hz, 1H, -C(5)H_2-), 3.30 (d, *J* = 14.7 Hz, 1H, -C(4)H_2-), 3.24 (d, *J* = 13.5 Hz, 1H, -C(1)H_2-), 3.23 (d, *J* = 12.6 Hz, 1H, -C(3)H_2-), 3.19 (d, *J* = 11.7 Hz, 1H, -C(2)H_2-), 1.66 (br d, *J* = 9.6 Hz, 1H, -NH_2-), 1.04 (br d, *J* = 9.6 Hz, 1H, -NH_2-), 0.42 (s, 9H, -OSi(CH_3)$_3$), 0.27 (s, 4H, -Si(H)(NH_2)$_2$), 0.24 (s, 4H, -Si(H)(NH_2)$_2$) ppm. ^{13}C NMR (C_6D_6, 25 °C) δ 156.1, 154.4, 152.0, 151.6, 151.1, 150.8 (*ipso*-C), 136.8, 136.6, 136.4, 136.1, 135.9, 135.2, 134.5, 133.3, 132.8, 132.6, 132.1, 132.0 (*meta*-C), 131.0, 130.8, 130.7, 130.5, 130.4, 130.3, 129.8, 129.7, 129.4, 129.3, 129.1, 128.8 (*ortho*-C), 123.6, 122.7, 122.3, 122.2, 120.9, 120.8 (*para*-C), 34.2, 34.0, 33.9, 33.4, 33.1, 31.1 (-*C*H_2-), 1.6 (-OSi(*C*H_3)$_3$) ppm. ^{29}Si{^{1}H} NMR (C_6D_6, 25 ° C): δ 21.63, 21.17, and 21.07 ppm. IR (Nujol): 3348, 3266, 3255, 2720, 2664, 2288, 1916,

1859, 1807, 1713, 1661, 1589 cm^{-1}. Anal. Calcd. for $C_{45}H_{51}Ge_2N_5O_6Si_3$: C, 54.74; H, 5.21. Found: 54.15; H, 5.41%.

NMR scale reaction of calix[6]arene with 3 equivaents of $Ge[N(SiMe_3)_2]_2$

A solution of calix[6]arene (0.050 g, 0.078 mmol) in benzene-d_6 (.25 ml) was treated with a solution of $Ge[N(SiMe_3)_2]_2$ (0.093 g, 0.24 mmol) in benzene-d_6 (.25 ml) in a screw-cap NMR tube.

NMR scale reaction of calix[6]arene with 2 equivaents of $Ge[N(SiMe_3)_2]_2$

A solution of calix[6]arene (0.050 g, 0.078 mmol) in benzene-d_6 (.25 ml) was treated with a solution of $Ge[N(SiMe_3)_2]_2$ (0.062 g, 0.16 mmol) in benzene-d_6 (.25 ml) in a screw-cap NMR tube.

NMR scale reaction of calix[6]arene with 2 equivaents of $Ge[N(SiMe_3)_2]_2$

A solution of calix[6]arene (0.050 g, 0.078 mmol) in benzene-d_6 (.25 ml) was treated with a solution of $Ge[N(SiMe_3)_2]_2$ (0.031 g, 0.079 mmol) in benzene-d_6 (.25 ml) in a screw-cap NMR tube.

Synthesis of calix[6]arene-d_6

To a solution of calix[6]arene (0.300 g, 0.471 mmol) in diethyl ether (30 ml) was added a solution of 2.5 M Bu^nLi in hexanes (1.51 ml, 3.78 mmol) at -78 ºC. The reaction mixture was allowed to come to room temperature and was stirred for 4 h. The reaction mixture was quenched with D_2O (5 ml) at -78 ºC via cannula from a sure-seal bottle. The

organic layer was separated and dried over anhydrous $MgSO_4$ and the solvent was removed in *vacuo* to yield calix[6]arene-d_6 (0.221 g, 72%). The ^{1}H-NMR spectrum of the product recorded in benzene-d_6 did not exhibit an –OH resonance.

NMR scale reaction of calix[6]arene-d_6 with 3 equivaents of $Ge[N(SiMe_3)_2]_2$

To a solution of calix[6]arene-d_6 (0.057 g, 0.088 mmol) in benzene-d_6 (0.35 ml) was added a solution of $Ge[N(SiMe_3)_2]_2$ (0.107 g, 0.272 mmol) in benzene-d_6 (0.30 ml). The reaction mixture was heated in an oil bath for 48 h and the ^{1}H-NMR spectrum was recorded.

X-ray crystal structure of 1· 0.5(C_6H_6)

Diffraction intensity data were collected with a Siemens P4/CCD diffractometer. Absorption corrections were applied for all data by SADABS. The structures were solved using direct methods, completed by Fourier synthesis, and refined by full-matrix least squares procedures on F^2. All non-hydrogen atoms were refined with anisotropic displacement coefficients, and hydrogen atoms were treated as idealized contributors. Contributions from the benzene solvent molecule were removed using SQUEEZE. All software and sources of scattering factors are contained in the SHEXTL (5.10) program package (G. Sheldrick, Bruker XRD, Madison, WI). ORTEP diagrams were drawn using the ORTEP3 program (L.J. Farrugia, Glasgow).

Crystallographic data for **1· 0.5(C_6H_6)**: Crystal size: 0.23 x 0.22 x 0.17 mm. Crystal color and habit: colorless block. Empirical formula: $C_{48}H_{54}Ge_2N_5O_6Si_3$. Formula weight: 1026.42. Wavlength: 0.71073 Å. Temperature: 100(2) K. Crystal system: triclinic. Space group: P-1. Unit cell dimensions: *a* = 13.199(2) Å, *b* = 14.774(2) Å; *c* =

16.569(4) Å; α = 105.373(4) °; β = 102.641(4) °; γ = 115.225(3) °. Volume = 2606.5(9) Å^3. Z = 2. D_{calc} = 1.309 g/cm^3. Absorption coefficient = 1.274 mm^{-1}. F(000) = 1064. θ-Range for data collection = 1.67 – 25.00 °. Index ranges: - 14 ≤ h ≤ -15; -15 ≤ k ≤ 17; -19 ≤ l ≤ 19. Reflections collected = 15228. Independent reflections = 9124 (R_{int} = 0.0295). Completeness to θ = 99.2 % (θ = 25.00 °). Absorption correction = multi-scan. Refinement method = full-matrix least-squares on F^2. Data/restraints/parameters = 9124/0/584. Goodness-of-fit on F^2 = 1.014. Final R indices [$I > 2\sigma(I)$]: R_1 = 0.0581; wR_2 = 0.1414. R indices (all data): R_1 = 0.0884; wR_2 = 0.1580. Largest difference in peak and hole = 0.512 and -0.547 eÅ^{-3}.

References

(1) Neumann, W. P. *Chem. Rev.* **1991**, *91*, 311-334.
(2) Lappert, M. F.; Rowe, R. S. *Coordination Chemistry Reviews* **1990**, *100*, 267-292.
(3) Cotton, J. D.; Davidson, P. J.; Lappert, M. F. *Dalton Trans.* **1976**, *21*, 2275-2286.
(4) Chorley, R. W.; Hitchcock, P. B.; Lappert, M. F.; Leung, W. P.; Power, P. P.; Olmstead, M. M. *Inorg. Chim. Acta* **1992**, 203-209.
(5) Davidson, P. J.; Harris, D. H.; Lappert, M. F. *Dalton Trans.* **1976**, *21*, 2268-2274.
(6) Goldberg, D. E.; Hitchcock, P. B.; Lappert, M. F.; MarkThomas, K.; Thorne, A. J.; Fjeldberg, T.; Haaland, A.; Schilling, B. E. R. *J. Chem. Soc., Dalton Trans.* **1986**, 2387-2394.
(7) Miller, K. A.; Bartolin, J. M.; O'Neill, R. M.; Sweeder, R. D.; Thomas M. Owens; Kampf, J. W.; Holl, M. M. B.; Wells, N. J. *J. Am. Chem. Soc.* **2003**, *125*, 8986-8987.
(8) Miller, K. A.; Watson, T. W.; John E. Bender, I.; Holl, M. M. B.; Kampf, J. W. *J. Am. Chem. Soc.* **2001**, *123*, 982-983.
(9) Walker, R. H.; Miller, K. A.; Scott, S. L.; Cygan, Z. T.; Bartolin, J. M.; Kampf, J. W.; Holl, M. M. B. *Organometallics* **2009**, *28*, 2744–2755.
(10) Sweeder, R. D.; Miller, K. A.; Edwards, F. A.; Wang, J.; Holl, M. M. B.; Kampf, J. W. *Organometallics* **2003**, *22*, 5054-5062.
(11) Gynane, M. J. S.; Harris, D. H.; Lappert, M. F.; Power, P. P.; Riviere, P.; Riviere-Baudet, M. *Dalton Trans.* **1977**, *20*, 2004-2009.
(12) Lappert, M. F.; Power, P. P.; Sanger, A. R.; Srivastava, R. C. *Metal and Metalloid Amides*; John Wiley & Sons: New York, 1980.
(13) Zhu, Q.; Ford, K. L.; Roskamp, E. J. *Heteroatom Chemistry* **1992**, *3*, 647-9.
(14) Litz, K. E.; John E. Bender, I.; Kampf, J. W.; Holl, M. M. B. *Angew. Chem. Int. Ed. Engl.* **1997**, 496-498.
(15) Gehrhus, B.; Hitchcock, P. B.; Lappert, M. F. *Angew. Chem. Int. Ed. Engl.* **1997**, *36*, 2514-2516.
(16) Dickie, D. A.; Maclntosh, I. S.; Ino, D. D.; He, Q.; Labeodan, O. A.; Jennings, M. C.; Schatte, G.; Walsby, C. J.; Clyburne, J. A. C. *Can. J. Chem.* **2008**, *86*, 20-31.
(17) Glidewell, C.; Lloyd, D.; Lumbard, K. W. *J. Chem. Soc., Dalton Trans.* **1987**, 501-508.
(18) HITCHCOCK, P. B.; JASIM, H. A.; LAPPERT, M. F.; LEUNG, W.-P.; RAI, A. K.; TAYLOR5, R. E. *Polyhedron* **1991**, *10*, 1203-1213.
(19) Weinert, C. S.; Fenwick, A. E.; Fanwick, P. E.; Rothwell, I. P. *J. Chem. Soc., Dalton Trans.* **2003**, 532-539.
(20) Cetinkays, B.; Giimriikcii, I.; Lappert, M. F.; Atwood, J. L.; Shakir, R. *J. Am. Chem. Soc.* **1980**, *102*, 2088-2089.
(21) Nelson, T. D.; Crouch, D. R. *Synthesis* **1996**, *9*, 1031-1069.
(22) Clarke, P. A.; Martin, W. H. C. *Annu. Rep. Prog. Chem., Sect. B* **2003**, *99*,

84-103.
(23) Green, T. W.; Wuts, P. G. M. *Protective Groups in Organic Synthesis*; 3rd ed.; John Wiley and Sons: New York, 1999.
(24) Jarowicki, K.; Kocien´ski, P. *J. Chem. Soc., Perkin Trans. 1* **1999**, 1589-1615.
(25) Jarowicki, K.; Kocienski, P. *Contemporary Organic Synthesis* **1995**, *2*, 315-336.
(26) Jarowicki, K.; Kocienski, P. *Contemporay Organic Synthesis* **1996**, *3*, 397-431.
(27) Jarowicki, K.; Kocienski, P. *Contemporary Organic Synthesis* **1997**, *4*, 454-492.
(28) Jarowicki, K.; Kocienski, P. *J. Chem. Soc., Perkin Trans. 1* **1998**, 4005-4037.
(29) Jarowicki, K.; Kocienski, P. *J. Chem. Soc., Perkin Trans. 1* **2000**, 2495-2527.
(30) Jarowicki, K.; Kocienski, P. *J. Chem. Soc., Perkin Trans. 1* **2001**, 2109-2135.
(31) Muzart, J. *Synthesis* **1993**, 11-27.
(32) Spivey, A. C.; Leese, D. *Annu. Rep. Prog. Chem., Sect. B* **2002**, *98*, 41-60.
(33) Spivey, A. C.; Srikaran, R. *Annu. Rep. Prog. Chem., Sect. B* **2001**, *97*, 41-59.
(34) Karimi, B.; Golshani, B. *J. Org. Chem.* **2000**, *65*, 7228-7230.
(35) Gautret, P.; El-Ghammarti, S.; Legrand, A.; Couturier, D.; Rigo, B. *Synth. Commun.* **1996**, *26*, 707-713.
(36) Langer, S. H.; Connell, S.; Wender, I. *J. Org. Chem.* **1958**, *23*, 50-58.
(37) Bruynes, C. A.; Jurriens, T. K. *J. Org. Chem.* **1982**, *20*, 3966-3969.
(38) Akhlaghinia, B.; Asadi, M.; Safaee, E.; Heydarpoor, M. *Phosphorus, Sulfur, Silicon Relat. Elem.* **2004**, *179*, 2099-2104.
(39) Harada, T.; Kurokawa, H.; Kagamihara, Y.; Tanaka, S.; Inoue, A.; Oku, A. *J. Org. Chem.* **1992**, *57*, 1412-1421.
(40) Tanabe, Y.; Mubakami, M.; Kitaichi, K.; Yoshida, Y. *Tetrahedron Lett.* **1994**, *35*, 8409-8412.
(41) Firouzabadi, H.; B.Karimi *Synth. Commun.* **1993**, *23*, 1633-41.
(42) Firouzabadi, H.; Sardarian, A. R.; Khayat, Z.; B.Karimi; Tangcstanincjad, S. *Synth. Commun.* **1997**, *27*, 2709-2719.
(43) Firouzabadi, H.; Iranpoor, N.; Amani, K.; Nowrouzi, F. *J. Chem. Soc., Perkin Trans. 1* **2002**, 2601–2604.
(44) Shirini, F.; Zolfigol, M. A.; Mohammadi, K. *Phosphorus, Sulfur, Silicon Relat. Elem.* **2003**, *178*, 1567–1570.
(45) Curhi, M.; Epifano, F.; Marcotullio, M. C.; Rosati, O. *Synth. Commun.* **1999**, *29*, 541-546.
(46) Zhang, Z.-H.; Li, T.-S.; Yang, F.; Fu, C.-G. *Synth. Commun.* **1998**, *28*, 3105-31 14.
(47) Tillu, V. H.; Jadhav, V. H.; Borate, H. B.; Wakharkar, R. D. *ARKIVOC* **2004**, 83-88.
(48) Chaudhary, S. K.; Hernandez *Tetrahedron Lett.* **1979**, *2*, 99 - 102.

(49) D'Sa, B. A.; McLeod, D.; Verkade, J. G. *J. Org. Chem.* **1997**, *62*, 5057-5061.
(50) Hayashi, M.; Matsuura, Y.; Watanabe, Y. *Tetrahedron Lett.* **2004**, *45*, 1409–1411.
(51) Huang, X.; Craita, C.; Awad, L.; Vogel, P. *Chem. Commun* **2005**, 1297–1299.
(52) Ito, H.; Takagi, K.; Miyahara, T.; Sawamura, M. *Organic Letters* **2005**, *7*, 3001-3004.
(53) Wetherby, A. E., Jr. ; Benson, S. D.; Weinert, C. S. *Inorg. Chim. Acta* **2007**, *360*, 1977–1986.
(54) Wetherby, A. E., Jr.; Goeller, L. R.; DiPasquale, A. G.; Rheingold, A. L.; Weinert, C. S. *Inorg. Chem.* **2007**, *46*, 7579-7586.
(55) Wetherby, A. E., Jr.; Goeller, L. R.; DiPasquale, A. G.; Rheingold, A. L.; Weinert, C. S. *Inorg. Chem.* **2008**, *47*, 2162-2170.
(56) Nöth, H.; Schlosser, D. *Inorg. Chem.* **1983**, *22*, 2700-2703.
(57) Nöth, H.; Schlosser, D. *Eur. J. Inorg. Chem.* **2003**, 2245-2254.
(58) Chadwick, S.; Englich, U.; Ruhlandt-Senge, K. *Angew. Chem. Int. Ed* **1998**, *37*, 3007-3009.
(59) Wiberg, N.; Uhlenbrock, W. *Chem. Ber.* **1971**, *104*, 2643.
(60) Emsley, J. *The Elements*; 3rd ed.; Clarendon Press: Oxford, 1998.
(61) Arnold, P. L.; Natrajan, L. S.; Hall, J. J.; Bird, S. J.; Wilson, C. *J. Organomet. Chem.* **2002**, *647*, 205–215.
(62) Corden, J. P.; Errington, W.; Moore, P.; Partridge, M. G.; Wallbridge, M. G. H. *Dalton Trans.* **2004**, 1846-1851.
(63) Dong, C.; Zhang, J.; Zheng, W.; Zhang, L.; Yu, Z.; Choi, M. C. K.; Chan, A. S. C. *Tetrahedron: Asymmetry* **2000**, *11*, 2449-2454.
(64) Geldbach, T. J.; Chaplin, A. B.; Ha¨nni, K. D.; Scopelliti, R.; Dyson, P. J. *Organometallics* **2005**, *24*, 4974-4980.
(65) Nagataki, T.; Tachi, Y.; Itoh, S. *J. Mol. Catal. A: Chem.* **2005**, *225*, 103–109.
(66) Natrajan, L. S.; Blake, A. J.; Wilson, C.; Weinsteinand, J. A.; Arnold, P. L. *Dalton Trans.* **2004**, 3748-3755.
(67) Natrajan, L. S.; Wilson, C.; Okuda, J.; Arnold, P. L. *Eur. J. Inorg. Chem.* **2004**, 3724-3732.
(68) Yu, X.; Marks, T. J. *Organometallics* **2007**, *26*, 365-376.
(69) Pearson, R. G. *Inorg. Chem.* **1988**, *27*, 734-740.
(70) Weinert, C. S.; Fanwick, P. E.; Rothwell, I. P. *J. Chem. Soc., Dalton Trans.* **2002**, 2948–2950.
(71) Mori, K.; Masuda, Y.; Kashino, S. *Acta Cryst.* **1993**, *C49*, 1224-1227.
(72) Shriver, D. F.; Drezdzon, M. A. *The Manipulation of Air Sensitive Compounds*; 2nd ed.; John Wiley and Sons: New York, 1986.
(73) Buisman, G. J. H.; Veen, L. A. v. d.; Klootwijk, A. l.; Lange, W. G. J. d.; Kamer, P. C. J.; Leeuwen, P. W. N. M. v.; Vogt, D. *Organometallics* **1997**, *16*, 2929-2939.
(74) Gynane, M. J. S.; Harris, D. H.; Lappert, M. F.; Power, P. P.; Rividre, P.; Rividre-Baudet, M. *J. Chem. Soc., Dalton Trans.* **1977**, 2004-2009.

(75) Buerger, H.; Forker, C.; Goubeau, J. *Monatsh. Chem.* **1965**, *96*, 597-601.
(76) Bradley, D. C.; Hursthouse, M. B.; Ibrahim, A. A.; Malik, K. M. A.; Motevalli, M.; Moseler, R.; Powell, H.; Runnacles, J. D.; Sullivan, A. C. *Polyhedron* **1990**, *9*, 2959-2964.
(77) Engelhardt, L. M.; Jolly, B. S.; Junk, P. C.; Raston, C. L.; Skelton, B. W.; White, A. H. *Australian Journal of Chemistry* **1986**, *39*, 1337-45.
(78) Westerhausen, M. *Inorg. Chem.* **1991**, *30*, 96-101.
(79) Buerger, H.; Sawodny, W.; Wannagat, U. *J. Organomet. Chem.* **1965**, *3*, I I 3-120.
(80) Deleuze, M. S. *J. Chem. Phys.* **2002**, *116*, 7012-7026.
(81) Dimitrakopoulos, C. D. *P.R. L. Malenfant* **2002**, *99*, 99-117.
(82) Dotz, F.; Brand, J. D.; Ito, S.; Gherghel, L.; Mu1llen, K. *J. Am. Chem. Soc.* **2000**, *122*, 7707-7717.
(83) Klauk, H.; Halik, M.; Zschieschang, U.; Schmid, G.; Radlik, W. *J. Appl. Phys.* **2002**, *92*, 5259-5263.
(84) Mori, T.; Takeuchi, H.; Fujikawa, H. *J. Appl. Phys.* **2005**, *97*, 066101-066103.
(85) Müller, M.; Kübel, C.; Müllen, K. *Chem. Eur. J.* **1998**, *4*, 2099-2109.
(86) Ramamurthy, V.; Schanze, K. S. *Eds. Solid State and Surface Photochemistry*; CRC Press: New York, 2000.
(87) Asari, T.; Kobayashi, N.; Naito, T.; Inabe, T. *Bull. Chem. Soc. Jpn.* **2001**, *74*, 53-58.
(88) Hjorth, M.; Thorup, N.; Frederiksen, P.; Bechgaard, K. *Acta. Chem. Scand.* **1994**, *48*, 139-43.
(89) Asari, T.; Ishikawa, M.; Naito, T.; Matsuda, M.; Tajima, H.; Inabe, T. *Chem. Lett.* **2005**, *34*, 936-937.
(90) Asari, T.; Naito, T.; Inabe, T.; Matsuda, M.; Tajima, H. *Chem. Lett.* **2004**, *33*, 128-129.
(91) Inabe, T. *Mol. Cryst. Liq. Cryst.* **2002**, *376*, 225-232.
(92) Inabe, T.; Asari, T.; Hasegawa, H.; Matsuda, M.; Gacho, E. H.; Matsumura, N.; Takeda, S.; Takeda, K.; Naito, T. *Synth. Met.* **2003**, *133-134*, 515-518.
(93) Takano, S.; Naito, T.; Inabe, T. *Chem. Lett.* **1998**, 1249-1250.
(94) Hanasaki, N.; Matsuda, M.; Tajima, H.; Naito, T.; Inabe, T. *Synth. Met.* **2003**, *133-134*, 519-521.
(95) Matsuda, M.; Asari, T.; Naito, T.; Inabe, T.; Hanasaki, N.; Tajima, H. *Bull. Chem. Soc. Jpn.* **2003**, *76*, 1935–1940.
(96) Matsuda, M.; Hanasaki, N.; Tajima, H.; Naito, T.; Inabe, T. *J. Chem. Phys. Solids* **2004**, *65*, 749-752.
(97) Doi, S.; Fujita, A.; Ikeura, S.; Inabe, T.; Matsunaga, Y. *Bull. Chem. Soc. Jpn.* **1979**, *52*, 2494-2500.
(98) Ikegami, K.; Matsunaga, Y.; Osafune, K.; Osawa, E. *Bull. Chem. Soc. Jpn.* **1975**, *48*, 341-342.
(99) Sugimoto, A.; Kato, S.; Inoue, H.; Imoto, E. *Bull. Chem. Soc. Jpn.* **1976**, *49*, 337-338.
(100) Pummerer, R.; Prell, E.; Rieche, A. *Chem. Ber.* **1926**, *59*, 2159-2161.

(101) Lau, W.; Kochi, J. K. *J. Org. Chem.* **1986**, *51*, 1801-1811.
(102) Lau, W.; Kochi, J. K. *J. Am. Chem. Soc.* **1986**, *108*, 6720-6732.
(103) Taylor, R. *Electrophilic Aromatic Substitution*; John Wiley & Sons: Chichester, 1991.
(104) Bockman, T. M.; Kosynkin, D.; Kochi, J. K. *J. Org. Chem.* **1997**, *62*, 5811-5820.
(105) Boga, C.; Vecchio, E. D.; Forlani, L. *Eur. J. Org. Chem.* **2004**, 1567-1571.
(106) Hubig, S. M.; Kochi, J. K. *J. Org. Chem.* **2000**, *65*, 6807-6818.
(107) Atherton, J. H.; Moodie, R. B.; Noble, D. R. *J. Chem. Soc., Perkin Trans. 2* **1999**, 699-705.
(108) Hubig, S. M.; Kochi, J. K. *J. Am. Chem. Soc.* **2000**, *122*, 8279-8288.
(109) Morley, J. O.; Roberts, D. W. *J. Org. Chem.* **1997**, *62*, 7358-7363.
(110) Foster, D. j.; Tobler, E. *J. Am. Chem. Soc.* **1961**, *83*, 851-855.
(111) Fields, R.; Haszeldlne, R. N.; Palmer, P. J. *Tetrahedron Lett.* **1971**, 1879-1882.
(112) Foster, D. J.; Tobler, E. *J. Org. Chem.* **1962**, *27*, 834-837.
(113) Blackburn, G. M.; Cameron, D. W.; Chan, H. W.-S. *J. Chem. Soc. C* **1966**, 1836-1842.
(114) Brevard, C.; Granger, P. *Handbook of High Resolution Multinuclear NMR*; John Wiley & Sons: New York, 1981.
(115) Sens, M. A.; Wilson, N. K.; Ellis, P. D.; Odom, J. D. *J. Mag. Reson.* **1975**, *19*, 323-336.
(116) Asfari, Z.; Bohmer, V.; Harrowfield, J.; Vincens, J. *Calixarenes 2001*; Kluwer Academic Publishers: Dordrecht, The Netherlands, 2001.
(117) Bohmer, V. *Angew. Chem. Int. Ed. Engl.* **1995**, *34*, 713-745.
(118) de Namor, A. F. D.; Cleverley, R. M.; Zapata-Ormachea, M. L. *Chem. Rev.* **1998**, *98*, 2495-2525.
(119) Gutsche, C. D. *Calixarenes Revisited*; Royal Society of Chemistry: Cambridge, 1998.
(120) Hof, F.; Craig, S. L.; Nuckolls, C.; Rebek, J., Jr. *Angew. Chem. Int. Ed.* **2002**, *41*, 1488-1508.
(121) Pochini, A.; Ungaro, R. *In Comprehensive Supramolecular Chemistry*; Atwood, J. L., Davis, J. E. D., MacNicol, D. D.,Vogtle, F., Pergamon Press: New York, 1996; Vol. 2.
(122) Vincens, J.; Bohmer, V. *Calixarenes, A Vesatile Class of Macrocyclic Compounds*; Kluwer Academic Publishers: Dordrecht, The Netherlands, 1991.
(123) Brown, M.; Jablonski, C. *Can. J. Chem.* **2001**, *79*, 463-471.
(124) Coquiere, D.; Marrot, J.; Reinaud, O. *Chem. Commun.* **2006**, 3924-3926.
(125) Cotton, F. A.; Daniels, L. M.; Lin, C.; Murillo, C. A. *Inorg. Chim. Acta* **2003**, *347*, 1-8.
(126) Dorta, R.; Shimon, L. J. W.; Rozenberg, H.; Ben-David, Y.; Milstein, D. *Inorg. Chem.* **2003**, *42*, 3160-3167.
(127) Durr, S.; Bechlars, B.; Radius, U. *Inorg. Chim. Acta* **2006**, *359*, 4215-4226.
(128) Estler, F.; Herdtweck, E.; Anwander, R. *J. Chem. Soc., Dalton Trans.*

2002, 3088–3089.
(129) Jeunesse, C.; Armspach, D.; Matt, D. *Chem. Commun.* **2005**, 5603–5614.
(130) Khasnis, D. V.; Burton, J. M.; Lattman, M.; Zhang, H. *J. Chem. Soc. Chem. Commun.* **1991**, 562-563.
(131) Khasnis, D. V.; Lattman, M. *J. Am. Chem. Soc.* **1990**, *112*, 9423-9425.
(132) Kotzen, N.; Goldberg, I.; Vigalok, A. *Inorg. Chem. Commun.* **2005**, *8*, 1028-1030.
(133) Loffler, F.; Luning, U.; Gohar, G. *New J. Chem.* **2000**, *24*, 935-938.
(134) MacLachlan, E. A.; Fryzuk, M. D. *Organometallics* **2006**, *25*, 1530-1543.
(135) Marcos, P. M.; Mellah, B.; Ascenso, J. R.; Michel, S.; Hubscher-Bruderd, V. r.; Arnaud-Neu, F. *New J. Chem.* **2006**, *30*, 1655-1661.
(136) Pellet-Rostaing, S.; Regnouf-de-Vains, J.-B.; Lamartine, R.; Fenet, B. *Inorg. Chem. Commun.* **1999**, *2*, 44-47.
(137) Petrella, A. J.; Raston, C. L. *J. Organomet. Chem.* **2004**, *689*, 4125-4136.
(138) Radius, U. *Z. Anorg. Allg. Chem.* **2004**, *630*, 957-972.
(139) Redshaw, C.; Rowan, M. A.; Warford, L.; Homden, D. M.; Arbaoui, A.; Elsegood, M. R. J.; Dale, S. H.; Yamato, T.; Casas, C. P.; Matsui, S.; Matsuura, S. *Chem. Eur. J.* **2007**, *13*, 1090-1107.
(140) Seitz, J.; Maas, G. *Chem. Commun.* **2002**, 338-339.
(141) Sliwa, W. *Croat. Chem. Acta* **2002**, *75*, 131-153.
(142) Sliwa, W. *J. Inclusion Phenom. Macrocyclic Chem.* **2005**, *52*, 13-37.
(143) Xie, D.; Gutsche, C. D. *J. Org. Chem.* **1998**, *63*, 9270-9278.
(144) Shang, S.; Khasnis, D. V.; Zhang, H.; Small, A. C.; Fan, M.; Lattman, M. *Inorg. Chem.* **1995**, *34*, 3610-3615.
(145) Hascall, T.; Rheingold, A. L.; Guzeib, I.; Parkin, G. *Chem. Commun.* **1998**, 101-102.
(146) Hockeymeyer, J.; Valentin, B.; Castel, A.; Riviere, P.; Satge, J.; Cardin, C. J.; Teixeira, S. *Main Group Met. Chem.* **1997**, *20*, 775-781.
(147) McBurnett, B. G.; Cowley, A. H. *Chem. Commun.* **1999**, 17-18.
(148) Ohta, T.; Sakurai, T.; Fujiwara, K. *Appl. Organometal. Chem.* **2004**, *18*, 431-437.
(149) Sakurai, T.; Takeuchi, Y. *Heteroat. Chem.* **2003**, *14*, 365-373.
(150) Sakurai, T.; Takeuchi, Y. *Appl. Organometal. Chem.* **2005**, *19*, 372-376.
(151) Takeuchi, Y.; Sakurai, T.; Tanaka, K. *Main Group Met. Chem.* **2000**, *23*, 311-316.
(152) Weinert, C. S.; Fanwick, P. E.; Rothwell, I. P. *Acta Crystallogr.* **2002**, *E58*, m718-m720.
(153) Weinert, C. S.; Fanwick, P. E.; Rothwell, I. P. *Inorg. Chem.* **2003**, *42*, 6089-6094.
(154) Weinert, C. S.; Fenwick, A. E.; Fanwick, P. E.; Rothwell, I. P. *J. Chem. Soc., Dalton Trans.* **2003**, 532-539.
(155) Lang, J.; Deckerova, V.; Czernek, J.; Lhotak, P. *J. Chem. Phys.* **2005**, *122*, 0445061-04405611.
(156) Emsley, J. *The Elements, 2cnd ed.*; Clarendon Press: Oxford, 1991.
(157) Hitchcock, P. B.; Lappert, M. F.; Thomas, S. A.; Thorne, A. J.; Carty, A. J.; Taylor, N. J. *J. Organomet. Chem.* **1986**, *315*, 27-44.

(158) Green, R. A.; Rheingold, A. L.; Weinert, C. S. *Inorg. Chim. Acta* **2009**, *362*, 3159–3164.
(159) Chin, H. B.; Smith, M. B.; Wilson, R. D.; Bau, R. *J. Am. Chem. Soc.* **1974**, *96*, 5285-5287.
(160) Anema, S. G.; Barris, G. C.; Mackay , K. M.; Nicholson, B. K. *J. Organomet. Chem.* **1988**, *350*, 207-215.
(161) Batsanov, A. S.; Rybin, L. V.; Rybinskaya, M. I.; Struchkov, Y. T. *J. Organomet. Chem.* **1983**, *249*, 319-326.
(162) Melzer, D.; Weiss, E. *J. Organomet. Chem.* **1983**, *255*, 335-344.
(163) Anema, S. G.; Mackay , K. M.; McLeod, L. C.; Nicholson, B. K.; Whittaker, J. M. *Angew. Chem. Int. Ed. Engl.* **1986**, *25*, 759-760.
(164) Anema, S. G.; Mackay , K. M.; Nicholson, B. K. *Inorg. Chem.* **1989**, *28*, 3158-3164.
(165) Bonny, A.; Mackay, K. M. *J. Chem. Soc., Dalton Trans.* **1978**, 722-726.
(166) Bonny, A.; Mackay, K. M.; Wong, F. S. *J. Chem. Res., Synop.* **1985**, *2*, 40-41.
(167) Kawano, Y.; Sugawara, K.; Tobita, H.; Ogino, H. *Chem. Lett.* **1994**, 293-296.
(168) Mohamed, B. A. S.; Kikuchi, M.; Hashimoto, H.; Ueno, K.; Tobita, H.; Ogino, H. *Chem. Lett.* **2004**, *33*, 112-113.
(169) Anema, S. G.; Lee, S. K.; Mackay, K. M.; McLeod, L. C.; Nicholson, B. K.; Service, M. *J. Chem. Soc., Dalton Trans.* **1991**, 1209-1217.
(170) Anema, S. G.; Lee, S. K.; Mackay, K. M.; Nicholson, B. K.; Service, M. *J. Chem. Soc., Dalton Trans.* **1991**, 1201-1208.
(171) Foster, S. P.; Mackay, K. M. *J. Organomet. Chem.* **1982**, *238*, C46-C48.
(172) Gerlach, R. F.; Graham, B. W. L.; Mackay , K. M. *J. Organomet. Chem.* **1979**, *182*, 285-298.
(173) Gerlach, R. F.; Mackay, K. M.; Nicholson, B. K. *J. Chem. Soc., Dalton Trans.* **1981**, 80-84.
(174) Lee, S. K.; Mackay, K. M.; Nicholson, B. K.; Service, M. *J. Chem. Soc., Dalton Trans.* **1992**, 1709-1716.
(175) Wong, F. S.; Mackay , K. M. *J. Chem. Res., Synop.* **1980**, 180.
(176) Anema, S. G.; Mackay, K. M.; Nicholson, B. K. *J. Chem. Soc., Dalton Trans.* **1996**, 3853-3858.
(177) Anema, S. G.; Mackay, K. M.; Nicholson, B. K.; Tiel, M. V. *Organometallics* **1990**, *9*, 2436-2442.
(178) Duffy, D. N.; Mackay, K. M.; Nicholson, B. K.; Thomson, R. A. *J. Chem. Soc., Dalton Trans.* **1982**, 1029-1034.
(179) Whitmire, K. H.; Lagrone, C. B.; Churchill, M. R.; Fettinger, J. C.; Robinson, B. H. *Inorg. Chem.* **1987**, *26*, 3491-3499.
(180) Evans, C.; Mackay, K. M.; Nicholson, B. K. *J. Chem. Soc., Dalton Trans.* **2001**, 1645-1649.
(181) Foster, S. P.; Mackay, K. M.; Nicholson, B. K. *J. Chem. Soc. Chem. Commun.* **1982**, 1156-1157.
(182) Foster, S. P.; Mackay, K. M.; Nicholson, B. K. *Inorg. Chem.* **1985**, *24*, 909-913.

(183) Gerlach, R. F.; Mackay, K. M.; Nicholson, B. K. *J. Organomet. Chem.* **1979**, *178*, C30-C32.
(184) Lee, S. K.; Mackay, K. M.; Nicholson, B. K. *J. Chem. Soc., Dalton Trans.* **1993**, 715-722.
(185) Audett, J. A.; Mackay, K. M. *J. Chem. Soc., Dalton Trans.* **1988**, 2635-2643.
(186) Bonny, A.; Mackay, K. M. *J. Chem. Soc., Dalton Trans.* **1978**, 1569-1573.
(187) Lei, D.; Hampden-Smith, M. J.; Duesler, E. N.; Huffman, J. C. *Inorg. Chem.* **1990**, *29*, 795-798.
(188) Anema, S. G.; Audett, J. A.; Mackay, K. M.; Nicholson, B. K. *J. Chem. Soc., Dalton Trans.* **1988**, 2629-2634.
(189) Anema, S. G.; Barris, G. C.; Mackay, K. M.; Nicholson, B. K. *J. Organomet. Chem.* **1992**, *441*, 35-43.
(190) Anema, S. G.; Mackay, K. M.; Nicholson, B. K. *J. Organomet. Chem.* **1989**, *371*, 233-246.
(191) Elder, M.; Hutcheon, W. L. *J. Chem. Soc., Dalton Trans.* **1972**, 175-180.
(192) Gynane, M. J. S.; Harris, D. H.; Lappert, M. F.; Power, P. P.; Riviere, P.; Riviere-Baudet, M. *J. Chem. Soc., Dalton Trans.* **1977**, 2004-2009.
(193) Harris, D. H.; Lapper, M. F. *J. Chem. Soc. Chem. Commun.* **1974**, 895-896.
(194) Zhu, Q.; Ford, K. L.; Roskamp, E. J. *Heteroat. Chem.* **1992**, *3*, 647-649.
(195) Fan, M.; Shevchenko, I. V.; Voorhies, R. H.; Eckert, S. F.; Zhang, H.; Lattman, M. *Inorg. Chem.* **2000**, *39*, 4704-4712.
(196) Fan, M.; Zhang, H.; Lattman, M. *Organometallics* **1996**, *15*, 5216-5219.
(197) Fan, M.; Zhang, H.; Lattman, M. *Chem. Commun.* **1998**, 99-100.
(198) FAN, M.; ZHANG, H.; LATTMAN, M. *Phosphorus, Sulfur, Silicon Relat. Elem.* **1999**, *144-146*, 257-260.
(199) Fan, M.; Zhang, H.; Lattman, M. *Phosphorus, Sulfur, Silicon Relat. Elem.* **2002**, *177*, 1549-1551.
(200) Fan, M.; Zhang, H.; Lattman, M. *Inorg. Chem.* **2006**, *45*, 6490-6496.
(201) Khasnis, D. V.; Burton, J. M.; McNeil, J. D.; Santini, C. J.; Zhang, H.; Lattman, M. *Inorg. Chem.* **1994**, *33*, 2657-2662.
(202) Khasnis, D. V.; Burton, J. M.; McNeil, J. D.; Zhang, H.; Lattman, M. *Phosphorus, Sulfur, Silicon Relat. Elem.* **1993**, *75*, 253-256.
(203) Lattman, M. In *Modern Aspects of Main Group Chemistry*; Kemp(Ed.), R. A., Ed.; ACS Symposium Series: 2006, p 237-251.
(204) Redkevich, D. M. *Angew. Chem. Int. Ed. Engl.* **2004**, *43*, 558.
(205) Shang, S.; Khasnis, D. V.; Burton, J. M.; Santini, C. J.; Fan, M.; Small, A. C.; Lattman, M. *Organometallics* **1994**, *13*, 5157-5159.
(206) Shevchenko, I.; Zhang, H.; Lattman, M. *Inorg. Chem.* **1995**, *34*, 5405-5409.
(207) Sood, P.; Koutha, M.; Fan, M.; Klichko, Y.; Zhang, H.; Lattman, M. *Inorg. Chem.* **2004**, *43*, 2975-2980.
(208) Sood, P.; Zhang, H.; Lattman, M. *Organometallics* **2002**, *21*, 4442-4447.
(209) Kanamathareddy, S.; Gutache, C. D. *J. Org. Chem.* **1992**, *57*, 3160-3166.
(210) Magrans, J. O.; Rincon, A. M.; Cuevas, F.; Lopez-Prados, J.; Nieto, P. M.;

Pons, M.; Prados, P.; de Mendoza, J. *J. Org. Chem.* **1998**, *63*, 1079-1085.
(211) Shinkai, S. *Tetrahedron* **1993**, *49*, 8933-8968.
(212) Gutsche, C. D.; Bauer, L. J. *J. Am. Chem. Soc.* **1985**, *107*, 6052-6059.
(213) Iglesias-Sanchez, J. C.; Souto, B.; Pastor, C. J.; de Mendoza, J.; Prados, P. *J. Org. Chem.* **2005**, *70*, 10400-10407.
(214) Belhamel, K.; Nguyen, T. K. D.; Benamor, M.; Ludwig, R. *Eur. J. Inorg. Chem.* **2003**, 4110-4116.
(215) Boulet, B.; Bouvier-Capely, C.; Cossonnet, C.; Cote, G. *Solvent Extr. Ion Exc.* **2006**, *24*, 319-330.
(216) Darbost, U.; Seneque, O.; Li, Y.; Bertho, G.; Marrot, J.; Rager, M.-N.; Reinaud, O.; Jabin, I. *Chem. Eur. J.* **2007**, *13*, 2078-2088.
(217) Eggert, J. P. W.; Harrowfield, J. M.; Luning, U.; Skelton, B. W.; White, A. H. *Lanthanide(III) ion coordination by a concave reagent* **2006**, *25*, 910-914.
(218) Izzet, G.; Akdas, H.; Hucher, N.; Giorgi, M.; Prange, T.; Reinaud, O. *Inorg. Chem.* **2006**, *45*, 1069-1077.
(219) Izzet, G.; Rager, M.-N.; Reinaud, O. *Dalton Trans.* **2007**, 771-780.
(220) Obora, Y.; Liu, Y. K.; Jiang, L. H.; Takenaka, K.; Tokunaga, M.; Tsuji, Y. *Organometallics* **2005**, *24*, 4-6.
(221) Obora, Y.; Liu, Y. K.; Kubouchi, S.; Tokunaga, M.; Tsuji, Y. *Eur. J. Inorg. Chem.* **2006**, 222-230.
(222) Rondelez, Y.; Seneque, O.; Rager, M.-N.; Duprat, A. F.; Reinaud, O. *Chem. Eur. J.* **2000**, *6*, 4218-4226.
(223) Seneque, O.; Rager, M.-N.; Giorgi, M.; Prange, T.; Tomas, A.; Reinaud, O. *J. Am. Chem. Soc.* **2005**, *127*, 14833-14840.
(224) Seneque, O.; Rager, M.-N.; Giorgi, M.; Reinaud, O. *J. Am. Chem. Soc.* **2000**, *122*, 6183-6189.
(225) Seneque, O.; Rondelez, Y.; Le Clainche, L.; Inisan, C.; Rager, M.-N.; Giorgi, M.; Reinaud, O. *Eur. J. Inorg. Chem.* **2001**, 2597-2604.
(226) Souane, R.; Hubscher, V.; Asfari, Z.; Arnaud, F.; Vicens, J. *Tetrahedron Lett.* **2003**, *44*, 9061-9064.
(227) Petrella, A. J.; Craig, D. C.; Lamb, R. N.; Raston, C. L.; Roberts, N. K. *Dalton Trans.* **2004**, 327-333.
(228) Petrella, A. J.; Roberts, N. K.; Craig, D. C.; Raston, C. L.; Lamb, R. N. *Chem. Commun.* **2003**, 2288-2289.
(229) Petrella, A. J.; Roberts, N. K.; Craig, D. C.; Raston, C. L.; Lamb, R. N. *Chem. Commun.* **2003**, 1014-1015.
(230) Stanciu, C.; Hino, S. S.; Stender, M.; Richards, A. F.; Olmstead, M. M.; Power, P. P. *Inorg. Chem.* **2005**, *44*, 2774-2780.
(231) Cetinkaya, B.; Gumrukcu, I.; Lappert, M. F. *J. Am. Chem. Soc.* **1980**, *102*, 2088-2089.
(232) Weinert, C. S.; Fanwick, P. E.; Rothwell, I. P. *Dalton Trans.* **2003**, 1795-1802.
(233) Chorley, R. W.; Hitchcock, P. B.; Lappert, M. F.; Leung, W. P.; Power, P. P.; Olmstead, M. M. *Inorg. Chim. Acta* **1992**, *198-200*, 203-209.
(234) Lappert, M. F.; Slade, M. J. *J. Chem. Soc. Chem. Commun.* **1980**, 621-

622.
(235) Benet, S.; Cardin, C. J.; Cardin, D. J.; Constantine, S. P.; Heath, P.; Rashid, H.; Teixeira, S.; Thorpe, J. H.; Todd, A. K. *Organometallics* **1999**, *18*, 389-398.
(236) Suh, S.; Hoffman, D. M. *Inorg. Chem.* **1996**, *35*, 6164-6169.
(237) Reiche, C.; Kliem, S.; Klingebiel, U.; Noltemeyer, M.; Voit, C.; Herbst-Irmer, R.; Schmatz, S. *J. Organomet. Chem.* **2003**, *667*, 24-34.
(238) Ruhland-Senge, K.; Barlett, R. A.; Olmstead, M. M.; Power, P. P. *Angew. Chem. Int. Ed.* **1993**, *32*, 425.
(239) Schraml, J.; Kvicalova , M.; Blechta, V.; Cermak, J. *Mag. Res. Chem.* **1997**, *35*, 659-662.
(240) Luo, B.; Young, V. G., Jr.; Gladfelter, W. L. *J. Organomet. Chem.* **2002**, *649*, 268-275.
(241) Carmalt, C. J.; Mileham, J. D.; White, A. J. P.; Williams, D. J.; Steed, J. W. *Inorg. Chem.* **2001**, *40*, 6035-6038.
(242) Schmidbaurr, H.; Findeiss, W. *Angew. Chem. Int. Ed.* **1964**, *3*, 696.

VITA

Anthony Edmund Wetherby Jr.

Candidate for the Degree of

Doctor of Philosophy

Dissertation: REACTION OF BULKY MAIN GROUP METAL (II) AMIDES WITH POLYFUNCTIONAL PHENOL SUBSTRATES

Major Field: Chemistry

Biographical:

Personal Data: Born in Glens Falls, New York on January 9, 1983

Education:

Bachelors of Science:

Chemistry, Clarkson University, December, 2004

Doctor of Philosophy:

Chemistry, Oklahoma State University, July 2009

Publications:

The author has published and presented work in seminars and national conferences.

Professional Memberships:

American Chemical Society (ACS)

Phi Lambda Upsilon (PLU): National Honorary Chemical Society

Name: Anthony E. Wetherby Jr. Date of Degree: July, 2009

Institution: Oklahoma State University Location: Stillwater, Oklahoma

Title of Study: REACTION OF BULKY MAIN GROUP METAL(II) AMIDES WITH POLYFUNCTIONAL PHENOL SUBSTRATES

Pages in Study: 177 Candidate for the Degree of Doctor of Philosophy

Major Field: Chemistry

Scope and Method of Study: The purpose of this study was to afford the selective protection of one functional group in the presence of others. This is an important process in synthetic chemistry. Several types of silylating agents have been reported for the protection of hydroxyl groups, with limited selectivity, harsh reaction conditions and long reaction times. In an attempt to increase silylation power and limit the complexity and harshness of these reactions we have developed a novel method using mild conditions to achieve silylation of one or two hydroxyl groups. Silyaltion reactions were investigated for the reaction between 3,3'-disubstituted-1,1'-bi-2,2'-napthol and various metal(II) amides. These reactions were monitored using ^{1}H-NMR spectroscopy. Studies were also done involving the reaction of $Ge[N(SiMe_3)_2]_2$ with calix[4], [6] and [8]arenes. Results were confirmed via ^{1}H-NMR and X-ray Crystallography

Findings and Conclusions: We have developed a novel method using metal (II) amides under mild conditions to achieve silylation of one or two hydroxyl groups with reaction times ranging from 10min-24hrs. Variation of the metal furnished different rates of reaction. The general trend in reaction rate was monitored by ^{1}H-NMR spectroscopy and decreases in the order M= Be>Zn>Ge>Mg, with no observable silylated products using Sn, Pb or Ca amides. Reactions employing a mercury (II) amide resulted in an unexpected outcome involving cyclization via formation of a C-O bond. The reaction of germanium (II) amide with calix[4], calix[6] and calix[8]arenes resulted in the formation of compounds containing germanium rhombi as well as the formation of a unique compound containing unusual diamidosilyl ether groups.

ADVISER'S APPROVAL: Dr. Charles S. Weinert